

**EVALUATION OF THE WATER
BUDGET COMPONENTS OF THE
BRAHMAPUTRA RIVER BASIN USING
SATELLITE DATA**

Thesis

Submitted in partial fulfilment of the requirements for the degree of

DOCTOR OF PHILOSOPHY

by

**SURAJIT DEB BARMA
155094AM15F10**



**DEPARTMENT OF WATER RESOURCES & OCEAN
ENGINEERING
NATIONAL INSTITUTE OF TECHNOLOGY KARNATAKA
SURATHKAL, MANGALORE – 575 025
OCTOBER 2023**

DECLARATION

by the Ph.D. Research Scholar

I hereby *declare* that the Research Thesis entitled **Evaluation of the water budget components of the Brahmaputra river basin using satellite data** which is being submitted to the **National Institute of Technology Karnataka, Surathkal** in partial fulfilment of the requirements for the award of the Degree of **Doctor of Philosophy in Water Resources and Ocean Engineering Department** is a *bonafide report of the research work* carried out by me. The material contained in this Research Thesis has not been submitted to any University or Institution for the award of any degree.

Surajit Deb Barma

155094AM15F10, SURAJIT DEB BARMA

(Register Number, Name & Signature of the Research Scholar)

Department of Water Resources and Ocean Engineering

Place: NITK-Surathkal

Date: *19.10.2023*

CERTIFICATE

This is to *certify* that the Research Thesis entitled **Evaluation of the water budget components of the Brahmaputra river basin using satellite data** submitted by **Mr. Surajit Deb Barma** (Register no: 155094AM15F10) as the record of the research work carried out by him, is *accepted as the Research Thesis submission* in partial fulfilment of the requirements for the award of degree of **Doctor of Philosophy**.



Prof. Amai Mahesha 10/23

Research Guide

(Name and Signature with Date and Seal)

Dr. MAHESHA AMAI
Professor

Dept. of Water Resources & Ocean Engineering
National Institute of Technology Karnataka
Surathkal, Srinivasnagara, Mangaluru - 575 025



Varija K
19.10.23

Chairman - DRPC

(Signature with Date and Seal)

Chairman (DRPC)
Dept. of Water Resources & Ocean Engineering

ACKNOWLEDGEMENT

To everyone who helped this Ph.D. thesis be completed successfully, I would like to offer my profound gratitude and admiration. Their assistance, direction, and encouragement have been priceless throughout this process.

First and foremost, I want to express my sincere gratitude to my Ph.D. supervisor Prof Amai Mahesha. His expertise, patience, and ongoing assistance have shaped this research project. I sincerely appreciate his professionalism and steadfast commitment.

I would also like to acknowledge the valuable contributions of Dr B Manu, Department of Civil Engineering, Dr Ramesh H, and the late Prof P.C. Deka, who served as my research committee members. Their insightful feedback, constructive criticism, and scholarly guidance have greatly enriched this thesis. I am indebted to them for their time and expertise.

I would like to thank the Head of the department, Dr Varija K, for her constant encouragement and support. I am grateful for her leadership and vision, which have fostered an environment conducive to research and intellectual growth. I would also like to acknowledge the contributions of former heads of the department, Prof Dwarakish G S, Prof A. Mahesha, Prof Amba Shetty and Prof B M Dodamani, for their contributions to the department and for creating a supportive environment for research.

Furthermore, I sincerely thank the institute Director, Prof Prasad Krishna, for his visionary leadership and commitment to academic excellence. Also, thanks to former directors, Prof K. Umamaheshwar Rao and Prof Sawapan Bhattacharya for their continuous support and encouragement throughout my research journey.

I would like to thank the former and present department staff, Mr. Anil Kumar, Mr. Balakrishna, Mr. Seetharam, Mr. Jagadeesh, and all teaching and non-teaching staff for their help and support. I am grateful for their assistance with my research and for making my time in the department pleasant.

I am also grateful to my present department Ph.D. colleagues, Vinod, Ayilo and Poojitha, and others, for their camaraderie, intellectual discussions, and valuable insights. Their support and encouragement have been instrumental in overcoming challenges and maintaining a productive research atmosphere. I would also like to acknowledge the contributions of former colleagues, Dr Sujay, Dr Chythanya, Dr Dinesh and Dr Pramodkumar, and others, whose intellectual discussion and fellowship have enriched my research expedition.

Last but not least, I want to express my deepest gratitude to my wife, daughter, mother, and father for their unwavering love, understanding, and support throughout this challenging endeavour. Their encouragement and belief in me have been a constant source of motivation.

I extend my heartfelt thanks to all those mentioned above and the countless others who have played a part in my academic and personal growth. This thesis would not have been possible without your contributions and support.

Thank you.

Surajit Deb Barma

ABSTRACT

The water budget can be described as the volume of water that enters a land area, remains stored within it, and eventually exits the land system during a specific time interval. The water budget of a river basin can be represented by equating key components of the hydrological cycle, which include precipitation, actual evapotranspiration (ET), runoff (Q), and changes in terrestrial water storage.

The current research is centred on the assessment of the water budget elements within the Brahmaputra river basin by utilizing satellite-derived data. The motivation for this PhD research is grounded in the complex and transboundary nature of the Brahmaputra River basin, which extends through several countries. A key challenge is the scarcity of hydrometeorological data within the basin, making it difficult to conduct comprehensive hydrological studies. To address this data deficiency, the study turns to space-borne data, as it can offer a more complete and cohesive view of the basin's water budget. The satellite precipitation data were evaluated against updated Brahmaputra River basin gauge data. We also assessed different precipitation data to determine the risk of hydrometeorological variables using dependence measures. We further assessed precipitation data for reconstructing significant water budget variables and innovative trend analysis (ITA) of those variables. The study

Five daily satellite precipitation products were evaluated against an updated Asian Precipitation Highly-Resolved Observational Data Integration Towards Evaluation of the Extreme Events version 2 (APHRODITE v2) using categorical and continuous metrics. Global precipitation measurement (GPM) resulted in the program known as the Integrated Multi-satellitE Retrievals for GPM (IMERG) was found to be the best-performing product daily, considering the spatial and temporal mean for the whole time series. The Climate Prediction Center (CPC) Morphing technique (CMORPH) was found to be the best-performing product considering the evaluation of metrics on a seasonal basis. The soil moisture to rain (SM2RAIN) of the European Space Agency (ESA) climate change

initiative (CCI) precipitation product was found to be the least-performing product on all counts.

Given precipitation quantity, the conditional bivariate copula concept predicted evapotranspiration, the Gravity Recovery and Climate Experiment terrestrial water storage change (GRACE TWSC), and river discharge. The optimal copula is Frank for all three precipitation-TWSC pairs, the European Centre for Medium-Range Weather and Forecasting (ECMWF) reanalysis ET (ERA5-ET) and ERA5-ET, and Clayton for the remaining pairs. Pearson's linear and Spearman's rank correlations for all the pairs of variables are significant for observed and simulated values. The non-exceedance probability of all the dependent variables (lower percentile) decreases with increased precipitation. However, the exceedance probability of the same variables (upper percentile) increases gradually with increased precipitation.

The water budget equation of a large basin based on the conservation of mass was used to reconstruct TWSC, ET, and runoff for the Brahmaputra basin. The reconstructed water budget variables are further assessed using a correlation coefficient to know the linear strength. Also, error metrics like absolute mean error and bias were used to determine how far we can see the variation, such as reconstruction against a gauge or quasi-gauge data. The ERA5-derived TWSCs and Qs tend to provide the highest linear strength expressed in the correlation coefficient on a monthly and seasonal basis. To a greater extent, the Tropical Rainfall Measuring Mission (TRMM), IMERG and the Climate Hazards group Infrared Precipitation with Stations (CHIRPS) also depict a closer correlation coefficient to that of ERA5-derived TWSCs and Qs. The linear strength of derived ETs shows that the inherent uncertainties in the water budget variables did not reconstruct ETs well. On a monthly basis, the TRMM-based TWSC reconstruction was the most optimal, and IMERG-driven ET and runoff were the most optimal. SM2RAIN-driven TWSC, ET, and Q were reported to be the least optimal. For most of the seasons, it was either TRMM or IMERG with the least error. However, the error in terms of the percentage of gauge precipitation for winter and post-monsoon seasons is staggeringly high. Even on a seasonal basis, SM2RAIN was

the least performing. Overall, TRMM, IMERG, and CHIRPS show much lesser uncertainties than other precipitation datasets, as evidenced by the raincloud plots.

The recently developed ITA and innovative polygon trend analysis (IPTA) were used to determine the trend of individual months, including the sub-trends based on different clusters (low, medium, and high) for complete time series and transition of trend between months, respectively. In addition, the traditional Mann-Kendall (MK) test was also conducted to compare the findings of trends. The monthly precipitation of seven precipitation data, four evapotranspiration data, river basin discharge, and GRACE TWSC were used in the study. The present findings are consistent, as reported in several studies on ITA and a few on sub-trends. What was commonly observed in all the water budget variables is the higher percentage of months detecting either increasing or decreasing significant trends using ITA compared to the classical MK test, which in most cases could not detect any significant trend. The sub-trends provided us with the trends in each of the three clusters. Only APHRODITE, TRMM, and IMERG showed more than 2.5 mm/month decreasing trend in the high category. Numerically, ETs showed insignificant trend variation in all the clusters. Discharge of the basin shows a high decreasing trend in the high cluster (339.01 m³/s) and a decreasing trend in the low cluster by a rate of 176.79 m³/s. Similarly, GRACE TWSC shows a decreasing trend of 7.75 mm/month in the high cluster and an 8.69 mm/month decreasing trend in the low cluster.

Keywords: innovative polygon trend analysis (IPTA), innovative trend analysis (ITA), risk assessment, satellite precipitation, water budget error

TABLE OF CONTENTS

| Sl. No | TITLE | Page. No. |
|-------------------------------------|--|------------------|
| | ABSTRACT | i-iii |
| | TABLE OF CONTENTS | v-ix |
| | LIST OF FIGURES | xi-xii |
| | LIST OF TABLES | xiii-xiv |
| | LIST OF ABBREVIATIONS | xv-xvi |
| CHAPTER 1: INTRODUCTION | | 1-8 |
| 1.1 | OVERVIEW | 1 |
| 1.2 | STUDY BACKGROUND | 2 |
| 1.3. | RESEARCH STATEMENT | 5 |
| 1.4 | RESEARCH AIM AND OBJECTIVES | 6 |
| 1.5 | ORGANISATION OF THE THESIS | 7 |
| CHAPTER 2: LITERATURE REVIEW | | 9-29 |
| 2.1 | BRIEF OVERVIEW | 9 |
| 2.2 | GLOBAL SATELLITE PRECIPITATION | 9 |
| 2.2.1. | Introduction | 9 |
| 2.2.2. | Assessment of satellite precipitation | 10 |
| 2.2.3. | Assessment of satellite precipitation in the Brahmaputra Basin | 12 |
| 2.3 | DEPENDENCE MODELLING OF HYDROMETEOROLOGICAL VARIABLES | 13 |
| 2.3.1 | Introduction | 13 |
| 2.3.2 | Application of copula in the probabilistic prediction of hydrometeorological variables | 15 |
| 2.4 | RECONSTRUCTION OF WATER BUDGET VARIABLES | 18 |
| 2.4.1 | Introduction | 18 |

| | | |
|--|---|--------------|
| 2.4.2 | Application of satellite data in the reconstruction of water budget variables | 18 |
| 2.5 | INNOVATIVE TREND ANALYSIS (ITA) OF HYDROMETEOROLOGICAL VARIABLES | 25 |
| 2.5.1 | Introduction | 25 |
| 2.5.2 | Application of ITA trend analysis of hydrometeorological variables | 25 |
| 2.6 | RESEARCH GAP | 27 |
| CHAPTER 3: STUDY AREA AND DATASETS | | 31-39 |
| 3.1 | STUDY AREA | 31 |
| 3.2 | DATASETS | 33 |
| 3.2.1. | Precipitation data | 33 |
| 3.2.2 | Evapotranspiration data | 36 |
| 3.2.3 | River discharge | 38 |
| 3.2.4 | GRACE TWSC | 38 |
| CHAPTER 4: EVALUATION OF SATELLITE PRECIPITATION OF A LARGE RIVER BASIN | | 41-74 |
| 4.1 | OVERVIEW | 41 |
| 4.2 | METHODS | 41 |
| 4.2.1. | Categorical error metrics | 41 |
| 4.2.2. | Continuous error metrics | 41 |
| 4.3 | RESULTS AND DISCUSSION | 43 |
| 4.3.1 | Metrics of daily precipitation of the basin | 43 |
| 4.3.2 | Metrics of daily precipitation in winter season | 58 |
| 4.3.3 | Metrics of daily precipitation in summer season | 61 |
| 4.3.4 | Metrics of daily precipitation in monsoon season | 63 |
| 4.3.5 | Metrics of daily precipitation in post monsoon season | 64 |
| 4.3.6 | Uncertainty analysis of precipitation across the basin | 66 |
| 4.4 | CONCLUSIONS | 72 |

| | | |
|--|---|---------------|
| CHAPTER 5: EVALUATION OF PRECIPITATION FOR RISK ASSESSMENT OF WATER CYCLE VARIABLES | | 75-94 |
| 5.1 | OVERVIEW | 75 |
| 5.2 | METHODS | 75 |
| 5.3 | RESULTS | 78 |
| 5.3.1 | Identification of Marginal Distribution of Precipitation, TWSC, ET, and Discharge | 78 |
| 5.3.2 | Dependence Modeling of Precipitation with TWSC, ET, and Discharge | 80 |
| 5.3.3 | Risk Evaluation of TWSC Conditioned on Different Precipitation Scenarios | 85 |
| 5.3.4 | Risk Evaluation of ET Conditioned on Different Precipitation Scenarios | 87 |
| 5.3.5 | Risk Evaluation of Q Conditioned on Different Precipitation Scenarios | 88 |
| 5.4 | DISCUSSION | 90 |
| 5.4.1 | Assessment of Risk of TWSC for given Precipitation Scenarios | 91 |
| 5.4.2 | Assessment of Risk of ET for given Precipitation Scenarios | 92 |
| 5.4.3 | Assessment of Risk of Q for given Precipitation Scenarios | 92 |
| 5.5 | CONCLUSIONS | 93 |
| CHAPTER 6: EVALUATION OF SATELLITE PRECIPITATION ESTIMATES TO RECONSTRUCT MAJOR WATER BUDGET COMPONENTS | | 95-116 |
| 6.1 | OVERVIEW | 95 |
| 6.2 | METHODS | 95 |
| 6.3 | RESULTS AND DISCUSSION | 96 |
| 6.3.1 | Assessment of monthly water budget components | 96 |
| 6.3.2 | Assessment of winter water budget components | 101 |
| 6.3.3 | Assessment of summer water budget components | 105 |
| 6.3.4 | Assessment of monsoon water budget components | 106 |
| 6.3.5 | Assessment of post-monsoon water budget components | 108 |

| | | |
|--|--|----------------|
| 6.3.6 | Uncertainty estimation of reconstructed monthly water budget variables | 111 |
| 6.4 | CONCLUSIONS | 115 |
| CHAPTER 7: INNOVATIVE TREND ANALYSIS OF WATER BUDGET COMPONENTS | | 117-141 |
| 7.1 | OVERVIEW | 117 |
| 7.2 | METHODS | 117 |
| 7.3 | RESULTS AND DISCUSSION | 119 |
| 7.3.1 | Innovative trend analysis of different precipitation products | 119 |
| 7.3.2 | Innovative trend analysis of ET, Q, and GRACE TWSC | 122 |
| 7.3.3 | Sub-trends of precipitation estimates, ET, Q and GRACE TWSC | 126 |
| 7.3.4 | Innovative polygon trend analysis of different precipitation products | 130 |
| 7.3.5 | Innovative polygon trend analysis of ET, Q, and GRACE TWSC | 135 |
| 7.4 | CONCLUSIONS | 140 |
| CHAPTER 8: SUMMARY AND CONCLUSIONS | | 143-149 |
| 8.1 | SUMMARY | 143 |
| 8.2 | CONCLUSIONS | 144 |
| 8.2.1 | General conclusions | 144 |
| 8.2.2 | Satellite data evaluation | 145 |
| 8.2.3 | Risk Assessment of water budget variables | 145 |
| 8.2.4 | Reconstruction of water budget variables | 146 |
| 8.2.5 | Innovative trend analysis of water budget variables | 146 |
| 8.3 | RESEARCH CONTRIBUTIONS | 147 |
| 8.4 | LIMITATIONS OF THE STUDY | 148 |
| 8.5 | SCOPE FOR FURTHER STUDY | 148 |
| REFERENCES | | 150 |
| APPENDIX | | 166 |

| | |
|---------------------|------------|
| PUBLICATIONS | 173 |
| BIOSKETCH | 175 |

LIST OF FIGURES

| Figure No. | Figure Caption | Page No. |
|-------------------|---|-----------------|
| 3.1 | Study area map of Brahmaputra basin | 32 |
| 3.2 | Elevation map of different zones of Brahmaputra | 32 |
| 4.1 | Map of mean daily (2001-2015) of gauge and satellite precipitation products | 44 |
| 4.2 | Probability of detection (POD) map of satellite precipitation products against gauge data | 47 |
| 4.3 | False alarm ratio (FAR) map of satellite precipitation products against gauge data | 50 |
| 4.4 | Critical success index (CSI) map of satellite precipitation products against gauge | 51 |
| 4.5 | Correlation of determination (R^2) map of satellite precipitation products against gauge data | 52 |
| 4.6 | Taylor's diagram of correlation between satellite precipitation and APHRODITE in different elevation-based zones of the basin | 53 |
| 4.7 | Relative bias (RBIAS) map of satellite precipitation products against gauge data | 54 |
| 4.8 | Mean error (ME) map of satellite precipitation products against gauge data | 56 |
| 4.9 | Mean absolute error (MAE) map of satellite precipitation products against gauge data | 57 |
| 4.10 | Root mean square error (RMSE) map of satellite precipitation products against gauge data | 59 |
| 4.11 | Violin plots of precipitation | 67 |
| 4.12 | Violin plots of precipitation in winter | 69 |
| 4.13 | Violin plots of precipitation in summer | 70 |
| 4.14 | Violin plots of precipitation in monsoon | 71 |
| 4.15 | Violin plots of precipitation in post-monsoon | 72 |

| | | |
|-----|---|-----|
| 5.1 | Cumulative distribution function plots of precipitation products | 79 |
| 5.2 | Cumulative distribution function plots of dependent variables | 80 |
| 5.3 | Scatter diagrams of different precipitation-TWSC pairs | 84 |
| 5.4 | Scatter diagrams of different precipitation-ET pairs | 84 |
| 5.5 | Scatter diagrams of different precipitation-Q pairs | 85 |
| 5.6 | Conditional distribution plots of TWSC given different precipitation products | 87 |
| 5.7 | Conditional distribution plots of ET given different precipitation products | 89 |
| 5.8 | Conditional distribution plots of Q given different precipitation | 90 |
| 6.1 | Time series of reconstructed dS/dt against GRACE TWSC | 98 |
| 6.2 | Time series of reconstructed ET against MOD16 ET | 102 |
| 6.3 | Time series of reconstructed Q against observed runoff | 103 |
| 6.4 | Raincloud plots of GRACE TWSC and derived TWSCs | 112 |
| 6.5 | Raincloud plots of MOD16 ET and derived ETs | 114 |
| 6.6 | Raincloud plots of observed runoff and derived runoffs | 114 |
| 7.1 | Subtrends of precipitation products using ITA | 127 |
| 7.2 | Subtrends of ET products using ITA | 129 |
| 7.3 | Subtrends of discharge and GRACE TWSC using ITA | 130 |
| 7.4 | IPTA diagram for mean of the precipitation | 131 |
| 7.5 | IPTA diagram for standard deviation of the precipitation | 134 |
| 7.6 | IPTA diagram for mean of the ET | 136 |
| 7.7 | IPTA diagram for standard deviation of the ET | 137 |
| 7.8 | IPTA diagram for the mean and standard deviation of discharge and GRACE TWSC | 140 |

LIST OF TABLES

| Table No. | Table Caption | Page No. |
|------------------|---|-----------------|
| 4.1 | Performance metrics for evaluation of satellite-based precipitation products | 42 |
| 4.2 | Daily metrics obtained for the evaluation of satellite precipitation of the basin | 45 |
| 4.3 | Daily metrics obtained for the evaluation of satellite precipitation of the upper section of the basin | 46 |
| 4.4 | Daily metrics obtained for the evaluation of satellite precipitation of the middle section of the basin | 48 |
| 4.5 | Daily metrics obtained for the evaluation of satellite precipitation of lower section of the basin | 48 |
| 4.6 | Daily metrics obtained for evaluation of satellite precipitation of winter season of the basin | 59 |
| 4.7 | Daily metrics obtained for evaluation of satellite precipitation of summer season of the basin | 62 |
| 4.8 | Daily metrics obtained for evaluation of satellite precipitation of monsoon season of the basin | 64 |
| 4.9 | Daily metrics obtained for evaluation of satellite precipitation of post monsoon season of the basin | 65 |
| 5.1 | Description of the most commonly used Archimedean copulas | 76 |
| 5.2 | KS statistics of different marginal distributions fitted to precipitation | 79 |
| 5.3 | KS statistics of different marginal distributions fitted to dependent variables | 80 |
| 5.4 | Performance statistics of precipitation-TWSC pair | 81 |
| 5.5 | Performance statistics of precipitation-ET pair | 81 |

| | | |
|-----|--|-----|
| 5.6 | Performance statistics of precipitation-Q pair | 82 |
| 5.7 | Performance measures of the optimal copula of different pairs of the water cycle variables | 83 |
| 5.8 | Magnitudes of precipitation corresponding to each percentile | 85 |
| 5.9 | Magnitudes of the dependent variable corresponding to each percentile | 86 |
| 6.1 | The evaluation of monthly precipitaton products with respect to three metrics (MOD16_0.5 ET) | 100 |
| 6.2 | The evaluation of winter precipitaton products with respect to three metrics (MOD16_0.5 ET) | 104 |
| 6.3 | The evaluation of summer precipitaton products with respect to three metrics (MOD16_0.5 ET) | 107 |
| 6.4 | The evaluation of monsoon precipitaton products with respect to three metrics (MOD16_0.5 ET) | 109 |
| 6.5 | The evaluation of postmonsoon precipitaton products with respect to three metrics (MOD16_0.5 ET) | 110 |
| 7.1 | ITA and MK trend tests of precipitation products | 121 |
| 7.2 | ITA and Sen's slopes of precipitation products | 123 |
| 7.3 | ITA and MK trend tests of ET, Q and TWSC | 124 |
| 7.4 | ITA and Sen's slopes of ET, Q and TWSC | 128 |
| 7.5 | IPTA of mean of precipitation products | 132 |
| 7.6 | IPTA of mean of ET, Q and TWSC | 133 |
| 7.7 | IPTA of standard deviation of precipitation products | 138 |
| 7.8 | IPTA of standard deviation of ET, Q and TWSC | 139 |

LIST OF ABBREVIATIONS

| Abbreviation | Definition |
|---------------------|---|
| AIC | Akaike Information Criterion |
| APHRODITE | Asian Precipitation Highly-Resolved Observational Data Integration Towards Evaluation of the Extreme Events |
| CCI | Climate change initiative |
| CDF | Cumulative distribution function |
| CHIRPS | Climate Hazards Group Infrared Precipitation with Stations |
| CLSM | Catchment Land Surface Model |
| CMORPH | CPC Morphing technique |
| CPC | Climate Prediction Center |
| CSI | critical success index |
| dS/dt | change in storage |
| ECMWF | European Centre for Medium-Range Weather and Forecasting |
| ERA5 | ECMWF reanalysis 5 th generation |
| ET | Evapotranspiration |
| FAR | false alarm ratio |
| GLDAS | Global Land Data Assimilation System |
| GPM | Global precipitation measurement |
| GRACE TWSC | Gravity Recovery and Climate Experiment Terrestrial Water Storage Change |
| IMERG | Integrated Multi-satellitE Retrievals for GPM |
| IPTA | Innovative polygon trend analysis |

| | |
|----------------|---|
| ITA | Innovative trend analysis |
| KS | Kolmogorov–Smirnov |
| MAE | Mean absolute error |
| ME | Mean error |
| MK | Mann-Kendall |
| MOD16/MODIS | Moderate Resolution Imaging Spectroradiometer |
| NSE | Nash-Sutcliffe efficiency |
| P | Precipitation/ rainfall |
| POD | probability of detection |
| Q | Discharge/ runoff |
| r | Correlation coefficient |
| R ² | Coefficient of determination |
| RBIAS | Relative bias |
| RMSE | Root mean square error |
| SM2RAIN-CCI | soil moisture to rain CCI |
| TRMM | Tropical Rainfall Measuring Mission |
| TWSA | Total water storage anomaly |

CHAPTER 1

INTRODUCTION

1.1 OVERVIEW

The present research focuses on evaluating the major water budget components of a large river basin using globally available satellite data. The data or estimates are used against gauge-based data or reference data to ascertain their ability to represent the satellite observations and gauge-based or reconstructed data, estimate the risk associated with a water budget variable, and determine the trends of each water budget variable. There are conflicting views on the performance of satellite-based rainfall estimates, especially the one merged with several other data sources (Beck et al. 2019; Lehmann et al. 2022). Also, the estimation of risk or probability of occurrence of a water budget variable given different sources of precipitation has been addressed (Uttarwar et al. 2020). In addition, how different precipitation data perform for the reconstruction of other water budget variables like evapotranspiration (ET), runoff (Q, discharge), and terrestrial water storage change (TWSC) in a given study have been rarely addressed (Zhang et al. 2016a). Then, the assessment of trend analysis using the recently developed innovative trend analysis (Şen 2017; Şen et al. 2019a) for the water budget variables is not yet highlighted (Oliveira et al. 2014).

Therefore, the main aim of the current research is to evaluate the water budget components using globally available data. This will achieve the objectives of evaluating different satellite precipitation estimates, assessing the risk of water budget variables given precipitation, evaluating different sources of precipitation data for water budget reconstruction, and assessing the trend of each water budget variable using innovative trend analysis.

This chapter provides an introduction to the study by first discussing the overview and background of the research, then stating the research problem, followed by the

research aim, objectives, and research questions, and then followed by research significance or contribution to the body of research, and finally, the limitations of the research and organization of the thesis.

1.2 STUDY BACKGROUND

Water budget may be defined as the amount of water entering a land, stored within and leaving the land system for a given time interval (Mitchell et al., 2003 ; Lorenz et al., 2014; Wang et al., 2014). A river basin water budget can be expressed as balancing major hydrological cycle components: precipitation, actual evapotranspiration, runoff and terrestrial water storage change (Gao et al., 2010). Hence, the water budget follows the conservation of mass principle. Interested readers may refer to a review article by Duffy (2017) for more information on the water budget from a historical perspective. The concept of the water budget in scientific hydrology has been around for some time (Xu and Singh, 1998), but it gained momentum only in recent times, especially in the first decade of the 21st century (Jothityangkoon et al., 2001; Marengo, 2005; Sheffield et al., 2009 among others.) More so after the year 2010 there have been resurgent interests in water budget estimation and closure (Azarderakhsh et al., 2011; Pan et al., 2012; Zhang et al., 2016). Several approaches have been attempted to estimate water budget at different spatial and temporal scales ranging from small catchments (Hentschel et al., 2013; Graf et al., 2014; Wei et al., 2016) to medium size catchments (Xue et al., 2013; Wu and Chen, 2013; Savéan et al., 2015) to large river basins (Wu and Chen, 2013; Armanios and Fisher, 2014; Abera et al., 2017) and continental/global river basins (Troy et al., 2011; Sahoo et al., 2011; Fersch et al., 2012; Pan et al., 2012; Corbari et al., 2014; Munier et al., 2014; Wang et al., 2014; Zhang et al., 2016).

Comprehensive information about the hydrological variables that make up the terrestrial water cycle is of great importance because it allows us to understand their dynamic changes over time and space (Sheffield et al., 2018). In addition to in situ monitoring networks, satellite remote sensing is increasingly used as a source of information and, in some situations, is the only practical source (Sheffield et al. 2018). The continuous development of space-borne sensors has enabled to have access to almost

all the major water budget components like precipitation (Ciabatta et al. 2017; Huffman et al. 2010, 2019; Joyce et al. 2004), evapotranspiration (Mu et al. 2011), terrestrial water storage change (Landerer and Swenson 2012) and discharge (Revel et al. 2023).

Out of all the major water budget variables, the estimation of space-borne precipitation is under continuous development and has more products than any other variables at a given time (Prakash 2019; Wei et al. 2021). Proportionately, it is also the major water budget component that is paid more attention than the rest of the variables, as evidenced from literature on the current sensors used and future planned sensors (Kidd et al. 2021). Precipitation is usually recorded by a tipping-bucket system (Sevruk 2006), which measures point precipitation and its measurement area is limited to the gauge itself. Despite its limitation, the gauge measurement is still the most preferred when satellite precipitation estimates are evaluated or corrected (Kidd et al. 2021; Michelson 2004). Low earth orbit satellites (LEO) come with four different sensors, namely, visible (VIS), infrared (IR), active microwave (AMW) and passive microwave (PMW) (Battaglia et al. 2020). However, geostationary satellites are limited to using the first two sensors because of the high altitude over which these kinds of satellites fly and the necessity for fine resolution estimation (Kidd et al. 2021). Some of the satellite-based precipitation products that are widely used are the TRMM (Huffman et al. 2010), GPM IMERG (Huffman et al. 2019), CMORPH (Joyce et al. 2004), CHIRPS (Funk et al. 2014, 2015), SM2RAIN (Brocca et al. 2014) and PERSIANN (Nguyen et al. 2018). These satellite precipitation estimates are evaluated based on categorical metrics like the probability of detection (POD), false alarm ratio (FAR) and critical success index (CSI) (AghaKouchak and Mehran 2013) and continuous metrics like mean error (ME), mean absolute error (MAE), mean square error (MSE) and root mean square error (RMSE) (Duan et al. 2016). In very recently published literature, CHIRPS was found to be mostly applied for drought or climatological studies (Ma et al. 2023), whereas GPM IMERG or just IMERG has been widely used to evaluate it against gauge data in several studies related to extreme precipitation events (Islam et al. 2020; Li et al. 2022; Liu et al. 2022a).

Understanding water resource evolution at the basin scale is necessary to achieve water security and enhance adaptability to hydrological extremes (Sheffield et al. 2018). Risk assessment of a hydrometeorological variable with respect to another variable was often carried out using the traditional bivariate modelling in which both the marginal distributions come from the same distribution. However, this is not the case with a copula connecting two continuous variables based on a dependence measure. The copula can handle the dependence measure irrespective of the marginal distributions of the two interacting variables (Genest and Favre 2007). The risk evaluation of the occurrence of an event is associated with the exceedance/ non-exceedance of the ET/Q/TWSC for a given threshold of explanatory variable precipitation (Liu et al. 2018; Salvadori and De Michele 2004). For example, for a given amount of precipitation, the groundwater level was predicted in different aquifers bivariate using conditional copula (Uttarwar et al. 2020; Wable and Jha 2018). Similarly, the probabilistic streamflow prediction concerning hydrometeorological variables was carried out in the Three Gorges dam in China (Liu et al. 2018). In recent years, copula methods have continued to find applications when there is a need to understand dependence measures. For instance, they have been used in the application of drought-fluvial identification (Liu et al. 2022b), environmental flow assessment (Liu et al. 2016) and streamflow-sediment-dependent structure (Yang et al. 2023), among others.

Water budget variables like ET, Q and TWSC (dS/dt) are reconstructed using the conservation of mass principle. The residual of precipitation (P) minus two of the above variables will yield the equivalence of the variable that was not considered. Under ideal conditions, the residual and the target variable should be equal resulting in zero when the difference between the two is taken. For example, it is desired to obtain ET ($=P - Q - TWSC$) or Q ($=P - ET - TWSC$) or dS/dt ($=P - ET - Q$). So, ET, Q and dS/dt are the reconstructed evapotranspiration, runoff/discharge and change in storage. Precipitation is a common variable in all three scenarios, so that the same precipitation data could be used. Accordingly, the reconstructed variables are compared with either gauge for the runoff, satellite-based observed ET for ET and satellite-based observed TWSC for dS/dt .

The assessment could be carried out using metrics like mean absolute or bias errors. For over a decade, satellite data have been extensively used to close the water budget, meaning to minimize the difference error between observed variables like GRACE TWSC and dS/dt or MOD16 ET and reconstructed ET. To close the water budget, several researchers attempted to constrain the closure error by using data assimilation technique (Sahoo et al. 2011a), correction model (Munier et al. 2014; Pellet et al. 2020), a blend of different sources of data (Zhang et al. 2016b), integrated model (Maxwell and Condon 2016), modelling framework (Abera et al. 2017), multiple combinations of data to close water budget for the land mass of the world excluding the pools (Lehmann et al. 2022), two-step water budget closure method (Luo et al. 2023).

The trend analysis of hydrological variables helps us to understand how the variable of interest could vary over different time scales and spatial variations. Trends analysis of water budget components has already been attempted either using the traditional MK test (Kendall 1938; Mann 1945) and Sen's slope (Sen 1968) or the linear regression method (Oliveira et al. 2014; Zhang et al. 2016a). However, they pose great uncertainty because of the data length and homogeneity (Dorigo et al. 2021). To overcome the above drawbacks of the traditional methods, a new method called innovative trend analysis (ITA), which is a numerical and graphical method, has been widely used in literature (Şen 2017). Also, the extended version of innovative trend analysis (IPTA) for trend transitions has found many applications (Deb Barma and Mahesha 2023; Şen et al. 2019b). Another advantage of the ITA method is the sub-trends of such variables. Such sub-trends are useful for deciding flood and drought (Chowdari et al. 2023).

1.3 RESEARCH STATEMENT

The Brahmaputra River basin is a transboundary basin that flows from China to Bhutan, India and Bangladesh. The sparseness of hydrometeorological data makes it difficult to carry out hydrological studies. However, space-borne data could come in handy given the size of the basin and when the average information is more compelling than fragmented information in the context of the water budget. Although the current state of the art on the

evaluation of satellite precipitation data is evolving with the addition of new satellites because of the development of new sensors (Kidd et al. 2021), there is not always an attempt to evaluate satellite precipitation estimates against existing gauge-based data (Ji et al. 2020). Even gauge-based precipitation data are interpolated over a large area from rainfall collected in different gauge locations. So, when the previous version of APHRODITE was used for the Brahmaputra basin, it always had the issue of the data being bias corrected using monthly data and the local timestamp instead of correcting the daily data with daily data and the local timestamp changed to UTC time zone making it suitable for analysis. Hence, to fill this gap, the existing satellite precipitation will be evaluated using the updated version of the gauge-based precipitation.

Risk assessment of different hydrometeorological studies has been an ongoing process, as seen from different works (Uttarwar et al. 2020; Yang et al. 2023), but what needs to be added is similar studies about water budget variables. So, the copula method was used to make probabilistic predictions of ET, Q and TWSC given precipitation data from various sources. If other variables besides precipitation influence these variables, then the Vine copula may be a better choice. Also, three different sources of precipitation were used to achieve the goal. Several recent studies have reported improving water budget constraints for better closure. However, it is still an ongoing process. Therefore, the present study will extend the work of Zhang et al. (2016a) to the Brahmaputra basin by using several precipitation data as the main input. Trend analysis of water budget components (Oliveira et al. 2014) may be affected by high uncertainties due to the sample size of the data and inhomogeneity (Kidd et al. 2021). In contrast, the ITA method does not have the limitations of the classical method. Therefore, ITA and IPTA will be used to determine the trend of each month individually. Also, the advantage of ITA to detect sub-trends will be used.

1.4 RESEARCH OBJECTIVES

Given the lack of precipitation evaluation for the whole basin concerning the updated precipitation, risk of water budget variables, water budget error with respect to different precipitation data and the innovative trend analysis of the variables, the present study is

aimed at evaluating the water budget components using satellite data. The research objectives are:

1. Evaluation of the satellite precipitation estimates of the Brahmaputra basin against updated gauge-based APHRODITE v2 precipitation.
2. Evaluation of the ERA5 and IMERG precipitation data for risk assessment of water cycle variables of the Brahmaputra basin using satellite data and Archimedean copulas.
3. Evaluation of satellite precipitation estimates to reconstruct major water budget components of the Brahmaputra basin.
4. Investigation of the innovative trend analysis of water budget components of the Brahmaputra basin.

1.5 ORGANISATION OF THE THESIS

The remainder of the thesis is organised in the following manner:

Chapter 2 - Literature Review

The literature review chapter provides a comprehensive overview of the existing literature on evaluating satellite precipitation, risk assessment of water budget variables, reconstruction of water budget variables, and innovative trend analysis. The chapter identifies the gaps in the literature and how this research addressed them.

Chapter 3 - Study Area and Datasets

Chapter three describes the basin in detail, including its physical characteristics, climate, and water resources. The chapter also identifies the key water budget variables of interest and discusses the availability of data for each variable.

Chapter 4 - First Objective: Evaluation of Satellite Precipitation

Chapter four focuses on the first objective of our study, which involves evaluating five different satellite datasets. The chapter also presents the results of the evaluation, including the strengths and weaknesses of each dataset. Finally, the chapter discusses the implications of the results and summarizes with conclusions.

Chapter 5 - Second Objective: Risk Assessment of Water Budget Variables

Chapter five addresses the second objective, centred on the risk assessment of key water budget variables, including ET, Q, and GRACE TWSC. This section outlines the methodologies used and presents the results, followed by a comprehensive discussion. It concludes with key conclusions of the findings.

Chapter 6 - Third Objective: Reconstruction of Water Budget Variables

This chapter describes the methods used to reconstruct ET, Q and GRACE TWSC. The chapter also presents the results of the reconstruction, including the reconstructed time series of each water budget variable. It offers a thorough analysis of the results, followed by key conclusions of the chapter.

Chapter 7 - Fourth Objective: Innovative Trend Analysis

This chapter, fourth and final objective, describes the innovative trend analysis methods used in this study. The chapter also presents the results of the trend analysis, including the trends in each water budget variable and the associated uncertainties. The chapter also compares the results of the innovative trend analysis methods with the results of the traditional Mann-Kendall test and Sen's slope estimator. It ends with the key conclusions of the results.

Chapter 8 - Summary, Conclusions, and Future Directions

The final chapter, chapter eight, provides a summary of the work, concluding remarks, and insights gained from the study. Additionally, it discusses the limitations of the research and suggests areas for future exploration and development.

CHAPTER 2

LITERATURE REVIEW

2.1 BRIEF OVERVIEW

This chapter discusses recent advances in satellite data for hydrological applications, especially in water budget variable reconstruction, probabilistic prediction, and innovative trend analysis. For a large river basin like Brahmaputra, precipitation, evapotranspiration (ET), discharge, and terrestrial water storage change (TWSC) significantly influence water budget variables. However, precipitation is the most influencing water budget variable in the Brahmaputra River basin because its contribution to the discharge is over 70% of the flow in the river.

2.2 GLOBAL SATELLITE PRECIPITATION

2.2.1 Introduction

The precipitation retrieved from gauge measurements may have certain drawbacks because of the instrumentation issues (Villarini et al. 2008). Though gauge measurement may still be better at representing precipitation, the sparseness of rain gauges will render an inaccurate representation of rainfall events. Since precipitation exhibits significant temporal and regional variability, precise data with high spatial and temporal precision are greatly desired (Duan and Bastiaanssen 2013). The availability of observed precipitation over the global land surface remains small (Kidd et al. 2017).

On the other hand, high spatial and temporal resolution precipitation variability detection using satellite remote sensing data is a newer way of understanding precipitation distribution (Duan et al. 2016). The satellite precipitation comes from both infra-red, either microwave measurements or the merging of both sensors (Prakash 2019). However, such precipitation data are evaluated against gauge measurements (Kidd and Huffman 2011).

Access to gauge precipitation in the Brahmaputra basin is difficult with complex terrain. Therefore, with even improvement in gauge precipitation, it becomes customary to assess the satellite precipitation against updated gauge-based data like APHRODITE v2 (Deb Barma et al. 2022; Yatagai et al. 2012).

2.2.2 Assessment of satellite precipitation

The satellite precipitation estimates are assessed against gauge data using categorical and continuous metrics (Duan et al. 2016). Prakash (2019) conducted an assessment of four monthly precipitation datasets for the whole of India from 1998 to 2015. This research evaluated the effectiveness of four recent versions of multi-satellite precipitation products in India. The four products under consideration are (i) Climate Hazards group Infrared Precipitation with Stations (CHIRPS), which combines infrared precipitation data with station data, (ii) Multi-Source Weighted-Ensemble Precipitation (MSWEP), a precipitation ensemble that incorporates multiple sources, (iii) soil moisture to rain climate change initiative (SM2RAIN-CCI), which utilizes the SM2RAIN algorithm in the Climate Change Initiative; and (iv) Tropical Rainfall Measuring Mission Multi-satellite Precipitation Analysis (TRMM MPA or TMPA). The evaluation was conducted by comparing these products with gauge-based observations over a monthly period from 1998 to 2015. The study found that CHIRPS and TMPA performed similarly to gauge-based precipitation estimates in India. SM2RAIN-CCI consistently underestimated precipitation and needed bias correction. CHIRPS can be confidently used for long-term precipitation analyses.

Gupta et al. (2019) investigated the ability of three satellite-based precipitation datasets to capture extreme precipitation events in India. The datasets are the Climate Hazards Group InfraRed Precipitation with Station data (CHIRPS), Satellite Soil Moisture to Rain (SM2RAIN-ASCAT), and Tropical Rainfall Measuring Mission (TRMM). The study found that all three datasets could capture extreme precipitation events, but their accuracy needed more consistency. TRMM was the most accurate dataset, followed by CHIRPS and SM2RAIN-ASCAT. The study also found that the accuracy of the datasets varied depending on the location in India. The results of this study are important for understanding

the accuracy of satellite-based precipitation datasets and for developing better methods for predicting extreme precipitation events.

Another study (Liu et al. 2020) evaluates the performance of three satellite precipitation products (GPM IMERG, CHIRPS, and GSMaP) over Bali Island, Indonesia. The study uses a variety of metrics to assess the performance of the products, including bias, root mean square error (RMSE), and Nash-Sutcliffe efficiency (NSE). The study results show that IMERG outperforms the other two products on all metrics and has the lowest bias, RMSE, and highest NSE values. CHIRPS has the second-best performance, followed by GSMaP. The study also finds that IMERG is more accurate at detecting rainfall events at different altitudes. However, IMERG tends to overestimate rainfall events at high altitudes. Overall, the study finds that IMERG is the most accurate satellite precipitation product for Bali Island. The study recommends that IMERG be used for applications that require high accuracy, such as hydrological modeling and drought monitoring.

Cavalcante et al. (2020) evaluated the performance of the CHIRPS satellite precipitation product in estimating extreme rainfall indices over the Brazilian Amazon. The study uses a variety of metrics to assess the product's performance, including bias, root mean square error (RMSE), and Nash-Sutcliffe efficiency (NSE). The results show that CHIRPS had an excellent performance in estimating extreme rainfall indices over the Brazilian Amazon. However, CHIRPS tends to underestimate the values of extreme rainfall indices for the rainiest months. The study also finds that CHIRPS performs better in estimating extreme rainfall indices in the eastern Amazon than in the western Amazon. Overall, it is evident that CHIRPS is a reliable satellite precipitation product for estimating extreme rainfall indices over the Brazilian Amazon. However, users should be aware of the underestimation of extreme rainfall indices for the rainiest months and the better performance of CHIRPS in the eastern Amazon.

The study by Zhang et al. (2020) evaluated two types of satellite precipitation products over mainland China from 2012 to 2017. The top-down product used in the study is the Integrated Multi-satellite Retrievals for Global Precipitation Measurement (IMERG).

IMERG is a product of the National Oceanic and Atmospheric Administration (NOAA). The bottom-up product used in the study is the SM2RAIN-ASCAT product. SM2RAIN-ASCAT is a product of the European Space Agency (ESA).

They found that IMERG was better at capturing large-scale precipitation patterns, while SM2RAIN-ASCAT was better at capturing small-scale precipitation patterns. The study also found that the accuracy of both products can vary depending on the season and the location. The study then integrated the two products to create a more comprehensive and accurate precipitation product. The integrated product was more accurate than either of the individual products. The results of this study are important for improving the accuracy of satellite precipitation products and for developing better methods for monitoring and predicting precipitation over mainland China.

2.2.3 Assessment of satellite precipitation in the Brahmaputra Basin

Ji et al. (2020) investigated the ability of four different bias correction methods to improve the accuracy of APHRODITE data in a large Himalayan basin (530,000 km²). The methods are Local scaling (LS): This method adjusts the APHRODITE data by multiplying it by a spatially varying factor. Locally Optimized Canonical Correlation Analysis (LOCI): This method adjusts the APHRODITE data by finding a linear combination of the observed and simulated data that minimizes the error. Cumulative distribution function (CDF): This method adjusts the APHRODITE data by transforming it to match the cumulative distribution function of the observed data. LS-CDF: This method combines the LS and CDF methods. The study found that all four methods could improve the accuracy of the APHRODITE data, but that the LS-CDF method was the most effective. The LS-CDF method was able to improve the Nash-Sutcliffe efficiency (NSE) of the hydrological simulations by an average of 0.15. The results of this study are important for improving the accuracy of hydrological simulations in large Himalayan basins. The LS-CDF method is promising for correcting the bias in APHRODITE data and improving the accuracy of hydrological simulations.

Luo et al. (2020) investigated the ability of bias correction to improve the analysis of extreme precipitation in the Yarlung Tsangpo–Brahmaputra River basin. This study aimed to make APHRODITE precipitation estimates more accurate in the YBRB. It used different correction methods and evaluated their impact on extreme precipitation indices. Bias correction significantly improved extreme precipitation analysis. The effectiveness of correction methods in adjusting wet-day frequency and coefficient of variation varied, resulting in differences in extreme precipitation indices. Notably, Local intensity scaling (LOCI) and quantile–quantile mapping (QM) outperformed linear scaling (LS) and power transformation (PT). The study provides guidance for using gridded precipitation data in extreme precipitation analysis and selecting appropriate bias-correction methods in data-sparse regions.

Zhu et al. (2020) studied the spatial distribution and temporal trends of daily precipitation concentration in the Yarlung Tsangpo River basin. The basin is located in the eastern Himalayas and is a major water source for China and India. The study used a dataset of daily precipitation observations from 1970 to 2017. The study found that the spatial distribution of daily precipitation concentration is uneven, with the highest concentrations in the western and central parts of the basin. The study also found that the temporal trends of daily precipitation concentration are variable, with some areas showing increasing trends and other areas showing decreasing trends. The results of this study are important for understanding the water resources of the Yarlung Tsangpo River Basin. The study findings can be used to improve the management of water resources in the basin and to mitigate climate change impacts.

2.3 DEPENDENCE MODELLING OF HYDROMETEOROLOGICAL VARIABLES

2.3.1 Introduction

The relationship between precipitation and hydrologic variables is critical in understanding the occurrence of such variables in a hydrologic system. In order to attain water security and improved flexibility to hydrologic extrema, a pragmatic discernment of water resource

evolution at the basin level is necessary (Sheffield et al. 2018). This is evident when dealing with the water budget of large river basins. Pearson's correlation coefficient has been widely used in hydrology to relate one variable with another. Still, this statistical metric follows the assumption that the data follow a normal distribution and are linear.

Moreover, the correlation coefficient is very sensitive to outliers (Legates and McCabe 1999). However, hydrometeorological variables are often non-linear, and rank-based correlation coefficients like Spearman's rho and Kendal's tau are preferred (Li et al. 2015a; Uttarwar et al. 2020). Accordingly, the prediction of a hydrological variable is carried out using various methods, namely, ordinary least square (OLS) (Hasan and Tarhule 2020), multiple linear regression (MLR) (Jato-Espino et al. 2017; Ndehedehe et al. 2016; Sinha et al. 2019), partial least squares regression (PLSR) (Abudu et al. 2010; Hu et al. 2021; Yuan et al. 2019; Zhou et al. 2020), principal component analysis/regression (PCA/PCR) (Abudu et al. 2010; Almanaseer and Sankarasubramanian 2012) and geographically weighted regression (GWR) (Li et al. 2020; Li and Quiring 2021), empirical method- Budyko framework (Li and Quiring 2021), machine learning algorithms (Han et al. 2021; Seyoum and Kwon 2020; Sinha et al. 2019; Sun et al. 2014), conceptual hydrological model (Poncelet et al. 2017) and semi-distributed/ distributed models (Sahana and Timbadiya 2020; Sridhar et al. 2019).

For example, Hasan and Tarhule (2020) investigated the long-term terrestrial water storage anomaly from GRACE data as affected by precipitation, runoff, surface water storage, soil moisture storage and population density using geographically multiple regression (GMR), ordinary least square (OLS) and geographically weighted regression (GWR). It is reported that GWR is important for accounting for the spatial locations to characterize the variability of GRACE TSWA long-term trends in space. In the assessment of watershed characteristics on long-term water balances, machine learning algorithms like neural network (ANN) and relevance vector machine (RVM) were found to perform better than MLR in determining the watershed parameter (Sinha et al. 2019). PLSR and global hydrological models were used to predict terrestrial water storage (TWS) over central Asia

using multiple satellite data (Hu et al. 2021). PLSR was found to be useful for the simulation of the hydroclimatic variables and prediction of TWS.

Poncelet et al. (2017) used a large sample hydrological approach and a conceptual lumped hydrological model to estimate runoff variations over different landscapes in Austria, France and Germany. The consistency of four precipitation products and GRACE TWS over the Arabian Peninsula was assessed using a multivariate statistical approach and Pearson's correlation coefficient (Wehbe et al. 2018). In another study, satellite-based precipitations TRMM and CHIRPS were assessed against gauge-based precipitation to evaluate their performance in reproducing streamflow and hydrological signatures of a humid tropical catchment in India (Sharannya et al. 2020). However, limited studies have focused on the probabilistic dependence of precipitation and other water cycle variables using copula.

2.3.2 Application of copula in the probabilistic prediction of hydrometeorological variables

The dependence structure between the water cycle variables needs to be achieved using copulas to obtain the probabilistic prediction. Copulas are multivariate techniques that derive the dependence structure between two or more continuous/discrete variables (Genest and Favre 2007; Nelsen 2006). Copulas have been extensively applied in various fields. For example, in the area of hydrologic sciences, copulas find applications in the dependence of hydroclimatic variables (Uttarwar et al. 2020), drought characterization (Sajeev et al. 2021), flood frequency analysis (Muthuvel and Mahesha 2021), compound climate extreme events (Hao et al. 2018; Tavakol et al. 2020; Zscheischler and Seneviratne 2017), variance-based sensitivity analysis (Sheikholeslami et al. 2021), among others.

Liu et al. (2018) carried out the joint dependence of river water temperature, air temperature, and discharge in the Yangtze River. The study found that the joint dependence of these variables is complex and varies over time. The study also found that the Three Gorges Dam has significantly impacted the joint dependence of these variables. The study used a dataset of daily observations of river water temperature, air temperature, and

discharge from 1975 to 2014. The joint dependence of these variables is strongest in the summer and weakest in the winter. The joint dependence of these variables is more pronounced in the upstream reaches of the river than in the downstream reaches. The Three Gorges Dam has significantly impacted the joint dependence of river water temperature, air temperature, and discharge. The dam has reduced the variability of river water temperature and discharge. The dam has also changed the timing of peak river water temperature and discharge. The results of this study are important for understanding the impacts of the Three Gorges Dam on the Yangtze River. The study findings can be used to improve the Yangtze River management and mitigate the impacts of climate change.

Liu and Menzel (2018) conducted the probabilistic dependence between streamflow and hydroclimatic variables in Baden-Württemberg, Southwest Germany. The study found that streamflow is positively correlated with precipitation and soil moisture, and negatively correlated with temperature. The study also found that large-scale atmospheric circulation patterns can significantly impact streamflow. The study used a dataset of daily observations of streamflow, precipitation, temperature, and soil moisture from 1961 to 2016. The probabilistic dependence between streamflow and hydroclimatic variables is strongest in the summer and weakest in the winter. The probabilistic dependence between streamflow and hydroclimatic variables is more pronounced in the upstream reaches of the river than in the downstream reaches. It was found that large-scale atmospheric circulation patterns can have a significant impact on streamflow. The study also found that the westerlies play an important role in favoring warm and moist airstreams from the Atlantic Ocean towards the study area. The results of this study are important for understanding the streamflow regime in Baden-Württemberg, Southwest Germany. The study findings can be used to improve water resources management in the region and mitigate climate change impacts.

In another study (Qian et al. 2020), the use of coupled copulas to model the relationship between two precipitation variables was investigated. The study found that coupled copulas can be used to model the dependence pattern between two precipitation variables, and that they can be used to improve the accuracy of hydrological simulations. The study used a dataset of daily precipitation observations from two stations in the Jinghe River basin. The

study found that the coupled copula could accurately model the dependence pattern between the two precipitation variables. The study also found that the coupled copula improved the accuracy of hydrological simulations.

Qian et al. (2021) examined the variability in the relationship between runoff and sediment discharge in the Xiliugou River basin in China. The study found that the dependence structure between runoff and sediment discharge exhibits temporal variations, with a significant shift in 2000. The strength of the dependence structure was also found to be stronger in the upstream reaches of the river. The study attributes the observed variation in the dependence structure to climate and land use changes, such as increased precipitation and deforestation in the upstream region. The findings of this study can be used to improve water resource management practices and mitigate the adverse effects of climate change.

Seo et al. (2022) used a copula to identify the risk of river water temperature stress under meteorological drought conditions. The study found that the model could accurately predict the risk of river water temperature stress for various meteorological drought conditions. The model identified the areas of the Yangtze River basin most vulnerable to river water temperature stress under meteorological drought conditions. The areas of the basin that are most vulnerable to river water temperature stress are the areas that are located in the upstream reaches of the basin.

The study by Yang et al. (2023) used a hybrid copula model to analyze the joint probability of streamflow and sediment load. The model was able to predict the joint probability under various conditions accurately. The study found that the model was able to identify areas within the Yangtze River basin that are particularly vulnerable to high streamflow and sediment load. The findings of this study are important for the advancement of water resource management strategies in the Yangtze River basin.

A conditional copula model was used to identify the response of runoff probability to climatic factors in the Poyang Lake basin in China (Han et al. 2023). The study found that the model could accurately predict the response of runoff probability to climatic factors for various climatic conditions. The study also found that the model identified the areas of the

basin most vulnerable to changes in runoff probability due to climatic factors. The areas of the basin that are most vulnerable to changes in runoff probability due to climatic factors are the areas that are located in the upstream reaches of the basin. The results of this study are important for improving the management of water resources in the Poyang Lake basin.

2.4 RECONSTRUCTION OF WATER BUDGET VARIABLES

2.4.1 Introduction

Water budget may be defined as the amount of water entering a land, stored within and leaving the land system for a given time interval (Mitchell et al., 2003 ; Lorenz et al., 2014; Wang et al., 2014). A river basin water budget can be expressed as the balance between major hydrological cycle components, namely, precipitation, actual evapotranspiration, runoff and terrestrial water storage change (Gao et al., 2010). Hence, the water budget follows the conservation of mass principle.

2.4.2 Application of satellite data in the reconstruction of water budget variables

One of the earliest works on the GEWEX Continental-Scale International Project (GCIP) for Arkansas and Red River basins by Abdulla et al. (1996) applied a macro-scale two-layer variable infiltration capacity (VIC) model forced by gridded station precipitation and potential evapotranspiration. The study found an underestimation of seasonal peak streamflow in late spring, an overestimation during late summer, and a minimum in early fall. Partly averaged evapotranspiration over the whole basins derived from the model was compared to the one obtained from atmospheric moisture budget of the basins. There was a close agreement from late winter to midsummer for both the estimates in mean seasonal cycles. They found that VIC model estimated less evapotranspiration in fall and greater in midwinter as compared to that of atmospheric budget. The first paper by Ropelewski and Yarosh (1998) in the series of papers that investigate the mean annual atmospheric and terrestrial water budgets over the central United States for a period of 20 years (1973-1992) led to the development of a baseline or reference climatology for applying both in observational and experimental studies as a part of GCIP. Insufficient spatial and temporal sampling by radiosonde network might have led to discrepancy between the budgets. In

another GEWEX study, Strong et al.(2002) attempted to close the atmospheric moisture budget of Mackenzie river basin using WATFLOOD model and gridded data and vindicate it against the surface water budget at annual and monthly temporal scales. Near-closure of the basin budget could be attained at monthly scales for 1994/95 to 1996/97 water years. The Large Scale Biosphere Atmosphere (LBA) Experiment in the Amazon basin as a part of GEWEX by Marengo (2005) focused on the spatial and temporal variability of water budget and its closure. The average imbalance or non-closure of the water budget for the basin was estimated at 51 % as compared to earlier studies by Zeng (1999) and Roads et al. (2002) for the same basin. The key contribution of this work has been the exemplification of chief differences in the behaviour of water budget between the southern and northern parts of the basin.

Comparisons of terrestrial water storage (TWS) obtained from combined atmospheric and surface water balance approach to that of simulated ECMWF 40 year Re-Analysis (ERA-40) indicate that there is substantial underestimation of seasonal cycle amplitude for 37 midlatitude basins (Hirschi et al. 2006). However, ERA-40 was found to have agreement with in situ data as compared to two other precipitation products while being forced to variable infiltration capacity model (VIC) at global level (Voisin et al., 2008). This might be due to mismatch in the length and spatial scale of datasets since GRACE data was only available from 2002 in the first case. Lorenz and Kunstmann (2012) reported similar finding in which ERA-40 reanalysis performed better than its other counterparts in atmospheric and terrestrial water budget closure, whereas in La Plata basin, South America ERA-40 did not balance either atmospheric or terrestrial water budget (Su and Lettenmaier, 2009). Evapotranspiration obtained as the difference between precipitation and runoff (neglecting storage term for long term) in ERA-40 seasonally is close to the value obtained from observations than that obtained annually in Amazon basin (Fernandes et al. 2008).

Music and Caya (2007, 2009) examined sensitivity of the water budget in the Canadian Regional Climate Model (CRCM) to a more accurate representation of the land surface processes including radiation, cloud cover, and atmospheric boundary layer mixing for Mississippi river for the first study and in addition St. Lawrence, and the Mackenzie River

basins for the second study. Removal of the water budget closure error could be achieved by introducing a little modification to the specific humidity values at each grid point that takes into account the impreciseness related to the semi Lagrangian numerical scheme.

Pan and Wood (2006) developed constrained ensemble Kalman filter (CEnKF) to overcome the shortcoming of ensemble Kalman filter (EnCF) in order to maintain water budget closure. This new data assimilation technique in conjunction with VIC model was applied in southern Great Plains region of the United States (75, 000 km²). The filtering technique has two steps: in the first step in-situ measurements of water budget assimilation into VIC model was carried out and second step involved optimal distribution of imbalance term among water budget terms according to correlation and variances between the terms by constrained assimilation. They reported that CEnKF was able to reduce imbalance/non-closure of water budget. Pan et al. (2008) extended the work by incorporating more techniques for Arkansas-Red river basins. In a similar study Sahoo et al. (2011) applied CEnKF technique, but in a non-ensemble manner (Simon and Chia, 2002) to close the water budget over ten large river basins across the globe including energy limited basin (wet system) like Amazon basin and water limited basins like the Niger and Murray-Darling building on previous studies (Gao et al., 2010; Sheffield et al., 2009). They merged individual biased estimates to budget closure-constrained best estimate. Their findings indicate that the influence of bias correction is related to the skill and accuracy of the non-satellite target variable merged estimate over a given river basin. However, Another follow-up study by Pan et al. (2012) attempted to merge global datasets including in situ observations, remote sensing retrievals, land surface model simulations and global re-analyses in order to create long-term global data record for the terrestrial water budget based on each individual dataset error. Runoff or storage change was not merged as they had only one dataset each.

Gao et al.(2010) and Sheffield et al.(2009) attempted to close water budget without applying any constraining technique. Hence, the errors were estimated to be more in both cases and perhaps Sheffield et al. (2009) paper was the first to present the estimates of large terrestrial water budget purely based on remote sensing retrievals. However, in situ

discharge was used to compare with the residual discharge obtained from water balance equation. In the ensuing years that followed, many researchers have also attempted to close water budget in different parts of the world using similar techniques. For example, in Rufiji river basin, Tanzania, Armanios and Fisher (2014) explored the feasibility of entirely satellite remote sensing data for water budget closure. They used Global land Data Assimilation System (GLDAS) product to validate Gravity Recovery and Climate Experiment (GRACE) data. In Australia Wang et al. (2014) examined water balance over the continent with limited annual streamflow using three commonly used satellite based water cycle components: precipitation (P) from the Tropical Rainfall Measuring Mission (TRMM), evapotranspiration (ET) from the Moderate Resolution Imaging Spectroradiometer (MODIS), and terrestrial water storage change (DS) from the Gravity Recovery and Climate Experiment (GRACE). Their results show more recurrent and improved closure and uniformity in the water balance from above three components over central part of Western Australia having low rainfall, greater elevation and low relief. The data sets were found to be more articulate at seasonal and annual scales than monthly ones. In Yangtze river basin (Chang Jiang), China Corbari et al. (2014) estimated actual evapotranspiration from water budget closure. In the same basin, total discharge was obtained from water balance equation (Ferreira et al., 2013); evaluation of global satellite precipitation products for multiscale hydrologic applications including annual water budgeting (Li et al., 2012 ;Li et al., 2015); assessment of the suitability of popular satellite products (Zhang et al., 2016); in tropical Amazon river basin the water budget components and their spatial and temporal variability were diagnosed using monthly mean satellite retrieval data from September 2002 to December 2006 (Azarderakhsh et al. 2011), but closure was not possible. The merged datasets outperform the individual datasets of water budget components in a study in northern China (Yao et al. 2014).

Another noteworthy study (Aires, 2014; Munier et al., 2014) discussed the applicability of water budget closure for Mississippi river basin by employing closure correction model (CCM), which permits to independently correct each observation data set. It was also used to reconstruct missing values in any water budget component. CCM permits to achieve

standardization for each component and decrease water budget imbalance/ residual to a great extent. This method is simple and does not use any data assimilation technique and model to close the water budget. This has advantages over data assimilation technique and land surface model being computationally demanding.

What sets apart the study conducted by Zhang et al.(2016) from others is that they provide the first comparison between water budget closure using purely satellite products and a complete blend of remote sensing, land surface model outputs (LSM) and reanalysis products on a pseudo-global level. They found that gradual removal of non-satellite data products would degrade closure errors in the budget estimates. The worst error was seen when satellite retrievals P, ET and terrestrial water storage change (TWSC) and runoff (R) from LSM were used. This study, however, still used data assimilation algorithm, which assumes normal distribution.

An interesting aspect of terrestrial water budget is the trend analysis of each water budget component carried out by Oliveira et al.(2014) for the Brazilian Cerrado using entirely remote sensing data (2003-2010) along with long-term discharge data. Uncertainties and water budget closure were determined for the three largest river basins in the Cerrado. Temporal trends in the water balance components and measured river discharge were analyzed using Mann-Kendall test. Their findings indicate that (i) mean annual evapotranspiration over the entire Cerrado of 51 ± 15 mm/year with significant rise (ii) in the north eastern region of the Brazilian Cerrado the terrestrial water storage rising of 11 ± 6 mm/year (iii) reduction of 72 ± 11 mm/year runoff in isolated spots and in the western part. Similarly, Zhang et al.(2016) presented a study on Yangtze river basin and concluded that satellite products are more suitable for studying annual temporal trends than monthly.

Some of the most recent water budget studies conducted on large scales that find worth mentioning are the works of Lv et al.(2017), Troy et al.(2011), Wang et al. (2014), Wang et al.(2014) and Wang et al.(2015). Previous studies on Yangtze river basin (Corbari et al., 2014; Ferreira et al., 2013; Zhang et al., 2016) have not considered human interventions in the basin unlike the study of Lv et al.(2017). To the best of our knowledge, this is one of

its kind where water diversion in the basin was considered in water balance analysis using global data products. Evapotranspiration (ET) was reconstructed using the GLDAS-1 land surface models, the high-quality observation-based precipitation, naturalized streamflow and the irrigation water. After the ET reconstruction, the average absolute non-closure value decreased from 3.31 cm/year to 1.69 cm/year and from 15.40 cm/year to 1.96 cm/year over the Yellow and Yangtze River Basins, respectively. Due to the data limitation of naturalized streamflow, irrigation water and water diversion, the annual temporal scale is the smallest time scale used for the analysis in this study.

Troy et al. (2011) use datasets from various sources to determine the terrestrial water budget and its uncertainties over the period 1950–2006 in northern Eurasia to develop a water budget closure-based method to combine these independent bases of information and observed streamflow to make better estimates of the terrestrial water cycle. For long-term annual temporal scale, the storage term may be neglected, and streamflow data was found to have the least error among the four water budget terms. The method was found robust in that the weightings for each variable were assigned such that the values were bracketed within the minimum and maximum values of the corresponding variable, say precipitation, for example.

In continental size Canada, though at the watershed level, Wang et al. (2014) presented a first attempt at surface water budget closure for the whole country. They investigated the long-term water budget closures for 370 watersheds by using 30 years (1981–2010) data products recently produced for precipitation (P) gridded using climate station measurements, land surface evapotranspiration (ET), and water surface evaporation (E_0) obtained by the Ecological Assimilation of Land and Climate Observations (EALCO) model and observed streamflow (Q). For a time-independent state watershed at long-term scales and when the study phase starts and ends at the same time of the year, the change in storage (ΔTWS) is small in the yearly hydrological cycles of the watershed. It may be neglected as compared to the total amounts of P, ET, and Q in that phase. Another study by Wang et al.(2014) made the first attempt to investigate the spatial and seasonal variations of the terrestrial water budget by using state-of-the-art datasets for sixteen large Canadian

river basins with a total area of 3.2 million km². The accrued water budget non-closure over the seven years of 2002–2008 ranged between close to zero to ± 10 mm/month. The positive and negative non-closure among the sixteen basins was nullified mainly, and the all-basin non-closure was close to 0. Similarly, Wang et al. (2015) assessed long-term (1979–2008) water budget closures for 19 large cold region basins in Canada.

Lehmann et al. (2022) investigated the global water budget using precipitation, evapotranspiration, and runoff data at the catchment scale. They found that TWS changes derived from the water balance equation were more accurate than the long-term and monthly mean of the GRACE time series in the corresponding basins. They also found that the nature of the catchment dynamics and balance between components affects the optimum combination of datasets. Ultimately, they concluded that their results provide a road map for studying the water budget at the catchment scale. To elaborate on the first finding, the researchers used 189 river basins covering more than 90% of the continental land area. They compared TWS changes derived from the water balance equation to GRACE data using two metrics: the Nash–Sutcliffe efficiency (NSE) and the cyclostationary NSE. They found a positive NSE and cyclostationary NSE in 99% and 62% of the basins examined. To elaborate on the second finding, the researchers identified that some good results were obtained due to the cancellation of errors in poor estimates of water budget components. They used variation coefficients to determine a data product's relative quality. They found that water budget components from ERA5-Land and the Catchment Land Surface Model (CLSM) performed better than other products for most climatic zones. To elaborate on the third finding, the researchers found that the latest version of CLSM, v2.2, performed poorly for evapotranspiration in snow-dominated catchments. The researchers' findings provide valuable insights into the global water budget and the optimum combination of datasets for studying it at a catchment scale.

2.5 INNOVATIVE TREND ANALYSIS (ITA) OF HYDROMETEOROLOGICAL VARIABLES

2.5.1 Introduction

The need for freshwater continues to rise as various sectors encounter many requirements daily. Precipitation is the primary component of the hydrologic cycle. The Mann-Kendall test is a nonparametric test that can identify monotonic trends in time series data (Kendall 1938; Mann 1945). It is based on comparing the ranks of the data values over time. It is also one of the most widely used methods for trend analysis (Chowdari et al. 2023; Singh et al. 2021b; a). However, the recently developed innovative trend analysis (ITA) has been widely used to analyse hydrometeorological variables (Şen 2012, 2017). The present study will address the shortcomings of the MK test using the ITA method.

2.5.2 Application of ITA trend analysis of hydrometeorological variables

Praveen et al. (2020) used non-parametric and machine-learning approaches to analyse the trend and forecast rainfall changes in India. They use non-parametric methods to identify monotonic trends in the rainfall data, and they use machine learning methods to forecast future rainfall. They find that there is a significant decreasing trend in rainfall in India. They also find that the decreasing trend is more pronounced in the southern and western parts of India. They forecast that the decreasing trend in rainfall will continue in the future. Their findings have important implications for water management in India. The decreasing trend in rainfall will decrease the amount of water available for irrigation, drinking, and other uses. This will require India to develop new water management strategies to ensure enough water to meet the needs of its growing population.

Similarly, the study by Singh et al. (2021a) uses an innovative trend analysis method to investigate the spatiotemporal rainfall variations in India during 1901-2019. The study finds significant trends in rainfall in India, with increasing trends in the monsoon season and decreasing trends in the winter season. The study also finds that the trends in precipitation are different across India, with some regions experiencing more significant trends than others. The study's findings have important implications for water management in India. The increasing trends in monsoon rainfall will increase the amount of water

available for irrigation, drinking, and other uses. However, the decreasing trends in winter rainfall will lead to reduced water availability for these uses. The study's findings suggest that climate change is having a significant impact on rainfall patterns in India. This is important because India is an extensive and populous country heavily dependent on rainfall for its water supply. The study's findings suggest that India will need to adapt to the impacts of climate change on its rainfall patterns.

Caloiero (2020) used ITA to evaluate rainfall trends in the South Island of New Zealand. They found that rainfall is increasing, especially in the western and central parts of the island. The trend is more pronounced in the summer months. The findings have implications for water management, as the increasing trend in rainfall will lead to an increase in the amount of water available. However, the trend is not uniform across the island, and some regions may experience more significant trends than others. This will require water managers to develop new strategies to ensure enough water to meet the needs of the growing population. The change in trend is likely due to climate change, which is causing the Earth's atmosphere to warm and leading to changes in rainfall patterns. The findings suggest that climate change significantly impacts rainfall patterns in the South Island and that the region will need to adapt to the impacts of climate change on its rainfall patterns.

The ITA method was used to analyse annual and seasonal rainfall data from 14 stations in the Yangtze River Delta (Wang et al. 2020). The results showed significant increasing trends in annual rainfall at all stations and in summer and winter rainfall. There were decreasing trends in spring and autumn rainfall. Contrasting trends were found for extreme rainfall, with strong increasing trends in high rainfall in summer and winter and falling trends in low rain in spring and autumn. These additional details provide more information about the trends in rainfall in the Yangtze River Delta. They suggest significant annual and seasonal rainfall trends, likely impacting the region's water resources significantly. In particular, the increasing trends in annual and seasonal rainfall in summer and winter will likely lead to an increase in the risk of flooding in these seasons. The decreasing trends in spring and autumn rainfall will likely increase the drought risk in these seasons. These

changes in rainfall patterns will likely significantly impact the region's agriculture, ecosystems, and water resources.

Chowdari et al. (2023) conducted a similar study to extend it to the semi-arid region of Karnataka, India. The ITA method was used to analyze seasonal and annual rainfall data from 11 districts in semi-arid Karnataka. The results showed significant increasing trends in annual rainfall in most districts and in summer and monsoon rainfall. There were decreasing trends in winter rainfall. The ITA test was able to detect trends that traditional methods were unable to detect. The results of this study suggest significant trends in seasonal and annual rainfall in semi-arid Karnataka and that these trends are likely to impact the region's water resources significantly.

For trend transition between months/ weeks/ days/ seasons, Şen et al. (2019) extended the ITA method. After that, many studies on applying the ITA method have been conducted. For example, Şan et al. (2021) compared three different ways: IPTA, ITA with the Significance Test, and Mann-Kendall (MK), in analyzing the monthly total rainfall trends of 15 stations in the Vu Gia-Thu Bon River Basin (VGTBRB) in Vietnam. The data spans from 1979 to 2016. The findings reveal that rainfall generally increases in March and decreases in June across most stations. IPTA and ITA with the Significance Test are more sensitive in detecting trends than the MK method. Approximately 90% of all months showed trends when using IPTA and ITA with the Significance Test, while the MK test detected trends in only 23%. Additionally, although the average rainfall patterns over the 1-year hydrometeorological cycle appear consistent at most stations, the standard deviations show irregular variations. October emerges as the most critical month for trend transitions between consecutive months in all stations, with an average negative trend slope of -1.35 and a range of -3.98 to -0.21, indicating a decreasing trend.

Several studies are similar to the above research on the IPTA method reported elsewhere (Ahmed et al. 2022; Akçay et al. 2021; Ceribasi and Ceyhunlu 2021; Şan et al. 2021b; Sezen 2022).

2.6 RESEARCH GAP

Though several studies have been conducted on evaluating satellite data in different parts of the world, applying several satellite data against the new version APHRODITE v2 still needs to be undertaken, even though the gauge-based data itself has been tested against point measurements. In this research, the first objective will address the gap of evaluating various satellite-based precipitation against the newly updated APHRODITE v2 for the Brahmaputra basin.

The above literature shows that the dependence measure between precipitation and the other three water budget variables (evapotranspiration, runoff and terrestrial water storage change) were not conducted holistically, that is the measurement of risk (probability) of the three variables given the precipitation (satellite, reanalysis and gauge) amount is not reported in literature. Hence, the culmination of our work (Deb Barma et al. 2022) to address the second objective.

The water budget closure has been performed for several basins for over a decade, either using a process-based or empirical model or using only data. However, the reconstruction of water budget variables like evapotranspiration, runoff and terrestrial water storage change using various satellite precipitation data have not been addressed much using the empirical water budget equation in literature. To this end, several precipitation data were used to reconstruct the remaining variables by extending the work of Oliveira et al. (2014) and Zhang et al. (2016a) to the Brahmaputra basin to achieve the third objective of this study.

There is hardly any study on the trend analysis of water budget variables reported in the literature using the innovative trend analysis (ITA) method (Şen 2017) and IPTA method (Deb Barma and Mahesha 2023; Şen et al. 2019b). To fill this research gap, in the fourth objective the trend analysis of several precipitation products (gauge, satellite and reanalysis), evapotranspiration data (satellite and reanalysis), runoff (observed) and terrestrial water storage change (GRACE TWSC) of Brahmaputra basin was conducted for each individual month using the classical MK-test and modified MK-test, innovative trend

analysis (ITA) and innovative polygon trend analysis (IPTA). Also, sub-trend analysis was the first attempt for water budget variables.

STUDY AREA AND DATASETS

3.1 STUDY AREA

The Brahmaputra basin lies between 25° – 32° North latitude and 82° – 98° East longitude. The basin, with an average discharge of about $20,000 \text{ m}^3\text{s}^{-1}$, is the fourth largest river in terms of the quantity of runoff in the world (Jian et al. 2009). The total drainage basin area is about $517,224 \text{ km}^2$ at Bahadurabad gauging station. Bhutan and Bangladesh share about 8% each, about 34% in India, and about 50% in China (Immerzeel 2008) (Fig.3.1). The Brahmaputra's source originates from the Chemayungdung Glacier and throughout the upper part of Tibet, it is known by Tsangpo (purifier in Tibet) and in Chinese "Yarlung Zangbo" (Ahmad and Lodrick 2017). In contrast, the lower part of the river in India and Bangladesh is known as the Brahmaputra ("son of Brahma"). From the origin, it flows for about 1150 km eastwards (Fig.3.2(b)). Then it enters the northern-most point of Arunachal Pradesh (India), turns southwards, and courses for nearly 500 km (Fig.3.2(c)); it directs towards west-flowing through the states of Arunachal Pradesh, Assam, and Meghalaya for next about 700 km before it finally moves into Bangladesh (Futter et al. 2015) (Fig.3(d)). The Tibetan Plateau bifurcates the basin into two unique zones of climate: (1) the northern part of the basin is dominated by mountain climate and is characterized as cold and dry, and (2) the southern part is dominated by the tropical monsoon climate and is categorized as humid and warm thereby receiving a high amount of precipitation under the impact of the Indian summer monsoon (Pervez and Henebry 2015). The Brahmaputra is characterized by braided channels, whereas Ganga meandering channels (Futter et al. 2015). It is topographically and ecologically abundant in crops and natural biodiversity falling into three distinct topographic areas: (a) the Tibetan Plateau covering 44% of the area with 3500 m and above high, (b) the Himalayan section covering 29% with 100 – 3500 m and (c) the floodplains covering 27% with below 100 m elevation (Immerzeel

2008). The river is a lifeline to nearly 70 million people who depend on water resources for food production (Hasson et al. 2013).

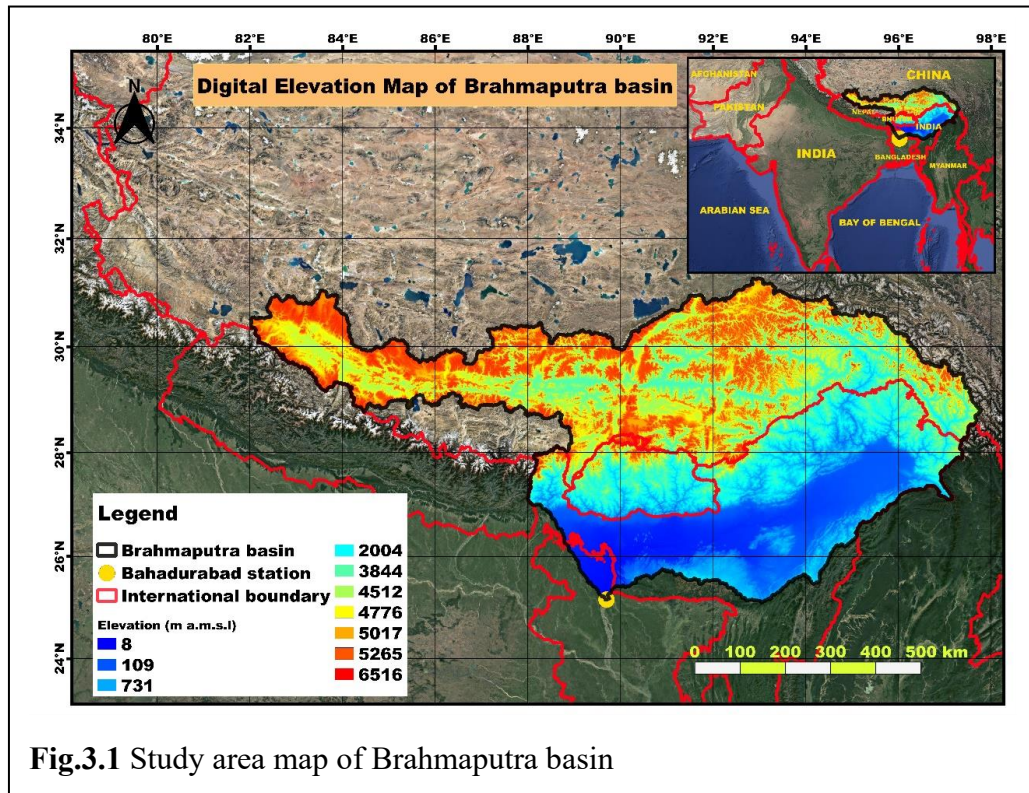


Fig.3.1 Study area map of Brahmaputra basin

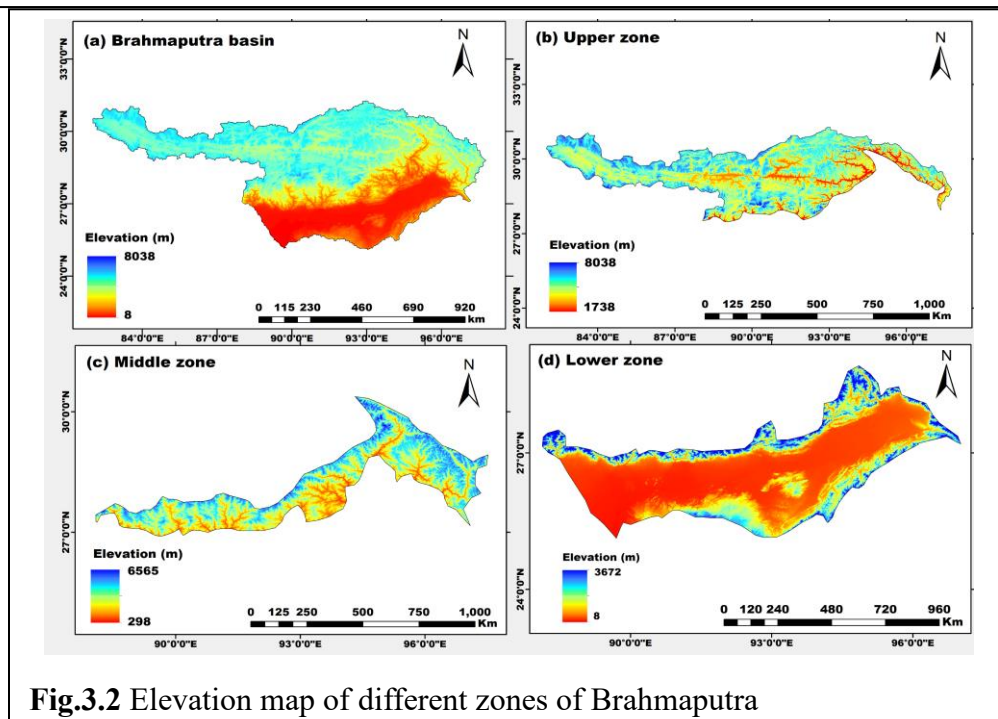


Fig.3.2 Elevation map of different zones of Brahmaputra

3.2 DATASETS

3.2.1 Precipitation data

a. APHRODITE gauge data

The Asian Precipitation Highly-Resolved Observational Data Integration Towards Evaluation of the Extreme Events (APHRODITE) V1101 is available on the daily scale for the year 1951-2007 (Yatagai et al. 2012) at 0.25/0.50 degrees spatially, but APHRODITE-2 (V1901) is available from 1998 to 2015 for the exact spatiotemporal resolution for whole of Asia. The main improvement of V1901 is the 24-hour accumulation period adjustment to the 00 - 24 UTC of the stamped date. The other improvement in APHRODITE-2 (V1801 and V1901) is the daily climatology used as a ratio of daily rainfall to the climatology to interpolate the gauge data. In contrast, monthly climatology was used for older versions. The long-term performance has been applied in various studies and performed well. However, the newer version is yet to be evaluated on a large scale though it was found to perform well with respect to gauge data (Ji et al. 2020) in the Brahmaputra basin. In V1801 and V1901, the end of the day (EOD) was matched using the satellite-based precipitation CMORPH, and the extreme values were identified using CMOPRH and TRMM-3B42. The monthly areal average precipitation for the Brahmaputra basin was derived from daily data from 2003 to 2014 for the current study from <http://aphrodite.st.hirosaki-u.ac.jp/download/>.

b. ERA5 reanalysis data

The ERA5 (Hersbach et al. 2020) is the 5th reanalysis product and replacement to ERA-Interim and all previous versions of the European Centre for Medium-Range Weather and Forecasting (ECMWF) reanalysis. In a comparative study of ERA-Interim and Global Precipitation Climatology Project (GPCP) as the base data for the 1979–2018 period, Nogueira (2020) found that ERA5 showed lower bias as well as unbiased root-mean-squared error and higher correlations over most of the tropics and limited regions of mid-latitudes. However, ERA-Interim outperformed ERA5 over the Himalayas. Overall, ERA5 has improved parameterization and resolution, leading to trade-off performances over most

regions. The monthly areal mean ERA5 precipitation (0.25-degree lat/long) data were downloaded from the Google Earth Engine platform from 2003 to 2014.

c. CMORPH

The CMORPH- Climate Data Record (CDR) satellite precipitation product was developed by the National Centers for Environmental Information (NCEI), NOAA using the Climate Prediction Center (CPC) Morphing technique (CMORPH). The precipitation data was retrieved from passive microwave (PMW) from low earth orbit (LEO) satellites, and where PMW precipitation measurement is missing, the estimates from infrared (IR) brightness temperature (TBB) data from geostationary (GEO) satellites are utilized (Joyce et al. 2004). The precipitation data comes in three spatio-temporal resolutions: 8 km x 8 km – half-hourly, 0.25° x 0.25° – 3-hourly, and daily from 1998 to 2020. Unlike other satellite precipitation estimates, CMORPH data is bias-corrected against CPC daily gauge precipitation measurements. The daily 0.25° spatial resolution precipitation was obtained from <https://www.ncei.noaa.gov/data/cmorph-high-resolution-global-precipitation-estimates/access/daily/>.

d. CHIRPS

The Climate Hazards group Infrared Precipitation with Stations (CHIRPS) dataset was jointly developed by the United States Geological Survey (USGS) and the Climate Hazard Group (CHG) of the University of California, Santa Barbara, for environmental change and drought monitoring. The TRMM v7 was used to calibrate global Cold Cloud Duration (CCD) rainfall amounts of the CHIRPS and incorporate gauge data (Funk et al. 2015). Over the land within 50°S – 50°N latitudinal extent with a spatial resolution of 0.05° x 0.05° degree and temporal resolution of daily, 5-daily, and monthly, CHIRPS v2.0 is currently available from 1981 to the present. Daily CHIRPS v2.0 also comes at 0.25° x 0.25° resolution, which was evaluated against APHRODITE for the current study. The data is available at https://data.chc.ucsb.edu/products/CHIRPS-2.0/global_daily/netcdf/p25/.

e. SM2RAIN

The soil moisture to rain (SM2RAIN) of the European Space Agency (ESA) climate change initiative (CCI) precipitation product (SM2RAIN-CCI) was derived by the application of the SM2RAIN algorithm (Brocca et al. 2014) to ESA CCI soil moisture Active and Passive products. The soil moisture-derived precipitation is available at 0.25° spatial resolution on a daily cumulative from 00 UTC to 23:59 UTC time from 1998 to 2015 over the whole globe after masking out regions with highly complex topography, frozen soil, the chance of snow occurrence, and tropical forests (Ciabatta et al. 2018). A monthly precipitation climatology was used to bias correct the product, whereas a daily dataset of Global Precipitation Climatology Centre Full-Data (GPCC-FDD) was applied to calibrate the SM2RAIN-CCI dataset. Hereafter, SM2RAIN-CCI is referred to as SM2RAIN for brevity. The precipitation data were obtained from <https://zenodo.org/record/1305021#.YXOO5IVBzIU>.

f. TRMM

The Tropical Rainfall Measuring Mission 3B42 version 7 algorithm (TRMM 3B42 v7) Multi-Satellite Precipitation Analysis (TMPA) was developed by the National Aerospace and Space Administration (NASA) and the Japanese Aerospace Exploration Agency (JAXA) to detect precipitation in the tropical and subtropical regions (50°S – 50°N latitude) with quasi-global coverage (Huffman et al. 2007, 2010). It is derived from the blend of gauge and microwave-IR precipitation estimates from several independent satellites. The spatial resolution of the product is 0.25° x 0.25° with temporal resolutions of 3 hours, daily and monthly, from 1998 to 2019. The daily and monthly TRMM 3B42 v7 are upscaled from 3-hourly precipitation data. The diurnal rainfall data was obtained from https://disc.gsfc.nasa.gov/datasets?keywords=TRMM_3B42_Daily_007 to evaluate it against APHRODITE data.

g. GPM IMERG

The final run (FR) global precipitation measurement (GPM) resulted in the program known as the Integrated Multi-satellitE Retrievals for GPM (IMERG). The rainfall was derived from several satellite passive microwave (PMW) sensors encompassing the GPM collection using the Goddard Profiling Algorithm of 2017(GPROF2017) (Huffman et al. 2019). The inter-calibration of the gridded data ($0.1^{\circ} \times 0.1^{\circ}$; June 2000 onwards) to the Combined Ku Radar-Radiometer Algorithm (CORRA) of the GPM product on a 30-minute basis with adjustment to Global Precipitation Climatology Project (GPCP) insitu-satellite product was carried out to rectify identified errors over the high-latitude ocean and tropical land. Though the precipitation product comes in half-hourly, daily, and monthly scales, the latter two were derived from the former. In this study, the monthly IMERG V06 data was obtained by summing the daily precipitation from https://disc.gsfc.nasa.gov/datasets/GPM_3IMERGDF_06/summary?keywords=GPM. Li et al. (2021) conducted a comparative study of two products (ER=early run and FR) of IMERG for two decades over the whole globe. ER estimated 12% more annual rainfall than FR over the land and 33% greater extreme precipitation over the earth. Since the FR is gauge-adjusted, it is used for long-term hydrometeorological studies, whereas ER is useful for short-term real-time studies like floods.

3.2.2 Evapotranspiration data

a. MOD16 ET

Evapotranspiration forms a significant part of the water cycle that influences irrigation planning and crop water requirement. This study uses the MOD16 ET product, the GMAO (Global Meteorological Assimilation Office) climate derivative, and MODIS global terrestrial evapotranspiration dataset obtained via the Penman-Monteith equation per Mu et al. (2011). The cumulative evapotranspiration includes day and night components with soil heat flux calculation and improvement estimates of stomatal conductance from damp topsoil and plant covering surfaces. MOD16 is also one of the most widely used ET products. A monthly product at a spatiotemporal resolution of 0.05 degrees from the 1st

month of 2003 to the last month of 2014 was used for the study after downloading from http://files.ntsg.umt.edu/data/NTSG_Products/MOD16/. The dataset was spatially averaged over the Brahmaputra basin for further analysis.

b. GLDAS CLSM ET

The NASA Global Land Data Assimilation System Version 2 (GLDAS-2) comprises three parts: GLDAS-2.0, GLDAS-2.1, and GLDAS-2.2. GLDAS-2.0 delivers a temporally consistent dataset from 1948 to 2014 and is forced totally with the Princeton meteorological forcing input data. Combining model and observation data from 2000 to the present, GLDAS-2.1 is forced. The GLDAS-2.2 product suites use data assimilation (DA), but not by the "open-loop" (i.e., data assimilation-free) GLDAS-2.0 and GLDAS-2.1 products. Different GLDAS-2.2 packages use different forcing data, DA observation sources, variables, and schemes. This data product contains monthly 1.0-degree GLDAS-2.1 Catchment data from the main production stream. The Land Information System (LIS) Version 7's Catchment-F2.5 Land Surface Model was used to simulate 3-hourly GLDAS-2.1 data to create it. 34 land surface fields from January 2000 to the present are included in the data product. In NetCDF format, the GLDAS-2.1 data are archived and made available (Li et al. 2020; Rodell et al. 2004).

c. GLDAS Noah ET

The GLDAS-2.1 data products are currently accessible in two production streams, one processed without this forcing data (the early production stream) and the other forced with combined forcing data that includes GPCP version 1.3. The GLDAS-2.1 data products are first developed without the GPCP Version 1.3 data because it has a 3–4 month latency, and they are referred to as Early Products (EPs), with a 1.5-month lag. The GLDAS-2.1 data products are processed in the main production stream and deleted from the Early Products repository once the GPCP Version 1.3 data are accessible. This data package, reprocessed in January 2020, replaces the previous one and is for GLDAS-2.1 Noah monthly 1.0 degree data from the main production stream (Beaudoin and Rodell 2020; Rodell et al. 2004).

d. TerraClimate ET

TerraClimate is a dataset that covers the global terrestrial surfaces from 1958 to 2019 and provides monthly climate and climatic water balance data. These data serve as crucial inputs for ecological and hydrological research that call for time-varying data and high spatial resolution. All data have a spatial resolution of about 4 km (1/24th degree) and a temporal resolution of one month. The information spans the years 1958 to 2020. The approach creates a high-spatial-resolution dataset with a broader temporal record by interpolating time-varying anomalies from CRU Ts4.0/JRA55 to the WorldClim high-spatial resolution climatology (Abatzoglou et al. 2018).

3.2.3 River discharge

The daily water level (5 times a day) and weekly discharge (using the velocity-area method) of the Brahmaputra basin at Bahadurabad station are recorded by the Hydrology Division belonging to the Bangladesh Water Development Board (BWDB) (Masood et al. 2015). The daily water level and weekly discharge were used to construct rating curves (personal communication) to calculate the daily discharge. The daily discharge for 2003-2014 was converted to monthly values by averaging the daily discharge in cumecs (m^3/s).

3.2.4 GRACE TWSC

The monthly variations of the earth's gravity field obtained by determining the length between two orbiting satellites since April 1st, 2002, have been provided by the Gravity Recovery and Climate Experiment (GRACE) satellites (Tapley et al. 2004). For regions of 200,000 km^2 or more, GRACE data provide unprecedented accessibility to terrestrial water storage changes (with a precision of 1.5 cm equivalent water height) with respect to climate change, global change, human water use, groundwater extraction, which is unmeasured and unmanaged in several parts of the world. The GRACE data may be freely accessed from three different sources: the Jet Propulsion Laboratory (JPL), the Center for Space Research (CSR) at the University of Texas, and Geoforschungs Zentrum Potsdam (GFZ). These three products were obtained following the spherical decomposition of GRACE

records. Using the average of the three products is usually recommended to reduce uncertainty. Another category of GRACE records is the MASCON (mass concentration) dataset, which comes independently from JPL and CSR (Watkins et al. 2015). The solution from JPL is explicit, whereas the one from CSR is first spherically decomposed. In the current study, the solution from JPL is used because it is independent (Pellet et al., 2020). In this study, a simple derivative method representing the total water storage change (TWSC) between two data points in terms of mass anomalies is used, which may be found elsewhere may be presented (Oliveira et al. 2015; Wang et al. 2014). The basin average of GRACE data was used for the current analysis.

EVALUATION OF SATELLITE PRECIPITATION OF THE BRAHMAPUTRA RIVER BASIN

4.1 OVERVIEW

Despite the ubiquitous of application of satellite precipitation data in hydrological studies, they are not free from errors and uncertainties. Hence, the common practice is to assess such precipitation data against gauge or measured data, even though they are often sparse in a topographically complex terrain like Brahmaputra river basin. It is imperative that the satellite data be assessed using categorical metrics (Duan et al. 2016) and continuous metrics AghaKouchak and Mehran (2013). In this study the daily satellite based precipitation estimates were assessed against an updated version of APHRODITE, which is the version 2 of earlier precipitation known by the same or APHRODITE v1.

4.2 METHODS

4.2.1 Categorical error metrics

The equations for all the categorical statistics (error metrics) are described in Table 4.1. The Probability of Detection (POD) is the ratio of hit (H) to the sum of H and miss (M). As the phrase suggests, the False Alarm Ratio (FAR) is the ratio of false (F) to the sum of F and H. The Critical Success Index (CSI) is the ratio of H to the sum of H, M, and F. More details are available reported by AghaKouchak and Mehran (2013).

4.2.2 Continuous error metrics

Table 4.1 describes the equations for continuous error metrics in detail. Though there are two variants of the coefficient of determination (Chicco et al. 2021; Legates and McCabe 1999), the square of correlation coefficient (r), which is known as the coefficient of determination (R^2), is considered for the current study. The R^2 describes the degree of collinearity between the gauge and satellite rainfall. Also, it represents the fraction of the total variance in the gauge rainfall data, which can be explained by satellite precipitation

(Legates and McCabe,1999). The relative bias (RBIAS) estimates the mean propensity of satellite precipitation to be lesser or larger than the gauge precipitation. The mean error (ME) is the average of the summation of the difference between satellite and gauge precipitation. The mean absolute error (MAE) is the average summation of the absolute difference between satellite and gauge precipitation. Root mean square error (RMSE) is the square root of the mean of the square of the difference between satellite and gauge precipitation. The R^2 and RBIAS do not possess units, whereas ME, MAE, and RMSE have units of the variables of interest. Spatial mean for both the categories is total values of the pixels by total pixel area.

Table 4.1 Performance metrics for evaluation of satellite-based precipitation products

| Performance metric | Equation | Range | Best value |
|--|--|------------------------|------------|
| Probability of detection (POD) | $POD = \frac{H}{H + M}$ | 0 to 1 | 1 |
| False alarm ratio (FAR) | $FAR = \frac{F}{H + F}$ | 0 to 1 | 0 |
| Critical success index (CSI) | $CSI = \frac{H}{H + M + F}$ | 0 to 1 | 1 |
| Coefficient of determination (R^2) | $R^2 = \left(\frac{\sum_{i=1}^n (O_i - \bar{O})(S_i - \bar{S})}{\sqrt{\sum_{i=1}^n (O_i - \bar{O})^2} \sqrt{\sum_{i=1}^n (S_i - \bar{S})^2}} \right)^2$ | 0 to 1 | 1 |
| Relative bias (RBIAS) | $RBIAS = \frac{\sum_{i=1}^n S_i}{\sum_{i=1}^n O_i} - 1$ | $-\infty$ to $+\infty$ | 0 |
| Mean error (ME) | $ME = \frac{\sum_{i=1}^n (S_i - O_i)}{n}$ | | 0 |

| | | | |
|--------------------------------------|--|---------------------------|---|
| | | $-\infty$ to $+\infty$ | |
| Mean absolute error (MAE) | $MAE = \frac{\sum_{i=1}^n S_i - O_i }{n}$ | 0 to $+\infty$ | 0 |
| Root mean square error (RMSE) | $RMSE = \sqrt{\frac{\sum_{i=1}^n (S_i - O_i)^2}{n}}$ | 0 to $+\infty$ | 0 |

Notations: H stands for the precipitation detected by satellite products when it has accrued; M stands for the missed precipitation by satellite products when it has accrued; F stands for the precipitation detected by satellite products when it has not occurred; n stands for a total number of samples (total days from 1.01.2001 to 31.12.2015); O_i and S_i are the gauged and satellite precipitation measurements, respectively; \bar{O} and \bar{S} are the means of gauged and satellite precipitation measurements, respectively.

4.3 RESULTS AND DISCUSSION

4.3.1 Metrics of daily precipitation of the basin

This section discusses the overall time series of daily rainfall (2001-2015) for the entire Brahmaputra River basin, including its upper, middle, and lower parts. Fig.4.1 displays the spatial extent of the 15-year mean precipitation over the basin, obtained from five satellite-based precipitation data (CHIRPS, CMORPH, IMERG, SM2RAIN and TRMM) and a gauged based APHRODITE data. At the same time, Table 4.2 presents the areal average of different metrics for all the products.

On visual inspection, the spatial mean precipitation of CMORPH is like that of APHRODITE, resulting in the basin average of spatial mean precipitation being 2.51 and 2.9 mm/day for both products, respectively. This similarity is because CMORPH products were derived using daily gauge precipitation for bias correction, whereas other precipitation products were bias corrected using monthly gauge precipitation data. TRMM

has the highest basin average of spatial mean precipitation at 3.98 mm/day, followed by IMERG (3.79 mm/day) and CHIRPS (3.38 mm/day). Meanwhile, SM2RAIN shows the lowest basin average of spatial mean precipitation at 1.5 mm/day.

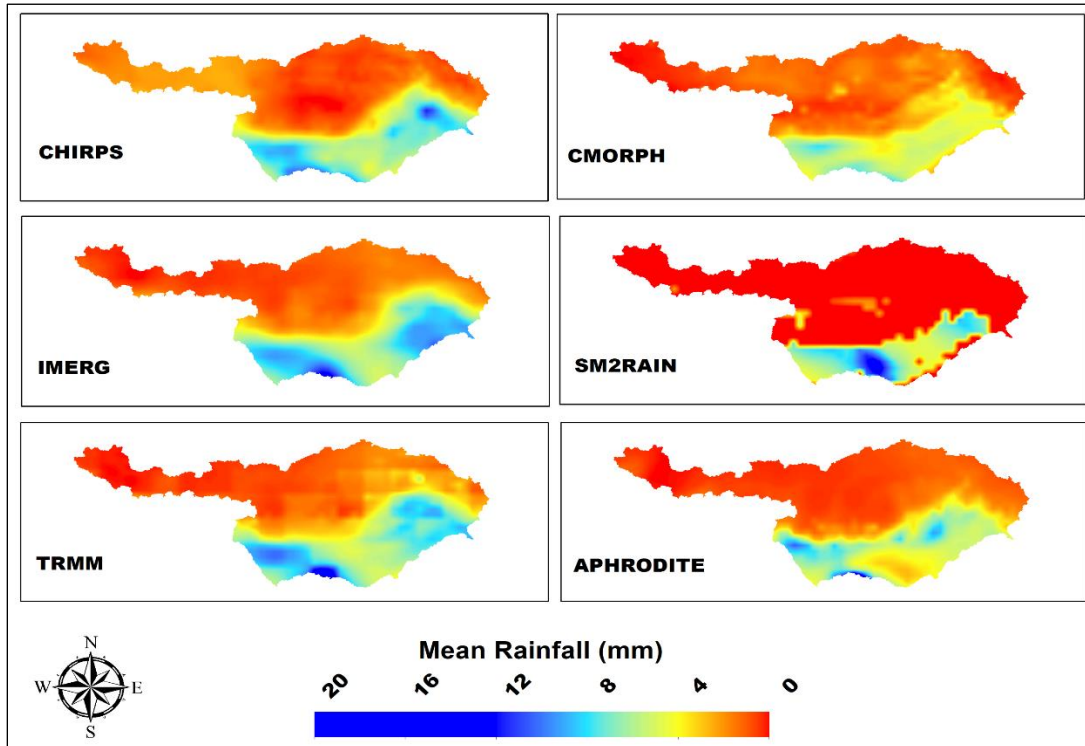


Fig. 4.1 Map of mean daily (2001-2015) of gauge and satellite precipitation products

One drawback of SM2RAIN is that it cannot capture precipitation from snow-exposed regions. It is unable to capture precipitation from snow-exposed regions, has frozen soil, are rainforest-dominated, and are located at high elevations. The mean precipitation at higher elevations is lower due to snowpacks and the sparse density of rain gauges. In contrast, the floodplain region receives much Indian monsoon rain. The basin's southern part, which mainly falls within India's northeast, also shows less rainfall for the gauge-based APHRODITE product than for the gauge-corrected satellite products such as CHIRPS, IMERG, and TRMM. This is partly due to a lower density of rain gauges, orography, and topographical setup in this region, leading to less rainfall recorded by the gauge product.

The scenario appears to be different in the upper part of the basin. The TRMM product shows the mean value, close to the gauge-based precipitation, of 3.56 mm/day against the mean of APHRODITE (3.65 mm/day), as shown in Table 4.3. The CHIRPS precipitation shows the highest value at 3.89 mm/day, while the least value was obtained by SM2RAIN (2.53 mm/day). The least mean value by SM2RAIN is consistent with its overall mean, probably because this product needs to be gauge corrected. In the middle portion of the basin (Table 4.4,) CHIRPS tends to be closer to APHRODITE in terms of the mean precipitation. Like in the upper basin, the TRMM and SM2RAIN exhibited the highest and least mean precipitation at 6.68 and 3.11 mm/day, respectively, as shown in Table 4.4. In the basin's lower section, the precipitation products' behaviour tends to differ from when considering the upper and middle regions of the basin. This is partly because the lower portion of the basin lies in the flood plains of northeast India and Bangladesh. In this portion of the basin, SM2RAIN tends to be closer to APHRODITE in terms of the mean precipitation (Table 4.5), which is partly due to this region not being covered by snowpacks. The sensor used to obtain precipitation by SM2RAIN product is based on soil moisture, unlike other sensors used to get precipitation products. The highest mean is shown by the IMERG product (9.38 mm/day), derived from the TRMM product (9.22 mm/day). This might be the reason why their mean values are closer to each other for all sections of the basin. The least mean value was demonstrated by CMORPH (7.01 mm/day), but this value is close from the mean of APHRODITE. All the gauge-corrected satellite precipitation products namely, CHIRPS, IMERG and TRMM, except CMORPH, show greater mean values than APHRODITE because the first three products were bias-corrected using monthly gauge data. At the same time, the CMORPH was bias-corrected using daily gauge data.

Table 4. 2 Daily metrics obtained for the evaluation of satellite precipitation of the basin

| Metrics | CHIRPS | CMORPH | IMERG | SM2RAIN | TRMM |
|---------|--------|--------|-------|---------|------|
| POD | 0.96 | 1 | 1 | 1 | 1 |
| FAR | 0.03 | 0.03 | 0.03 | 0.03 | 0.03 |
| CSI | 0.94 | 0.97 | 0.97 | 0.97 | 0.97 |

| | | | | | |
|----------------|------|--------------|-------------|-------|------|
| R ² | 0.65 | 0.74 | 0.83 | 0.62 | 0.76 |
| Mean (mm) | 3.38 | 2.51 | 3.79 | 1.5 | 3.98 |
| RBIAS | 0.16 | -0.14 | 0.31 | -0.48 | 0.37 |
| ME (mm) | 0.47 | -0.39 | 0.89 | -1.4 | 1.08 |
| MAE (mm) | 1.62 | 1.15 | 1.33 | 1.64 | 1.56 |
| RMSE (mm) | 2.87 | 1.85 | 2.41 | 2.87 | 2.85 |

Note: Daily mean of APHRODITE = 2.9 mm.

Table 4.3 Daily metrics obtained for the evaluation of satellite precipitation of the upper section of the basin.

| Metrics | CHIRPS | CMORPH | IMERG | SM2RAIN | TRMM |
|----------------|--------|--------|-------------|-------------|--------------|
| POD | 0.95 | 1 | 1 | 0.84 | 1 |
| FAR | 0.03 | 0.04 | 0.04 | 0.02 | 0.04 |
| CSI | 0.92 | 0.96 | 0.96 | 0.82 | 0.96 |
| R ² | 0.05 | 0.02 | 0.06 | 0.09 | 0 |
| Mean (mm) | 3.89 | 2.95 | 3.85 | 2.53 | 3.56 |
| RBIAS | 0.06 | -0.19 | 0.05 | -0.31 | -0.03 |
| ME (mm) | 0.24 | -0.7 | 0.19 | -1.12 | -0.1 |
| MAE (mm) | 2.65 | 2.68 | 2.43 | 2.73 | 3.1 |
| RMSE (mm) | 3.96 | 4.03 | 3.79 | 3.96 | 4.35 |

Note: Daily mean of APHRODITE = 3.65 mm.

The categorical metric POD in Fig.4.2 follows a similar pattern to other error metrics for SM2RAIN, with the southern region showing that it was able to represent actual precipitation. Precipitation for the other parts of the basin could not be captured by SM2RAIN, as confirmed with most of the continuous error metrics. Visually IMERG is the best-performing satellite precipitation, followed by TRMM, CMORPH and CHIRPS.

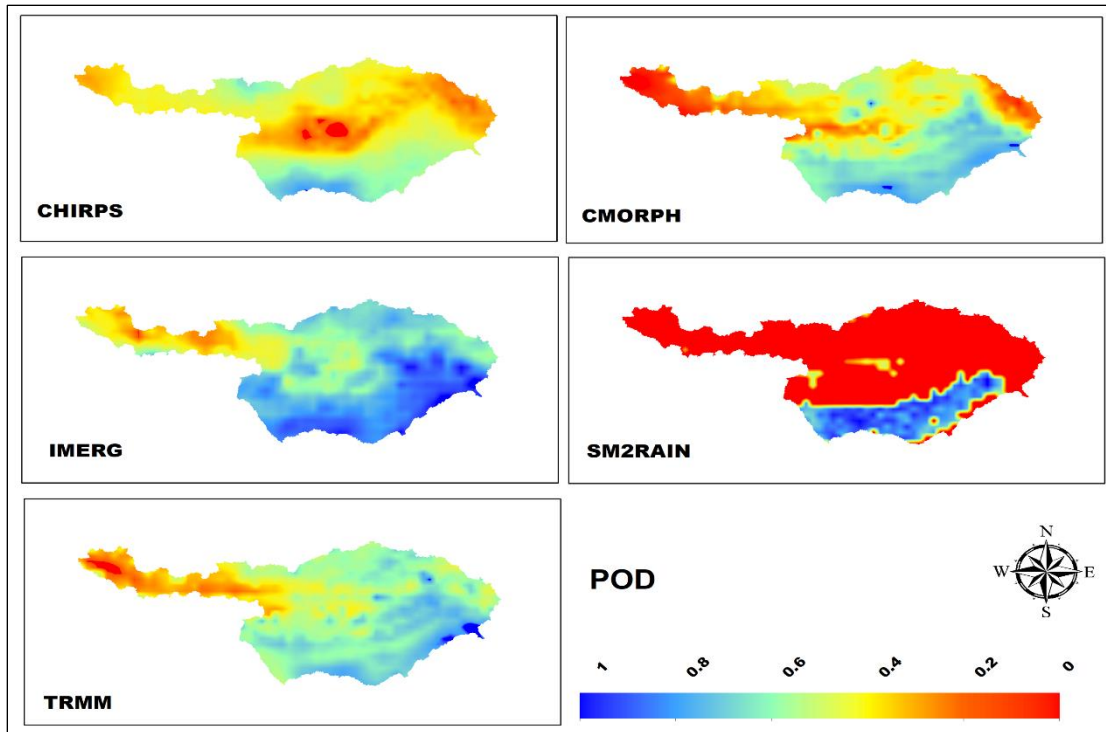


Fig. 4.2 Probability of detection (POD) map of satellite precipitation products against gauge data

The basin average also confirms this with the highest POD value of 0.59 for IMERG. SM2RAIN is the least-performing satellite product with a POD value of 0.16. The remaining products have POD values ranging from 0.3 – 0.5. However, when only the cells with precipitation values were considered in calculating the areal precipitation average, a different perspective is obtained as shown in Table 4.2. Except for the CHIRPS precipitation product, all precipitation products show a POD of unity value (1.00). Therefore, spatial variation of POD in the form of a map is indispensable to get a clearer picture of the metric. When the POD of precipitation products in the upper part of the basin (Table 4.3) was considered, the SM2RAIN product showed the least mean POD (0.84) when compared against other products that tend to show POD between 0.95 - 1.00. The POD of the precipitation products in the middle part of the basin (Table 4.4) again casts a similar pattern to the upper portion of the basin. The SM2RAIN again exhibits the least POD (0.7), whereas the remaining products show the metric ranging from 0.88- 1.00. In contrast, the lower portion of the basin depicts POD like that of the whole basin metric,

with all the precipitation products showing the metric ranging from 0.91 – 1.00, as shown in Table 4.5. This pattern was observed because the lower section of the basin is in the flood plains of India and Bangladesh, where moisture content uncovered by snowpacks is the basis for SM2RAIN precipitation products.

Table 4.4 Daily metrics obtained for the evaluation of satellite precipitation of the middle section of the basin

| Metrics | CHIRPS | CMORPH | IMERG | SM2RAIN | TRMM |
|----------------|-------------|------------|------------|---------|------|
| POD | 0.88 | 1 | 1 | 0.7 | 1 |
| FAR | 0.06 | 0.09 | 0.09 | 0.07 | 0.09 |
| CSI | 0.84 | 0.91 | 0.91 | 0.66 | 0.91 |
| R ² | 0.05 | 0 | 0.08 | 0 | 0.02 |
| Mean (mm) | 5.28 | 4.79 | 6.46 | 3.11 | 6.68 |
| RBIAS | 0.01 | -0.08 | 0.24 | -0.4 | 0.28 |
| ME (mm) | 0.06 | -0.43 | 1.24 | -2.11 | 1.46 |
| MAE (mm) | 4.35 | 4.33 | 4.2 | 5.21 | 5.25 |
| RMSE (mm) | 6.18 | 5.7 | 6.08 | 6.64 | 7.09 |

Note: Daily mean of APHRODITE = 5.22 mm.

Table 4.5 Daily metrics obtained for the evaluation of satellite precipitation of lower section of the basin

| Metrics | CHIRPS | CMORPH | IMERG | SM2RAIN | TRMM |
|----------------|-------------|--------|-------------|--------------|------|
| POD | 0.91 | 1 | 1 | 1 | 1 |
| FAR | 0.07 | 0.1 | 0.1 | 0.1 | 0.1 |
| CSI | 0.85 | 0.9 | 0.9 | 0.9 | 0.9 |
| R ² | 0.42 | 0.43 | 0.61 | 0.27 | 0.51 |
| Mean (mm) | 8.76 | 7.01 | 9.38 | 7.23 | 9.22 |
| RBIAS | 0.16 | -0.07 | 0.24 | -0.04 | 0.22 |
| ME (mm) | 1.22 | -0.53 | 1.84 | -0.31 | 1.68 |

| | | | | | |
|-----------|------|-------------|-------------|------|------|
| MAE (mm) | 5.04 | 4.22 | 4.22 | 4.3 | 4.9 |
| RMSE (mm) | 7.36 | 5.63 | 6.03 | 6.01 | 6.64 |

Note: Daily mean of APHRODITE = 7.54 mm.

Though FAR (Fig.4.3) seems negligible for SM2RAIN, only the southern part can represent precipitation occurrence to a certain extent. Hence, the least-performing product is SM2RAIN, with a FAR value of 0.16. The best-performing product is IMERG, with a FAR value of 0.06. The second-best performing product is CHIRPS, with a FAR value of 0.07. CMORPH and TRMM have FAR values of 0.15 and 0.12, respectively. Interestingly, CMORPH has higher FAR values over the centre, east, northwest, and upper most part of the basin. TRMM has some irregular pattern of higher FAR values over the northwest part. CHIRPS and IMERG have almost all the pixels having low FAR values. This is probably CMORPH was bias corrected by daily gauge data, which tends to have more with no rainy day counts than monthly scale that tends to have lesser counts with no rain.

Temporally, the FAR values range 0.02- 0.1 for all the precipitation products as shown in Table 4.2 – 4.5. As was the case with POD, which was high for all the precipitation products, the same is true for FAR magnitudes for all the precipitation products. The reason being the grid cells devoid of rainfall were not considered while these categorical metrics were calculated on areal average basis for each daily data.

The pixel-to-pixel CSI values in Fig.4.4 are very similar to POD. However, CSI is different from POD with the former having an additional additive term of FALSE counts of precipitation. The order of performance of the satellite products is the same as that of POD: IMERG (0.56) > TRMM (0.46) > CMORPH (0.4) > CHIRPS (0.37) > SM2RAIN (0.14). On temporal basis, CSI follows the same pattern of POD with its magnitude ranging 0.66 - 0.97 in which SM2RAIN's performance was the least in the upper and middle portions of the basin (Table 4.3 and 4.4). It is to be noted that earlier also the reason for SM2RAIN product performing the least in these sections of the basin was highlighted. The reason for better performance of the product in the lower part of the basin was also highlighted earlier.

The categorical metrics alone cannot help us decipher a clear picture on the performance of the satellite rainfall estimates. They are more to do with the occurrence of rainfall, whereas continuous metrics can provide better picture regarding the magnitude of rainfall. Categorical metrics could be used as the first step towards assessment of any precipitation products. However, continuous metrics can support the categorical metrics for a better assessment of how close satellite rainfall estimates are able to capture the actual occurrence of rainfall.

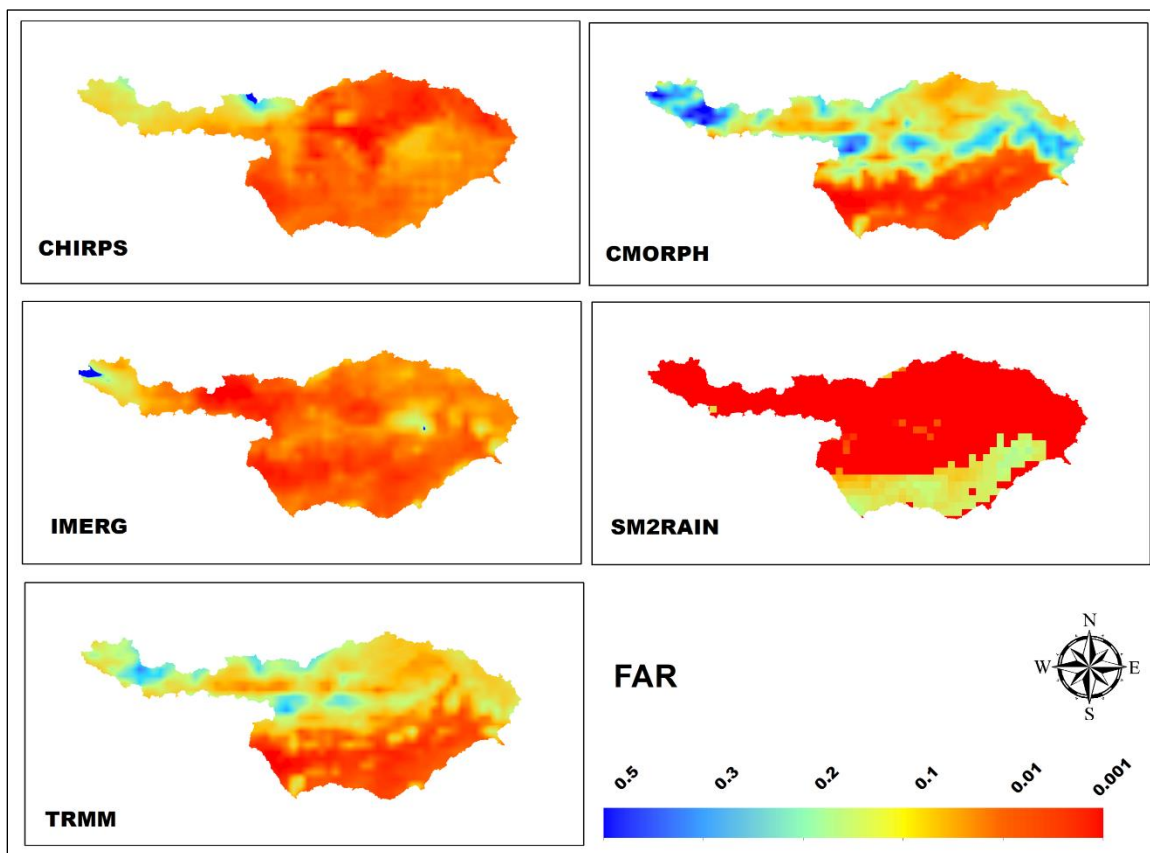


Fig. 4.3 False alarm ratio (FAR) map of satellite precipitation products against gauge data

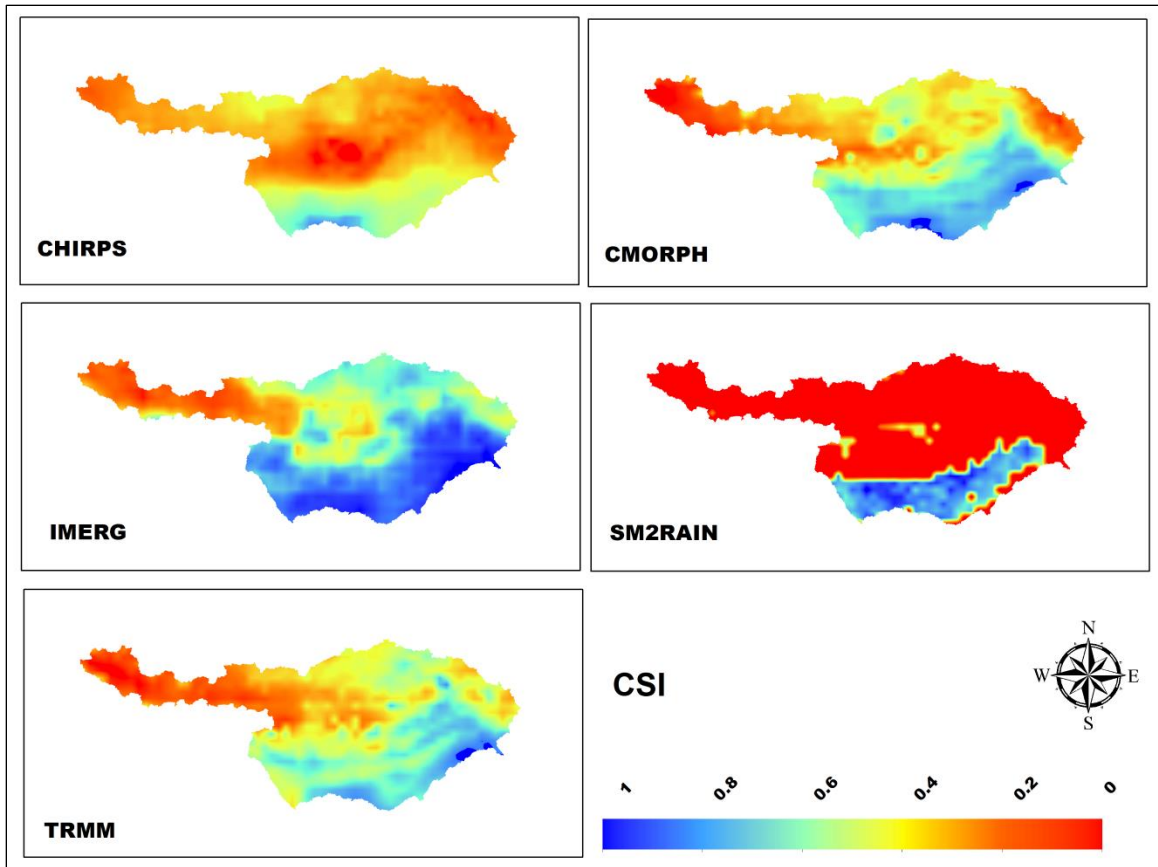


Fig.4.4 Critical success index (CSI) map of satellite precipitation products against gauge data

From Fig.4.5, CHIRPS, CMORPH, IMERG, and TRMM have the higher R^2 in the southwest of the basin, whereas CHIRPS and IMERG have the higher R^2 in the upper middle of the basin as compared to other products. SM2RAIN has no relationship with APHRODITE except in the lower part of the basin. IMERG has the highest average of spatial R^2 value at 0.4 followed by CHIRPS and TRMM at 0.28. The R^2 for the latter two products is consistent with the finding of Adige basin, Italy (Duan et al. 2016). Probably IMERG has higher spatial resolution and derived from multi-satellite missions, whereas CHIRPS was bias corrected using TRMM along with gauge data. CMORPH has basin average of R^2 value at 0.22 and SM2RAIN has the least basin average of R^2 at 0.17.

The temporal R^2 (Fig.4.6) for the all the precipitation products strike contrasting values as compared to what we have seen for the categorical metrics in which all the products show similar magnitude for a particular portion of the basin. Hence, unique R^2 is observed for the whole and lower portion of the basin (Table 4.2 and 4.5). IMERG has highest linear strength ($R^2 = 0.83$) for the basin as a whole, whereas the least linear strength ($R^2 = 0.62$) was depicted by SM2RAIN. Similarly, for the lower section of the basin, the highest and least linear strength (0.61 and 0.27) are shown by the same products. However, the linear strength measures are not true representation of the performance of non-linear variables like rainfall. Therefore, the R^2 for the upper and middle portion of the basin (Table 4.3 and 4.4) indicate a strong non-linear measure most likely because of snow covers and lesser rainfall events in these regions.

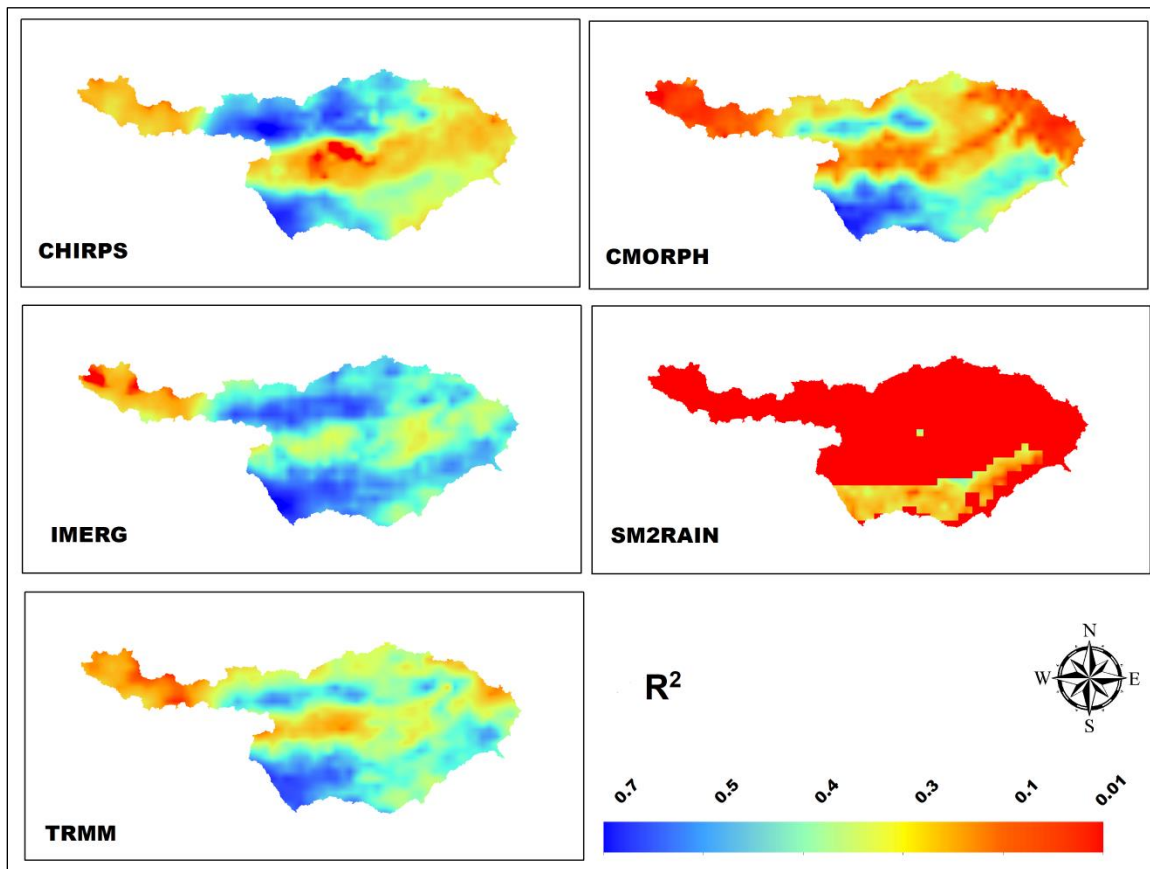


Fig.4.5 Correlation of determination (R^2) map of satellite precipitation products against gauge data

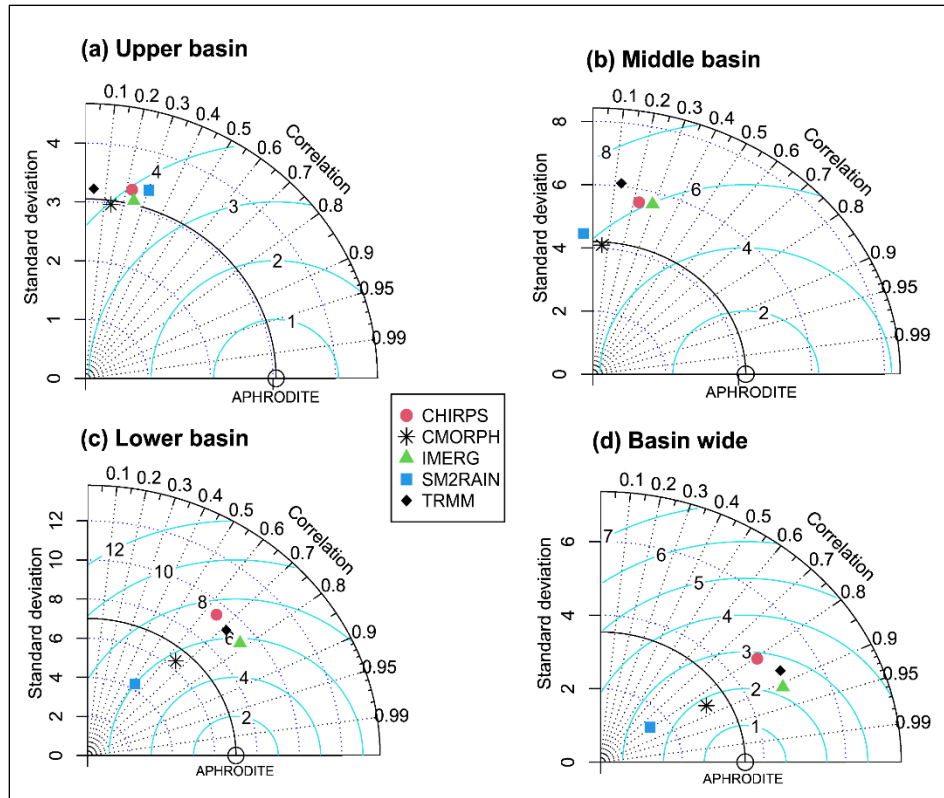


Fig. 4.6 Taylor's diagram of correlation between satellite precipitation and APHRODITE in different elevation-based zones of the basin

On closer inspection of the RBIAS of all the precipitation products in Fig.4.7, CMORPH has very close-to-zero basin-average estimate of RBIAS at -0.06, which affirms that CMORPH was bias corrected with daily gauge data. TRMM with basin-average RBIAS of 0.5 overestimated daily precipitation over the basin, while SM2RAIN underestimated the daily precipitation most with basin-average RBIAS of -0.6. CHIRPS and IMERG with RBIAS of 0.28 and 0.36, respectively overestimated precipitation over the basin.

Pixel-to-pixel analysis shows different pattern of RBIAS for CHIRPS and IMERG. But IMERG and TRMM look very much similar in pattern on spatial distribution of RBIAS. It indicates that depending on the analysis required one can choose satellite precipitation based on the error metrics obtained either pixel-to-pixel or basin-average

basis. CHIRPS underestimated precipitation over the central, northern and some parts of the north-eastern part of the basin, whereas the upper section of the basin it mostly overestimated precipitation. Some patches of central part of the basin are the flood plains of Assam, which receive high rainfall during monsoon season. The high rainfall of north-eastern India, in which Brahmaputra lies, is sparsely gauged because of which gauge-based APHRODITE may not fully reflect true precipitation recorded (Prakash et al. 2015). CMORPH underestimated precipitation for most part of the basin except the northern and southern part of the basin. Except most of the southern part of the basin and a small part of the centre, SM2RAIN underestimated precipitation over the basin. This was expected as SM2RAIN could not capture precipitation in certain conditions of the earth's surface and land cover. The high biases induced in the satellite precipitation products could be due to varying orography compounded by precipitation occurrences as reported by (Prakash 2019).

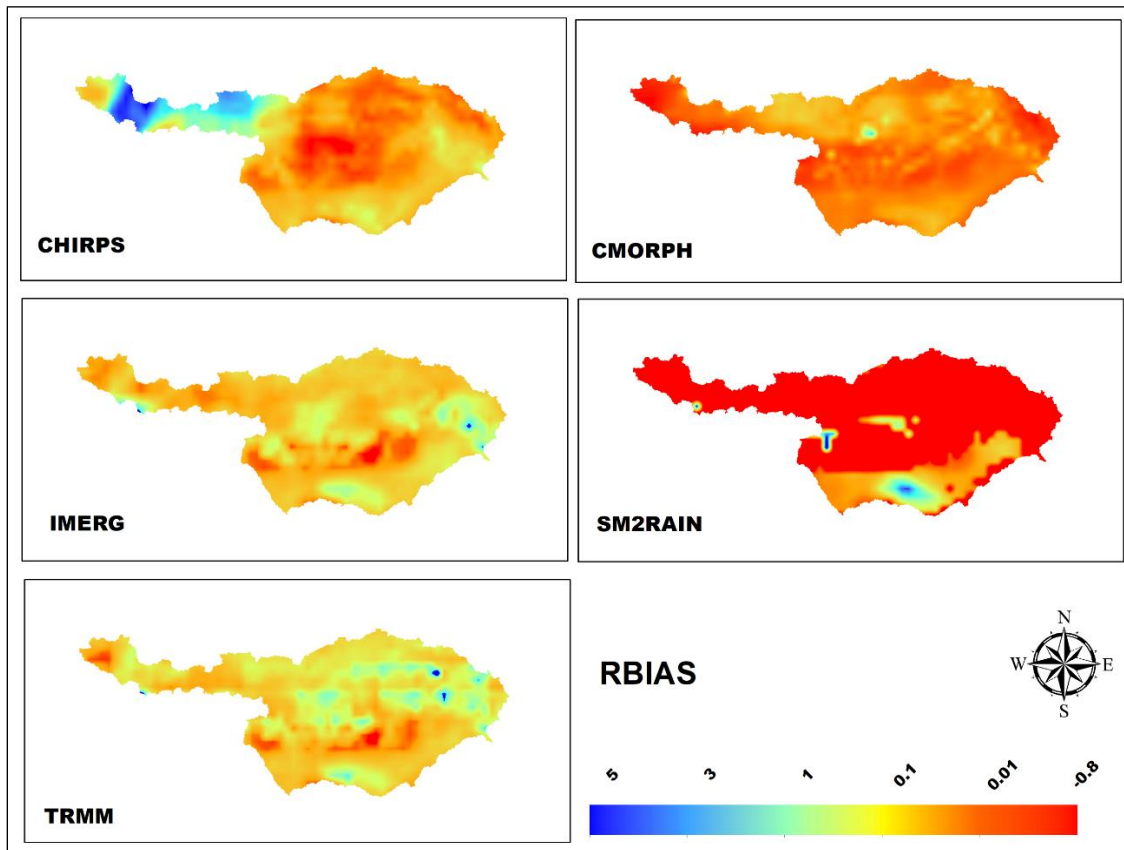


Fig.4.7 Relative bias (RBIAS) map of satellite precipitation products against gauge data.

On a temporal basis slightly underestimating (-0.14) the magnitude of precipitation, CMORPH is better than other products as shown in Table 4.2. SM2RAIN underpredicts (-0.48) precipitation the most as was expected because of it being not gauge-corrected, whereas TRMM (0.37) overpredicts the most. CHIRPS is the least overpredicting product and IMERG closely follows TRMM in overprediction of precipitation. The latter two products' overprediction is apparently because of the bias correction inherent in the product using monthly rainfall data. This pattern was noticed even in the areal averages of all the precipitation products.

Interestingly in Table 4.3, RBIAS values of CHIRPS, IMERG and TRMM products are almost same, in the upper section of the basin, with TRMM (-0.03) slightly on the underprediction side is the best performing product. The least performance is shown by SM2RAIN (-0.31). In middle and lower portions of the basin, TRMM and IMERG behave the same way as it is in the whole and upper portion of the basin (Table 4.4 and 4.5). But CHIRPS with an RBIAS = 0.01 is the best performing in middle section of the basin, whereas SM2RAIN (-0.04) is the best performing in the lower section of the basin. This finding is in consistent with other metrics of SM2RAIN, which performed well where there is non-existent of snow cover.

From Fig.4.8, SM2RAIN has the highest ME values on the southern part of the basin, whereas on a basin scale it has the least ME (-1.38 mm/day). On the other hand, TRMM has the maximum average ME value (1.06 mm/day). IMERG and TRMM appear to display similar ME values over the basin though the basin average ME for IMERG is slightly lesser at 0.85 mm/day. Except the upper part of the basin, CHIRPS also tend to exhibit similar pattern to IMERG and TRMM. However, CHIRPS has ME of 0.45 mm/day. CMORPH with ME value of - 0.38 mm/day tends to have the error closer to zero than other products.

In temporal terms, the mean ME pattern is similar to RBIAS with CMORPH (-0.39 mm/day) being the best for the whole basin (Table 4.2); TRMM (-0.1 mm/day) being the best for the upper part of the basin (Table 4.3); CHIRPS (0.06 mm/day) being the best for

the middle basin (Table 4.4) and SM2RAIN (-0.31 mm/day) performing the best in the lower part of the basin (Table 4.5). It is to be noted that the pattern for all continuous metrics is same until now.

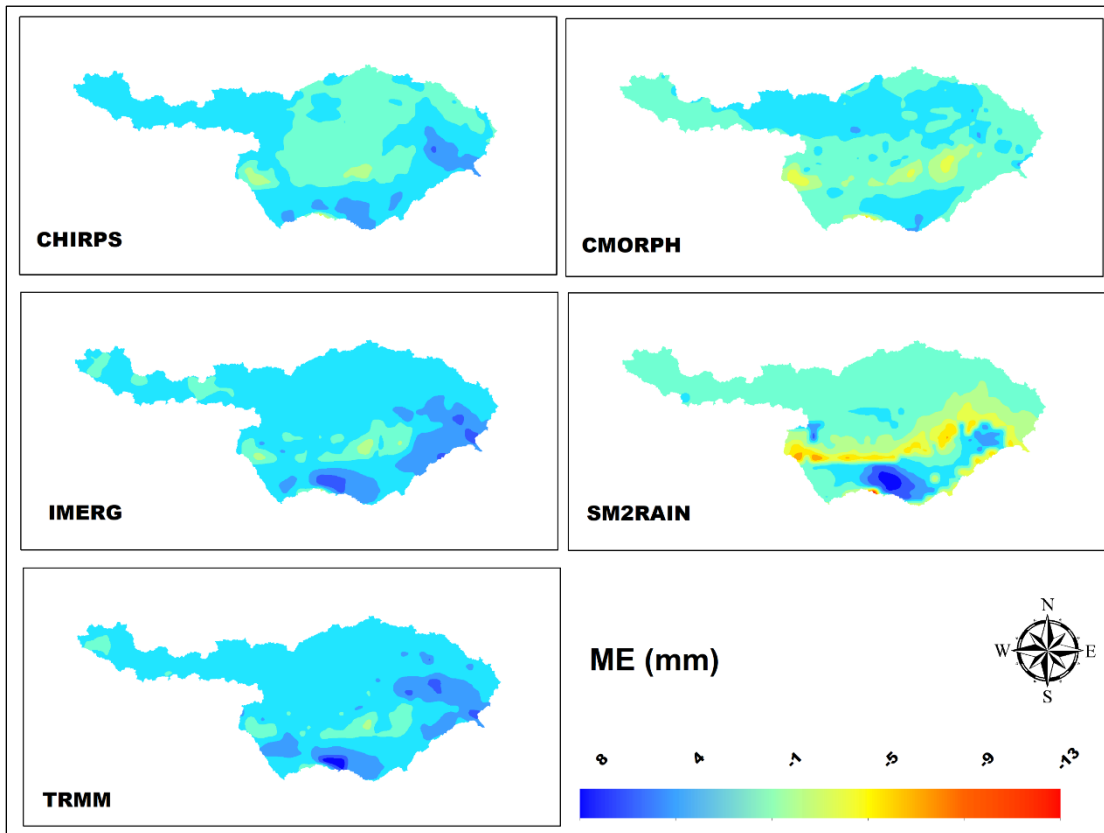


Fig.4.8 Mean error (ME) map of satellite precipitation products against gauge data

In Fig.4.9, the spatial MAE tends to be higher on south, southwest and southeast regions of the basin for all the precipitation products, whereas the remaining portion of the basin has lower magnitudes of MAE. The basin average MAE for all the data sets varies between 2 and 4 mm/day. CHIRPS (3.34 mm/day) and TRMM (3.44 mm/day) have the magnitudes of MAE on the higher side, while CMORPH (2.71 mm/day) and IMERG (2.8 mm/day) have MAE on the lower side.

The basin wide temporal mean MAE ranges 1.15-1.64 mm/day with CHIRPS being the best performer and SM2RAIN being the least performing product (Table 4.2). However,

for the upper portion of the basin, IMERG is the best (2.43 mm/day), whereas SM2RAIN (2.73 mm/day) is again the least performing product (Table 4.3). For the middle basin (Table 4.4), IMERG (4.2 mm/day) is again the best performing product, whereas TRMM (5.25) turns out to be the least performing product. Also, SM2RAIN with MAE= 5.21 mm/day is very close to TRMM. The lower portion of the basin (Table 4.5) shows that CMORPH and IMERG (4.22 mm/day) are the best performing products, whereas CHIRPS turns out to be the least performing product (5.04 mm/day).

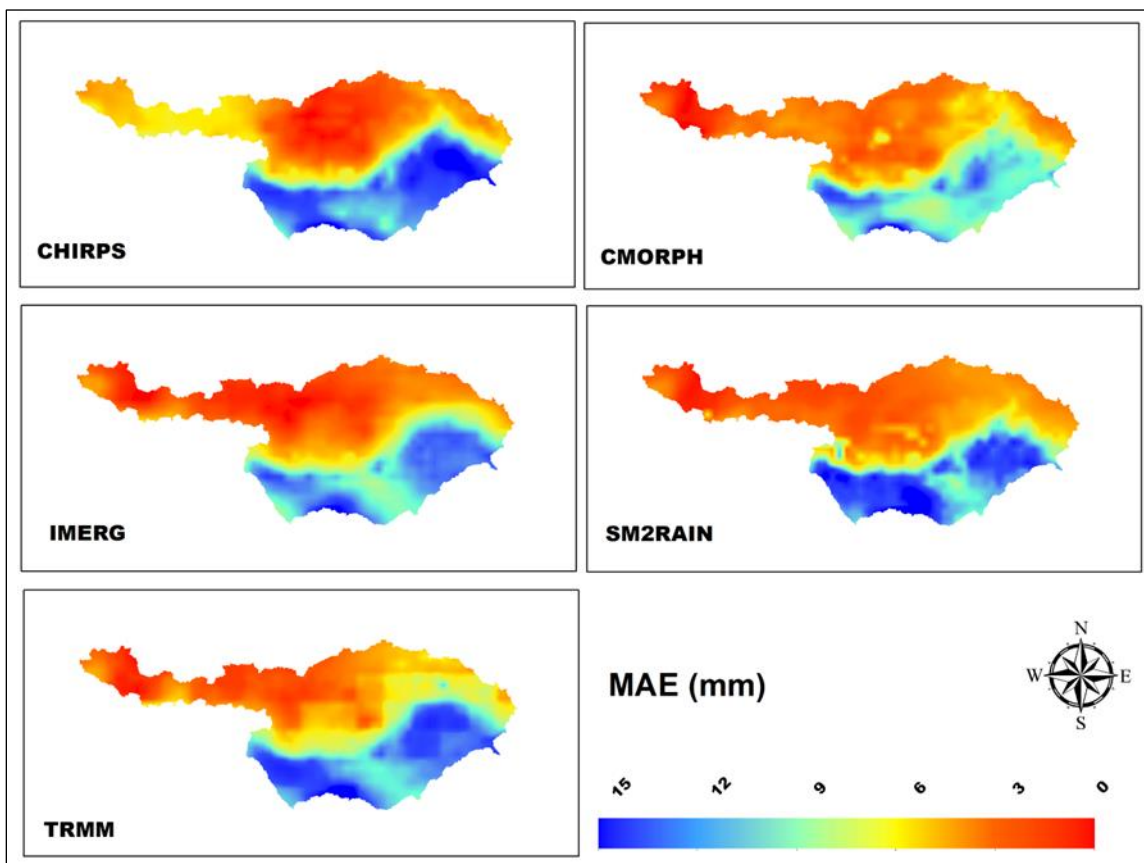


Fig.4.9 Mean absolute error (MAE) map of satellite precipitation products against gauge data

The RMSE in Fig.4.10 tends to follow similar pattern of MAE for precipitation products, with east, southeast, and southwest zones of the basin having higher RMSE. The remaining part has lower of the error metric. On the whole, TRMM has the highest RMSE

(8.09 mm/day) and SM2RAIN has the lowest RMSE (5.86 mm/day). In consistent with the previous error metrics, the RMSE for CHIRPS (7.21 mm/day) is closer to that of TRMM probably because of the bias correction of CHIRPS being done using TRMM. As with most of the metrics CMORPH has RMSE (5.93 mm/day), which is about the same to that of SM2RAIN. The RMSE for IMERG (6.36 mm/day) is consistent in pattern to other error metrics.

In terms of temporal assessment of the products in terms of RMSE, CMORPH is the best performing product, whereas CHIRPS and SM2RAIN are the least performing products for the whole basin (Table 4.2). With a RMSE of 3.79 mm/day, IMERG is the best performing rainfall product, while TRMM shows the least performance (4.35 mm/day) for the upper section of the basin (Table 4.3). For the middle and lower sections of the basin, CMORPH is the performing product (Table 4.4 and 4.5), whereas TRMM (7.09 mm/day) and CHIRPS (7.36 mm/day) are the least performing products the two sections, respectively.

4.3.2 Metrics of daily precipitation in winter season

In this section, the metrics of daily precipitation in winter season are considered for all the zones including the whole basin. Also, only the temporal areal mean of various metrics is considered henceforth.

As mentioned earlier, the categorical metrics of all the precipitation products tend to have similar values for the whole and the lower part of the basin because these metrics (Table 4.6 and AI.3) depend on whether precipitation products can capture rainfall in a particular day against rainfall observation unlike the continuous metrics that depend on the magnitude of rainfall occurrence not just occurrence. Also, for the same reason the upper and middle sections of the basin with snow-covered areas show similar pattern of the metrics (Table AI.1 and AI.2). For example, the SM2RAIN show POD for the whole and lower basin to be 1, whereas for the upper and middle portions of the basin 0.76 and 0.74, respectively. The latter two values are also amongst the least in comparison to other satellite products. In the light of the above discussion, the remaining discussion of the results will

centre around continuous metrics, which are known to vary across different satellite precipitation estimates.

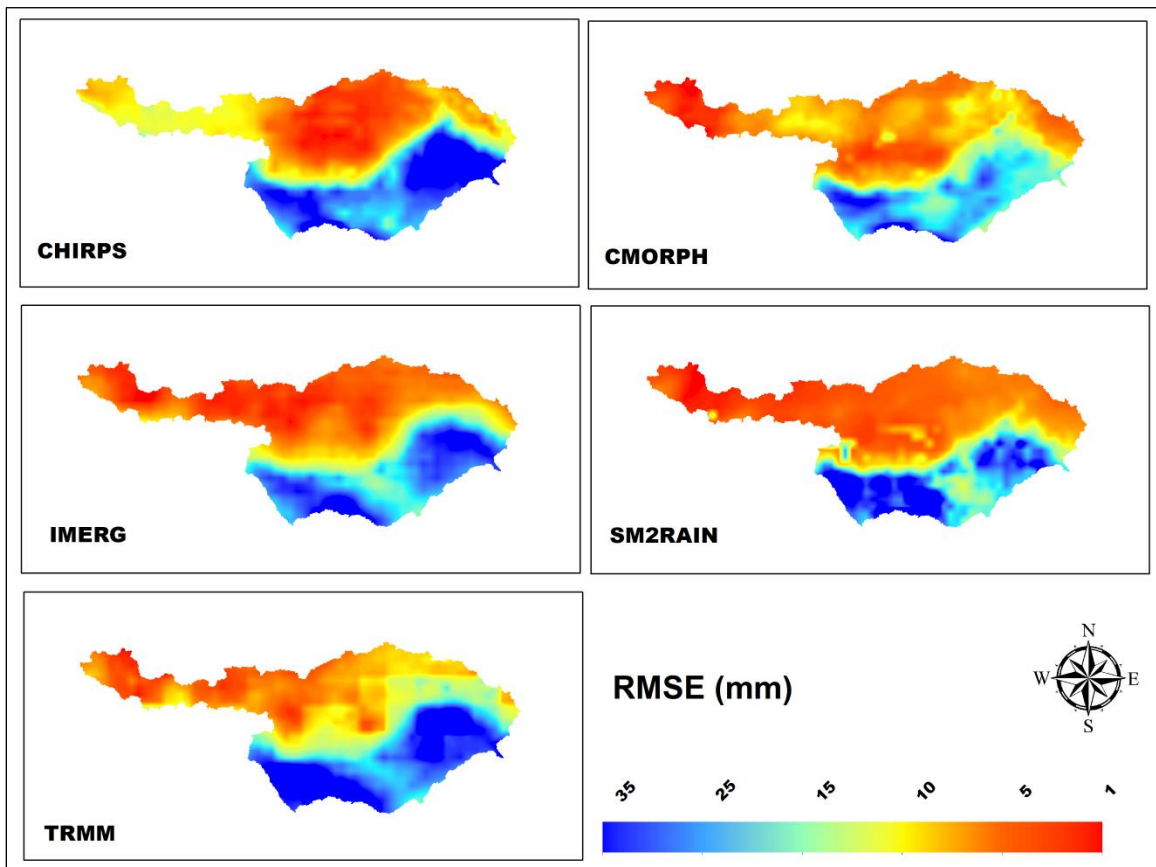


Fig.4.10 Root mean square error (RMSE) map of satellite precipitation products against gauge data

Table 4.6 Daily metrics obtained for evaluation of satellite precipitation of winter season of the basin

| Metrics | CHIRPS | CMORPH | IMERG | SM2RAIN | TRMM |
|----------------|-------------|-------------|-------------|---------|------|
| POD | 0.94 | 1 | 1 | 1 | 1 |
| FAR | 0.05 | 0.05 | 0.05 | 0.05 | 0.05 |
| CSI | 0.9 | 0.95 | 0.95 | 0.95 | 0.95 |
| R ² | 0.51 | 0.48 | 0.73 | 0.36 | 0.66 |
| Mean (mm) | 0.45 | 0.45 | 0.55 | 0.12 | 0.57 |

| | | | | | |
|-----------|--------------|-------|-------------|-------|------|
| RBIAS | -0.08 | -0.1 | 0.11 | -0.76 | 0.15 |
| ME (mm) | -0.04 | -0.05 | 0.06 | -0.38 | 0.08 |
| MAE (mm) | 0.39 | 0.4 | 0.3 | 0.42 | 0.35 |
| RMSE (mm) | 0.72 | 0.66 | 0.61 | 0.92 | 0.64 |

Note: Daily mean of APHRODITE = 0.49 mm.

The basin wide R^2 estimates show IMERG (0.73) to have the strongest linear relationship with the gauge-based APHRODITE and SMRAIN (0.36) to be the least. All the individual sections of the basin show R^2 estimates to be zero or negligible as shown in Table AI.1 – AI.3.

The CHIRPS and CMORPH products in the case of the basin show the mean to be closer to the gauge-based estimate (Table 4.6). The highest areal mean is depicted by TRMM (0.57 mm) and the least mean by SM2RAIN (0.12 mm). On other hand, SM2RAIN has the highest mean for all the individual portions of the basin as shown in Table AI.1 – AI.3. The nearest mean to the gauge data is shown by IMERG for the upper basin, CHIRPS for the middle basin and CMORPH for the lower basin. Though CMORPH was bias-corrected using daily gauge-based rainfall, it shows the least mean for the upper basin probably the magnitude of error is higher in this region attributed to sparse rain gauges. The near true reflection of the mean of the gauge-based rainfall can be seen in the lower basin because the rain gauges in the flood plains are relative higher in number. In absolute sense the northeast region of India, which forms part of the flood plain has lesser rain gauges. However, it is more conducive to reflect the true rainfall than in the upper inhospitable snow-covered terrain.

The basin wide RBIAS and ME depict CHIRPS to be the best performing rainfall estimate, whereas SM2RAIN underestimated the most (RBIAS=-0.76 mm/day, ME=-0.38 mm/day). Individual sections of the basin portray different scenarios. IMERG is the best product in the upper basin, CHIRPS in the middle basin and CMORPH in the lower basin. All the respective magnitudes are shown in Table AI.1 – AI.3.

On the other hand, SM2RAIN continues to be the least performing product in all the individual portions of the basin in terms of RBIAS and ME except CMORPH in the

upper portion of the basin. All these findings can be attributed to it being not gauge corrected.

The MAE (0.3 mm/day) and RMSE (0.61 mm/day) of IMERG of the basin exhibit to be least (highest performance) and that of SM2RAIN (MAE=0.42 and RMSE=0.92 mm/day) to be the highest (least performance) as shown in Table 4.6. In contrast, SM2RAIN is the best performing in the upper basin in terms of the two metrics, whereas TRMM is the least performing as noticed in Table AI.1. In the middle basin, CHIRPS emerges as the best product in terms of MAE (4.51 mm/day) and RMSE (6.44 mm/day), whereas TRMM is the least performing product (MAE=6.07 mm/day and RMSE=7.46 mm/day) (Table AI.2). With MAE=4.72 and RMSE=5.84 mm/day, TRMM is the least performing product and IMERG, which was derived from TRMM with more coverage and sensors happens to be the best performing product (MAE= 3.78 mm/day and RMSE =5.22 mm/day) in the lower section of the basin (Table AI.3).

4.3.3 Metrics of daily precipitation in summer season

The summer season shows no different variation in categorical metrics pattern to the winter season as evident from Table 4.7, AI.4, AI.5 and AI.6. The least POD was noticed for SM2RAIN in the upper (0.81) and middle (0.59) portions of the basin, while the basin wide and lower portion shows unity value.

In the basin wide and lower basin, the IMERG depicts the highest linear strength at 0.65 and 0.43, respectively. The least linear strength was shown by CHIRPS (0.38) in the basin and SM2RAIN (0.15) in the lower basin. The upper and middle portions of the basin show nonlinear strength to be prevalent.

The areal mean of CMORPH (2.33 mm/day) is the closest to the gauge product for the basin wide case, whereas the highest and least values are demonstrated by TRMM (3.6 mm/day) and SM2RAIN (1.34 mm/day). The highest and closest mean was shown by CHIRPS in the case of upper basin. The least mean precipitation was observed for CMORPH. The IMERG and TRMM emerge as the products having closer mean to the gauge-based rainfall for the middle and lower sections of the basin, respectively. In

addition, the IMERG has also the highest mean for the middle basin and CHIRPS demonstrates to have the highest mean for the lower basin. On the other hand, the soil moisture-based precipitation (SM2RAIN) depicts the least areal mean both for the middle and lower portions of the basin.

The optimal continuous metrics right from RBIAS down to RMSE is demonstrated by CMORPH for the whole basin (Table 4.7). When it comes to the highest values for RBIAS and ME, they were demonstrated by TRMM, whereas the highest MAE and RMSE values are demonstrated by CHIRPS. In the upper section, the optimal RBIAS and ME are demonstrated by CHIRPS (RBIAS = -0.19 mm/day, ME= -0.71) though the most underpredicting product is CMORPH (-0.54 mm/day) as shown in Table AI.4. The IMERG is represents the most optimal ME, MAE and RMSE values and the highest negative error by CMORPH, highest MAE and RMSE by TRMM.

In the middle portion of the basin, the optimal areal mean, RBIAS, ME and MAE are depicted by IMERG product. The least optimal representation of the above metrics and RMSE are demonstrated by SM2RAIN data. The optimal RMSE is, however, represented by CMORPH (5.34 mm/day).

The optimal metrics of mean, RBIAS and ME are shown by TRMM, whereas the optimal metrics of MAE and RMSE are depicted by CMORPH (Table AI.6) for the lower section of the basin. The least optimal metrics as mentioned above are shown by CHIRPS for mean, SM2RAIN for RBIAS and ME and CMORPH for MAE and RMSE.

Table 4.7 Daily metrics obtained for evaluation of satellite precipitation of summer season of the basin.

| Metrics | CHIRPS | CMORPH | IMERG | SM2RAIN | TRMM |
|----------------|--------|--------|-------------|---------|------|
| POD | 0.98 | 1 | 1 | 1 | 1 |
| FAR | 0 | 0 | 0 | 0 | 0 |
| CSI | 0.98 | 1 | 1 | 1 | 1 |
| R ² | 0.38 | 0.54 | 0.65 | 0.46 | 0.51 |

| | | | | | |
|-----------|------|--------------|------|-------|------|
| Mean (mm) | 3.01 | 2.33 | 3.3 | 1.34 | 3.6 |
| RBIAS | 0.13 | -0.12 | 0.24 | -0.49 | 0.35 |
| ME (mm) | 0.35 | -0.32 | 0.64 | -1.31 | 0.94 |
| MAE (mm) | 2.06 | 1.25 | 1.34 | 1.56 | 1.66 |
| RMSE (mm) | 3.36 | 1.83 | 2.14 | 2.44 | 2.8 |

Note: Daily mean of APHRODITE = 2.66 mm.

4.3.4 Metrics of daily precipitation in monsoon season

The basin wide, upper, middle and lower sections of the basin show all the categorical metrics like POD, FAR and CSI follow similar pattern as well in their magnitudes except for SM2RAIN in the middle section of the basin (POD and CSI =0.79). These findings are slightly in contrast to the findings of winter and summer seasons, especially for SM2RAIN product in the upper section of the basin. This might be because the sensor used for this product might be able to capture soil moisture given the occurrence of rain during this season in this part of the basin.

The highest temporal areal average of linear strength (R^2) between the satellite precipitation and gauge-based rainfall is demonstrated by IMERG for the basin and all three different sections as shown in Table 4.8, AI.7-AI.9, whereas the least linear strength is depicted by SM2RAIN. The CMORPH shows the most optimal metrics right from areal mean to RMSE in the basin wide as well as upper basin assessment, the least optimal metrics being shown by SM2RAIN. In the middle section of the basin, the CMORPH emerges to have the most optimal mean (5.46 mm/day), RBIAS (-0.06 /day) and ME (-0.37 mm/day), whereas for the same metrics plus MAE the SM2RAIN depicts the least optimal values (mean = 0.13 mm/day, RBIAS = -0.98 mm/day, ME= -5.71 mm/day and MAE = 5.71 mm/day).The optimal MAE and RMSE are shown by CMORPH with TRMM is found to show the least optimal RMSE (7.01 mm/day).

Table 4.8 Daily metrics obtained for evaluation of satellite precipitation of monsoon season of the basin

| Metrics | CHIRPS | CMORPH | IMERG | SM2RAIN | TRMM |
|----------------|--------|--------------|-------------|---------|------|
| POD | 1 | 1 | 1 | 1 | 1 |
| FAR | 0 | 0 | 0 | 0 | 0 |
| CSI | 1 | 1 | 1 | 1 | 1 |
| R ² | 0.5 | 0.56 | 0.72 | 0.33 | 0.61 |
| Mean (mm) | 6.97 | 4.98 | 7.84 | 3.14 | 8.13 |
| RBIAS | 0.19 | -0.15 | 0.33 | -0.47 | 0.38 |
| ME (mm) | 1.09 | -0.9 | 1.97 | -2.74 | 2.26 |
| MAE (mm) | 2.68 | 1.96 | 2.44 | 3.06 | 2.84 |
| RMSE (mm) | 3.74 | 2.63 | 3.49 | 4.17 | 4.08 |

Note: Daily mean of APHRODITE = 5.88 mm.

In the lower part of the basin, the optimal mean (10.54 mm/day) and RBIAS (-1.43 mm/day) are shown by SM2RAIN, the least optimal being shown by IMERG at mean = 15.07 mm/day and RBIAS = 3.1 mm/day. The most optimal metrics of ME (4.73 mm/day) and MAE (6.23 mm/day) are shown by CMORPH, whereas the least optimal metrics are shown by CHIRPS (ME = 5.97 mm/day, MAE = 8.04 mm/day). The optimal RMSE is shown by SM2RAIN and the least optimal RMSE (3.1 mm/day) is depicted by IMERG

4.3.5 Metrics of daily precipitation in post monsoon season

The post monsoon season shows the categorical statistics to be similar in pattern to other seasons in the basin wide as well as the upper basin assessments, except that CHIRPS and SM2RAIN show their ability to capture about 88% and 70% of areal average of POD in the upper part (Table 4.9 and AI.10). The CSI of SM2RAIN being 0.67 in the upper portion (Table AI.10). In the middle section of the basin, CMORPH, IMERG and TRMM show the highest POD at unity value. On the other hand, CHIRPS and SM2RAIN show POD of 0.75 and 0.66, respectively. The FAR metric appears to be similar in magnitude for a given basin section and this pattern is seen across different sections of the basin as well as the basin

itself. As in case of POD, CSI metric variation is similar to it because CSI differs from POD only with an additional additive term in the denominator.

The highest linear strength ($R^2=0.86$) is observed for IMERG product and least (0.41) for the soil moisture-based precipitation (SM2RAI) in the total basin wide assessment. However, there is no linear strength associated with any of the product in the upper and middle sections of the basin. However, there is apparently some linear relationship that could be seen in the lower section of the basin assessment.

The continuous metrics ranging from areal mean to RMSE for CMORPH are the most optimal ones in the basin wide analysis, whereas SM2RAIN shows the least optimal metrics. In the upper basin section analysis, the CMORPH represents the most optimal mean, RBIAS and Me, whereas TRMM represents the least optimal metrics right from the mean to RMSE. However, the optimal MAE and RMSE are represented by SM2RAIN. Interestingly, CHIRPS, SM2RAIN and TRMM portray the optimal mean at 5.05 mm/day in the middle part of the basin analysis. The least optimal mean being represented by CMORPH. The CHIRPS represents the most optimal metrics from RBIAS to RMSE including a tie representation of ME metric by SM2RAIN. The least optimal metrics are represented by TRMM not just for the middle section of the basin, but for the lower part of the basin as well. The optimal metrics of mean, RBIAS and ME are represented by SM2RAIN in the lower basin part analysis, while the best optimal ME and RMSE are represented by IMERG and CMORPH, respectively.

Table 4.9 Daily metrics obtained for evaluation of satellite precipitation of post monsoon season of the basin

| Metrics | CHIRPS | CMORPH | IMERG | SM2RAIN | TRMM |
|-----------|--------|-------------|-------------|---------|------|
| POD | 0.91 | 1 | 1 | 0.99 | 1 |
| FAR | 0.08 | 0.09 | 0.09 | 0.09 | 0.09 |
| CSI | 0.84 | 0.91 | 0.91 | 0.9 | 0.91 |
| R^2 | 0.72 | 0.82 | 0.86 | 0.41 | 0.82 |
| Mean (mm) | 0.87 | 0.74 | 0.99 | 0.39 | 1.06 |

| | | | | | |
|-----------|------|--------------|------|-------|------|
| RBIAS | 0.14 | -0.02 | 0.31 | -0.48 | 0.4 |
| ME (mm) | 0.11 | -0.02 | 0.23 | -0.36 | 0.3 |
| MAE (mm) | 0.57 | 0.47 | 0.5 | 0.62 | 0.55 |
| RMSE (mm) | 1.61 | 0.91 | 1.44 | 1.8 | 1.44 |

Note: Daily mean of APHRODITE = 0.76 mm.

4.3.6 Uncertainty analysis of precipitation across the basin

In this subsection, we discuss how areal mean daily precipitation varies across different precipitation products, basins, and sections of basins. We also discuss the variation of precipitation for different seasons.

Violin plots are a useful tool for visualising the distribution (kernel density) of continuous data, especially when the data are not normally distributed. Violin plots provide more information than boxplots, which only provide summary statistics. The width of the violin plot at any given point is proportional to the density of data points at that value. Thicker sections of the violin plot indicate higher density, while thinner sections indicate lower density. In Fig.4.11(a), CHIRPS has the highest precipitation, whereas SM2RAIN has the least. However, APHRODITE and CMORPH have similar distributions, which is attributed to the latter being bias corrected using daily precipitation as opposed to using monthly precipitation for bias correction of IMERG and TRMM. This pattern of variation was also evident when continuous metrics were discussed. Additionally, CHIRPS, IMERG, and TRMM are the only products with maximum values exceeding 40 mm/day. Excluding the ungauged-corrected SM2RAIN, all the remaining precipitation products have similar distribution patterns. Furthermore, all the products exhibit bimodal distributions. What does it mean is there are two dominant frequencies of precipitation. One distribution is between zero and 5 mm/day and the other between 5 and 10 mm/day. The trends appear to be same for all the precipitation products for the middle and lower sections Fig.4.11(c)-(d) of the basin in comparison to upper part (Fig.4.11(b)).

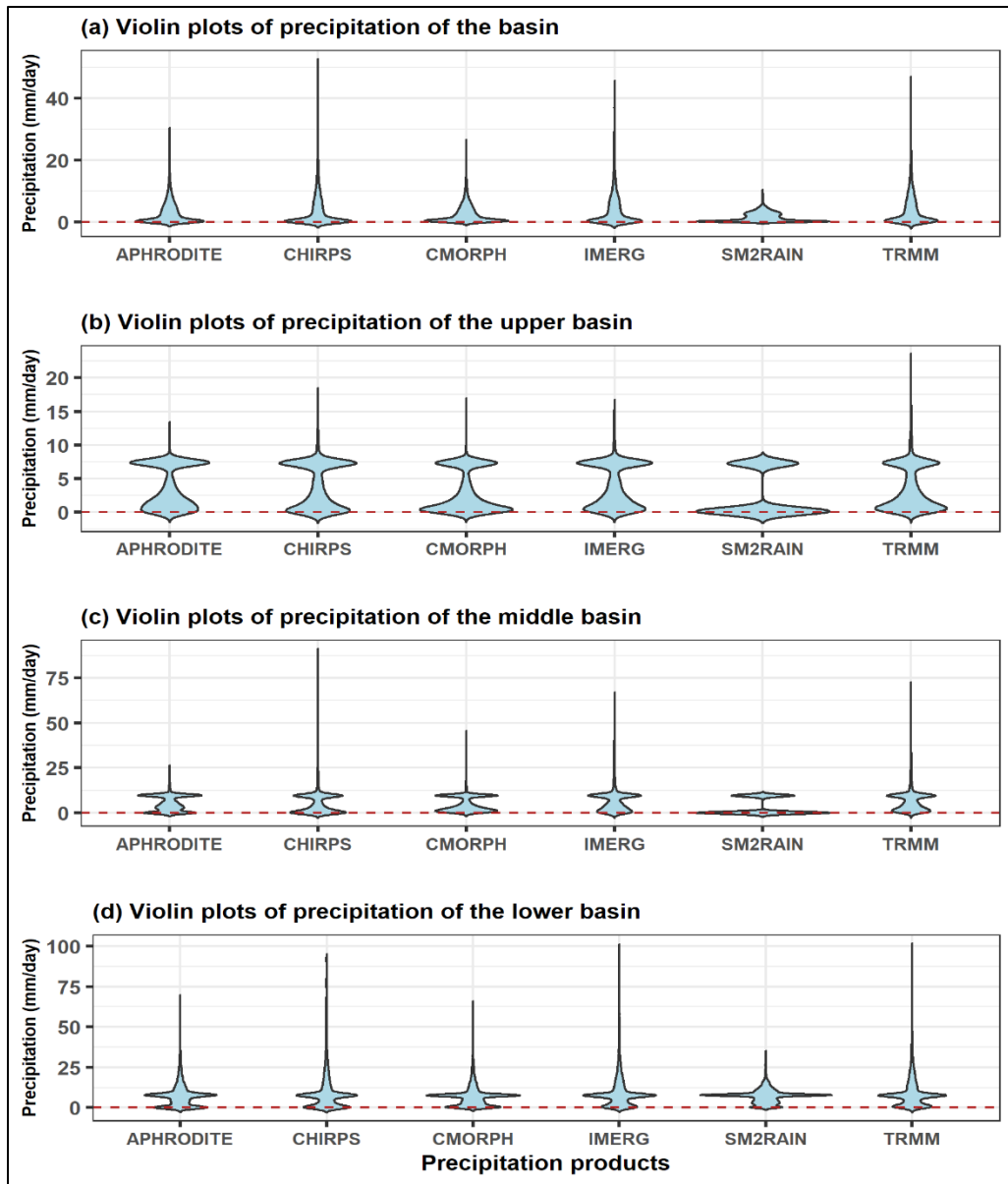


Fig.4.11 Violin plots of precipitation

The kernel density plots in Fig.4.12 show the distribution of precipitation in the winter season. The basin as a whole and the lower part do not show any distribution of rainfall magnitude (Fig.4.12(a) and (b)) because the lower section of the basin does not receive rainfall during the months of January and February (winter season). However, the upper and middle sections of the basin show a different picture, with each product following the same pattern when transitioning from one section to the other. The frequency

of lower magnitude rainfall in the upper part is skewed towards zero, whereas the upper frequency is skewed towards the range 4-8 mm/day. Similarly, the frequency of the lower magnitude of the middle basin is similar to that of the previous section, but the higher magnitude hovers around 5-10 mm/day frequency. The findings convey that winter precipitation is prevalent in the upper and middle sections of the basin.

The trends in rainfall distribution for the summer season (Fig.4.13) are similar when compared to the total time series of the basin (Fig.4.11). The magnitude of frequency of a given rainfall occurrence also appears to be similar.

In Fig.4.14, the rainfall characteristics appear to be very different for the monsoon season compared to other seasons discussed so far. All the products captured precipitation on the extremes. The flood plain of the Brahmaputra basin lies in the lower section of the basin, which is why the rainfall distribution from the monsoon season contributes over 75% of the river flow. The violin plots are evident, with their width depicting only unimodal distribution (Fig. 4.14(d)). Therefore, while considering the whole basin, the same pattern is reflected in the distribution of rainfall. A slightly perceptible frequency distribution for the upper section is visible, while no such distribution is distinguishable in the middle section of the basin.

In the post-monsoon season, the basin does not reveal any clear distribution of the data of the precipitation though the extremes are still evident as shown in Fig4.15(a). The bimodal distributions as shown by kernel density in Fig.4.15(b) for the upper part resemble to the distribution of rainfall in winter season for the same section of the basin. The higher magnitude frequency is denser than the lower magnitude frequency for this section. The frequency distribution flattens for the middle basin (Fig.4.15(c)) though the magnitude of the frequency is greater than the upper portion of the basin. It is indicative of a particular value of precipitation occurrence is lesser in frequency that the kernel density with broader distribution of data. The lower section could be likened to the middle section (Fig.4.15(d)).

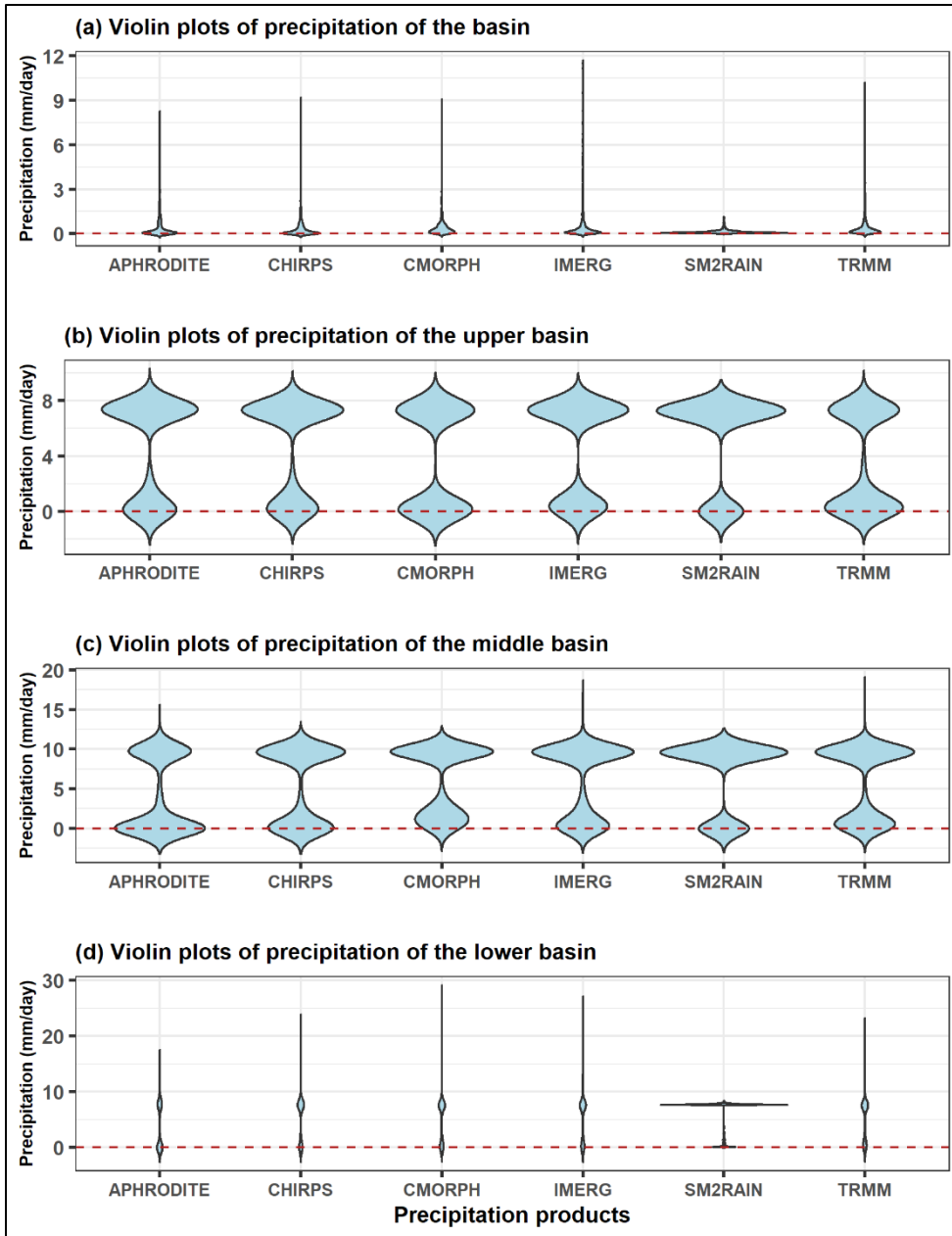


Fig.4.12 Violin plots of precipitation in winter

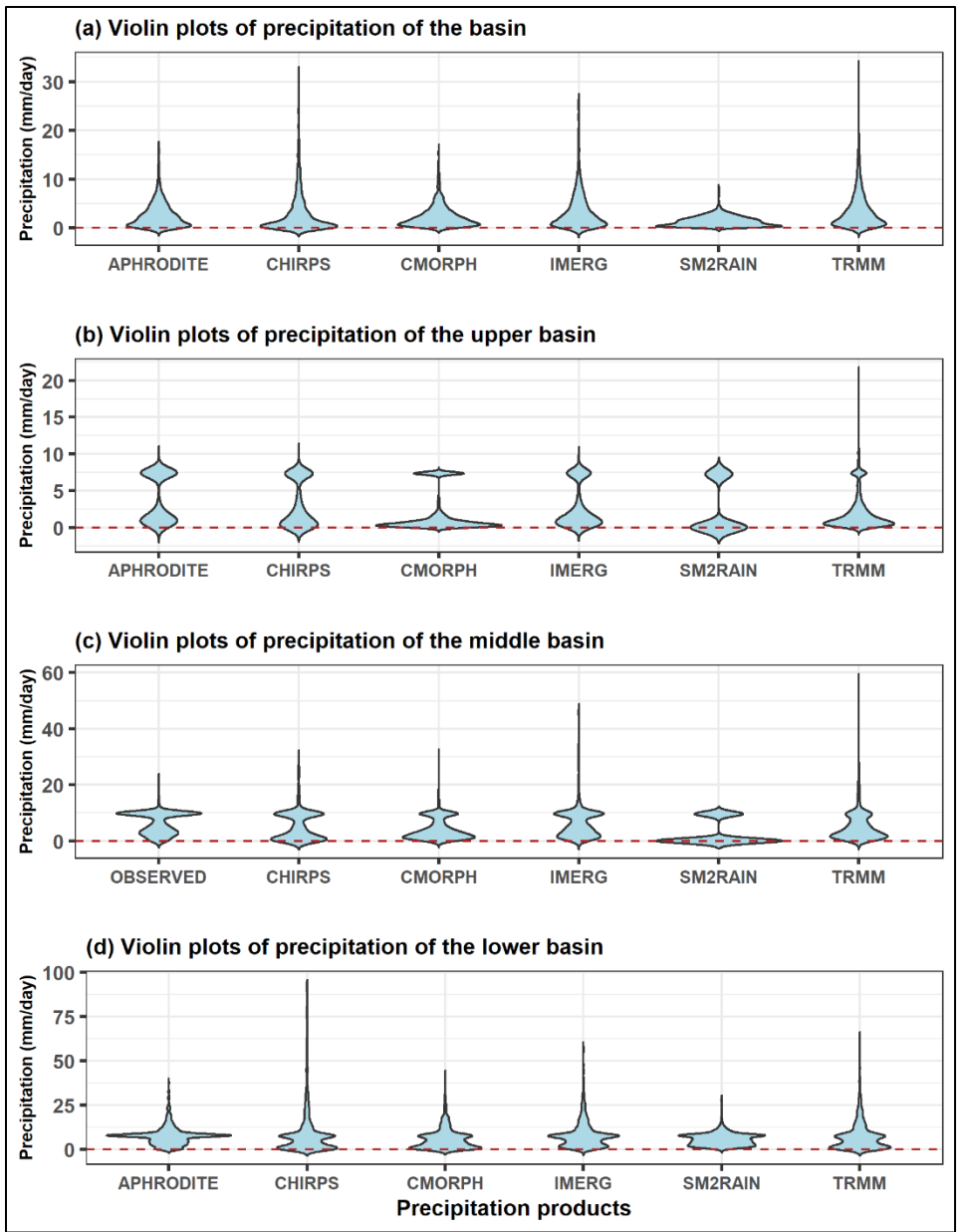


Fig.4.13 Violin plots of precipitation in summer

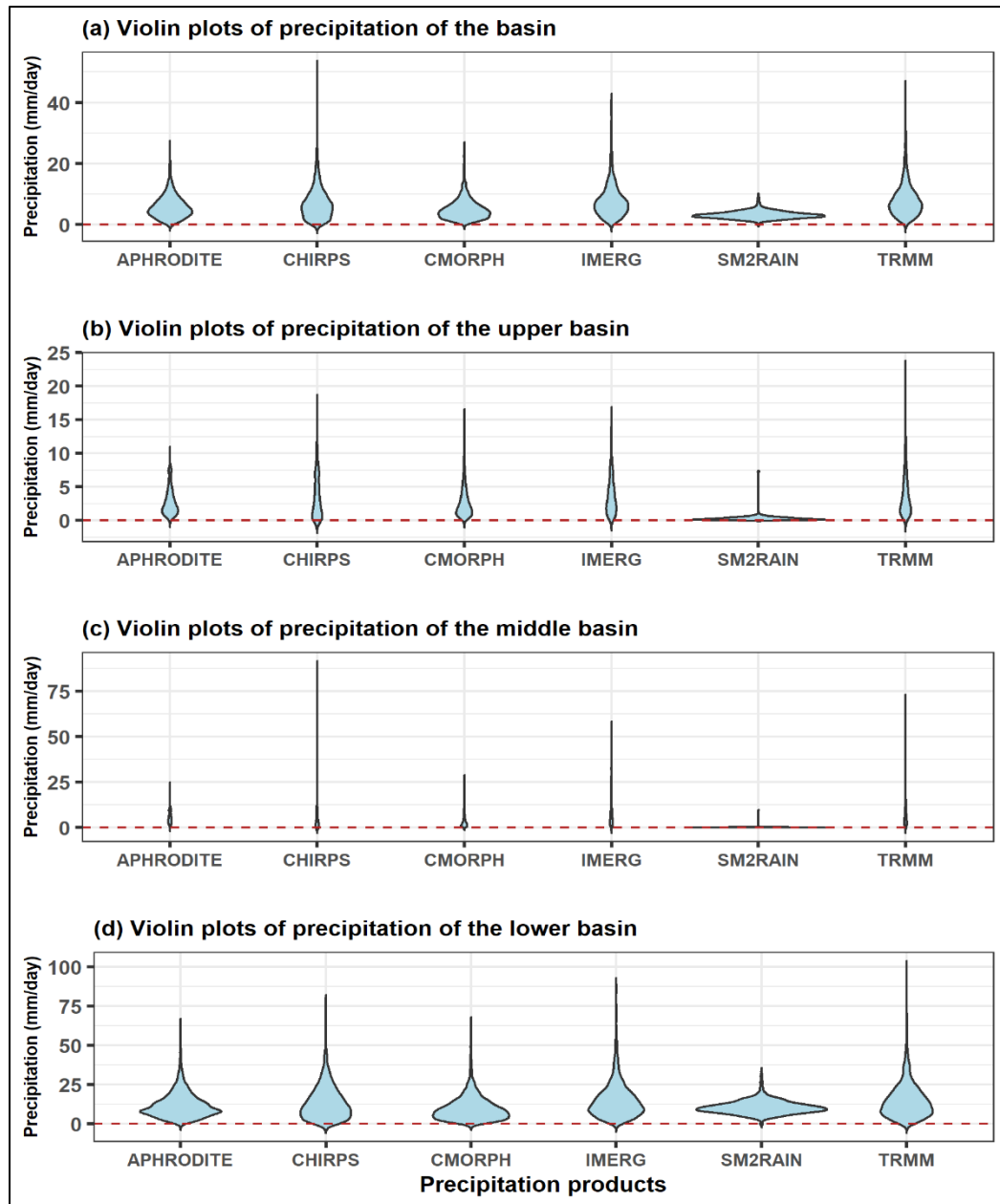


Fig.4.14 Violin plots of precipitation in monsoon

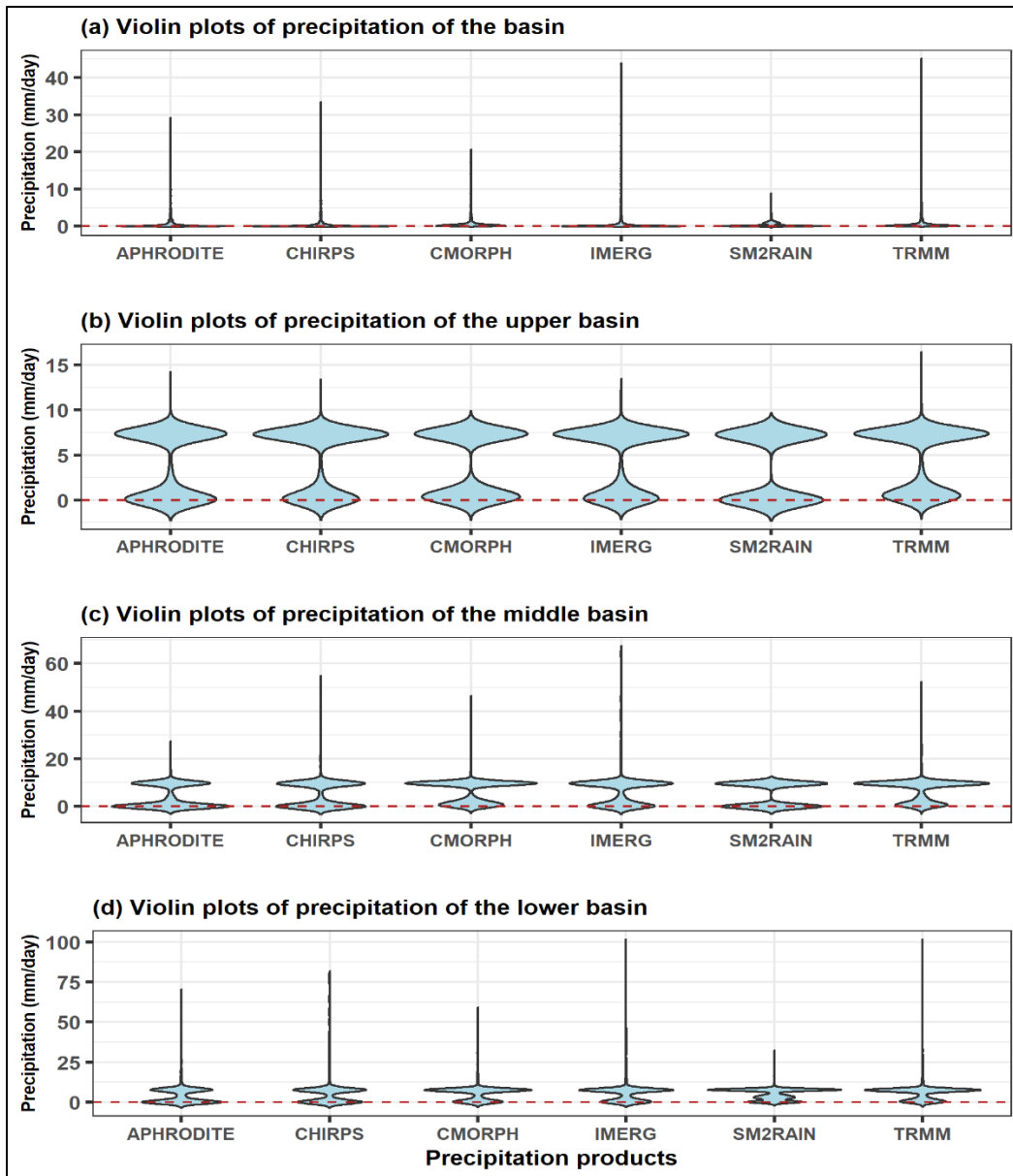


Fig.4.15 Violin plots of precipitation in post-monsoon

4.5 CONCLUSIONS

In this study, five satellite-based precipitation data were evaluated using both categorical and continuous statistical metrics against a recently updated gauge-based precipitation data on a daily basis for the whole basin as well as the different elevation-based zones of the Brahmaputra river basin. Also, temporal assessment of the precipitation

products was carried out. In addition, daily data were disaggregated in terms of winter, summer, monsoon and post-monsoon seasons. The time period of evaluation was 2001-2015.

Spatial performance:

- (a) GPM IMERG is the best-performing precipitation product overall, in terms of both POD and R2.
- (b) SM2RAIN is the worst-performing precipitation product overall.
- (c) TRMM and CMORPH perform similarly, with TRMM slightly better in terms of POD and CMORPH slightly better in terms of R2.
- (d) IMERG outperforms other precipitation products in terms of RMSE in almost all zones.

Temporal performance:

- (a) CMORPH is the best-performing precipitation product in terms of the number of optimal metrics it performs across the basin and the elevation-based zones for the whole time series.
- (b) IMERG is very close to CMORPH in terms of the total number of optimal metrics obtained for the whole-time length.
- (c) CMORPH is the best-performing precipitation product for the monsoon and post-monsoon seasons in terms of the total number of optimal metrics obtained.
- (d) IMERG is the best-performing precipitation product for the winter season in terms of the number of optimal metrics it performs.
- (e) CMORPH and IMERG are the best-performing precipitation products for the summer season.

Overall conclusion:

- (a) IMERG is the best-performing precipitation product overall, considering the spatial and temporal mean for the whole time series.
- (b) CMORPH is the best-performing precipitation product on a seasonal basis.

(c) SM2RAIN is the least-performing precipitation product on all counts.

EVALUATION OF PRECIPITATION FOR RISK ASSESSMENT OF WATER CYCLE VARIABLES

5.1 OVERVIEW

No water budget variable occurs in isolation because there is an interplay between different variables in a river basin like the Brahmaputra. To assess the risk associated with ET, Q and TWSC, three different precipitation data ranging from gauge to reanalysis data were used. IMERG was chosen because of its overall performance and ERA5 being a model-based precipitation product was introduced to compare its performance with IMERG and the gauge-based APHRODITE data. Bivariate copula dependence measure was used to predict the first three variables given certain thresholds of precipitation amount.

5.2 METHODS

The dependence measure between random variables is often determined using Pearson's correlation based on the normal distribution. However, such an assumption could be misleading while dealing with hydrometeorological variables having a nonlinear relationship between such random variables. Moreover, a nonlinear relationship also warrants the application of non-normal distributions. In this context, copula has been around for nearly two decades in hydrologic sciences opening new understanding and insights embedded in hydrometeorological variables. The copula is attractive and advantageous over traditional bivariate methods. It is flexible to model two random variables (bivariate case) irrespective of the marginal distributions and handle linear and nonlinear variables. According to Sklar's (1959) theorem, if X and Y are the continuous random variables, then their joint distribution $H_{XY}(x, y)$ and $C: [0,1]^2 \rightarrow [0,1]$ copula is connected as:

$$H_{XY}(x, y) = F_{XY}(x, y) = C[F_X(x), F_Y(y)] = C(u, v) \quad , x, y \in R \quad 5.1$$

where $F_X(x)$ and $F_Y(y)$ are the cumulative distribution functions of X and Y , respectively. In general, Archimedean copulas carry the following expressions:

$$C(u, v) = \phi^{[-1]}[\phi(u) + \phi(v)], \quad u, v \in [0, 1] \quad 5.2$$

where $\phi(\bullet)$ is a generator function of the copula and $\phi^{[-1]}(\bullet)$ is the pseudo-inverse of $\phi(\bullet)$. The flexibility and ease of construction make Archimedean copulas widely used in different research areas with well-established copula functions (Genest and Favre 2007; Nelsen 2006; Zhang and Singh 2006). The Archimedean copulas, viz., Clayton, Frank, and Gumbel-Hougaard copulas, were applied in this study. The details of such copulas are as shown in Table 5.1

Table 5.1 Description of the most commonly used Archimedean copulas

| Copula | CDF of copula, $C(u, v)$ | Function generator, ϕ_α | Range of parameter r | Kendall's tau, τ_α |
|-------------------|--|---|------------------------|---|
| Clayton | $(u^{-\alpha} + v^{-\alpha} - 1)^{-1/\alpha}$ | $(t^{-\alpha} - 1)/\alpha$ | $\alpha \geq -1$ | $\alpha/(\alpha + 2)$ |
| Frank | $-\left(\frac{1}{\alpha}\right) \ln \left[1 + \frac{(e^{-\alpha u} - 1)(e^{-\alpha v} - 1)}{(e^{-\alpha} - 1)} \right]$ | $-\ln \left(\frac{e^{-\alpha t} - 1}{e^{-\alpha} - 1} \right)$ | $\alpha \in R$ | $1 - \left(\frac{4}{\alpha}\right) + 4D_1(\alpha) / \alpha$ |
| Gumbel - Hougaard | $\exp(-[(-\ln u)^\alpha + (-\ln v)^\alpha]^{1/\alpha})$ | $(-\ln t)^\alpha$ | $\alpha \geq 1$ | $(\alpha - 1)/\alpha$ |

Note: $D_1(\alpha) = \int_0^\alpha \left(\frac{x}{\alpha}\right) / (e^x - 1) dx$ denotes the first Debye function.

The conditional distribution of a continuous variable for a value of another continuous variable could be obtained once the joint probability distribution function between the random variables is known. Then for the bivariate case, the probability

distribution of U conditioned on $V \leq v$ is given as (Uttarwar et al. 2020; Zhang and Singh 2006):

$$C_{(U|V \leq v)} = C(U \leq u | V \leq v) = \frac{C(u, v)}{v} \quad 5.3$$

In the present study, the single-parameter copulas were used to study the two extrema of TWSC, ET, and streamflow, viz., non-exceedance probability (\leq 5th percentile) for the lower extreme and the exceedance probability (\geq 95th percentile) for the upper extreme given different scenarios of precipitation (5th, 25th, 50th, 75th, and 95th percentiles).

The following steps were followed for the current study:

- (i) Select any two random variables between a precipitation dataset and TWSC or ET or streamflow.
- (ii) Determine the statistically significant dependence measure using rank based Spearman's rho (like Pearson's correlation, but calculated on ranked values) for the two selected variables, for example, precipitation and TWSC. It The correlation will help us decide whether to go ahead with dependence modelling.
- (iii) Fit the parametric theoretical distributions, viz., gamma, logistic, lognormal, and Weibull to precipitation, TWSC, ET, and streamflow. The best fit marginal distribution for each variable is obtained using the Kolmogorov–Smirnov (KS) goodness of fit test.
- (iv) Obtain copula parameter using the pseudo-maximum-log-likelihood (MLE) method (1000 simulations) for all the copulas.
- (iv) Obtain the best-fit copula based on Akaike Information Criterion (AIC), the lowest being the best.

$$AIC = -2 \ln MLE + 2 \text{ (no. of fitted parameters)} \quad 5.4$$

$$AIC = N \ln MSE + 2 \text{ (no. of fitted parameters)} \quad 5.5$$

$$AIC = 2 N \ln(RMSE) + 2 (\text{no. of fitted parameters}) \quad 5.6$$

The root mean square error ($RMSE$) is related to the mean square error (MSE) as $RMSE = \sqrt{MSE}$. Therefore, MSE may be expressed as (Chen and Guo 2019):

$$MSE = \frac{1}{n} \sum_{i=1}^n (C_n(u_i, v_i) - C_{\theta_m}(u_i, v_i))^2 \quad 5.7$$

where $C_n(u_i, v_i)$ is the empirical copula (observed) joint probability for the i^{th} observation and $C_{\theta_m}(u_i, v_i)$ is the simulated copula for m parameters in Θ .

In addition, the Nash-Sutcliffe efficiency equation (NSE) was used to confirm the findings of AIC by expressing it in the following:

$$NSE = 1 - \frac{\sum_{i=1}^n (C_{ei} - C_{fi})^2}{\sum_{i=1}^n (C_{ei} - \bar{C}_e)^2} \quad 5.8$$

where C_{ei} is the empirical copula of i^{th} observation, C_{fi} is the fitted copula of i^{th} observation and \bar{C}_e is the mean of the empirical copula of all the n observations.

(v) Derive conditional probability distribution of TWSC, ET, and streamflow given the explanatory variable, precipitation.

5.3 RESULTS

5.3.1 Identification of Marginal Distribution of Precipitation, TWSC, ET, and Discharge

The best marginal distribution for APHRODITE and IMERG precipitation is gamma at 5% significance level and lognormal for ERA5 precipitation at 10% significance level as per the KS statistics shown in Table 5.2. The optimal marginal distribution for ERA5 and the other two precipitations could be due to differences in magnitudes; lower values of ERA5 are higher than those of the other two precipitation products. Moreover, IMERG is gauge-corrected satellite precipitation, which could resemble APHRODITE derived from gauge precipitation.

Table 5.2 KS statistics of different marginal distributions fitted to precipitation

| Marginal distribution | APHRODITE | ERA5 | IMERG |
|-----------------------|-------------------------|--------------------------|--------------------------------|
| Gamma | 0.1112 (0.0539*) | 0.0769(0.3483) | 0.1120 (0.0506*) |
| Normal/Lognormal | 0.1428(0.0056) | 0.1021 (0.0945**) | 0.1515(0.002654), Lognormal |
| Weibull | 0.1128(0.0483) | 0.0771(0.3453) | 0.1143(0.0440) |

Note: * indicates p-value at 5% level of significance **indicates p-value at 10 % level of significance. Bold figures indicate optimal distribution.

The theoretical cumulative distribution curves are visually compared with the empirical distribution for each precipitation in Fig. 5.1. TWSC being in anomaly form, could be fitted only by kernel density functions like normal and quadratic, but among them only normal kernel density function was fitted in this study. Hence, no KS statistics were calculated, as shown in Table 5.3. Logistic and lognormal distributions, respectively, best represented ET and discharge. The cumulative distribution function curves of TWSC, ET, and discharge are presented in Fig. 5.2 compared to their corresponding empirical distribution curves.

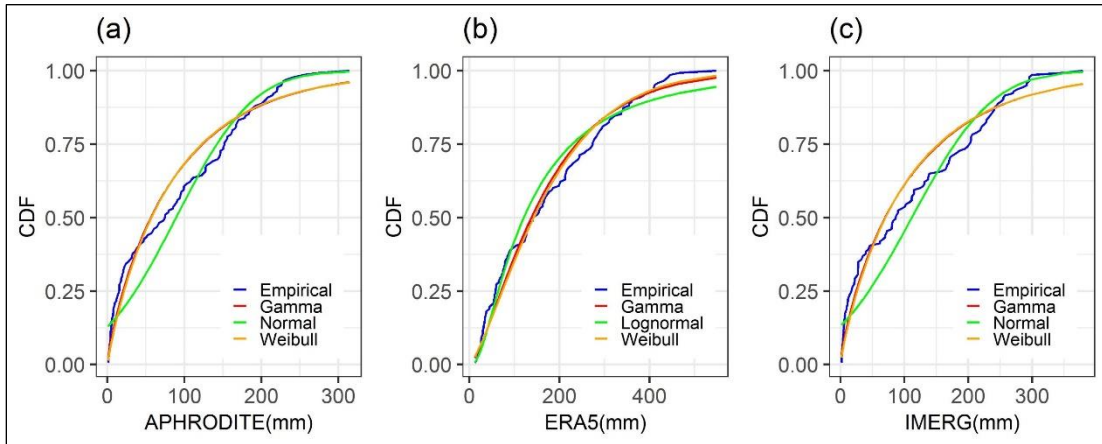


Fig.5.1 Cumulative distribution function plots of precipitation products.

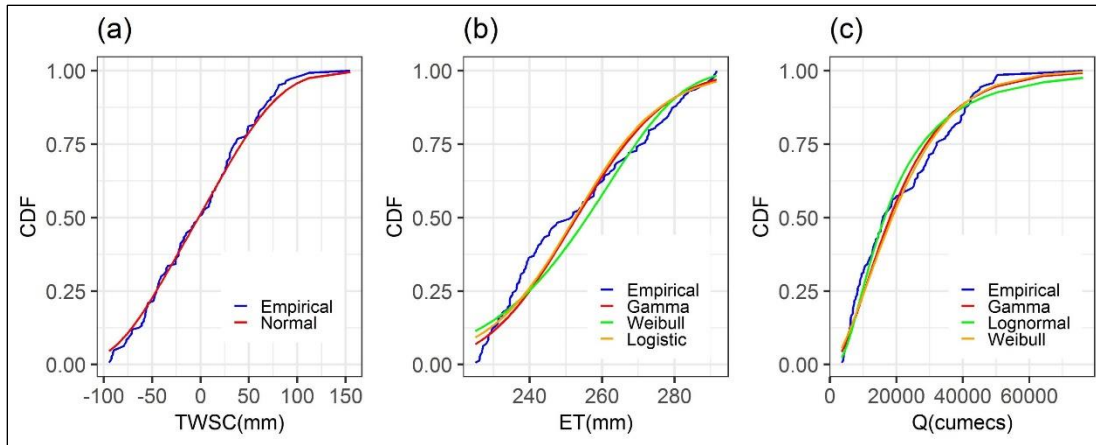


Fig.5.2 Cumulative distribution function plots of dependent variables

5.3.2 Dependence Modelling of Precipitation with TWSC, ET, and Discharge

The bivariate Archimedean copulas were constructed using the optimal marginal distribution for each variable. All the Archimedean copulas simulated for different pairs of precipitation and other water budget variables are shown in Table 5.4 - 5.6. Similar to the concept by Tao et al.(2020), Pearson's linear and Spearman's rank correlations were obtained for each pair of variables. All the pairs are either optimally represented by Frank or Clayton copulas, as shown in Table 5.7. The correlations (Pearson's and Spearman's) between all precipitation products (APHRODITE, ERA5, and IMERG) and TWSC and ET are significant for both observed and simulated data.

Table 5.3 KS statistics of different marginal distributions fitted to dependent variables

| Marginal distribution | TWSC | Evapotranspiration(ET) | Discharge(Q) |
|-----------------------|---------|-----------------------------------|-------------------------|
| Gamma | - | 0.1169(0.0369) | 0.0842(0.2483) |
| Weibull | - | 0.1282(0.0165) | 0.0832(0.2607) |
| Logistic/Lognormal | - | 0.1059 (0.0751**),logistic | 0.1095 (0.0599*) |
| Normal kernel | Optimal | - | - |

Note: * indicates 5% level of significance **indicates 10 % level of significance
 Bold figures indicate optimal distribution

Table 5.4 Performance statistics of precipitation-TWSC pair

| APHRODITE-TWSC | | | | |
|---------------------|-------------------------------|----------------|--------------|-------------|
| Copula | Copula parameter, α | AIC | RMSE | NSE |
| Clayton | 1.78 | -797.16 | 0.061 | 0.95 |
| Frank | 5.92 | -825.72 | 0.055 | 0.96 |
| Gumbel- Hougaard | 2.05 | -808.71 | 0.059 | 0.96 |
| ERA5-TWSC | | | | |
| Clayton | 1.25 | -933.54 | 0.038 | 0.98 |
| Frank | 6.39 | -994.14 | 0.031 | 0.99 |
| Gumbel- Hougaard | 2.23 | -991.25 | 0.031 | 0.99 |
| IMERG-TWSC | | | | |
| Clayton | 1.71 | -792.24 | 0.062 | 0.95 |
| Frank | 5.54 | -815.66 | 0.057 | 0.96 |
| Gumbel- Hougaard | 1.97 | -798.64 | 0.061 | 0.95 |

Table 5.5 Performance statistics of precipitation-ET pair

| APHRODITE-ET | | | | |
|---------------------|-------------------------------|----------------|--------------|-------------|
| Copula | Copula parameter, α | AIC | RMSE | NSE |
| Clayton | 2.20 | -896.69 | 0.043 | 0.98 |
| Frank | 10.09 | -887.83 | 0.045 | 0.98 |
| Gumbel- Hougaard | 3.04 | -851.67 | 0.051 | 0.97 |
| ERA5-ET | | | | |

| | | | | |
|---------------------|-------------|----------------|--------------|-------------|
| Clayton | 1.74 | -879.66 | 0.046 | 0.98 |
| Frank | 9.24 | -900.99 | 0.043 | 0.98 |
| Gumbel- Hougaard | 2.80 | -869.28 | 0.048 | 0.97 |
| IMERG-ET | | | | |
| Clayton | 2.36 | -892.72 | 0.044 | 0.98 |
| Frank | 10.88 | -881.32 | 0.046 | 0.98 |
| Gumbel- Hougaard | 3.19 | -843.36 | 0.052 | 0.97 |

Table 5.6 Performance statistics of precipitation-Q pair

| APHRODITE-Q | | | | |
|---------------------|-------------------------------|----------------|--------------|-------------|
| Copula | Copula parameter, α | AIC | RMSE | NSE |
| Clayton | 0.26 | -932.99 | 0.038 | 0.98 |
| Frank | 1.84 | -930.71 | 0.038 | 0.98 |
| Gumbel- Hougaard | 1.32 | -890.93 | 0.044 | 0.97 |
| ERA5-Q | | | | |
| Clayton | 0.15 | -947.51 | 0.036 | 0.98 |
| Frank | 1.63 | -956.96 | 0.035 | 0.98 |
| Gumbel- Hougaard | 1.29 | -917.88 | 0.040 | 0.98 |
| IMERG-Q | | | | |
| Clayton | 0.29 | -932.62 | 0.038 | 0.98 |
| Frank | 1.98 | -931.15 | 0.038 | 0.98 |
| Gumbel- Hougaard | 1.35 | -887.05 | 0.045 | 0.97 |

However, the correlations of the precipitation products with discharge are significant only for the observed values ($r=0.38-0.45$, $\rho=0.35-0.4$). In comparison, the correlations for simulated precipitation-discharge pairs are lesser ($r=0.09-0.22$, $\rho=0.19-0.6$). The correlations for precipitation-TWSC and precipitation-ET pairs are higher than those of precipitation-discharge pairs because the lags between the pairs may not influence much on the dependence measure of the first two pairs more than the last pair. This is true when precipitation occurs; ET also occurs without much time lag. The same is true with the occurrence of precipitation; the amount of TWSC is manifested with little elapse of time. The common rainfall-runoff concept demonstrates how rainfall occurring at a particular time in a given day or cumulative rainfall occurring in a given month may influence discharge at the outlet in days or months. As a result, the dependence measure expressed in Spearman's rank correlation and Pearson's linear correlation is found to be lesser for the precipitation-discharge pair than the other two pairs.

Table 5.7 Performance measures of the optimal copula of different pairs of the water cycle variables

| Pair | Optimal copula | Copula parameter (Θ) | Pearson's linear correlation (r) | | Spearman's rank correlation(ρ) | |
|--------------------|----------------|-------------------------------|----------------------------------|-----------|---------------------------------------|------------|
| | | | Observed | Simulated | Observed | Simulated* |
| APHRODITE_ TWSC | Frank | 5.9233 | 0.7639 | 0.5911 | 0.7658 | 0.7083 |
| ERA5_TWSC | Frank | 6.3882 | 0.7786 | 0.5553 | 0.7733 | 0.7511 |
| IMERG_TWSC | Frank | 5.5380 | 0.7437 | 0.6041 | 0.7517 | 0.7240 |
| APHRODITE_ ET | Clayton | 2.1978 | 0.9024 | 0.4989 | 0.8893 | 0.7007 |
| ERA5_ET | Frank | 9.2382 | 0.8895 | 0.6182 | 0.8718 | 0.8371 |
| IMERG_ET | Clayton | 2.3581 | 0.9107 | 0.5499 | 0.8956 | 0.7491 |
| APHRODITE_ Q | Clayton | 0.2606 | 0.4237 | 0.0903 | 0.3829 | 0.1863 |
| ERA5_Q | Frank | 1.6343 | 0.3871 | 0.2239 | 0.3514 | 0.5971 |

| | | | | | | |
|---------|---------|--------|--------|--------|--------|--------|
| IMERG_Q | Clayton | 0.2888 | 0.4531 | 0.1032 | 0.4008 | 0.1905 |
|---------|---------|--------|--------|--------|--------|--------|

Note: *Correlation is calculated from simulation values of 1000 data samples.

The scatter diagrams in Fig.5.3 and Fig.5.4 show that the simulated values of precipitation-TWSC and precipitation-ET pairs represent the observed values well. The scatter plots of APHRODITE and IMERG with TWSC look similar in pattern because both precipitations are connected to the gauge dataset. The scatter plots (Fig.5.5) for precipitation-discharge look different from the other two pairs, as evident from the linear and rank correlations.

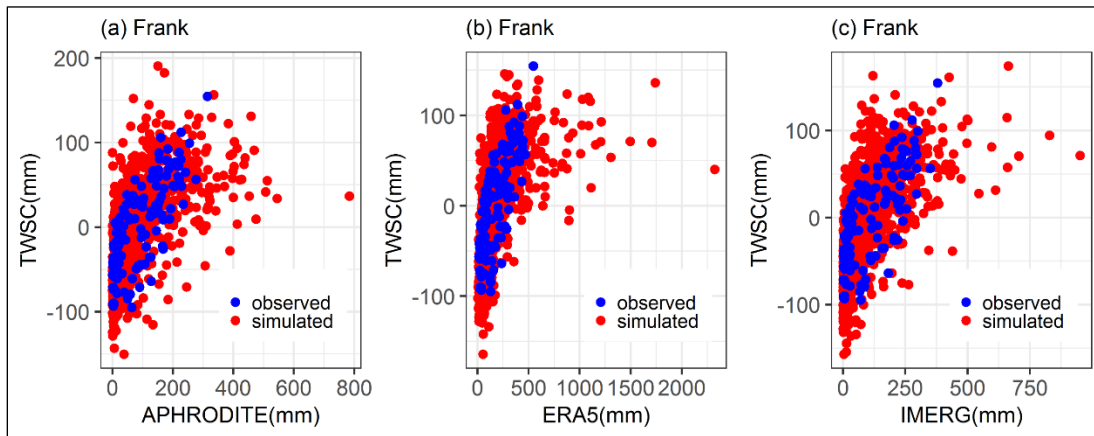


Fig.5.3 Scatter diagrams of different precipitation-TWSC pairs

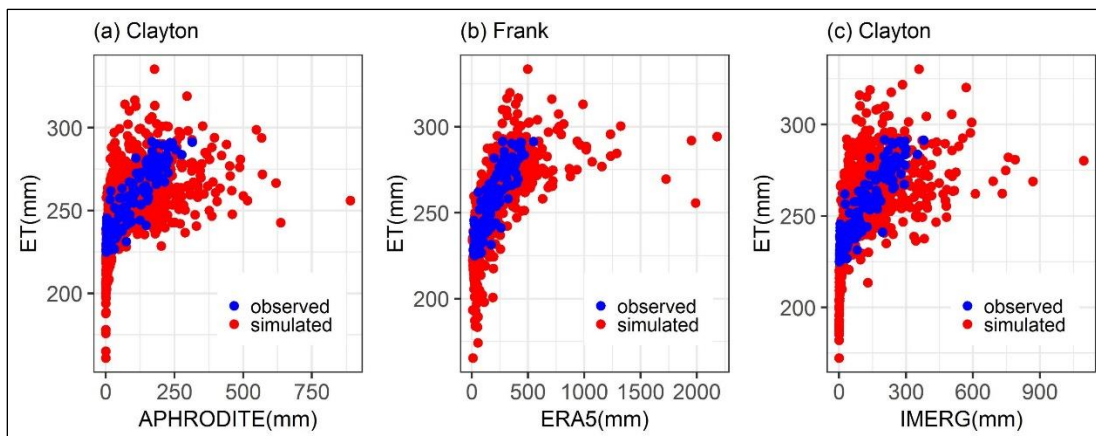


Fig.5.4 Scatter diagrams of different precipitation-ET pairs

5.3.3 Risk Evaluation Of Twsc Conditioned On Different Precipitation Scenarios

The conditional distribution of TWSC under different precipitation scenarios could be evaluated once the joint distribution between TWSC and a given precipitation scenario is obtained. The risk evaluation of the occurrence of an event is associated with the exceedance/ non-exceedance of the TWSC for a given threshold of explanatory variable precipitation (Liu et al., 2018; Salvadori and De Michele, 2004). The next step is to evaluate the probability of occurrence of TWSC under five different precipitation scenarios on establishing joint distribution, as shown in Table 5.7. To achieve this, two scenarios of TWSC were investigated ($TWSC \leq 5^{th}$ percentile and $TWSC \geq 95^{th}$ percentile as shown in Table 5.9) for every precipitation scenario. For example, the probabilities of occurrence of an event ($TWSC \leq 5^{th}$ percentile from Fig. 5.6) for different scenarios of gauge-based APHRODITE precipitation are 28%, 26%, 16%, 10%, and 8%, corresponding to 5th, 25th, 50th, 75th, and 95th percentiles, respectively.

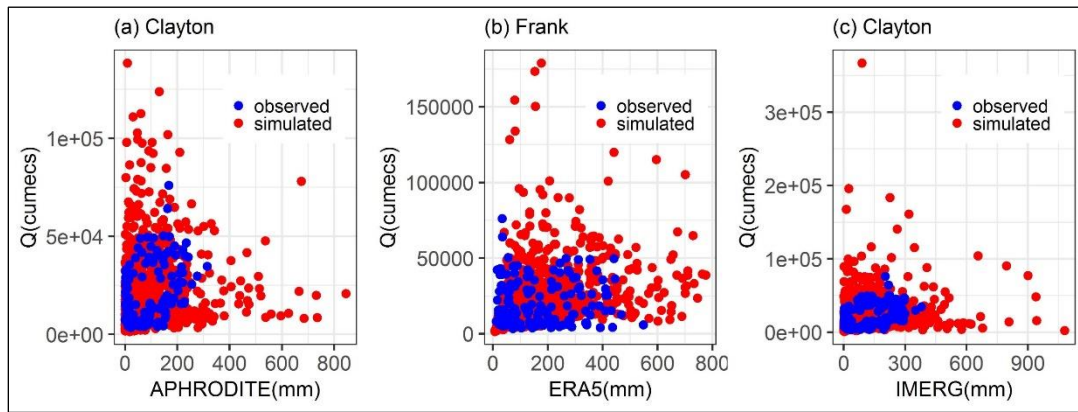


Fig.5.5 Scatter diagrams of different precipitation-Q pairs

Table 5.8 Magnitudes of precipitation corresponding to each percentile

| Precipitation | Percentile | | | | |
|-------------------|------------|---------|---------|----------|----------|
| | 5th | 25th | 50th | 75th | 95th |
| APHRODITE (mm) | 2.7453 | 15.2911 | 74.5768 | 151.8014 | 205.0797 |
| ERA5 (mm) | 24.2 | 58.5 | 144 | 274 | 361.6 |

| | | | | | |
|------------|----------|----------|----------|----------|----------|
| IMERG (mm) | 3.177638 | 17.78558 | 86.51642 | 201.9606 | 253.9442 |
|------------|----------|----------|----------|----------|----------|

Table 5.9 Magnitudes of the dependent variable corresponding to each percentile

| Dependent variable | Percentile | |
|----------------------------------|------------|----------|
| | 5th | 95th |
| TWSC (mm) | -84.1232 | 71.7037 |
| Evapotranspiration (ET) (mm) | 227.0304 | 281.7144 |
| Discharge(Q) (m ³ /s) | 4751.536 | 42238.01 |

Similarly, the probability of the lower value of TWSC ($\leq 5^{\text{th}}$ percentile) for the same precipitation scenarios of gauge-corrected satellite-based GPM-IMERG and reanalysis ERA5 follows a very similar pattern.

The conditional distribution of TWSC $\geq 95^{\text{th}}$ percentile (Fig.5.6) increases with precipitation (for the same precipitation scenarios). For example, the conditional distribution of TWSC for APHRODITE precipitation scenarios is less than 1% for 5^{th} ($100 - 99.718 = 0.28\%$), 25^{th} (0.32%) and 50^{th} (0.83%) percentiles. However, the conditional probabilities are about 4% and 8%, respectively, for precipitation less than equal to the 75^{th} and 95^{th} percentiles. Similar is the case for GPM-IMERG and ERA5.

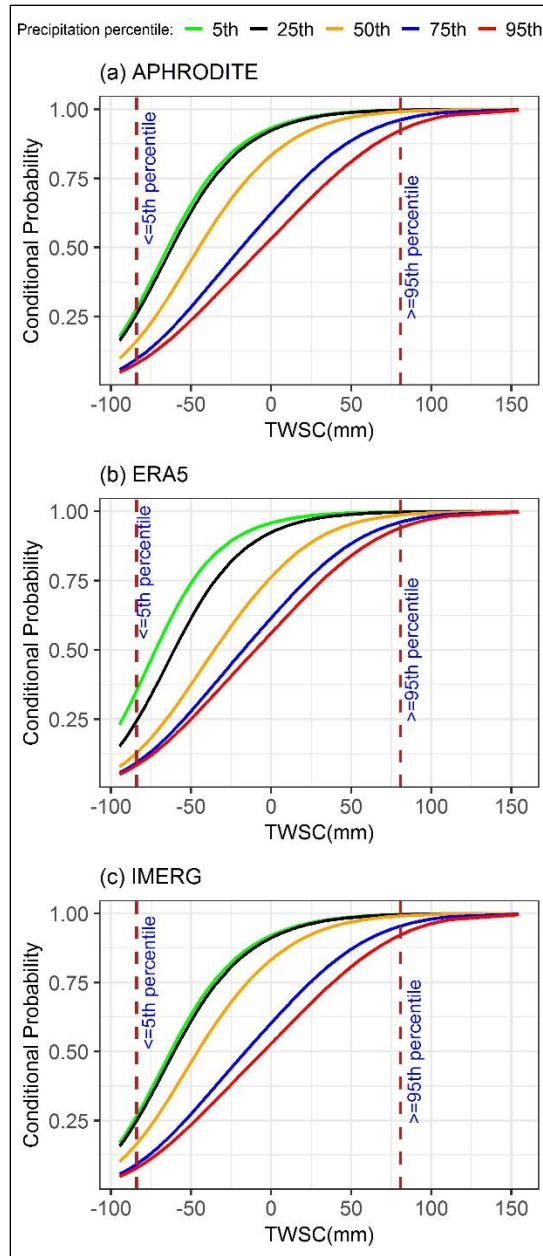


Fig.5.6 Conditional distribution plots of TWSC given different precipitation products

5.3.4 Risk Evaluation of ET Conditioned on Different Precipitation Scenarios

The joint distribution of APHRODITE-ET is applied to obtain the conditional distribution of ET for different scenarios of APHRODITE. The conditional probabilities of $ET \leq 5^{\text{th}}$ percentile (Table 5.9 and Fig. 5.7(a)) are 92, 48, 18, 13, and 12 %, corresponding to the APHRODITE precipitation values at 5th, 25th, 50th, 75th, and 95th percentiles.

Similarly, the conditional probabilities of ET at its lower end ($\leq 5^{\text{th}}$ percentile), given the precipitation scenarios of IMERG are almost identical to that of APHRODITE. However, the conditional probabilities of ET given the scenarios of ERA5 are lesser than that of the other two precipitation datasets up to $\leq 25^{\text{th}}$ percentile (Fig. 5.7(b)).

The conditional probability of mean ET ($\geq 95^{\text{th}}$ percentile) (Table 5.9 and Fig.5.7) for all the scenarios of precipitation lies between 0 and 5. It means that the higher events of precipitation have a lesser effect on the evapotranspiration process.

5.3.5 Risk Evaluation of Q Conditioned on Different Precipitation Scenarios

The conditional distribution of Q for different precipitation scenarios (5^{th} to 95^{th} percentiles) decreases with the increase in precipitation. The probabilities of the $Q \leq 5^{\text{th}}$ percentile (Table 5.9 and Fig. 5.8 (a)) are approximately 20%, 12%, 7%, 6% and 6 %, corresponding to APHRODITE precipitation at 5^{th} to 95^{th} percentiles, respectively.

Similarly, for IMERG precipitation, the probabilities of occurrence of $Q \leq 5^{\text{th}}$ percentile are approximately 22%, 13%, 8%, 6%, and 6 % (Fig. 5.8(c)) at 5^{th} to 95^{th} percentiles, respectively. Furthermore, for ERA5 precipitation, the probabilities of occurrence of $Q \leq 5^{\text{th}}$ percentile are approximately 10%, 9%, 7%, 6%, and 6 %, (Fig. 5.8(b)) at 5^{th} to 95^{th} percentiles, respectively.

The conditional probabilities of the $Q \geq 95^{\text{th}}$ percentile (Table 5.9 and Fig.5.8) for different scenarios of precipitation increase with the increase in precipitation. Also, given the scenarios of all three precipitation products, the probability of occurrence is between 4 and 9 %.

Precipitation percentile: 5th 25th 50th 75th 95th

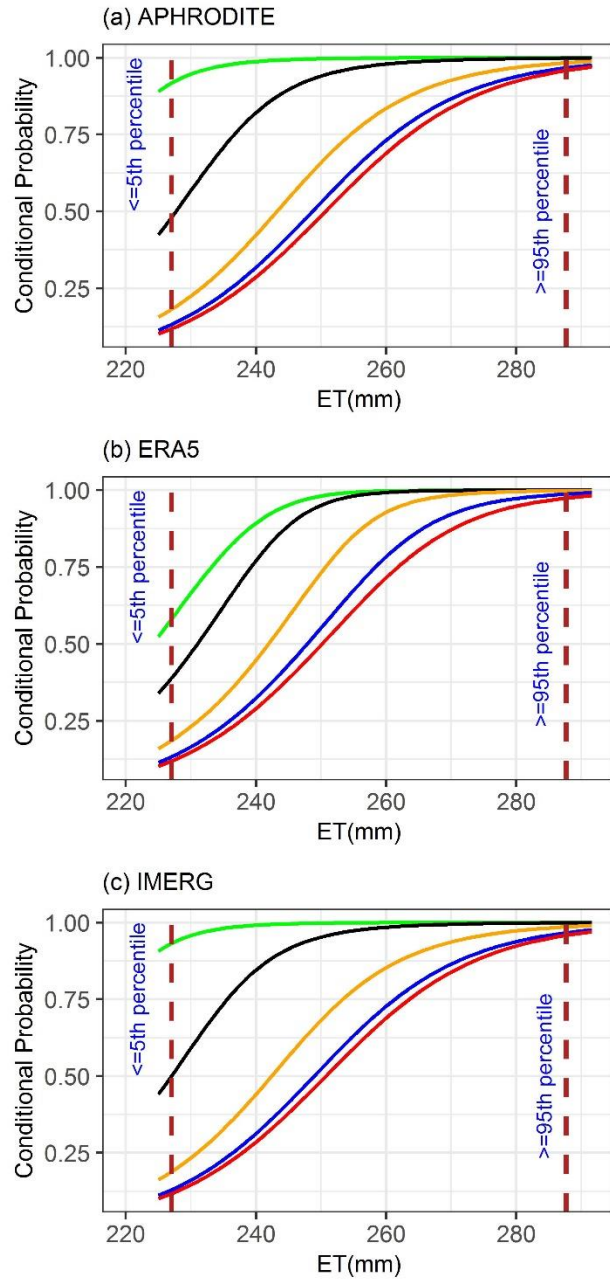


Fig. 5.7 Conditional distribution plots of ET given different precipitation products

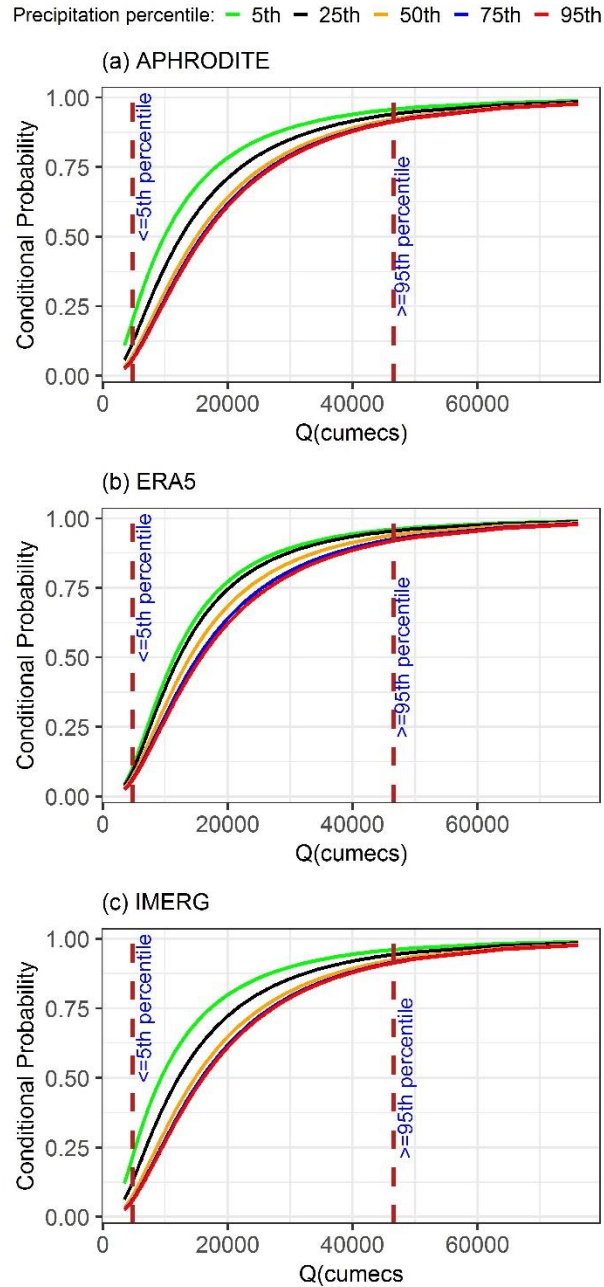


Fig.5.8 Conditional distribution plots of Q given different precipitation products

5.4 DISCUSSION

The risk assessment of the occurrence of an event is the exceedance/ non-exceedance probability of the GRACE terrestrial water storage change (TWSC), evapotranspiration (MODIS-16 ET), and discharge (Q) for a given threshold of explanatory variable

precipitation derived from in-situ measurement (APHRODITE), model-based reanalysis (ERA5), and gauge corrected satellite-based data (GPM IMERG). The study attempted to probabilistically predict the dependent water budget variables, namely, TWSC, ET, and Q for five scenarios of precipitation derived from various sources. We proved the hypothesis that precipitation data ERA5 and IMERG are equally helpful as APHRODITE to predict the non-exceedance and exceedance probabilities of the dependent variables.

5.4.1 Assessment of Risk of TWSC for given Precipitation Scenarios

The magnitude of the non-exceedance probability of TWSC (≤ 5 percentile) for different scenarios of ERA5 follow a very similar pattern to that of when obtained for the scenarios of APHRODITE. In contrast, the conditional distributions of TWSC with respect to IMERG lie between the other two products. It is observed that lower values of TWSC are more sensitive to lower precipitation values for all the precipitation products. In contrast, the sensitivity of TWSC reduces with an increase in precipitation. For instance, when precipitation is less than equal to the 95th percentile, the sensitivity of TWSC reduces by about a third/fourth of when precipitation is less than equal to the 5th percentile. This could be because smaller rainfall events have more opportunity for infiltration and get into the groundwater system than for larger storm events, which could flow as runoff to surface water bodies.

The harmonization of low extremes precipitation and TWSC occur during November – January and high extremes during June – September, which is similarly reported by Jia et al.(2020). Though the periods of harmonization are different, the present study covers not only the upper part of the Brahmaputra basin but also the whole basin. Moreover, there was a modulation between wetness and dryness of the lower and upper parts of the basin (Chun et al. 2020). The dependence structure of the joint distribution of TWSC-precipitation can evaluate the risk to about the same degree irrespective of precipitation data (Bibi et al. 2019). This is helpful, particularly for Brahmaputra basin, which is poorly gauged due to inhospitable terrain and has varying topographic features and climate making it too difficult to record in-situ hydrometeorological data.

5.4.2 Assessment of Risk of ET for given Precipitation Scenarios

ET is the link between water and energy budgets. Hence, it is necessary to understand its role in water budget and cycle components assessment. ET estimation could be useful to determine the water availability of the basin (Li et al. 2019).

The non-exceedance probability of ET beyond 25th percentile of ERA5 is similar to that of the other two precipitation data. This behavior of lower probabilities of occurrence of ET may be attributed to the higher precipitation amount of ERA5 for lower percentiles ($\leq 5^{\text{th}}$, 25th) because it is seen that with the increase in the precipitation, the probabilities of ET decrease.

Lower precipitation events have higher chances of evaporating than higher ones. It is evident from the values of APHRODITE and IMERG precipitation (Fig.5.7 (a), (c)) at $\leq 5^{\text{th}}$ percentile, which is about 1/8 of ERA5, as shown in Table 5.8. It is more than 1/3 of ERA5 for APHRODITE and IMERG precipitation $\leq 25^{\text{th}}$ percentile. It is noteworthy that beyond 25th percentile of precipitation, ERA5 precipitation is a little more than one time of the other two precipitation products.

The exceedance probabilities of ET increase with the increase in precipitation. Such probabilities are negligible during the non-monsoon season because it is very much less likely for a small amount of rainfall to contribute to a large amount of ET.

5.4.3 Assessment of Risk of Q for given Precipitation Scenarios

It is to be noted that the probabilities of occurrence of Q for APHRODITE and IMERG are very similar in pattern to each other, probably since IMERG is gauge-corrected satellite precipitation leading to a closer estimate of precipitation. However, the probabilities of occurrence of Q given ERA5 differ for scenarios up to $\leq 5^{\text{th}}$, 25th compared to given APHRODITE and IMERG. Though the magnitude of ERA5 $\leq 5^{\text{th}}$ percentile is about eight times (Table 5.8) that of APHRODITE and IMERG ($\leq 5^{\text{th}}$ percentile), the probability of occurrence of Q ($\leq 5^{\text{th}}$ percentile) given ERA5 is only about one half when compared to given APHRODITE and IMERG in this scenario.

The non-exceedance predictive capability of APHRODITE and IMERG for discharge is very similar as both the products are linked to in-situ measurements. Though APHRODITE and IMERG are better at predicting low flows, all three products equally perform to predict high flows. The non-exceedance probabilities of Q decrease with the increase in precipitation by almost three times (from 5th to 95th percentile).

In contrast, the exceedance probabilities increase with the increase in precipitation by about two times. This is because higher precipitation has a greater likelihood of causing a flood or a high flow. It is well known that the Brahmaputra basin experiences flooding every year when maximum precipitation occurs during the monsoon season, leading to an increased flow level in the river. Hence, the copula concept in this context could be used for water supply management and flood control (Liu et al. 2016; Liu and Menzel 2018). Copula could also be helpful in determining the threshold of low flow for the ecological balance of the Brahmaputra River.

The limitation of bivariate copula is that if a variable is controlled by more than one variable (Bibi et al. 2019), the probabilistic prediction may not represent the actual prediction. However, as a preliminary study, the present research could be extended to more than two variables. To further explore this investigation, it is recommended to use hierarchical/ vine copulas to model the dependence structure of more than two variables. Also, the interaction between ET-Q, ET - TWSC, and TWSC-Q pairs could be explored. In addition to these combinations, TWSC was not subdivided into different components like snow water equivalent storage (SWE), groundwater storage (GWS) and soil moisture storage (SMS). Future studies could look into the probabilistic prediction of the sub-components of TWSC for the same scenarios of a given precipitation used in this study by extending the work of Shamsudduha and Taylor (2020). Probabilistic predictions could also be carried out on a seasonal basis (Bibi et al. 2019).

5.5 CONCLUSIONS

Precipitation is known to be the major component of the terrestrial water cycle. Precipitation data obtained from gauge records is plagued by wind-induced under-catch

and altitude bias. It is also sparsely recorded in mountainous regions. Reanalysis data are derived from the model and are not gauge-corrected. Satellite-based precipitation has wide coverage but can under/over predict low/high precipitation depending on the climate of a region. For a transboundary basin like Brahmaputra, where gauge data of hydrometeorological variables are rarely available in the public domain, the alternative is to use the data sets obtained from various types, as stated above.

This study is the first attempt to conduct a comparative analysis of APHRODITE, ERA5, and IMERG to probabilistically predict TWSC, ET, and Q for a large river basin, the Brahmaputra using the concept of dependence structure and copulas. This study constructed a bivariate dependence structure to predict the conditional distributions of TWSC, ET, and Q for different precipitation scenarios.

- (a) The optimal marginal distributions for the variables are:
 - Gamma for APHRODITE and IMERG precipitation
 - Lognormal for ERA5 precipitation and discharge
 - Normal kernel density function for TWSC
 - Logistic for ET
- (b) The optimal copula function for all three precipitation-TWSC pairs, ERA5-ET, and ERA5-ET is the Frank copula.
- (c) The optimal copula function for the remaining pairs is the Clayton copula.
- (d) Pearson's linear and Spearman's rank correlations for all the pairs of variables are significant for observed and simulated values.
- (e) The non-exceedance probability of all the dependent variables (lower percentile) decreases with increased precipitation, while the exceedance probability of the same variables (upper percentile) increases gradually with increased precipitation.

EVALUATION OF SATELLITE PRECIPITATION ESTIMATES TO RECONSTRUCT MAJOR WATER BUDGET COMPONENTS

6.1 OVERVIEW

Precipitation is the major water budget variable, so it is essential to understand how to reconstruct other water budget variables like ET, Q and TWSC. Several studies have examined water budget error closure, including how the error is distributed among the variables. However, simply following the water budget equation based on mass conservation (in this study) can provide information on how these errors vary across different precipitation products. In addition to using statistical metrics, visual plots like rainclouds can offer insights beyond boxplots and scatter diagrams.

6.2 METHODS

There are several studies conducted on water budget closure. Nevertheless, only some studies exist on evaluating satellite precipitation to reconstruct water budget variables like evapotranspiration, change in storage and runoff. The monthly water budget equation (Oliveira et al. 2014) for the Brahmaputra basin is based on the conservation of mass principle, which can be expressed as:

$$\frac{dS}{dt} = P - ET - Q \quad 6.1$$

where dS/dt is the change in storage, P is precipitation, ET is evapotranspiration and Q is runoff.

The change in storage ($TWSC$) derived from GRACE total water storage anomaly ($TWSA$) may be derived from the following relationship:

$$\frac{dS}{dt} = TWSC(t) = TWSA_{t+1} - TWSA_t \quad 6.2$$

$TWSC$ is the difference between two consecutive monthly anomalies. Since $TWSC$ is derived from the anomalies of $TWSA$, we also express all other water budget terms in anomaly form in equation 6.1. Therefore, equation 6.1 may be written as (Oliveira et al. 2014):

$$\frac{dS}{dt} = \left(\frac{P_{t+1} - P_t}{2} \right) - \left(\frac{ET_{t+1} - ET_t}{2} \right) - \left(\frac{Q_{t+1} - Q_t}{2} \right) \quad 6.3$$

The residual dS/dt from equation 6.3 is compared with the $TWSC$ from equation 6.2 using the correlation coefficient. Then, the water budget error is estimated as the difference between $GRACE$ $TWSC$ and dS/dt as (Zhang et al. 2016):

$$\varepsilon(t) = TWSC(t) - \frac{dS}{dt} \quad 6.4$$

The mean absolute error in mm/month for the given time frame is expressed as (Zhang et al. 2016):

$$\bar{\varepsilon} = \frac{1}{n} \sum_{t=1}^n |\varepsilon(t)| \quad 6.5$$

The bias (mm/month) is expressed as (Zhang et al. 2016):

$$\bar{\varepsilon}_b = \frac{1}{n} \sum_{t=1}^n \varepsilon(t) \quad 6.6$$

Equations 6.4 – 6.6 were applied to ET and Q as well. The error analysis for precipitation was not carried out because the present study was aimed at assessing the ability of different precipitation for how well $TWSC$, ET and Q could be reconstructed and the errors thereof.

6.3 RESULTS AND DISCUSSION

6.3.1 Assessment of monthly water budget components

In Fig.6.1, the reconstructed change in storage term (dS/dt) of the water budget equation (equation (6.1)) is compared against GRACE $TWSC$ derived monthly time series. The time series plots and the corresponding scatter plot is placed on the right hand side of the figure.

It is to be mentioned here that the MOD16 derived ET and the in-situ runoff (Q) are subtracted from each precipitation product resulting in different residuals (dS/dt). The correlation between these residuals and GRACE TWSC show that the residual reconstructed using ERA5 precipitation has the highest linear strength (0.82). The least optimal correlation coefficient is shown by SMRAIN (0.08). The CMORPH (0.31) is the other precipitation product that shows a lesser correlation than that obtained by gauged-based precipitation APHRODITE.

In addition to ERA5, the CHIRPS (0.69), TRMM (0.78) and IMERG (0.73) show greater correlation because these products overestimated precipitation, whereas the remaining products underestimated precipitation amount. The same pattern could be seen by using MOD16, while maintaining the same discharge and precipitation products. Another reason for the lesser correlation coefficient is the residuals for the APHRODITE, CMORPH and SM2RAIN is that these residuals lag the GRACE TWSC. So, it could improve marginally by considering lags for these residuals. Similarly, the correlation coefficients are depicted in the first row in Table 6.1.

An interesting picture emerges when referring Fig.6.2 in which the derived ETs were not reconstructed well as evidenced from the correlation with the MODIS16 ET (Fig.6.2 and Table 6.1). The reconstructed ETs were obtained by subtracting GRACE TWSC and in-situ discharge from individual precipitation products. Though a similar pattern in the correlation coefficient of derived ETs and MODIS16 ET is seen as compared to that of the reconstructed dS/dt and GRACE TWSC, the linear strength appears to be insignificant for those derived using APHRODITE, CMORPH and SM2RAIN. However, there is a strong correlation for those reconstructions using ERA5 (0.68) and TRMM (0.51). A moderate linear strength for IMERG (0.40) and a weaker correlation for CHIRPS (0.29) were noticed. The results are tabulated in the second row of Table 6.1.

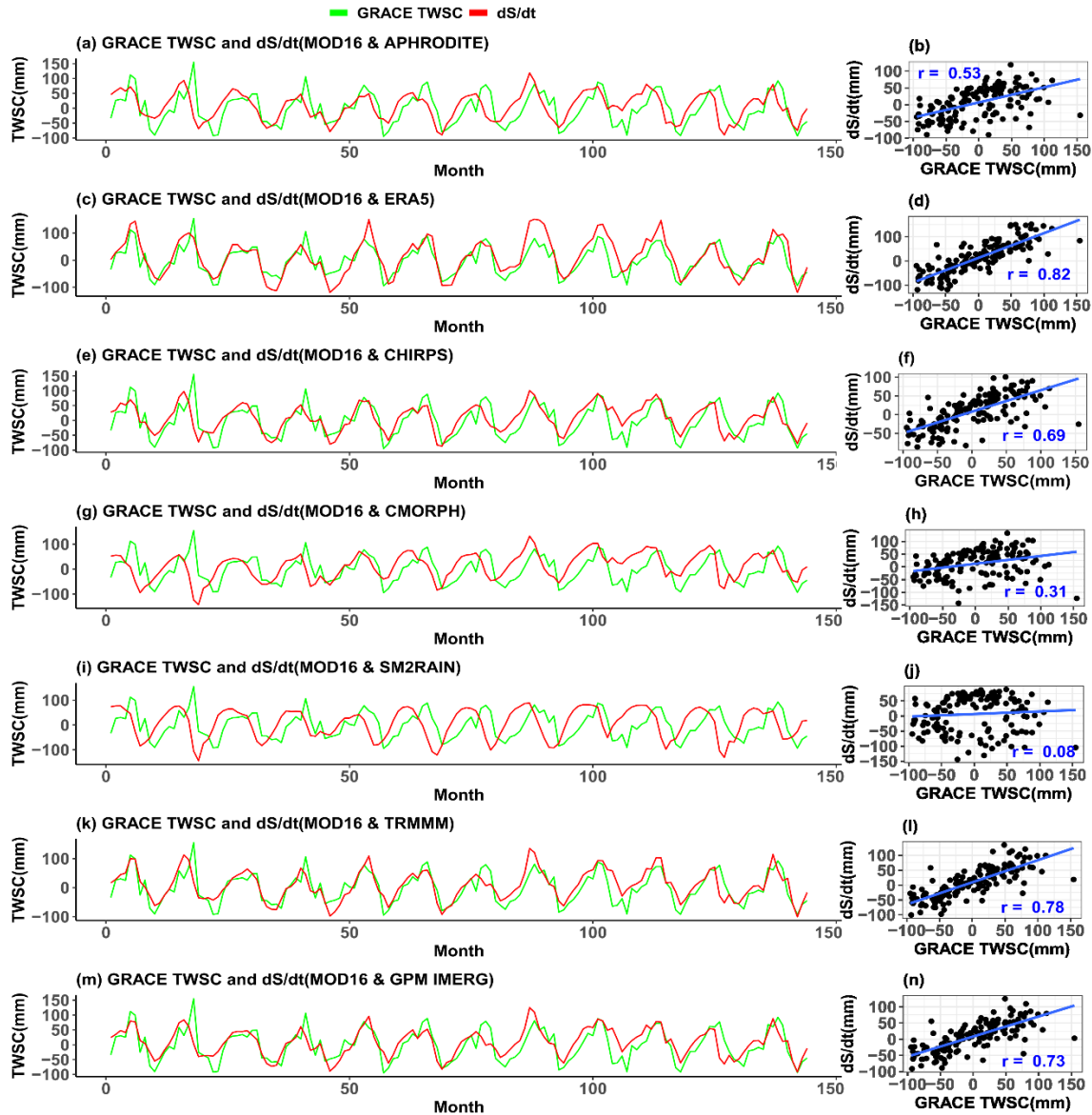


Fig.6.1 Time series of reconstructed dS/dt against GRACE TWSC

In contrast to the reconstructions of dS/dt and ET , the correlation coefficient of the reconstructed runoffs with in-situ runoff shows a different outcome. From Fig.6.3, the reconstructed runoff time series data are plotted against the in-situ runoff. The reconstructed runoff was obtained by subtracting MODIS16 ET and GRACE TWSC from the individual precipitation products using equation 6.2. Though IMERG (0.89) derived runoff is the most optimal correlation, there is hardly much deviation in terms of absolute

value as compared to those derived using the gauge-based APHRODITE (0.85), ERA5 (0.83), CHIRPS (0.88) and TRMM (0.87). As expected, the non-gauge corrected SM2RAIN (0.40) shows the least correlation strength and the much relative better CMORPH (0.68). All the correlation coefficient values have been recorded in third row of Table 6.1.

The mean absolute error ($\bar{\epsilon}$) or which is also known as water balance error was calculated using equation (6.5) and the corresponding bias using equation (6.6). From Table 6.1, the mean absolute error ($\bar{\epsilon}$) of TWSC derived using TRMM precipitation, MODIS16 ET and in-situ runoff is the most optimal one at 26.44 mm/month, amounting to 30% of gauge-based APHRODITE precipitation (mean rainfall at 88.48 mm/month for 2003-2014). The least optimal being captured by SM2RAIN at 65.17 mm/month, amounting to 74% of the gauge-based rainfall. This pattern has been clearly visible whenever the non-gauge corrected SM2RAIN was used. However, the findings of this study are more reasonable than a claim by Zhang et al. (2016) that overestimated TRMM resulted in lower absolute bias magnitudes. It is clearly seen that the mean precipitation of SM2RAIN is the least in comparison to other precipitation products. So, its low magnitude is attributed to the higher magnitude of water balance error.

On the other hand, the mean absolute error with the least value (optimal) is IMERG for ET reconstruction at 31.31 mm/day (Table 6.1), which is about 35% of the gauge-based APHRODITE precipitation. The SM2RAIN shows the highest mean absolute error at 57.53 mm/day that works out to be about 65% of the gauge precipitation. The higher error is attributed to the lesser precipitation captured the product and the lower error due to higher capturing of precipitation. Similarly, in Table 6.1, the IMERG driven runoff shows the least absolute error at 28.6 mm/day, which amounts to about 32% of the gauge precipitation and the highest absolute error at 59.15 mm/day working out to be about 67% of gauge precipitation.

Table 6.1 The evaluation of monthly precipitaton products with respect to three metrics (MOD16_0.5 ET)

| Metrics | APHRODITE | ERA5 | CHIRPS | CMORPH | SM2RAIN | TRMM | IMERG |
|--------------------------------------|--------------|-------------|--------|--------|---------|--------------|--------------|
| r_{TWSC} | 0.53 | 0.82 | 0.69 | 0.31 | 0.08 | 0.78 | 0.73 |
| r_{ET} | -0.06 | 0.68 | 0.29 | -0.29 | -0.68 | 0.51 | 0.40 |
| r_Q | 0.85 | 0.83 | 0.88 | 0.68 | 0.40 | 0.87 | 0.89 |
| $\bar{\epsilon}_{TWSC}$ (mm/month) | 39.75 | 30.25 | 31.18 | 50.75 | 65.17 | 26.44 | 28.65 |
| $\bar{\epsilon}_{ET}$ (mm/month) | 36.92 | 40.53 | 30.80 | 46.53 | 57.53 | 31.57 | 31.31 |
| $\bar{\epsilon}_Q$ (mm/month) | 36.95 | 36.58 | 30.89 | 47.80 | 59.15 | 29.13 | 28.60 |
| $\bar{\epsilon}_{b,TWSC}$ (mm/month) | -7.49 | -12.44 | -8.31 | -13.03 | -7.63 | -9.67 | -8.67 |
| $\bar{\epsilon}_{b,ET}$ (mm/month) | -7.62 | -12.38 | -8.39 | -13.19 | -7.88 | -9.69 | -8.73 |
| $\bar{\epsilon}_{b,Q}$ (mm/month) | -7.81 | -12.75 | -8.63 | -13.35 | -7.94 | -9.99 | -8.99 |

Note: bold figures represent the best value. GRACE TWSC, MOD16_0.5, in-situ Q were used for evaluation.

The negative biases of TWSC, ET and Q indicate that the reconstructed values overpredicted the observed values. However, in the absence of measured TWSC and ET the associated uncertainties could be high enough to obscure the true reflection of those variables. Nevertheless, they are still able to provide insights on the dynamics of hydrological variables. Each precipitation driven biases for the three water budget variables appear to be almost same in magnitude. It will become clearer when the analysis is carried out on a seasonal basis in the subsequent sections.

6.3.2 Assessment of winter water budget components

The assessment of water budget variables for the winter season was done by considering these variables only for the month of January and February from 2003- 2014. From Table 6.2, the TWSC is the only variable that could be successfully reconstructed using APHRODITE, ERA5, CHIRPS, TRMM and IMERG. The ERA5 product emerges as the product having the highest linear strength (0.88), followed by TRMM (0.78) and IMERG (0.74). The ETs and runoffs did not reconstruct well as revealed from the correlation coefficient tabulated in the second and third rows of Table 6.2.

The mean absolute error ($\bar{\epsilon}$) associated with TWSC reveals that TRMM (21.18 mm/year) and SM2RAIN (68.23 mm/year) to be the best and least performing precipitation product, respectively. The errors are at staggering figures of about 144% (TRMM) and 462% (SM2RAIN) of the winter precipitation (14.76 mm/year). The best and the least mean absolute error for ET are demonstrated by the TRMM and SM2RAIN at 16.15 mm/year and 66.42 mm/year, working out to be 109% and 450% of the winter precipitation. Similarly, the TRMM and SM2RAIN are the best and least performing precipitation estimates for runoff reconstruction with the mean absolute error at 21.27 mm/year and 67.87 mm/year, amounting to about 144% and 460% of the total gauge precipitation. It is clear that all the reconstruction of water budget variables shows similar magnitudes of the error. All the biases are negative, meaning reconstructed variables were overpredicted.

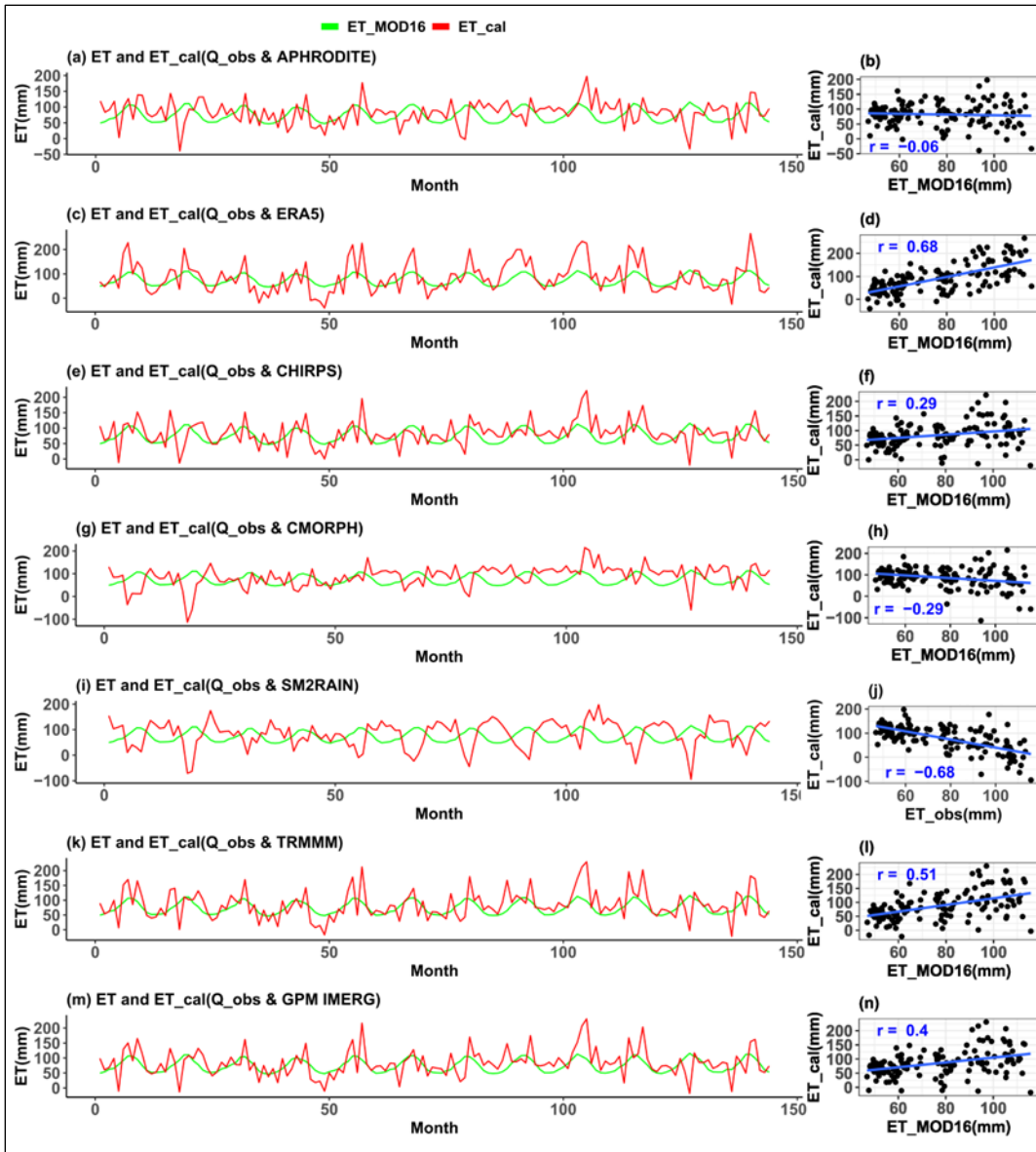


Fig.6.2 Time series of reconstructed ET against MOD16 ET

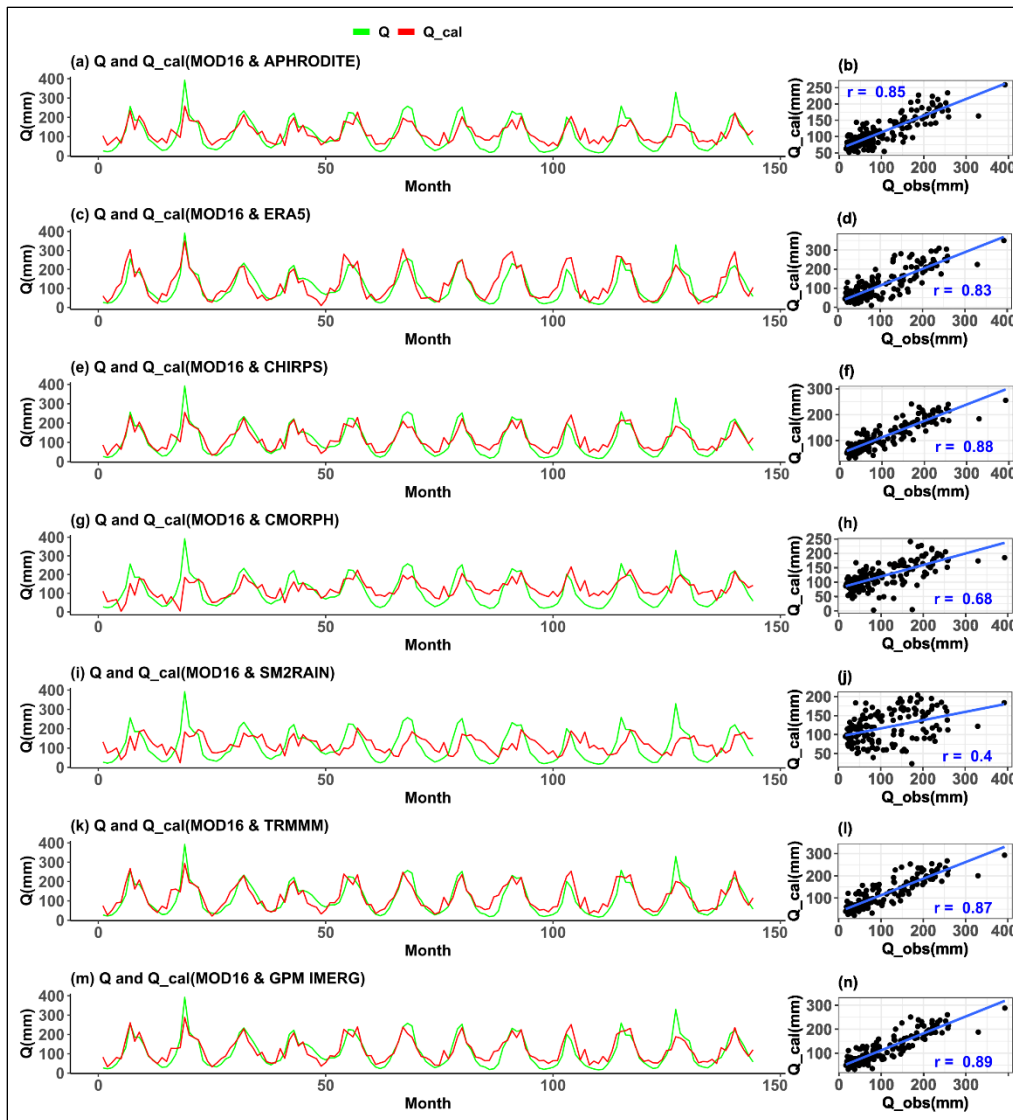


Fig.6.3 Time series of reconstructed Q against observed runoff

Table 6.2 The evaluation of winter precipitaton products with respect to three metrics (MOD16_0.5 ET)

| Metrics | APHRODITE | ERA5 | CHIRPS | CMORPH | SM2RAIN | TRMM | IMERG |
|-------------------------------------|-----------|---------------|--------|--------|--------------|--------------|--------|
| r_{TWSC} | 0.5 | 0.88 | 0.61 | 0 | 0.05 | 0.78 | 0.74 |
| r_{ET} | 0.21 | 0.3 | 0.12 | 0.09 | 0.01 | 0.21 | 0.2 |
| r_Q | -0.13 | -0.51 | -0.08 | -0.18 | -0.06 | -0.16 | -0.25 |
| $\bar{\epsilon}_{TWSC}$ (mm/year) | 41.9 | 21.7 | 27.84 | 53.98 | 68.23 | 21.18 | 27.16 |
| $\bar{\epsilon}_{ET}$ (mm/year) | 37.32 | 19.59 | 23.84 | 50.08 | 66.42 | 16.15 | 20.93 |
| $\bar{\epsilon}_Q$ (mm/year) | 41.97 | 22.57 | 27.68 | 54.06 | 67.87 | 21.27 | 27 |
| $\bar{\epsilon}_{b,TWSC}$ (mm/year) | -40.54 | -10.34 | -24.04 | -53.92 | -68.23 | -14.41 | -22.22 |
| $\bar{\epsilon}_{b,ET}$ (mm/year) | -34.21 | 4.58 | -19.09 | -48.78 | -66.42 | -5.23 | -14.05 |
| $\bar{\epsilon}_{b,Q}$ (mm/year) | -40.17 | -9.97 | -23.68 | -53.55 | -67.87 | -14.04 | -21.85 |

Note: bold figures represent the best value. GRACE TWSC, MOD16_0.5, in-situ Q were used for evaluation.

6.3.3 Assessment of summer water budget components

The water budget variables for the summer season were assessed considering the months of March through May from 2003 to 2014. The reconstruction of TWSC (dS/dt) was successful using all the precipitation estimates except SM2RAIN for which the linear strength was weak (Table 6.3). However, ERA5, CHIRPS, TRMM and IMERG show greater correlation than APHRODITE and CMORPH. The reason being the first four precipitation measures slightly overestimated precipitation, which might in fact be a better representation of observed rainfall because of their ability to detect precipitation over a large spatial extent as opposed to point measurement estimates like APHRODITE. The CMORPH comes with bias correction using daily gauge precipitation. As already known SM2RAIN was not gauge corrected. The product with the highest linear strength is the TRMM (0.83), followed by ERA5 and IMERG (0.81) and CHIRPS (0.79). According to the correlation coefficient listed in the second row of Table 6.3, the ETs did not reconstruct well because of uncertainties in the satellite products. Though the runoff reconstruction was similar in pattern to that of TWSC reconstruction, the correlation coefficient is only significant for ERA5, CHIRPS, TRMM and IMERG. The highest linear strength was demonstrated by TRMM (0.63), whereas the least linear strength was depicted by SM2RAIN (-0.03).

The best and least performing precipitation estimates, respectively, are IMERG (22.15 mm/year) and SM2RAIN (37.3 mm/year) as per the mean absolute error values for TWSC reconstruction. The error works out to be about 27% and 46% of the average summer precipitation of 81.13 mm. The IMERG and ERA5 show the best and the least mean absolute error for ET at 31.05 mm/year and 38.78 mm/year, or 38% and 48% of the winter precipitation, respectively. Similarly, the IMERG and ERA5 provide the best and least runoff reconstruction estimates, respectively, with mean absolute errors of 30.35 mm/year and 44.11 mm/year, or about 37% and 54% of the total gauge precipitation. The findings lead to the fact that SM2RAIN was able to reconstruct similar to other products like TRMM, ERA5 and CMORPH, may be because the soil moisture sensor was able to detect moisture during summer season when rainfall events are not frequent.

Another factor could be the runoff contribution from rainfall also will be lesser than the runoff from snowmelts. The Brahmaputra River basin has over 75% of its runoff contribution coming from monsoon rainfall that occurs between June and September. What is interesting is the bias errors are all negative values, which mean overestimation of the water budget variables. This is apparently clear from the biases from the reconstruction of the variables using ERA5 and TRMM estimates.

6.3.4 Assessment of monsoon water budget components

In Table 6.4, the months of June through September were considered for the reconstruction of TWSC, ET and runoff for the same period used in other seasons. Interestingly, the reconstruction of TWSC using ERA5 (0.84) and TRMM (0.77) depicts to have among the highest linear strength. The CHIRPS and IMERG have closer correlation values of 0.68 and 0.72, respectively. Then, with a much lower correlation values of APHRODITE (0.5) and CMORPH (0.39). The least performing precipitation estimates being SM2RAIN (0.01). Except ERA5 with a lesser significant correlation of 0.27, the reconstruction of ET did not project well when compared with MOD16 ET. However, all most all the precipitation data aided in reconstructing runoff with correlation ranging from 0.35 – 0.62. This means that GRACE TWSC and MOD16 ET might have been able to capture storage change and evapotranspiration in proportion to what the variables captured in summer season.

With absolute errors of 32.64 mm/year (18% of 179.56 mm/year gauge precipitation) and 78.92 mm/year (44% of the same seasonal average), the TRMM and SM2RAIN are the best and least performing precipitation estimates for reconstructing TWSC. However, for reconstruction of ET, the CMORPH turns to be having the least error at 39.39 mm/year (22%) as opposed to the highest error of SMRAIN at 69.42 mm/year (39%). In continuation, though the SM2RAIN shows the highest error at 73.45 mm/year (41%), the least error is exhibited by IMERG at 32.16 mm/year (18%) for runoff reconstruction. It is also interesting to note that most of the precipitation estimates show positive biases, which mean underprediction of rainfall. As expected, the SM2RAIN depicts the highest positive biases indicating the under representation of high rainfall.

Table 6.3 The evaluation of summer precipitaton products with respect to three metrics (MOD16_0.5 ET)

| Metrics | APHRODITE | ERA5 | CHIRPS | CMORPH | SM2RAIN | TRMM | IMERG |
|-------------------------------------|-----------|--------|--------|--------|--------------|-------------|--------------|
| r_{TWSC} | 0.69 | 0.81 | 0.79 | 0.52 | 0.28 | 0.83 | 0.81 |
| r_{ET} | -0.19 | 0.14 | -0.04 | -0.25 | -0.56 | 0.16 | -0.05 |
| r_Q | 0.35 | 0.59 | 0.6 | 0.11 | -0.03 | 0.63 | 0.58 |
| $\bar{\epsilon}_{TWSC}$ (mm/year) | 28.34 | 30.56 | 24.08 | 35.3 | 37.03 | 25.07 | 22.15 |
| $\bar{\epsilon}_{ET}$ (mm/year) | 33.61 | 38.78 | 31.32 | 36.14 | 35.29 | 32.48 | 31.05 |
| $\bar{\epsilon}_Q$ (mm/year) | 32 | 44.11 | 34.1 | 42.38 | 35.27 | 36.48 | 30.35 |
| $\bar{\epsilon}_{b,TWSC}$ (mm/year) | -6.96 | -22.61 | -11.49 | -12.08 | -1.96 | -16 | -7.73 |
| $\bar{\epsilon}_{b,ET}$ (mm/year) | -8.45 | -11.05 | -4.92 | -16.94 | -11.02 | -6.83 | -2.31 |
| $\bar{\epsilon}_{b,Q}$ (mm/year) | -25.4 | -41.05 | -29.93 | -30.53 | -20.4 | -34.44 | -26.18 |

Note: bold figures represent the best value. GRACE TWSC, MOD16_0.5, in-situ Q were used for evaluation.

6.3.5 Assessment of postmonsoon water budget components

Similar to monsoon seasonal assessment of the water balance variable reconstruction, the ERA5 (highest at 0.85), CHIRPS, TRMM and IMERG show a strong linear strength and relatively lower strength for APHRODITE and CMORPH (Table 6.5). The least strength being shown by SM2RAIN (0.05). Also, the first four precipitation estimates show relatively significant correlation for ET reconstruction. However, all the rainfall estimates show similar kind of correlation for runoff estimation.

The TRMM and SM2RAIN are respectively the most optimal and least optimal estimates for TWSC, ET and Q. Therefore, the errors are 23.03 mm/year (98% of 23.51 mm/year) and 72.95 mm/year (310% of 23.51 mm/year), respectively, for TWSC estimation. The errors for ET estimation are 21.63 mm/year and 57.98 mm/year, respectively following the sequence of the least and highest errors. Similarly, 22.53 mm/year and 58.15 mm/year, respectively, for the estimation of Q.

In a striking contrast to the evaluation of rainfall estimates in monsoon season, ERA5 turned out to be demonstrating positive bias, thereby confirming lesser rainfall amount being captured by ERA5. Overall, the least bias was depicted by TRMM and highest biases by SM2RAIN.

Table 6.4 The evaluation of monsoon precipitaton products with respect to three metrics (MOD16_0.5 ET)

| Metrics | APHRODITE | ERA5 | CHIRPS | CMORPH | SM2RAIN | TRMM | IMERG |
|-------------------------------------|-------------|-------------|--------------|--------|---------|--------------|--------------|
| r_{TWSC} | 0.5 | 0.84 | 0.68 | 0.39 | 0.01 | 0.77 | 0.72 |
| r_{ET} | -0.12 | 0.27 | -0.17 | -0.14 | -0.44 | -0.02 | -0.04 |
| r_Q | 0.62 | 0.53 | 0.59 | 0.41 | 0.35 | 0.6 | 0.62 |
| $\bar{\epsilon}_{TWSC}$ (mm/year) | 46.5 | 39.04 | 38.02 | 56.46 | 78.92 | 32.64 | 35.25 |
| $\bar{\epsilon}_{ET}$ (mm/year) | 43.62 | 60.19 | 39.39 | 54.16 | 69.42 | 46.05 | 43.53 |
| $\bar{\epsilon}_Q$ (mm/year) | 42.45 | 41.03 | 34.15 | 51.99 | 73.45 | 32.5 | 32.16 |
| $\bar{\epsilon}_{b,TWSC}$ (mm/year) | 31.68 | -20.6 | 15.41 | 38.58 | 67.42 | 0.73 | 6.58 |
| $\bar{\epsilon}_{b,ET}$ (mm/year) | 19.4 | -43.81 | -0.92 | 28.79 | 60.67 | -18.18 | -9.72 |
| $\bar{\epsilon}_{b,Q}$ (mm/year) | 32.44 | -19.84 | 16.17 | 39.35 | 68.19 | 1.49 | 7.34 |

Note: bold figures represent the best value. GRACE TWSC, MOD16_0.5, in-situ Q were used for evaluation.

Table 6.5 The evaluation of postmonsoon precipitaton products with respect to three metrics (MOD16_0.5 ET)

| Metrics | APHRODITE | ERA5 | CHIRPS | CMORPH | SM2RAIN | TRMM | IMERG |
|-------------------------------------|-----------|-------------|--------|--------|---------|--------------|-------------|
| r_{TWSC} | 0.5 | 0.85 | 0.71 | 0.43 | 0.05 | 0.8 | 0.73 |
| r_{ET} | 0.12 | 0.5 | 0.32 | 0.01 | -0.25 | 0.41 | 0.37 |
| r_Q | 0.67 | 0.65 | 0.7 | 0.64 | 0.59 | 0.72 | 0.72 |
| $\bar{\epsilon}_{TWSC}$ (mm/year) | 40.73 | 23.93 | 31.4 | 56.44 | 72.95 | 23.03 | 27.33 |
| $\bar{\epsilon}_{ET}$ (mm/year) | 31.02 | 30.01 | 23.45 | 44.37 | 57.98 | 21.63 | 22.18 |
| $\bar{\epsilon}_Q$ (mm/year) | 31.23 | 32.45 | 25.49 | 43.46 | 58.15 | 22.53 | 23.18 |
| $\bar{\epsilon}_{b,TWSC}$ (mm/year) | -38.22 | 7.23 | -26.26 | -55.53 | -72.95 | -14.06 | -20.92 |
| $\bar{\epsilon}_{b,ET}$ (mm/year) | -25.07 | 16.88 | -14.7 | -41.7 | -57.09 | -4.22 | -10.27 |
| $\bar{\epsilon}_{b,Q}$ (mm/year) | -22.31 | 23.15 | -10.35 | -39.62 | -57.04 | 1.86 | -5 |

Note: bold figures represent the best value. GRACE TWSC, MOD16_0.5, in-situ Q were used for evaluation.

6.3.6 Uncertainty estimation of reconstructed monthly water budget variables

The raincloud plots provide a transparent and robust visualisation of original sample data, probability density and important summary statistics like median, mean and pertinent confidence intervals (Allen et al. 2019). The plots are useful beyond just using boxplots, which provide summary statistics or violin plots that provide information on the spread of data. Raincloud plots are not a new technique of visualisation, but a combination of the existing plots like boxplots, half-violin plots and spread of data.

In this section, the uncertainty assessment of reconstructed water budget variables will be discussed only for monthly scale. In Fig.6.4, the x-axis denotes the TWSC measures and on y-axis various TWSCs derived using equation 6.3. On visual inspection, the interquartile (difference between 3rd quartile and 1st quartile) range of SM2RAIN derived TWSC is the highest, followed by the ERA5 derived TWSC. However, the interquartile ranges of APHRODITE, CHIRPS, TRMM and IMERG are the least. These interquartile ranges are very close to the interquartile range of GRACE TWSC. These are to some extent consistent with the correlation coefficient and mean absolute error in Table 6.1. However, ERA5 stands out to be different here compared to the better performance of the indicators in Table 6.1. It is worth mentioning here that ERA5 is not a direct measure of rainfall, but model derived precipitation obtained using various sources of data as inputs including satellite data, gauge measurement and climate data. Therefore, even though ERA5 tends to perform better than some of the precipitation data for reconstructing water budget variables, its uncertainty analysis offered a better understanding.

Lesser the interquartile, better the spread of data. Therefore, GRACE TWSC and the TWSC derived from the best performing precipitation data have better spread of data than those TWSCs derived from ERA5, CMORPH and SM2RAIN. These findings can be complemented by looking at the shape of half-violin plots representing kernel densities of various TWSCs. Interestingly, TWSC derived ERA5 shows a flat density curve with no skewness despite the second largest interquartile range. This could be because the spread of data is less dense, albeit uniform.

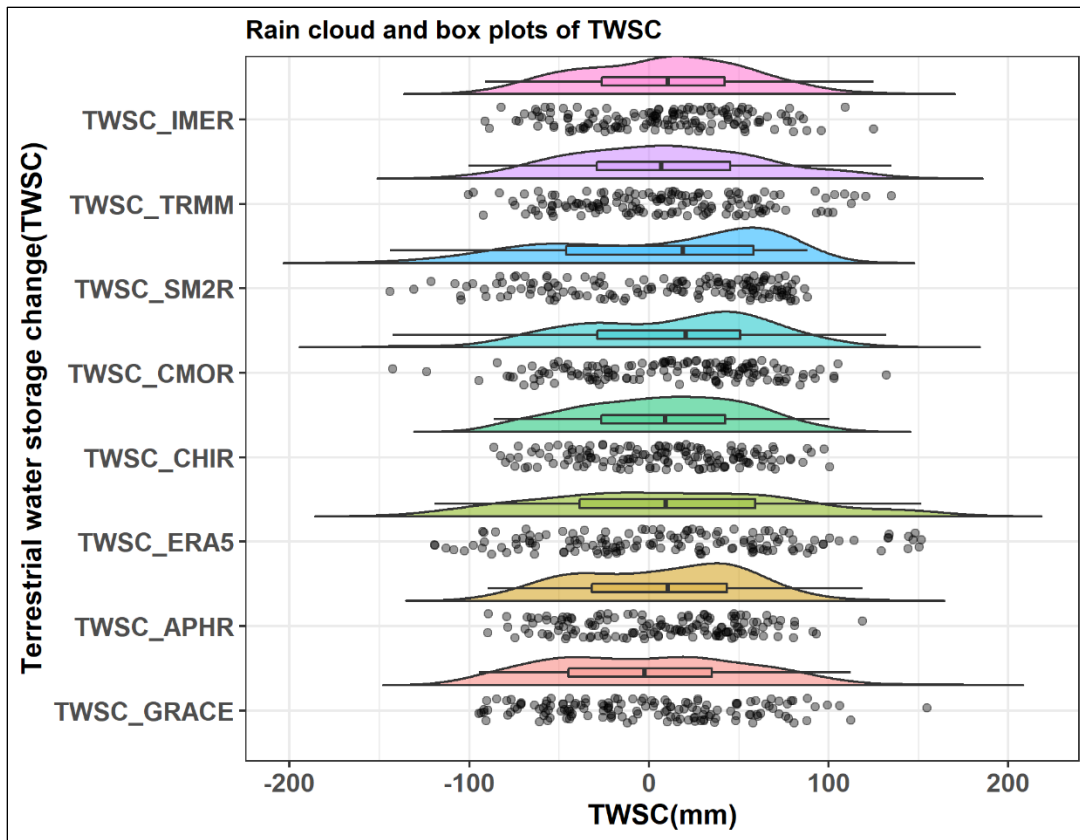


Fig.6.4 Raincloud plots of GRACE TWSC and derived TWSCs

The density curves of TWSCs derived using APHRODITE, CMORPH and SM2RAIN show the data skewed towards right. In other words, these findings complement the reason why the mean absolute errors of these TWSCs show relatively higher than those derived using the remaining precipitation measures as shown in Table 6.1. To some degree, IMERG derived TWSC also tend to be slightly positively skewed. However, its curve is bimodal shape that might have contributed to still have lesser error. In fact, only TWSCs derived from TRMM and CHIRPS did show a unimodal distribution of data and ERA5 to some extent.

From Fig.6.5, the derived ETs from APHRODITE, CHIRPS and IMERG appear to show similar interquartile ranges to that of MOD16 ET. These confirm from the mean absolute errors for ETs shown in Table 6.1. The higher interquartile ranges are demonstrated by ETs derived from SM2RAIN and ERA5, but the correlation coefficient depicted by ERA5 is the highest. Therefore, correlation coefficient is not a good measure for assessing performance non-linear variables. That might be the reason why ET derived from ERA5 shows a higher error as compared to those ETs performing better. It is known that MOD16 ET is a satellite-based ET data, which comes with uncertainties and ETs derived using all the precipitation and GRACE TWSC and in-situ runoff also do have different uncertainties. GRACE TWSC is also a satellite-based TWSC measure and the runoff measure derived from the discharge at the outlet of Brahmaputra basin dividing it by the area of the basin will also contribute to lots of uncertainties, especially GRACE TWSC. Hence, most of the density curves of derived ETs do not resemble MOD16 ET.

In Fig.6.6, though the interquartile ranges of runoffs derived using ERA5, TRMM and IMERG are higher than those runoffs derived using APHRODITE, CMORPH and SM2RAIN, they are very close to the interquartile range of in-situ runoff. Another interesting finding is that though CHIRPS derived runoff shows in between interquartile range its correlation coefficient and error values in Table 6.1 tend to be closer to that of IMERG and TRMM. This is possibly the spread of data is similar to each other when considering the density plots of in-situ runoff and runoffs derived using ERA5, CHIRPS, TRMM and IMERG.

The above findings indicate that a single metric is not recommended to decide the ability of precipitation data for water budget variables reconstructions. Multiple metrics can complement a visualisation tool like raincloud plots to make better informed decision in wate management.

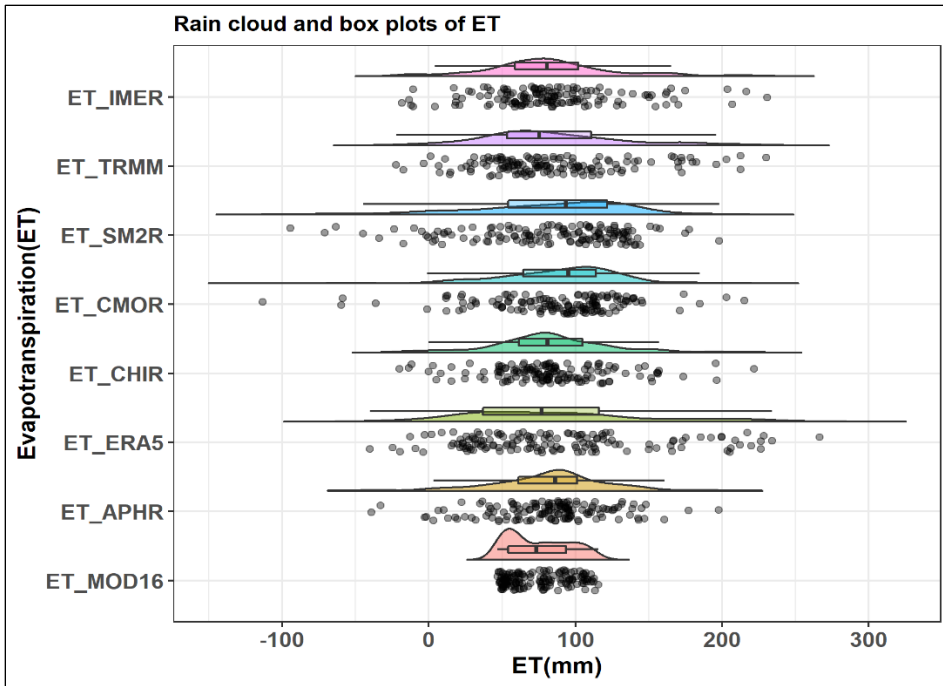


Fig.6.5 Raincloud plots of MOD16 ET and derived ETs

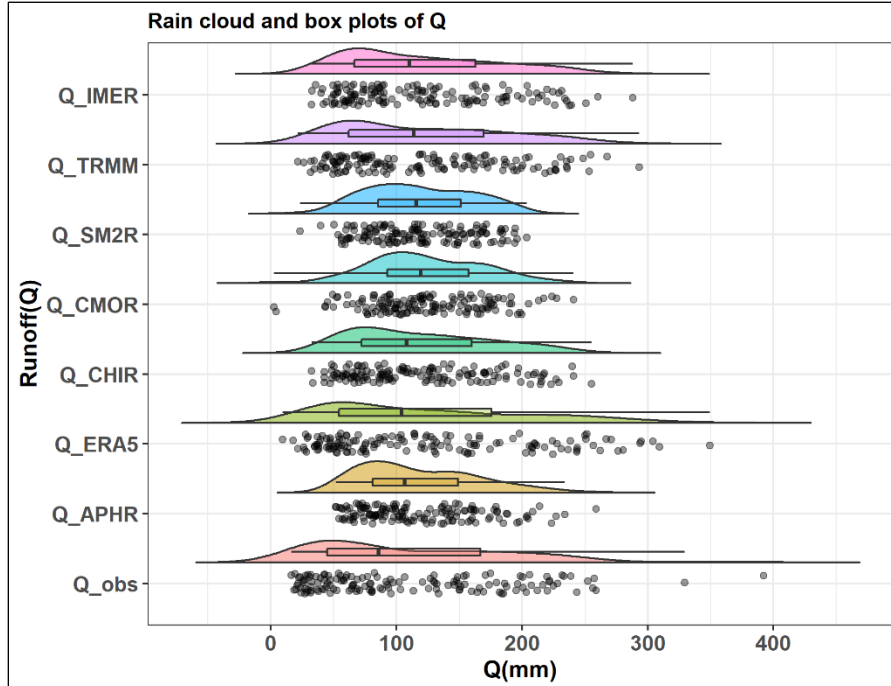


Fig.6.6 Raincloud plots of observed runoff and derived runoffs

6.4 CONCLUSIONS

The reconstruction (estimation) of water budget variables like dS/dt , ET and Q using different precipitation data on a monthly and seasonal basis from 2003 to 2014 for the Brahmaputra basin. The present study is one of the few studies in the context of water budget analysis that used empirical water budget equation for a large river basin using different datasets instead of using merged precipitation so as to know the strengths and weaknesses of such datasets on a standalone basis.

ERA5-derived TWSCs and Qs provide the highest linear correlation with gauge-based data.

TRMM, IMERG, and CHIRPS also show a closer correlation with ERA5-derived TWSCs and Qs, to a greater extent than other precipitation datasets.

The linear strength of derived ETs shows that the inherent uncertainties in the water budget variables did not reconstruct ETs well.

On a monthly basis:

- (a) TRMM-derived TWSCs have the lowest mean absolute error (MAE) at 26.44 mm/month, amounting to 30% of gauge-based APHRODITE precipitation.
- (b) IMERG has the lowest MAE for ET reconstruction at 31.31 mm/day, which is about 35% of gauge-based APHRODITE precipitation.
- (c) SM2RAIN shows the highest MAE for TWSC and ET reconstruction at 57.53 mm/day and 66.42 mm/day, respectively.
- (d) IMERG-derived runoff shows the least absolute error at 28.6 mm/day, which amounts to about 32% of the gauge precipitation, and the highest absolute error by SM2RAIN at 59.15 mm/day, about 67% of gauge precipitation.

For the winter season:

- (a) TRMM demonstrates the best mean absolute error for ET at 16.15 mm/year, 109% of the winter precipitation.
- (b) SM2RAIN shows the least mean absolute error for TWSC reconstruction at 37.3 mm/year, 46% of the average summer precipitation.

- (c) TRMM and IMERG provide the best and least mean absolute error for runoff reconstruction, respectively.

For the summer season:

- (a) IMERG and SM2RAIN are the best and least performing precipitation estimates for TWSC reconstruction, respectively.
- (b) IMERG and ERA5 show the best and the least mean absolute error for ET at 31.05 mm/year and 38.78 mm/year, respectively.
- (c) IMERG and ERA5 provide the best and least runoff reconstruction estimates, respectively.

For the monsoon season:

- (a) TRMM and SM2RAIN are the best and least performing precipitation estimates for reconstructing TWSC.
- (b) CMORPH has the least error for ET reconstruction at 39.39 mm/year, 22% of the monsoon precipitation.
- (c) IMERG exhibits the least error for runoff reconstruction at 32.16 mm/year, 18% of the total gauge precipitation.

For the post-monsoon season:

- (a) TRMM and SM2RAIN are the most and least optimal estimates, respectively, for TWSC, ET, and Q.
- (b) The errors are 23.03 mm/year (98% of gauge precipitation) and 72.95 mm/year (310% of gauge precipitation), respectively, for TWSC estimation.

Overall:

TRMM, IMERG, and CHIRPS show much lesser uncertainties than other precipitation datasets.

INNOVATIVE TREND ANALYSIS OF WATER BUDGET COMPONENTS

7.1 OVERVIEW

The trend analysis of water budget variables has been carried out in many studies, but most of them have concentrated on either precipitation or temperature. Though there has been surge in the applications of recently developed trend analysis method like innovative trend analysis (ITA), yet many findings were centred around precipitation. There are very few studies on the trend analysis of water budget using ITA. To fill the gap, all the major components of water budget were used to analyse trend analysis of individual months and trend transitions between months. Sub-trend was also carried out.

7.2 METHODS

The innovative trend analysis (ITA) (Şen 2012) has recently gained attention, as evident from several studies reported in the literature. However, most of them were concentrated on a variable or two. Therefore, to extend the works for trends of major water budget components (Oliveira et al., 2014; Zhang et al., 2016) the present study was attempted. It does not dependent on serial correlation, normality, and sample size of data. The following procedures were followed to carry out the ITA test (Chowdari et al., 2023):

- (i) Two equal subseries were extracted from the original rainfall time series (first and second halves).
- (ii) The two separate datasets were then placed in ascending order.
- (iii) In the Cartesian coordinate system, the first sub-series of data were plotted on the x-axis and the second on the y-axis. When coordinates fall on the 45° line, there is no trend. Below the line, there is a downward trend, and above the line, there is an upward trend.

Unlike conventional approaches, which can only detect monotonic trends, the ITA test can also discover sub-trends (Şen 2012). The sub-trends in this study were

determined using specific thresholds. Based on such threshold points, three clusters were consequently developed (Chowdari et al., 2023; Wang et al., 2020). On the x-axis (or y-axis), the low cluster is defined as all values lower than the 10th percentile of the original time series' first (or second) half. The high cluster, in a similar manner, is for values that are above the 90th percentile of the first (second) half of the time series. The middle cluster is found between values in the first (second) half of the original data that are larger than or equal to the 10th percentile and less than or equal to the 90th percentile. It is worth to mention here that the trend in the high cluster indicates the likelihood of a flood event, while the trend in the low cluster indicates the likelihood of a drought occurrence (Chowdari et al., 2023; Öztopal and Şen 2017)

The monthly ITA slope (s) was calculated as (Şen 2017):

$$s = \frac{2(\bar{y}_2 - \bar{y}_1)}{n} \quad 7.1$$

where \bar{y}_2 is the mean of the ordered second half time series, \bar{y}_1 is the mean of the ordered first half-time series, and n is the total number of samples in the original time series. At 5% significance level (critical value of $s_{cri} = \mp 1.96$), s is significant if $s < (0 - 1.96 * \sigma_s)$ and $s > (0 + 1.96 * \sigma_s)$. The σ_s is the standard deviation of the slope, which may be expressed as (Şen 2017):

$$\sigma_s = \frac{2\sqrt{2}}{n\sqrt{n}} \sigma \sqrt{1 - r_{\bar{y}_1 \bar{y}_2}} \quad 7.2$$

where σ is the sample time series standard deviation, $r_{\bar{y}_1 \bar{y}_2}$ is the correlation between the means of first and second half ordered time series. Equations 7.1 and 7.2 were applied to the monthly precipitation, evapotranspiration, change in storage and runoff of the Brahmaputra basin for innovative trend analysis. The results were compared with the traditional MK-test (Kendall 1938; Mann 1945). The innovative polygon trend analysis (IPTA) developed by Şen et al. (2019) was also used in this study to determine the trend volume (TV) and trend slope (TS) of the long-term mean water budget components. If X_1 and X_2 are the long-term mean/ standard deviation of two consecutive months (January and February, for example) of the first half time series of a variable and if Y_1 and Y_2 are

long-term mean/ standard deviation of two consecutive months, e.g., January and February) of second half time series of the variable, then the trend length (TL)/volume (TV) is given by:

$$TL/TV = \sqrt{(X_2 - X_1)^2 + (Y_2 - Y_1)^2} \quad 7.3$$

And the trend slope (TS) is given by:

$$TS = \frac{(Y_2 - Y_1)}{(X_2 - X_1)} \quad 7.4$$

7.3 RESULTS AND DISCUSSION

7.3.1 Innovative trend analysis of different precipitation products

The monthly ITA and MK tests and Sen's slopes were obtained for eight precipitation estimates, including the ensemble of those estimates: APHRODITE, ERA5, CHIRPS, CMORPH, SM2RAIN, TRMM, and IMERG. The monthly trend slopes of evapotranspiration (ET) (MOD16, CLSM, Noah, and, TerraClimate), runoff (Q), and GRACE TWSC were also evaluated. In addition, IPTA was employed to determine the trend length/volume (TL/TV) and trend slope (TS) for two consecutive months covering all the months in a year.

From Table 7.1, 75% of the months show a significant decreasing trend, and 25% of the months show an insignificant increasing trend using APHRODITE precipitation for ITA. In contrast, the MK test indicates about 8% of the month with a significant decreasing trend, 25% of the months with an insignificant positive trend, and about 67% of the month's insignificant negative trend.

The ITA for ERA5 precipitation reveals about 33% of the months to be a significant increasing trend, 50% of the months have a significant decreasing trend, and about 17% have an insignificant positive trend. In contrast, the MK test reveals about 33% of the month's insignificant increasing trend and about 67% of the months insignificant decreasing trend.

The ITA test of CHIRPS shows 17% of the months significantly increasing trend, about 67% of the months significantly decreasing trend, and about 8% each for both

insignificantly increasing and decreasing trend. On the other hand, the MK test depicts about 25% and 75% insignificantly increasing and decreasing trends, respectively.

The CMORPH for ITA indicates approximately 75% of the months with a significant positive trend, 8% with a significant downward trend, and 17% with an insignificant positive trend. MK test, in comparison, finds a 33% positive, a 58% insignificantly negative trend, and 8% of the months positively insignificant trend.

SM2RAIN (ITA) shows a significant positive trend of about 17% of the month, a significant negative trend of about 75%, and an insignificant decreasing trend of about 8%. In contrast, the MK test shows a significant negative trend in 25% of the months, an insignificant positive trend of 17%, and a much greater insignificant negative trend of 58%.

According to the ITA for TRMM, there is a significant positive trend in 17% of the months, a major significant negative trend in 58% of the months, and an insignificant negative trend in around 25%. On the other hand, the MK test shows that about 25% of the months had an insignificant increasing trend, and a high 75% had an insignificant falling trend.

The IMERG precipitation (ITA) shows about 17% of the month's positive significant trend, about 67% significant decreasing trend, about 8% insignificant increasing trend, and 8% insignificant decreasing trend. In contrast, the MK test reveals 25% of the month's insignificant positive and 75% insignificant negative trends.

The ensemble findings then reveal that roughly 33% of the months had a significant positive trend, whereas approximately 42% had a significant falling trend. Additionally, 17% of the months had an insignificant falling trend, while 8% had an insignificant ascending trend. The MK test, however, showed that 42% of the months had an insignificant positive trend and 58% had an insignificant descending trend.

From Table 7.2, July shows the highest trend magnitude at 6.44 mm/year significant downward trend for APHRODITE using the ITA test. In contrast, October (6.23 mm/year) reveals the highest significant downward trend as per Sens's slope.

Table 7.1 ITA and MK trend tests of precipitation products

| Variable | Trend slope | Jan | Feb | Mar | Apr | May | Jun | Jul | Aug | Sep | Oct | Nov | Dec |
|-----------|-------------|-----|-----|-----|-----|-----|-----|-----|-----|-----|-----|-----|-----|
| APHRODITE | ITA | -* | -* | -* | -* | + | -* | -* | + | + | -* | -* | -* |
| | MK | - | - | - | - | | - | - | + | + | -* | - | - |
| ERA5 | ITA | -* | -* | -* | -* | * | + | -* | * | * | -* | + | +* |
| | MK | - | - | - | - | + | - | - | + | + | - | - | + |
| CHIRPS | ITA | -* | -* | -* | -* | + | - | -* | +* | +* | -* | -* | -* |
| | MK | - | - | - | - | + | - | - | + | + | - | - | - |
| CMORPH | ITA | + | +* | +* | +* | +* | +* | +* | +* | +* | -* | + | +* |
| | MK | + | + | + | + | +* | +* | + | +* | +* | - | + | + |
| SM2RAIN | ITA | -* | -* | -* | -* | - | -* | -* | +* | +* | -* | -* | -* |
| | MK | - | - | - | - | - | - | - | + | + | -* | -* | -* |
| TRMM | ITA | -* | -* | - | -* | - | -* | -* | +* | +* | -* | -* | - |
| | MK | - | - | - | - | - | + | - | + | + | - | - | - |
| IMERG | ITA | -* | -* | - | -* | + | -* | -* | +* | +* | -* | -* | -* |
| | MK | - | - | - | - | + | - | - | + | + | - | - | - |
| Ensemble | ITA | -* | -* | - | -* | * | + | -* | * | * | -* | - | * |
| | MK | - | - | - | - | + | + | - | + | + | - | - | + |

Note: * indicates significance at 5% level.

August shows the highest trend at 6.86 mm/year significant increasing trend for ERA5 precipitation (ITA test), whereas Sen's slope shows no significant trend for any month. Similarly, CHIRPS detected a significantly decreasing trend (3.58 mm/year) for April using ITA and an insignificant trend for any month from Sen's slope values. Interestingly, CMORPH captured a significant upward ITA trend of 7.91 mm/year for August and a significant ascending trend of 6.79 mm/year for May using Sen's slope. The month of July for SM2RAIN shows a significant downward trend of 2.49 mm/year as per ITA, whereas Sen's slope for November and December shows a 2.81 mm/year significant downward trend. With no significant trend as per Sen's slope for TRMM, the ITA reveals a 5.92 mm/year significant downward trend for July. Similarly, for the same month, IMERG shows 6.02 mm/year significant decreasing trend (ITA) with no significant trend for any month using Sen's slope. The ensemble precipitation also does not show any significant trend from Sen's slope measures for any month, but the ITA test reveals a significant positive trend for August. Our study corroborates with the findings of previous research (Chowdari et al., 2023; Marak et al., 2020; Singh et al., 2021)

7.3.2 Innovative trend analysis of ET, Q, and GRACE TWSC

Extracting data from Table 7.3, the ITA test of MOD16 ET exhibits about 67% of the 12 months' significant upward trends, about 17% significant decreasing trend, and about 8% of each insignificant increasing and decreasing trend. However, the MK test reveals about 17% significant increasing trends, about 58% of insignificant increasing trends, and 25% of insignificant decreasing trends. The CLSM ET ITA test shows around 58% of the month's significant positive trend, 33% a significant negative trend, and 8% insignificant downward trend. The MK test, however, reveals that only 8% of the months in which trends are significantly increasing, 17% are significantly declining, a high of 50% are insignificantly increasing, and 25% are decreasing. The Noah ET ITA reveals that approximately 17% of the months had a significant positive trend, 57% a significant negative trend, and 8% each for insignificant upward and downward trends. However, the MK test shows that only 8% of the months have a significant uptrend, a 17% (significant) downtrend, up to 17% (insignificant) uptrend, and a high 58% (insignificant) downtrend.

Table 7.2 ITA and Sen's slopes of precipitation products

| Variable | Trend slope | Jan | Feb | Mar | Apr | May | Jun | Jul | Aug | Sep | Oct | Nov | Dec |
|-----------|-------------|--------|--------|--------|--------|-------|--------|--------|-------|-------|--------|--------|--------|
| APHRODITE | ITA | -0.86* | -2.06* | -0.87* | -1.35* | 1.29 | -1.98* | -6.44* | 0.57 | 0.22 | -4.86* | -0.30* | -0.13* |
| | Sen's | -0.52 | -1.14 | -1.83 | -4.93 | 0.22 | -1.11 | -5.88 | 0.63 | 1.25 | -6.23* | -0.3 | -0.24 |
| ERA5 | ITA | -1.14* | -1.53* | -1.64* | -2.22* | 5.03* | 1.75 | -3.11* | 6.86* | 3.89* | -3.03* | 0.58 | 1.5* |
| | Sen's | -0.64 | -2 | -2.39 | -4.46 | 2 | -0.48 | -5.6 | 4.57 | 4.15 | -4 | -0.76 | 0.67 |
| CHIRPS | ITA | -0.61* | -0.93* | -0.53* | -3.58* | 1.16 | -0.34 | -3.15* | 3.3* | 1.35* | -3.12* | -0.29* | -0.09* |
| | Sen's | -0.32 | -0.35 | -1.07 | -4.84 | 1.64 | -0.95 | -1.93 | 1.26 | 0.77 | -3.48 | -0.17 | -0.1 |
| CMORPH | ITA | 0.1 | 0.4* | 2.25* | 2.75* | 6.73* | 7.13* | 1.57* | 7.91* | 5.01* | -1.61* | 0.31 | 0.52* |
| | Sen's | 0.62 | 1.1 | 1.76 | 2.17 | 6.79* | 8.1* | 3.38 | 5.76* | 4.85* | -1.51 | 0.65 | 0.59 |
| SM2RAIN | ITA | -0.07* | -0.53* | -0.52* | -1.56* | -0.08 | -1.3* | -2.49* | 1.31* | 1.19* | -1.97* | -0.21* | -0.07* |
| | Sen's | -1.44 | -1.58 | -1.17 | -1.71 | -0.21 | -0.62 | -1.3 | 1.44 | 1.71 | -1.99* | -2.81* | -2.81* |
| TRMM | ITA | -0.66* | -2.12* | -0.82 | -1.04* | -1.01 | -0.86* | -5.92* | 5.56* | 3.38* | -3.75* | -0.27* | -0.01 |
| | Sen's | -0.23 | -0.67 | -0.82 | -4.76 | -1.18 | 1.28 | -6.57 | 4.13 | 3.1 | -3.8 | -0.05 | -0.16 |
| IMERG | ITA | -0.8* | -1.5* | -0.47 | -1.18* | 0.47 | -1.61* | -6.02* | 3.97* | 2.44* | -4.08* | -0.75* | -0.08* |
| | Sen's | -0.24 | -0.79 | -0.09 | -4.53 | 0.53 | -1.06 | -5.42 | 2.2 | 2.77 | -5.09 | -0.1 | -0.16 |
| Ensemble | ITA | -0.58* | -1.18* | -0.37 | -1.17* | 1.94* | 0.4 | -3.65* | 4.21* | 2.5* | -3.2* | -0.13 | 0.24* |
| | Sen's | -0.14 | -0.38 | -0.76 | -2.82 | 1.43 | 1.22 | -3.23 | 2.41 | 2.16 | -3.47 | -0.05 | 0.12 |

Note: * indicates significance at 5% level. The units of slopes are in mm/year.

Table 7.3 ITA and MK trend tests of ET, Q, and TWSC

| Variable | Trend slope | Jan | Feb | Mar | Apr | May | Jun | Jul | Aug | Sep | Oct | Nov | Dec |
|---------------|-------------|-----|-----|-----|-----|-----|-----|-----|-----|-----------|-----|-----|-----|
| MOD16 ET | ITA | + | -* | -* | - | +* | +* | +* | +* | +* | +* | +* | +* |
| | MK | + | - | - | - | + | + | +* | + | + | +* | + | + |
| GLDAS CLSM ET | ITA | -* | +* | - | +* | +* | +* | +* | +* | +* | -* | -* | -* |
| | MK | - | - | + | + | + | +* | + | + | + | - | -* | -* |
| GLDAS Noah ET | ITA | -* | -* | -* | -* | - | +* | -* | -* | -* | + | +* | -* |
| | MK | - | - | -* | - | + | +* | - | - | -* | - | + | - |
| Terra ET | ITA | -* | -* | -* | -* | -* | +* | - | +* | - | -* | -* | -* |
| | MK | -* | - | - | - | - | + | + | + | No | + | - | - |
| Ensemble (ET) | ITA | -* | -* | -* | -* | + | +* | +* | +* | +* | -* | -* | -* |
| | MK | -* | -* | - | - | + | +* | + | + | + | - | - | -* |
| Runoff (Q) | ITA | -* | -* | -* | -* | -* | -* | -* | + | -* | -* | -* | -* |
| | MK | - | - | - | - | - | - | - | + | - | - | - | - |
| GRACE TWSC | ITA | -* | -* | -* | +* | -* | - | +* | -* | No | + | -* | +* |
| | MK | - | -* | - | + | - | + | + | - | - | - | - | + |

Note: * indicates significance at 5% level.

According to the TerraClimate ET ITA, there were significant upward trends in about 17% of the months, significant downward trends in 66% of the months, and insignificant downward trends in 17% of the months. MK test, however, reveals that just 8% have a significant downtrend, up to 33% have an insignificant trend, and as high as 58% have an insignificant downtrend. With a significant uptrend of 34% of the months, the ensemble ET shows a staggering 58% significant downtrend. It only shows just 8% insignificant uptrend. The MK test for the ensemble shows a mere 8% of the months with significant uptrend, a higher 25% significant downtrend and a little higher 33% each for insignificant uptrend and downtrend.

The ITA test of in-situ runoff shows about 92% of the months with a significant decreasing trend and just about 8% insignificant decreasing trend, whereas in MK test, about 8% show insignificant uptrend and about 92% insignificant downtrend. The ITA test of GRACE TWSC shows 25%, 50%, 8% and 17% of the months significant up and down trends and insignificant up and down trends, respectively. The MK test shows about 8%, 33% and 59% of the months significant down trend, insignificant up and down trends, respectively.

Referring Table 7.4, MOD16 ET shows the highest significantly up trend of 0.86 mm/year for the month of July, whereas Sen's slope shows about the same significant uptrend of 0.9 mm/year for the same month. For the month of June, CLSM ET shows the highest significant uptrend of 1.62 and 1.93 mm/year as per ITA and Sen's slope, respectively. For the months of July (ITA) and March (Sen's slope), Noah ET reveals the significant downtrends are respectively 0.84 mm/year and 0.96 mm/year. For the months of April (ITA) and January (Sen's slope), TerraClimate ET shows downtrends of 0.83 mm/year and 0.31 mm/year, respectively. The ensemble ET reveals significant up trends of 0.84 and 0.94 mm/year, respectively for ITA and Sen's slope.

While Sen's slope reveals no significant trend in Q, the ITA test shows the highest significant downtrend of 1073 cumecs/year for the month of November. ITA test for the GRACE TWSC depicts an upward trend of 4.15 mm/year for June, whereas a significant decreasing trend of 2.26 mm/year was noticed for February.

The above results are in consistent with the results found elsewhere (Chowdari et al. 2023; Marak et al. 2020; Singh et al. 2021).

7.3.3 Sub-trends of precipitation estimates, ET, Q and GRACE TWSC

Since the ITA method has the advantage of detecting the hidden trends, sub-trend analysis was carried out on continuous monthly data instead of the individual months for the sake of maintaining brevity and to better understand how ITA is different from traditional MK tests. Red (low), green (middle), and blue (high) represent different clusters, reflecting the sub-trends. Brick red symbolizes the original time series trend.

In Fig.7.1(a), the APHRODITE shows the highest downtrend of 3.3425 mm/month in the higher percentile cluster. This is closely followed by a downtrend in IMERG data (3.2626 mm/month), as shown in Fig.7.1(g). However, SM2RAIN (Fig.7.1(e)) shows the least downtrend at 1.3043 mm/month in the same cluster. CMORPH is the only data to show an increasing trend at 0.883 mm/month in this category in Fig.7.1(d).

With a magnitude of 0.3487 mm/month, CMORPH Fig.7.1(d) reveals the highest uptrend in the medium cluster. While the highest decreasing trend in this category is depicted by APHRODITE (Fig.7.1(a)) at 0.1235 mm/month, and the least decreasing trend is seen in TRMM (0.0325 mm/month) in Fig.7.1(f).

In the low cluster in Fig.7.1(d), CMORPH shows the highest uptrend of 0.631 mm/month, whereas the highest downtrend of 0.0669 mm/month was seen in CHIRPS (Fig.7.1(c)). The least uptrend is seen in IMERG (0.0424 mm/month), while the least downtrend is noticed in APHRODITE data at 0.0377 mm/month (Fig.7.1(a)).

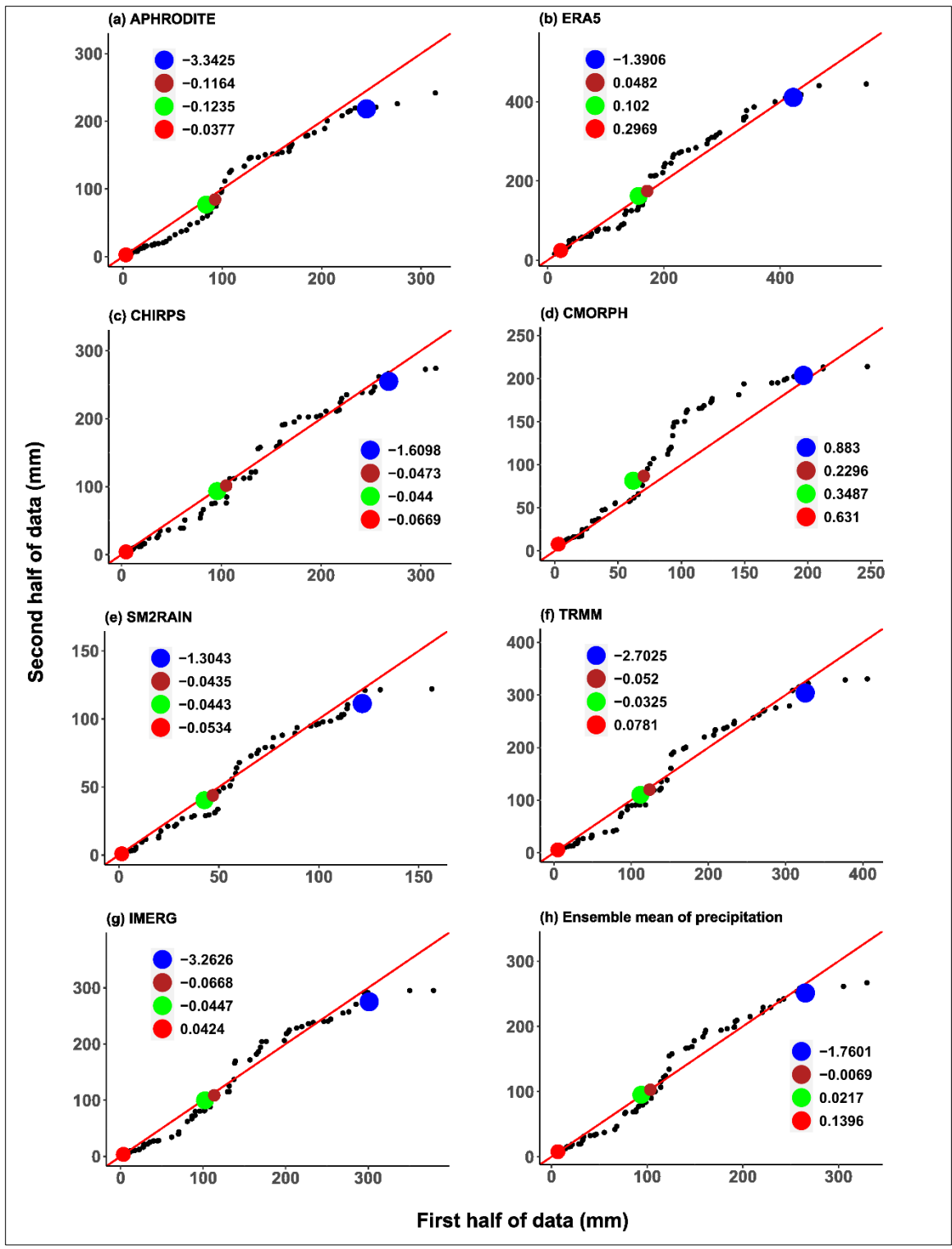


Fig.7.1 Subtrends of precipitation products using ITA

Table 7.4 ITA and Sen's slopes of ET, Q, and TWSC

| Variable | Trend slope | Jan | Feb | Mar | Apr | May | Jun | Jul | Aug | Sep | Oct | Nov | Dec |
|---------------|-------------|--------|--------|--------|--------|--------|-------|--------|--------|--------|--------|--------|--------|
| MOD16 ET | ITA | 0.05 | -0.19* | -0.18* | -0.03 | 0.29* | 0.58* | 0.86* | 0.32* | 0.53* | 0.42* | 0.19* | 0.09* |
| | Sen's | 0.08 | -0.08 | -0.09 | -0.21 | 0.34 | 0.57 | 0.9* | 0.17 | 0.59 | 0.5* | 0.18 | 0.14 |
| GLDAS | ITA | -0.73* | 0.13* | -0.08 | 0.37* | 0.62* | 1.62* | 1.1* | 0.68* | 0.21* | -0.56* | -1.39* | -1.51* |
| CLSM ET | Sen's | -0.54 | -0.24 | 0.08 | 0.85 | 0.63 | 1.93* | 1.53 | 0.56 | 0.03 | -0.42 | -1.14* | -1.18* |
| GLDAS | ITA | -0.25* | -0.23* | -0.87* | -1.17* | -0.02 | 0.65* | -0.84* | -0.24* | -0.51* | 0.01 | 0.22* | -0.22* |
| Noah ET | Sen's | -0.23 | -0.28 | -0.96* | -0.74 | 0.19 | 0.58* | -0.77 | -0.6 | -0.56* | -0.07 | 0.16 | -0.2 |
| Terra ET | ITA | -0.39* | -0.44* | -0.41* | -0.83* | -0.69* | 0.51* | -0.13 | 0.34* | -0.05 | -0.1* | -0.17* | -0.17* |
| | Sen's | -0.31* | -0.24 | -0.55 | -0.5 | -0.07 | 0.57 | 0.28 | 0.32 | 0 | 0.13 | -0.13 | -0.21 |
| Ensemble (ET) | ITA | -0.33* | -0.18* | -0.38* | -0.42* | 0.05 | 0.84* | 0.25* | 0.27* | 0.05* | -0.05* | -0.29* | -0.45* |
| | Sen's | -0.28* | -0.21* | -0.4 | -0.21 | 0.23 | 0.94* | 0.42 | 0.17 | 0.06 | -0.02 | -0.22 | -0.33* |
| Runoff (Q) | ITA | -445* | -496* | -555* | -459* | -387* | -629* | -477* | 6 | -717* | -629* | - | -748* |
| | Sen's | -284 | -172 | -170 | -190 | -59 | -498 | -150 | 150 | -103 | -283 | -709 | -418 |
| GRACE | ITA | -3.29* | -1.09* | -1.24* | 2.85* | -1.97* | -0.23 | 4.15* | -2.33* | 0 | 0.2 | -0.75* | 1.93* |
| TWSC | Sen's | -1.77 | -2.26* | -1.98 | 3.57 | -2.52 | 0.89 | 4.28 | -3.26 | -0.53 | -0.06 | -0.27 | 0.52 |

Note: * indicates significance at 5% level. The units of slopes are in mm/year except for runoff (Q) which is in m³/s/ year.

From Fig.7.2(b), the highest uptrend in the high cluster is depicted by CLSM ET (0.5505 mm/month), whereas the least uptrend is observed in TerraClimate ET (0.0205 mm/month) as shown in Fig.7.2(d). In addition, the only downtrend is noticed for Noah ET (0.2208 mm/month) in Fig.7.2(c).

In the medium cluster, the highest and lowest uptrends are 0.024 mm/year (Fig.7.2(a)) for MOD16 ET and 0.0048 mm/month for CLSM ET (Fig.7.2(b), respectively. The highest and least down trends are shown by TerraClimate ET (0.0254 mm/month) in Fig.7.2(d) and ensemble ET (0.0055 mm/month) in Fig.7.2(e).

With a downtrend of 0.5246 mm/month, CLSM ET shows the highest decrease, as shown in Fig.7.2(b) in the low cluster. And the least downtrend being led by 0.1134 mm/month. MOD16 ET establishes the only uptrend at 0.0564 mm/month.

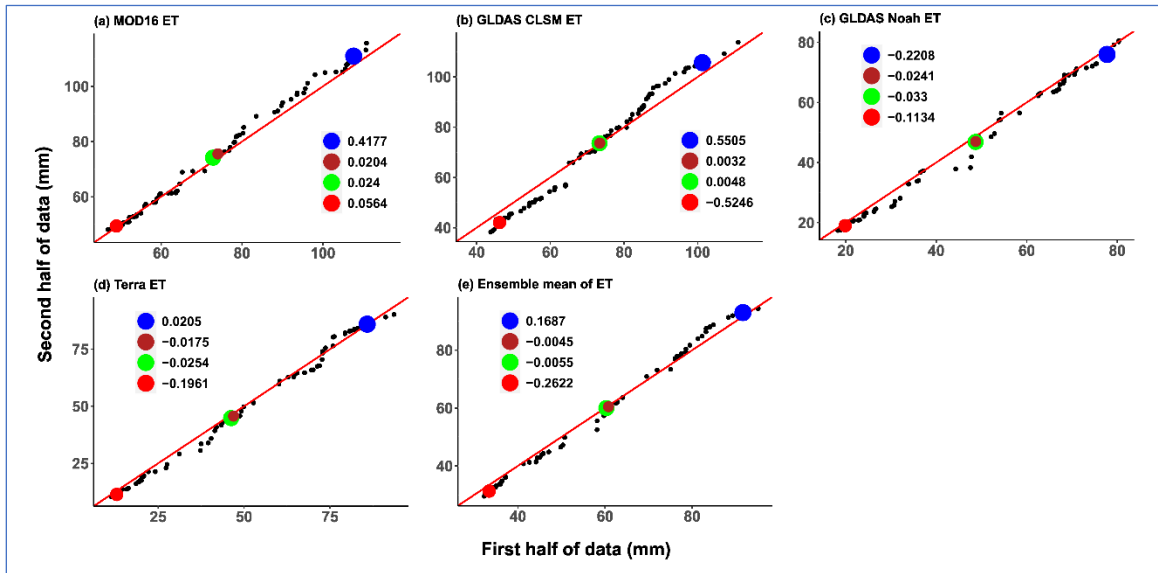


Fig.7.2 Subtrends of ET products using ITA

In Fig.7.3(a), the high cluster observed runoff at a decreasing trend of 339.0191 mm/month, whereas GRACE TWSC shows a downtrend of 7.7501 mm/month. The medium cluster shows discharge decreasing at 65.3471 mm/month and the GRACE TWSC at decreasing trend of 1.3522 mm/month. In the low cluster, a rate of 176.7871 mm/month and 8.6855 mm/month down trends were observed for observed discharge and GRACE TWSC. The findings are consistent with the sub-trend analysis reported elsewhere (Chowdari et al., 2023; Wang et al., 2020).

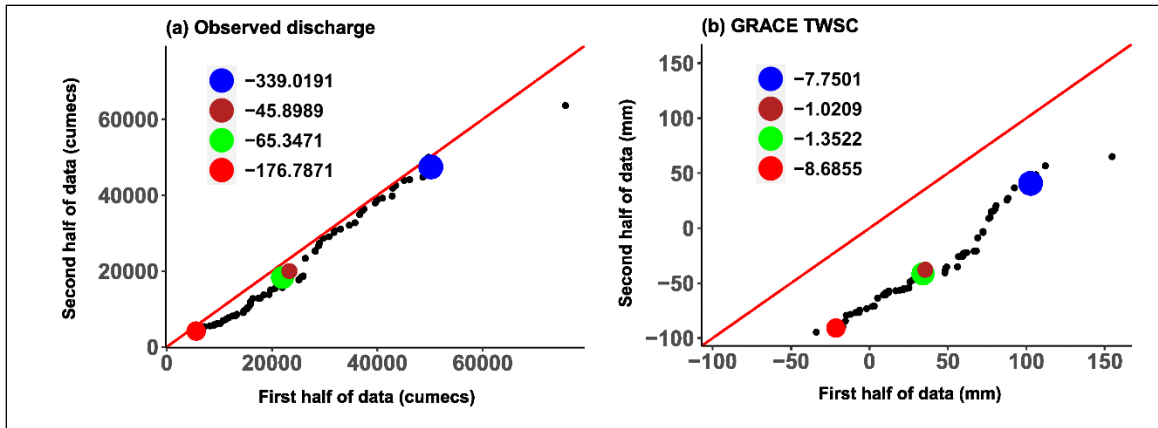


Fig.7.3 Subtrends of discharge and GRACE TWSC using ITA

7.3.4 Innovative polygon trend analysis of different precipitation products

The IPTA, as an extended version of the ITA method, is used to understand the transition behaviour of a water budget variable between months or seasons or any other suitable scale used in water resources management. Fig.7.4 is the representation of precipitation climatology (long-term mean), and Table 7.5 provides information on the trend length/volume (TL) and trend slope (TS) of monthly mean precipitation. The corresponding TL and TS for the long-term standard deviation of the rainfall estimates are shown in Table 7.6 along with Fig.7.5, which is the IPTA template like Fig.7.4.

In Fig.7.4(a), only the month of May is in trend increasing region (above 1:1 or 45°), whereas August, September, November, and December appear to be on the no-trend line (1:1), and the remaining months are in trend decreasing zone. There appear to be trend transitions from April to May and July to August. Also, the polygon seems to be more than one loop. Water budget variable like precipitation is more dynamic and chaotic. Hence, it is expected to have more than one polygon (Şen et al. 2019). The maximum trend length and slope for the APHRODITE climatology are 105.5 mm and 1.66, respectively. Similarly, all other rainfall products show similar shapes of the polygon. However, there could be some months of a precipitation measure like CMORPH in which many months of the year fall in the increasing zone of the IPTA (Fig.7.4(d)). February through September are in the growing region of the IPTA, whereas the remaining months are either on the no-trend line or in decreasing region. Since the

description of Fig.7.4 is self-explanatory, the explanation of one IPTA diagram is sufficient. Accordingly, the trend lengths (TL) of ERA5, CHIRPS, CMORPH, SM2RAIN, TRMM, IMERG, and ensemble precipitation are 168.4, 130.42, 92.2, 61.5, 149.9, 145.5 and 120.45 mm, respectively. Their corresponding trend slopes are 2.36, 3.24, 2.53, 1.72, 1.52, 1.48 and 1.69. It is also worth mentioning that the trend length transition occurred from September to October, except for SM2RAIN, which has the maximum trend length from May-June. The trend slopes occurred in April-May transition for all the precipitation climatology except for SM2RAIN, TRMM, and IMERG, whose maximum trend slopes occurred while transitioning from September – October.

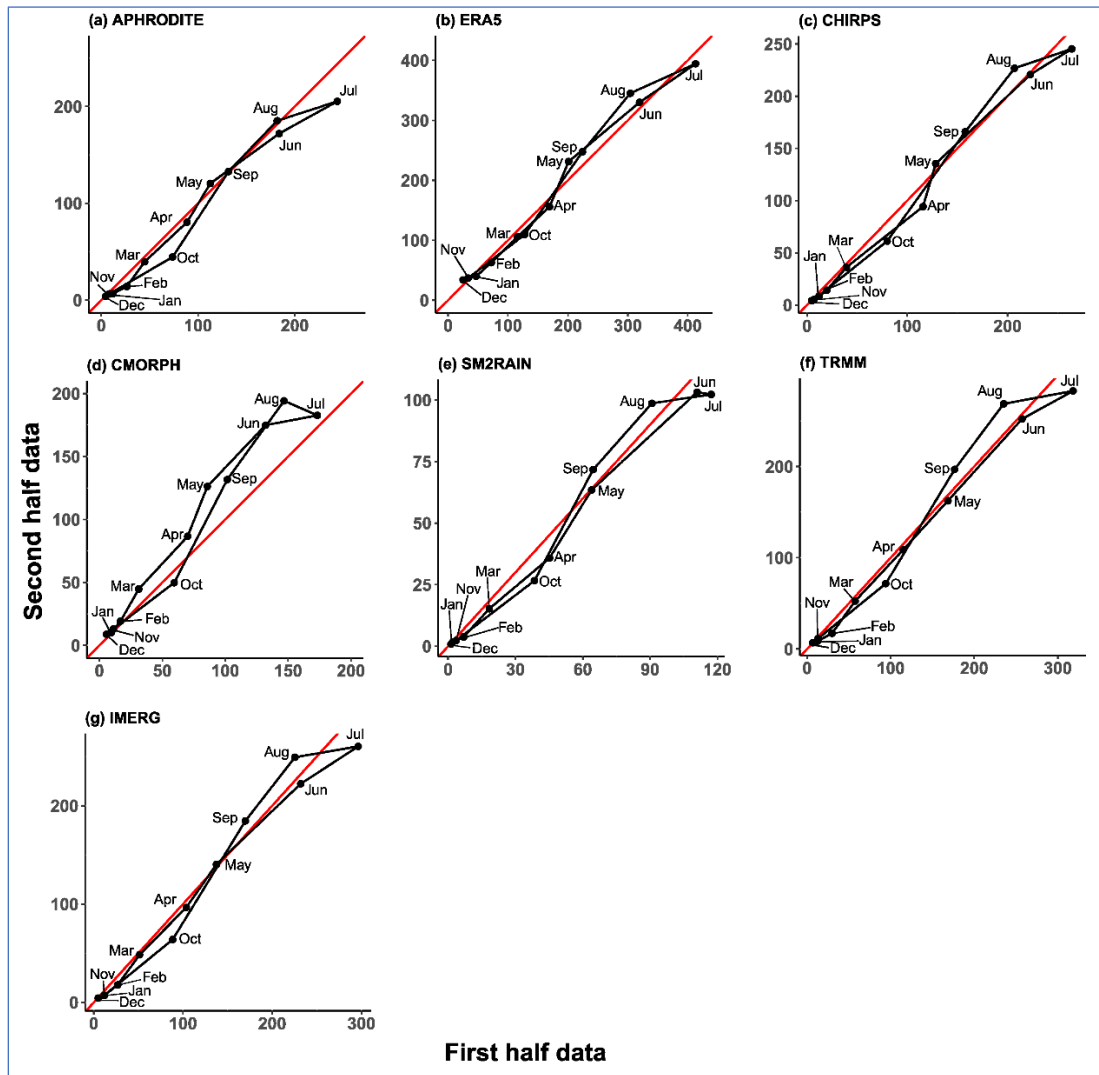


Fig.7.4 IPTA diagram for mean of the precipitation.

Table 7.5 IPTA of mean of precipitation products

| Variable | Trend | Jan- Feb | Feb- Mar | Mar- Apr | Apr- May | May- Jun | Jun- Jul | Jul- Aug | Aug- Sep | Sep- Oct | Oct- Nov | Nov- Dec | Dec- Jan |
|-----------|-------|-------------|-------------|-------------|-------------|-------------|-------------|-------------|-------------|-------------|-------------|-------------|-------------|
| APHRODITE | TL | 16.3 | 31.5 | 59.8 | 46.8 | 87.8 | 68.7 | 65.3 | 72.6 | 105.5 | 75.8 | 4.7 | 8.0 |
| | TS | 0.50 | 1.39 | 0.93 | 1.66 | 0.72 | 0.55 | 0.32 | 1.04 | 1.53 | 0.58 | 0.72 | 0.41 |
| ERA5 | TL | 34.0 | 61.3 | 73.2 | 82.0 | 154.1 | 113.5 | 119.6 | 126.1 | 168.4 | 119.1 | 9.0 | 22.8 |
| | TS | 0.91 | 0.98 | 0.93 | 2.36 | 0.83 | 0.69 | 0.45 | 1.22 | 1.43 | 0.77 | 0.35 | 0.28 |
| CHIRPS | TL | 9.64 | 29.37 | 96.07 | 43.05 | 127.17 | 48.24 | 60.17 | 78.28 | 130.42 | 91.94 | 2.54 | 8.42 |
| | TS | 0.75 | 1.12 | 0.76 | 3.24 | 0.9 | 0.59 | 0.32 | 1.24 | 1.34 | 0.77 | 0.47 | 0.57 |
| CMORPH | TL | 11.55 | 29.47 | 57.17 | 42.56 | 67.17 | 41.92 | 28.88 | 77.07 | 92.2 | 60.71 | 6.91 | 4.02 |
| | TS | 1.25 | 1.76 | 1.08 | 2.53 | 1.05 | 0.19 | -0.44 | 1.39 | 1.94 | 0.76 | 0.78 | 0.34 |
| SM2RAIN | TL | 5.3 | 16.15 | 33.86 | 33.42 | 61.5 | 6.32 | 26.64 | 37.58 | 52.18 | 42.49 | 2.72 | 1.14 |
| | TS | 0.43 | 1 | 0.77 | 1.47 | 0.84 | -0.14 | 0.14 | 1.03 | 1.72 | 0.7 | 0.63 | 0.99 |
| TRMM | TL | 19.24 | 44.85 | 80.52 | 75.75 | 126.07 | 68.32 | 84.17 | 92.8 | 149.9 | 100.97 | 7.68 | 6.05 |
| | TS | 0.49 | 1.28 | 0.98 | 1 | 1.01 | 0.5 | 0.17 | 1.22 | 1.52 | 0.74 | 0.74 | 0.32 |
| IMERG | TL | 18.1 | 39.4 | 71.0 | 55.3 | 125.0 | 75.0 | 72.0 | 85.2 | 145.5 | 95.7 | 7.3 | 7.7 |
| | TS | 0.71 | 1.25 | 0.92 | 1.29 | 0.87 | 0.59 | 0.16 | 1.17 | 1.48 | 0.74 | 0.40 | 0.40 |
| Ensemble | TL | 16.14 | 35.86 | 67.28 | 53.37 | 106.82 | 59.72 | 63.98 | 81.32 | 120.45 | 83.74 | 5.79 | 8.28 |
| | TS | 0.72 | 1.21 | 0.9 | 1.69 | 0.88 | 0.54 | 0.24 | 1.2 | 1.52 | 0.73 | 0.56 | 0.37 |

Table 7.6 IPTA of standard deviation of precipitation products

| Variable | Trend | Jan- Feb | Feb- Mar | Mar- Apr | Apr- May | May- Jun | Jun- Jul | Jul- Aug | Aug- Sep | Sep- Oct | Oct- Nov | Nov- Dec | Dec- Jan |
|-----------|-------|-------------|-------------|-------------|-------------|-------------|-------------|-------------|-------------|-------------|-------------|-------------|-------------|
| APHRODITE | TL | 4.17 | 20.09 | 23.73 | 10.51 | 6.64 | 20.24 | 20.08 | 18.95 | 5.71 | 30.57 | 3.62 | 6.95 |
| | TS | -0.21 | 1.51 | -9.21 | -3.21 | -0.74 | -0.69 | -4.93 | 0.5 | -2.88 | 0.95 | 1.29 | 0.72 |
| ERA5 | TL | 8.92 | 31.54 | 29.83 | 16.45 | 29.86 | 40.61 | 32.6 | 33.23 | 18.86 | 25.84 | 8.7 | 17.1 |
| | TS | 2.53 | 1.93 | -1.87 | -0.75 | 0.16 | -0.79 | -1.52 | 0.53 | 1.09 | 0.8 | 0.98 | 0.6 |
| CHIRPS | TL | 3.08 | 10.01 | 30.82 | 13.3 | 7.35 | 13.95 | 6.49 | 19.43 | 17.82 | 29.1 | 2.12 | 4.54 |
| | TS | 0.04 | 1.62 | 2.34 | 8.7 | 1.26 | -0.74 | 0.18 | -3.65 | 1.13 | 1.82 | 0.71 | 0.3 |
| CMORPH | TL | 5.76 | 8.5 | 21.71 | 14.02 | 6.45 | 16.11 | 2.57 | 30.32 | 15.16 | 14.56 | 8.39 | 7.25 |
| | TS | - 38.79 | 1.04 | 8.35 | -0.5 | -0.49 | -0.59 | 0.57 | -0.48 | 3.89 | 2.15 | 0.07 | 0.04 |
| SM2RAIN | TL | 1.13 | 5.53 | 6.15 | 4.76 | 3.23 | 8.46 | 5.55 | 10.07 | 8.24 | 10.17 | 0.56 | 0.31 |
| | TS | 0.68 | 1.16 | 2.21 | 0.12 | 2.71 | -0.63 | -0.37 | 0.08 | -1.37 | 0.41 | 0.74 | 1.42 |
| TRMM | TL | 5.33 | 24.17 | 37.88 | 29.27 | 9.93 | 36.75 | 12.25 | 22.37 | 15.87 | 36.65 | 8.15 | 5.49 |
| | TS | 0.41 | 1.82 | -10.09 | -1.35 | -2.69 | -0.47 | -0.11 | -0.8 | 2.09 | 1.34 | 0.66 | 0.36 |
| IMERG | TL | 2.03 | 24.09 | 30.15 | 18.58 | 7.75 | 29.15 | 13.59 | 22.93 | 18.65 | 34.43 | 8.4 | 7.41 |
| | TS | 0.45 | 1.77 | -6.25 | -1.59 | 0.24 | -0.58 | -0.25 | -1.76 | 2.16 | 1.59 | 0.29 | 0.28 |
| Ensemble | TL | 1.64 | 17.65 | 24.72 | 14.01 | 7.63 | 23.52 | 11.37 | 17.79 | 13.23 | 25.44 | 5.47 | 6.87 |
| | TS | 0.02 | 1.66 | -21.99 | -1.32 | 0.35 | -0.63 | -0.84 | -0.35 | 2.35 | 1.24 | 0.53 | 0.42 |

Note: TL=trend length, TS= trend slope; All TL are in mm and TS is unit less.

Fig.7.5 shows at least three loops for all the precipitation datasets except for CMORPH. The more the number of polygons, the more dynamic the variable is. For example, the standard deviation of APHRODITE in Fig.7.5(a) shows April, May, and June in the increasing region, whereas the remaining months are in the downtrend region. The increasing transitions occurred from March to April, August to September, whereas the decreasing transition occurred from September to October and June to July. The maximum trend length and trend slope are 30.57 mm and 1.51, as shown in Table 7.6.

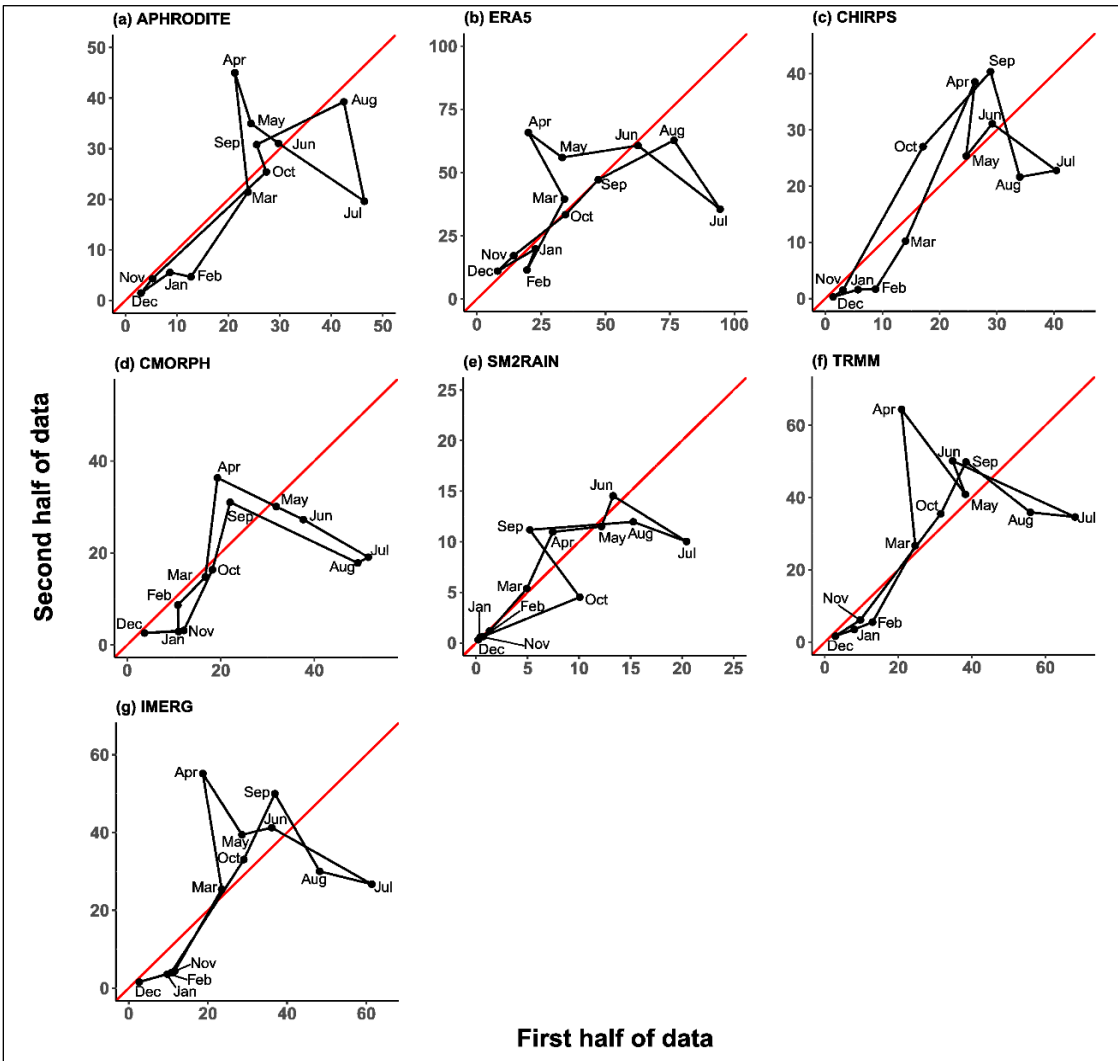


Fig.7.5 IPTA diagram for standard deviation of the precipitation

The maximum TL for the standard deviation of ERA5, CHIRPS, CMORPH, SM2RAIN,

TRMM, IMERG, and ensemble precipitation (no IPTA plot for ensemble precipitation) are 40.61, 30.82, 30.32, 10.17, 37.88, 34.43 and 25.44 mm, respectively. And the maximum trend slope for the standard deviation of ERA5, CHIRPS, CMORPH, SM2RAIN, TRMM, IMERG, and ensemble precipitation are 2.53, 2.34, 8.35, 2.71, 2.09, 2.16, and 1.66 respectively.

7.3.5 Innovative polygon trend analysis of ET, Q, and GRACE TWSC

From Fig.7.6, the polygons of the mean of ETs are not distinct for MOD16 ET, but CLSM ET and Noah ET tend to have more distinct polygons. For example, CLSM ET in Fig.7.7(b) was considered for the discussion. February to March lie on a 1:1 or no trend line, April to September in the increasing region. In contrast, October, November, December, and January lie in the decreasing region of the IPTA. September to October transitions from an increasing to decreasing region, while March to April transitions from a no trend to an increasing trend region. From Table 7.7, the maximum trend length (TL) of the mean of GLDAS CLSM ET is 23.63 mm, and the maximum slope is 3.81. Similarly, the maximum TL of the standard deviation of MOD16 ET, Noah ET, TerraClimate ET, and ensemble ET are 27.3, 24.86, 34.33, and 26.03 mm, whereas the corresponding trend slopes are 5.84, 1.75, 2.21, and 1.96.

In Fig.7.7(d), the vertices polygons of TerraClimate ET represent its monthly standard deviations. March, June, April, October, November, and December are in the increasing trend region, whereas the remaining months are in the decreasing trend region. The transition increase trend occurs between September to October, May to June, and decreasing transition between April to May and December to January. The maximum TL of the standard deviation of TerraClimate ET is 5.85 mm, and the maximum TS is 4.17. Similarly, the maximum TL of the standard deviation of MOD16 ET, CLSM ET, Noah ET, and ensemble ET are 2.31, 6.66, 4.16, and 2.59 mm, respectively (Table 7.8). The corresponding maximum TS are 7.69, 5.32, 19.22, and 4.7, respectively (Table 7.8).

In Fig.7.8(a), the observed discharge shows that all the months except August lie in decreasing trend region of the IPTA diagram. The month of August lies on no trend line. However, the standard deviation of the same variable in Fig.7.8(c) shows a different

scenario: Only April, May, October, and September lie in the uptrend region. In contrast, the rest lie in the downtrend region. The maximum TV of the mean of Q is 17276.6 m³/s, and the corresponding TS is 3, as shown in Table 7.7. Its corresponding maximum TV of the standard deviation of Q is 6648.5 m³/s, and the maximum TS is 21.83, as shown in Table 7.8. Similarly, the maximum TL of the mean of GRACE TWSC is 85.8 mm, and the maximum TS is 31.64 (Table 7.7). Also, the maximum TL of the standard deviation of GRACE TWSC is 29.06 mm, and the corresponding TS is 4.96.

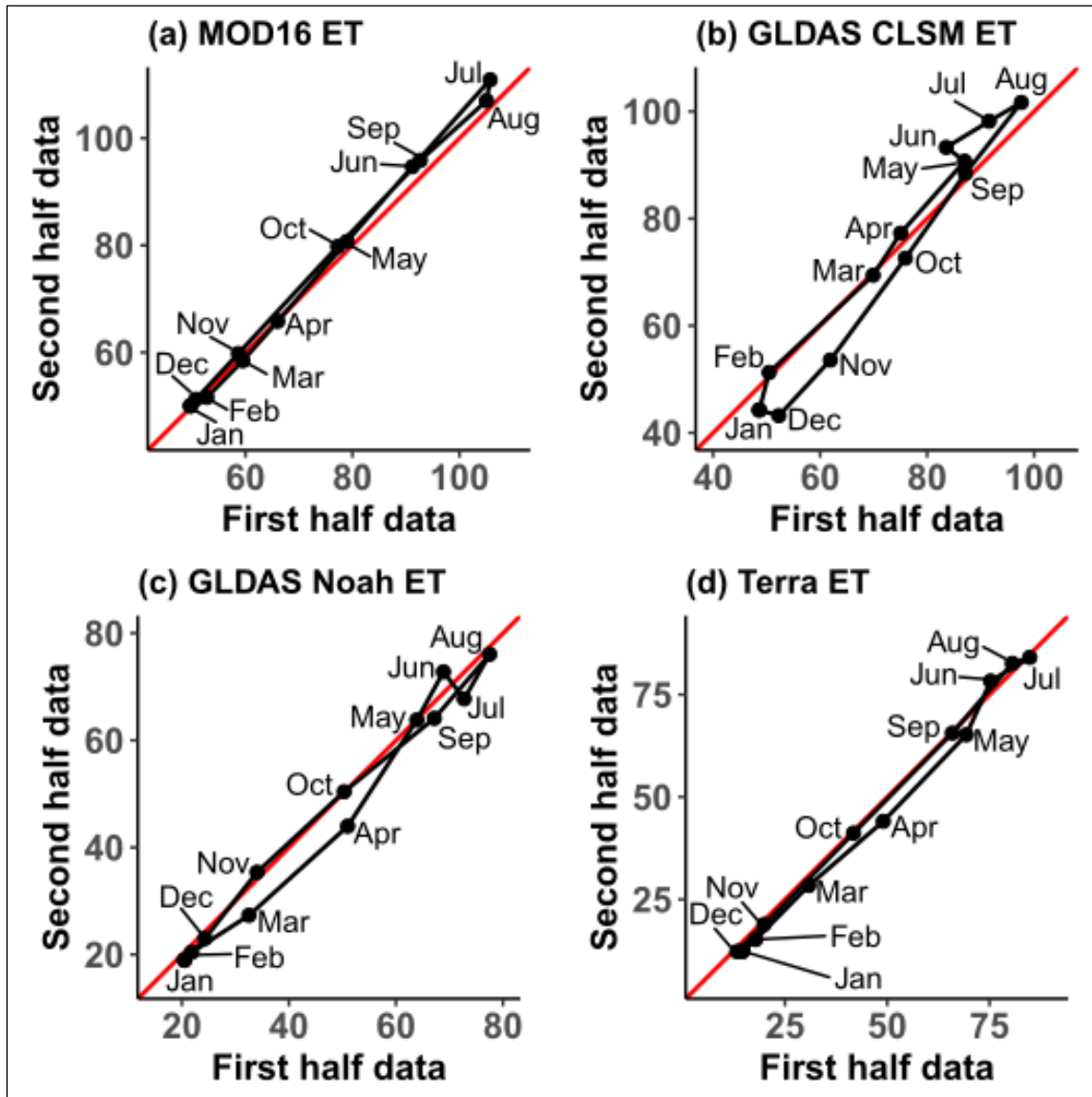


Fig.7.6 IPTA diagram for mean of the ET

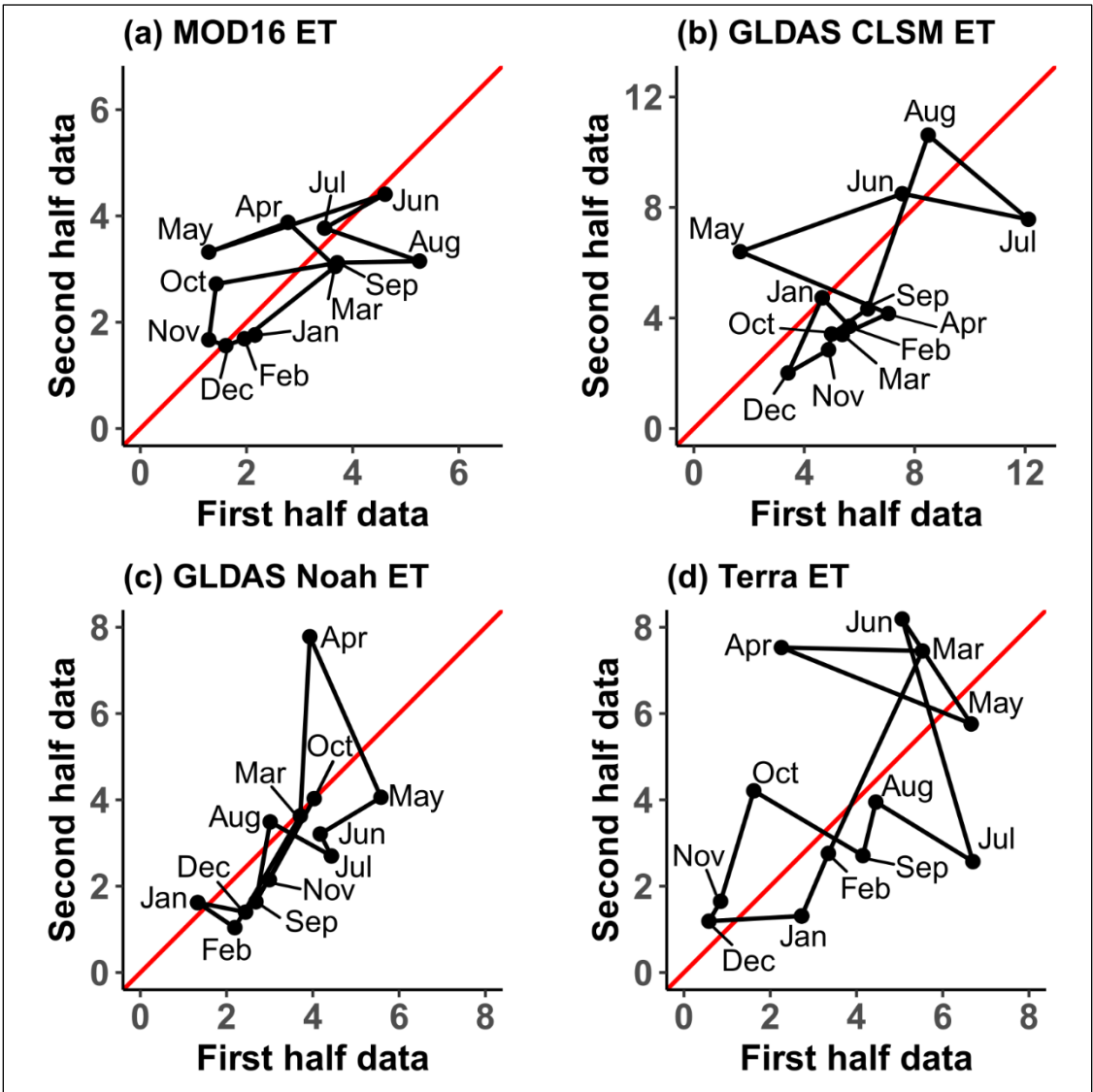


Fig.7.7 IPTA diagram for standard deviation of the ET

It is to be noted that the TL/TV tells us about the magnitude of transitioning of trend, whereas the magnitude of slope tells us about the intensity of occurrence of events. The lower the slope, the greater the intensity of the hydrological events. Our study corroborates previous findings on TL/TV and TS estimations (Akçay et al. 2021; Şen et al. 2019; Sezen 2022).

Table 7.7 IPTA of mean of ET, Q and TWSC

| Variable | Trend | Jan- Feb | Feb- Mar | Mar- Apr | Apr- May | May- Jun | Jun-Jul | Jul- Aug | Aug- Sep | Sep- Oct | Oct- Nov | Nov- Dec | Dec- Jan |
|-------------------|-------|-------------|-------------|-------------|-------------|-------------|---------|-------------|-------------|-------------|-------------|-------------|-------------|
| MOD16 ET | TL | 3.5 | 9.6 | 9.8 | 19.7 | 18.6 | 21.8 | 4.0 | 16.7 | 22.3 | 27.3 | 11.7 | 1.6 |
| | TS | 0.52 | 1.02 | 1.13 | 1.15 | 1.14 | 1.12 | 5.84 | 0.90 | 1.04 | 1.08 | 1.08 | 1.19 |
| GLDAS | TL | 7.25 | 26.6 | 9.39 | 17.98 | 4.31 | 9.4 | 6.96 | 16.88 | 19.4 | 23.63 | 14.13 | 3.82 |
| CLSM ET | TS | 3.81 | 0.93 | 1.53 | 1.12 | -0.75 | 0.61 | 0.58 | 1.27 | 1.41 | 1.36 | 1.08 | -0.28 |
| GLDAS | TL | 1.99 | 12.73 | 24.86 | 23.67 | 10.27 | 6.36 | 9.6 | 15.81 | 21.73 | 22.16 | 15.74 | 5.57 |
| Noah ET | TS | 1.08 | 0.65 | 0.9 | 1.53 | 1.81 | -1.3 | 1.75 | 1.16 | 0.81 | 0.92 | 1.27 | 1.05 |
| Terra ET | TL | 4.27 | 18.51 | 24.01 | 29.3 | 14.41 | 11.17 | 4.51 | 22.48 | 34.33 | 31.25 | 9.37 | 1.42 |
| | TS | 0.9 | 1.01 | 0.86 | 1.04 | 2.21 | 0.6 | 0.35 | 1.16 | 1.01 | 1.02 | 1 | 0.07 |
| Ensembl e (ET) | TL | 4 | 16.81 | 16.94 | 22.61 | 10.85 | 10.53 | 2.17 | 17.92 | 24.34 | 26.03 | 12.72 | 2.05 |
| | TS | 1.37 | 0.9 | 0.98 | 1.19 | 1.96 | 0.61 | 1.11 | 1.11 | 1.04 | 1.08 | 1.12 | 0.58 |
| Runoff (Q) | TV | 1835. | 1447. | 5957. | 8392. | 17276. | 26386. | 10962. | 6856. | 12500. | 14799. | 8649. | 5102. |
| | TS | 1 | 5 | 4 | 1 | 6 | 0 | 9 | 3 | 3 | 7 | 3 | 9 |
| GRACE TWSC | TL | 27.3 | 28.0 | 23.7 | 50.8 | 10.8 | 85.8 | 52.5 | 73.2 | 11.1 | 16.9 | 38.8 | 40.8 |
| | TS | 2.14 | 0.96 | -29.28 | 0.39 | 31.64 | 0.64 | 4.19 | 0.76 | 0.86 | 0.61 | 1.88 | 0.21 |

Note: TL=trend length, TV= trend volume, TS= trend slope; All TV in mm, except for runoff in m³/s. TS is unit less.

Table 7.8 IPTA of standard deviation of ET, Q and TWSC

| Variable | Trend | Jan- Feb | Feb- Mar | Mar- Apr | Apr- May | May- Jun | Jun-Jul | Jul- Aug | Aug- Sep | Sep- Oct | Oct- Nov | Nov- Dec | Dec- Jan |
|---------------------|-------|-------------|-------------|-------------|-------------|-------------|-------------|-------------|-------------|-------------|-------------|-------------|-------------|
| MOD16 ET | TL | 0.22 | 2.19 | 1.22 | 1.59 | 3.49 | 1.31 | 1.89 | 1.55 | 2.31 | 1.06 | 0.33 | 0.59 |
| | TS | 0.36 | 0.8 | -0.92 | 0.37 | 0.33 | 0.57 | -0.34 | 0.02 | 0.17 | 7.69 | -0.37 | 0.36 |
| GLDAS CLSM ET | TL | 1.43 | 0.4 | 1.83 | 5.82 | 6.23 | 4.66 | 4.74 | 6.66 | 1.6 | 0.57 | 1.7 | 2.99 |
| | TS | -1.05 | 1.2 | 0.46 | -0.42 | 0.36 | -0.2 | -0.84 | 2.88 | 0.69 | 5.32 | 0.57 | 2.19 |
| GLDAS Noah ET | TL | 1.03 | 2.99 | 4.16 | 4.08 | 1.65 | 0.57 | 1.62 | 1.87 | 2.74 | 2.14 | 0.93 | 1.13 |
| | TS | -0.67 | 1.7 | 19.22 | -2.25 | 0.6 | -1.95 | -0.56 | 5.51 | 1.77 | 1.82 | 1.36 | -0.2 |
| Terra ET | TL | 1.59 | 5.17 | 3.28 | 4.75 | 2.91 | 5.85 | 2.63 | 1.27 | 2.95 | 2.68 | 0.54 | 2.15 |
| | TS | 2.33 | 2.15 | -0.02 | -0.4 | -1.51 | -3.43 | -0.61 | 4.17 | -0.59 | 3.35 | 1.71 | 0.06 |
| Ensembl e (ET) | TL | 0.57 | 2.45 | 1.56 | 0.97 | 1.95 | 2.34 | 1.79 | 2.59 | 1.36 | 1.6 | 0.73 | 1.08 |
| | TS | -0.1 | 1.62 | -2.56 | 4.7 | 0.77 | -1.44 | -0.83 | 2.15 | -0.54 | 2.94 | 1.1 | 1.15 |
| Runoff (Q) | TV | 541.3 8 | 749.6 3 | 1696.8 9 | 3586.3 6 | 6209.0 8 | 4068.8 9 | 6648.5 1 | 2944. 4 | 2354.5 4 | 3684. 5 | 2249.7 3 | 948.1 6 |
| | TS | 21.83 | 4.44 | -1.29 | 1.85 | 0.51 | 0.35 | 0.7 | -3.47 | 0.79 | 8.84 | 1.82 | 1.25 |
| GRACE TWSC | TL | 6.02 | 15.26 | 14.09 | 29.06 | 16.05 | 15.35 | 15.2 | 22.7 | 8.36 | 5.48 | 1.38 | 13.33 |
| | TS | -1.2 | 4.96 | -1.24 | -1 | -0.16 | -1.65 | -1.05 | 2.72 | -2.68 | 4.81 | 0.29 | -5.88 |

Note: TL=trend length, TV= trend volume, TS= trend slope; All TV in mm, except for runoff in m³/s. TS is unit less.

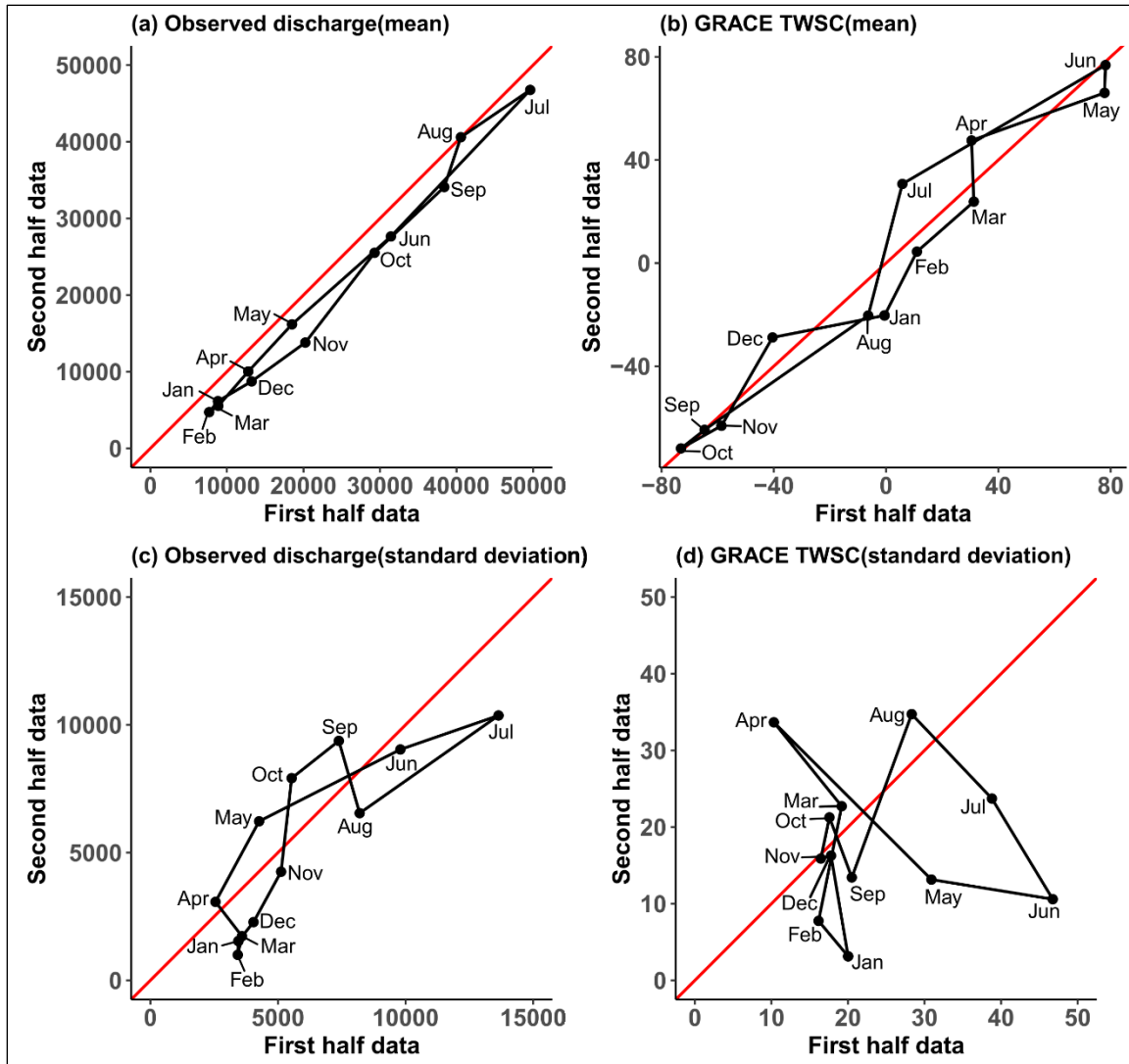


Fig.7.8 IPTA diagram for the mean and standard deviation of discharge and GRACE TWSC

7.4 Conclusions

In this study the innovative trend analysis of different precipitation products, ETs, discharge and GRACE TWSC of the Brahmaputra River basin for individual months from 2003 to 2014 was carried out.

- (a) Across multiple precipitation datasets, ITA consistently identified both rising and falling trends, albeit with varying proportions, while the MK test often failed to recognize significant trends. To elaborate, ITA pinpointed declining trends in APHRODITE, ERA5, CHIRPS, SM2RAIN, TRMM, and IMERG precipitation data, whereas CMORPH displayed notable upward trends. The ensemble findings revealed a mixture of positive and declining trends. In contrast, the MK test typically indicated the absence of significant trends in these datasets.
- (b) MOD16 ET and CLSM ET exhibited a substantial positive significant uptrend, whereas Noah ET, TerraClimate ET, and Ensemble ET showed a substantial negative significant downtrend using the ITA method. Using the MK-test, the ET products did not exhibit either positive or negative trends as significantly as with the ITA method. These analyses revealed diverse trends in ET across the datasets, with ITA and MK tests providing insights into the extent and significance of these trends.
- (c) In the case of in-situ discharge analysed using ITA, a substantial and consistent decreasing trend was observed throughout about 92% of the months. Surprisingly, the MK test did not detect any significant trend in this dataset.
- (d) For GRACE TWSC, the ITA analysis revealed a mixture of trends. Approximately 25% of the months showed significant increases in water storage, while 50% exhibited significant decreases. In contrast, the MK test only identified a significant downtrend in about 8% of the months.
- (e) The IPTA diagram provided the trend transition between months regarding the mean and standard deviation of all the variables used in this study. The trend slope provided information on how the intensity of events could vary.

CHAPTER 8

SUMMARY AND CONCLUSIONS

8.1 SUMMARY

The study focuses on evaluating the water budget components of the Brahmaputra river basin using satellite data. The basin is transboundary and has sparse hydrometeorological data, making it difficult to carry out hydrological studies. Satellite data can be useful for large basins like the Brahmaputra, but there is a need to evaluate satellite precipitation estimates against existing gauge-based data. Additionally, there is a need to assess the risk of water budget variables given precipitation data, reconstruct water budget variables using multiple precipitation data sources, and analyse the trend of water budget variables using innovative trend analysis.

In this regard, categorical and continuous metrics are used to assess the ability of satellite precipitation to capture rainfall quantity, the probabilistic prediction of evapotranspiration, discharge, and terrestrial water storage change given precipitation quantity using bivariate dependence measures like copula, water budget error analysis and application of innovative trend analysis to individual months.

The satellite precipitation data were assessed using categorical and continuous metrics, spatially and temporally considering the whole basin, upper, middle and lower sections of the basin based on elevation measure. Also, the analysis was carried out for winter, summer, monsoon and postmonsoon seasons.

The results obtained from the study are promising. Though satellite data come with uncertainties, they are useful, particularly for a large river basin like Brahmaputra, which is largely ungauged. Also, satellite data have a wider coverage than gauge data. The satellite precipitation data that are gauge corrected were found to perform well using both categorical and continuous statistics. The satellite precipitation was equally good as the gauged-based data in risk assessment of evapotranspiration, discharge and terrestrial water

storage change, while the reanalysis precipitation data slightly differed in the outcome of risk assessment.

Similarly, the gauge-corrected satellite precipitation data performed well in reconstructing the water budget variables, especially runoff and terrestrial water storage change. However, evapotranspiration could not be reconstructed well possibly due to uncertainties in precipitation, runoff and terrestrial water storage change apart from its own uncertainties. Also, as in most of the studies, the innovative trend analysis detected either positive or negative trends in precipitation data, substantial significant positive trends in evapotranspiration data, significant negative trends in discharge and a mixture of significant positive as well as negative trends in terrestrial water storage change. Subtrends using the innovative trend analysis (ITA) method also revealed differing pictures in all the variables. Then, the polygon version of the ITA method indicated the trend transition between months.

8.2 CONCLUSIONS

8.2.1 General conclusions

(a) IMERG is the most reliable for precipitation data, whereas CMORPH is best for seasonal use. SM2RAIN is generally unreliable.

(b) Copula functions reveal complex dependencies between variables, supporting model validation. Changing probabilities with precipitation offer insights for climate change adaptation.

(c) The ERA5 dataset is best for reconstructing total water storage change (TWSC) and streamflow (Q). Reconstructing evapotranspiration (ET) from precipitation data alone is difficult. The best dataset to use depends on the season and variable. SM2RAIN should be avoided.

(d) ITA outperforms the MK test in trend detection for precipitation. ET data shows diverse trends using ITA method. Consistent decreasing trends in discharge data emphasise the need for trend identification. ITA offers insights for water resource management and

drought monitoring by identifying subtrends, while IPTA diagrams and trend slopes aid water resources decision making.

8.2.2 Satellite data evaluation

- (a) IMERG emerges as the top-performing product in the evaluation of precipitation products, outperforming all other products in terms of both spatial and temporal accuracy. This finding has important implications for researchers and practitioners who rely on precipitation data, as it suggests that IMERG is the most reliable source of precipitation data available.
- (b) While CMORPH performs well overall, it is particularly suited for seasonal applications, given its strong performance during the monsoon and post-monsoon seasons.
- (c) SM2RAIN, on the other hand, is the least-performing precipitation product on all counts, suggesting that it is not a reliable source of precipitation data for most applications.

8.2.3 Risk assessment of water budget variables

- (a) The Frank copula is the optimal copula function for all three precipitation-TWSC pairs, ERA5-ET, and ERA5-ET, while the Clayton copula is the optimal copula function for the remaining pairs. This suggests that the dependence structure between these variables is complex and non-linear. This information can be used to develop more sophisticated models that capture the complex relationships between the variables.
- (b) Pearson's linear and Spearman's rank correlations for all the pairs of variables are significant for observed and simulated values. This indicates that there is a strong correlation between the variables, even though the dependence structure is complex. This information can be used to validate the models developed in this study.
- (c) The non-exceedance probability of all the dependent variables (lower percentile) decreases with increased precipitation, while the exceedance

probability of the same variables (upper percentile) increases gradually with increased precipitation. This is consistent with the expected impacts of climate change, which is projected to lead to more extreme precipitation events. This information can be used to assess the vulnerability of the Brahmaputra basin to climate change and to develop adaptation strategies.

8.2.4 Reconstruction of water budget variables

- (a) ERA5-derived TWSCs and Qs provide the highest linear correlation with gauge-based data, while TRMM, IMERG, and CHIRPS also show a closer correlation, to a greater extent than other precipitation datasets. This implies that ERA5 is the best precipitation dataset to use for reconstructing TWSCs and Qs, but TRMM, IMERG, and CHIRPS are also good options.
- (b) The linear strength of derived ETs shows that the inherent uncertainties in the water budget variables did not reconstruct ETs well. This means that it is difficult to accurately reconstruct ET using precipitation data alone, and other sources of data, such as satellite observations of vegetation and soil moisture, may be needed.
- (c) The linear strength of derived ETs shows that the inherent uncertainties in the water budget variables did not reconstruct ETs well. This means that it is difficult to accurately reconstruct ET using precipitation data alone, and other sources of data, such as satellite observations of vegetation and soil moisture, may be needed.
- (d) When choosing a precipitation dataset for reconstructing water budget variables, it is important to consider the season and the variable(s) of interest. TRMM, IMERG, and CHIRPS are generally good choices, but ERA5 may be better for some applications. SM2RAIN should be avoided.

8.2.5 Innovative trend analysis of water budget variables

- (a) ITA, compared to the MK test, consistently detects both rising and falling trends in precipitation datasets, yielding more robust and practical climate insights.

This can enhance our ability to make informed decisions in water resource management and climate adaptation.

- (b) ITA reveals diverse trends in evapotranspiration (ET) data, with some products showing substantial positive uptrends and others significant negative downtrends, making it crucial for assessing climate impacts on water resources and agricultural planning.
- (c) In-situ discharge data analyzed with ITA consistently reveals a significant decreasing trend in the majority of months, underscoring the importance of recognizing these trends for effective water resource planning and management. The ability to identify these trends is essential for effective water resource planning.
- (d) ITA analysis of GRACE Terrestrial Water Storage Change (TWSC) data reveals mixed trends, including both increases and decreases in water storage, offering comprehensive insights for water resource management and drought monitoring.
- (e) The IPTA diagram visually displays trend transitions between months for climate variables, while trend slopes help assess the intensity of climate events, aiding decision-making in various fields, including disaster preparedness and infrastructure planning.

8.3 RESEARCH CONTRIBUTIONS

(a) A comprehensive evaluation of several satellite precipitation products was conducted on a daily and seasonal basis. Additionally, temporal and spatial assessments of the precipitation products were performed.

(b) For the first time, satellite and reanalysis precipitation data, along with gauge data, were utilized to assess the risk of major water budget variables in the basin.

(c) Notwithstanding, a meticulous assessment of multiple precipitation products was undertaken, with the aim of reconstructing evapotranspiration, runoff, and terrestrial water storage through the utilization of water budget equations. This method is particularly

favoured when the financial constraints associated with elaborate modelling endeavours render them unfeasible.

(d) Innovative trend analysis and its extended version were employed to identify trends in water budget variables within the basin, incorporating various precipitation, evapotranspiration, river discharge, and terrestrial water storage data. A comprehensive subtrend analysis was also carried out.

8.4 LIMITATIONS OF THE STUDY

The seasonal precipitation variation was not evaluated based on the spatial distribution of rainfall. It is recommended to carry out the categorical and continuous metrics spatially for different seasons to understand rainfall distribution over the basin better. Also, bias correction of the satellite data might increase their performance. The bivariate copula may not be sufficient when more than one variable could influence a water budget. To overcome this limitation, it is recommended to use the trivariate or vine copula concept that can handle more than one controlling variable. The water budget error might change if it is enforced to distribute the errors, as seen in different studies. Though the innovative trend analysis is sample size independent, to make a fair comparison with the MK test, it may be advisable to use longer data because the MK test is affected by data length.

8.5 SCOPE FOR FURTHER STUDY

(a) The categorical and continuous metrics could be carried out based on elevation and rainfall intensities as reported in many other studies.

(b) Merging of two or more satellite precipitation data could be explored to ascertain whether it improves the performance of such merged products when compared against gauged data.

(c) Various bias correction methods of precipitation could be applied to assess the performance of bias corrected data.

(d) In real life water budget variables are interrelated to each other. Hence, the risk assessment of such variables may be assessed based on two or more other variables to be able to understand the risk variation. Therefore, vine copula is suggested for a similar analysis to the bivariate copulas.

(e) The merged as well as bias-corrected precipitation products could be used to reconstruct evapotranspiration, runoff and terrestrial water storage change.

(f) Extreme precipitation events over the basin could be identified using several trend detection methods.

(g) The wetness and dryness events could be related to both the phases of large atmospheric indices like ENSO, for example.

REFERENCES

- Abatzoglou, J. T., Dobrowski, S. Z., Parks, S. A., and Hegewisch, K. C. (2018). “TerraClimate, a high-resolution global dataset of monthly climate and climatic water balance from 1958–2015.” *Sci. Data*, 5(1), 170191.
- Abdulla, F. A., Lettenmaier, D. P., Wood, E. F., and Smith, J. A. (1996). “Application of a macroscale hydrologic model to estimate the water balance of the Arkansas-Red River Basin.” *J. Geophys. Res. Atmos.*, 101(D3), 7449–7459.
- Abera, W., Formetta, G., Brocca, L., and Rigon, R. (2017). “Modeling the water budget of the Upper Blue Nile basin using the JGrass-NewAge model system and satellite data.” *Hydrol. Earth Syst. Sci.*, 21(6), 3145–3165.
- Abudu, S., King, J. P., and Pagano, T. C. (2010). “Application of Partial Least-Squares Regression in Seasonal Streamflow Forecasting.” *J. Hydrol. Eng.*, 15(8), 612–623.
- AghaKouchak, A., and Mehran, A. (2013). “Extended contingency table: Performance metrics for satellite observations and climate model simulations.” *Water Resour. Res.*, 49(10), 7144–7149.
- Ahmad, N., and Lodrick, D. O. (2017). “Brahmaputra River.” *Br. Online Encycl.*, <<https://www.britannica.com/place/Brahmaputra-River>> (May 15, 2017).
- Ahmed, N., Wang, G., Booij, M. J., Ceribasi, G., Bhat, M. S., Ceyhunlu, A. I., and Ahmed, A. (2022). “Changes in monthly streamflow in the Hindukush–Karakoram–Himalaya Region of Pakistan using innovative polygon trend analysis.” *Stoch. Environ. Res. Risk Assess.* 36, 811–830.
- Aires, F. (2014). “Combining Datasets of Satellite-Retrieved Products. Part I: Methodology and Water Budget Closure.” *J. Hydrometeorol.*, 15(4), 1677–1691.
- Akçay, F., Kankal, M., and Şan, M. (2021). “Innovative approaches to the trend assessment of streamflows in the eastern Black Sea basin, Turkey.” *Hydrol. Sci. J.*
- Allen, M., Poggiali, D., Whitaker, K., Marshall, T. R., and Kievit, R. A. (2019). “Raincloud plots: a multi-platform tool for robust data visualization.” *Wellcome Open Res.*, 4, 63.
- Almanaseer, N., and Sankarasubramanian, A. (2012). “Role of Climate Variability in Modulating the Surface Water and Groundwater Interaction over the Southeast United States.” *J. Hydrol. Eng.*, 17(9), 1001–1010.
- Armanios, D. E., and Fisher, J. B. (2014). “Measuring water availability with limited ground data: assessing the feasibility of an entirely remote-sensing-based hydrologic budget of the Rufiji Basin, Tanzania, using TRMM, GRACE, MODIS, SRB, and AIRS.” *Hydrol. Process.*, 28(3), 853–867.

- Azarderakhsh, M., Rossow, W. B., Papa, F., Norouzi, H., and Khanbilvardi, R. (2011). "Diagnosing water variations within the Amazon basin using satellite data." *J. Geophys. Res. Atmos.*, 116(D24), n/a-n/a.
- Deb Barma, S., Uttarwar, S. B., Barane, P., Bhat, N., and Mahesha, A. (2022). "EVALUATION OF ERA5 AND IMERG PRECIPITATION DATA FOR RISK ASSESSMENT OF WATER CYCLE VARIABLES OF A LARGE RIVER BASIN IN SOUTH ASIA USING SATELLITE DATA AND ARCHIMEDEAN COPULAS." *Water Conserv. Manag.*, 6(1), 61–69.
- Battaglia, A., Kollias, P., Dhillon, R., Roy, R., Tanelli, S., Lamer, K., Grecu, M., Lebsock, M., Watters, D., Mroz, K., Heymsfield, G. M., Li, L., and Furukawa, K. (2020). "Spaceborne Cloud and Precipitation Radars: Status, Challenges, and Ways Forward." *Rev. Geophys.*
- Beaudoing, H., and Rodell, M. (2020). "GLDAS Noah Land Surface Model L4 monthly 1.0 x 1.0 degree V2.1, Greenbelt, Maryland, USA, Goddard Earth Sciences Data and Information Services Center (GES DISC)." NASA/GSFC/HSL.
- Beck, H. E., Wood, E. F., Pan, M., Fisher, C. K., Miralles, D. G., Dijk, A. van, McVicar, T. R., and Adler, R. F. (2019). "MSWEP V2 Global 3-Hourly 0.1° Precipitation: Methodology and Quantitative Assessment."
- Bibi, S., Wang, L., Li, X., Zhang, X., and Chen, D. (2019). "Response of Groundwater Storage and Recharge in the Qaidam Basin (Tibetan Plateau) to Climate Variations From 2002 to 2016." *J. Geophys. Res. Atmos.*, 124(17–18), 9918–9934.
- Brocca, L., Ciabatta, L., Massari, C., Moramarco, T., Hahn, S., Hasenauer, S., Kidd, R., Dorigo, W., Wagner, W., and Levizzani, V. (2014). "Soil as a natural rain gauge: Estimating global rainfall from satellite soil moisture data." *J. Geophys. Res. Atmos.*, 119(9), 5128–5141.
- Caloiero, T. (2020). "Evaluation of rainfall trends in the South Island of New Zealand through the innovative trend analysis (ITA)." *Theor. Appl. Climatol.*
- Cavalcante, R. B. L., Ferreira, D. B. da S., Pontes, P. R. M., Tedeschi, R. G., Costa, C. P. W. da, and Souza, E. B. de. (2020). "Evaluation of extreme rainfall indices from CHIRPS precipitation estimates over the Brazilian Amazonia." *Atmos. Res.*
- Ceribasi, G., and Ceyhunlu, A. I. (2021). "Analysis of total monthly precipitation of Susurluk Basin in Turkey using innovative polygon trend analysis method." *J. Water Clim. Chang.*, 12(5), 1532–1543.
- Chen, L., and Guo, S. (2019). *Copulas and Its Application in Hydrology and Water Resources*. Springer Water, Singapore: Springer Singapore.
- Chicco, D., Warrens, M. J., and Jurman, G. (2021). "The coefficient of determination R-squared is more informative than SMAPE, MAE, MAPE, MSE and RMSE in regression analysis evaluation." *PeerJ Comput. Sci.*, 7, e623.

- Chowdari, K., Deb Barma, S., Bhat, N., Girisha, R., Gouda, K. C., and Mahesha, A. (2023). "Trends of seasonal and annual rainfall of semi-arid districts of Karnataka, India: application of innovative trend analysis approach." *Theor. Appl. Climatol.*, 152(1–2), 241–264.
- Chun, K. P., He, Q., Fok, H. S., Ghosh, S., Yetemen, O., Chen, Q., and Mijic, A. (2020). "Gravimetry-based water storage shifting over the China-India border area controlled by regional climate variability." *Sci. Total Environ.*, 714, 136360.
- Ciabatta, L., Marra, A. C., Panegrossi, G., Casella, D., Sanò, P., Dietrich, S., Massari, C., and Brocca, L. (2017). "Daily precipitation estimation through different microwave sensors: Verification study over Italy." *J. Hydrol.*, 545, 436–450.
- Ciabatta, L., Massari, C., Brocca, L., Gruber, A., Reimer, C., Hahn, S., Paulik, C., Dorigo, W., Kidd, R., and Wagner, W. (2018). "SM2RAIN-CCI: a new global long-term rainfall data set derived from ESA CCI soil moisture." *Earth Syst. Sci. Data*, 10(1), 267–280.
- Corbari, C., Mancini, M., Su, Z., and Li, J. (2014). "Evapotranspiration estimate from water balance closure using satellite data for the Upper Yangtze River basin." *Hydrol. Res.*, 45(4–5), 603–614.
- Deb Barma, S., and Mahesha, A. (2023). "Discussion of 'Innovative approaches to the trend assessment of streamflows in the Eastern Black Sea basin, Turkey' *." *Hydrol. Sci. J.*, 68(5), 731–732.
- Dorigo, W., Dietrich, S., Aires, F., Brocca, L., Carter, S., Cretaux, J.-F., Dunkerley, D., Enomoto, H., Forsberg, R., Güntner, A., Hegglin, M. I., Hollmann, R., Hurst, D. F., Johannessen, J. A., Kummerow, C., Lee, T., Luoju, K., Looser, U., Miralles, D. G., Pellet, V., Recknagel, T., Ruz Vargas, C., Schneider, U., Schoeneich, P., Schröder, M., Tapper, N., Vuglinsky, V., Wagner, W., Yu, L., Zappa, L., Zemp, M., and Aich, V. (2021). "Closing the water cycle from observations across scales: Where do we stand?" *Bull. Am. Meteorol. Soc.*, 1–95.
- Duan, Z., and Bastiaanssen, W. G. M. (2013). "First results from Version 7 TRMM 3B43 precipitation product in combination with a new downscaling--calibration procedure." *Remote Sens. Environ.*
- Duan, Z., Liu, J., Tuo, Y., Chiogna, G., and Disse, M. (2016). "Evaluation of eight high spatial resolution gridded precipitation products in Adige Basin (Italy) at multiple temporal and spatial scales." *Sci. Total Environ.*, 573, 1536–1553.
- Duffy, C. J. (2017). "The terrestrial hydrologic cycle: an historical sense of balance." *Wiley Interdiscip. Rev. Water*, 4(4), e1216.
- Fernandes, K., Fu, R., and Betts, A. K. (2008). "How well does the ERA40 surface water budget compare to observations in the Amazon River basin?" *J. Geophys. Res.*, 113(D11), D11117.

- Ferreira, V., Gong, Z., He, X., Zhang, Y., and Andam-Akorful, S. (2013). “Estimating Total Discharge in the Yangtze River Basin Using Satellite-Based Observations.” *Remote Sens.*, 5(7), 3415–3430.
- Fersch, B., Kunstmann, H., Bárdossy, A., Devaraju, B., and Sneeuw, N. (2012). “Continental-Scale Basin Water Storage Variation from Global and Dynamically Downscaled Atmospheric Water Budgets in Comparison with GRACE-Derived Observations.” *J. Hydrometeorol.*, 13(5), 1589–1603.
- Funk, C., Peterson, P., Landsfeld, M., Pedreros, D., Verdin, J., Rowland, J., Romero, B. E., Husak, G., Michaelsen, J., and Verdin, A. (2014). “A quasi-global precipitation time series for drought monitoring.”
- Funk, C., Peterson, P., Landsfeld, M., Pedreros, D., Verdin, J., Shukla, S., Husak, G., Rowland, J., Harrison, L., Hoell, A., and Michaelsen, J. (2015). “The climate hazards infrared precipitation with stations—a new environmental record for monitoring extremes.” *Sci. Data*, 2, 150066.
- Futter, M. N., Whitehead, P. G., Sarkar, S., Rodda, H., and Crossman, J. (2015). “Rainfall runoff modelling of the Upper Ganga and Brahmaputra basins using PERSiST.” *Environ. Sci. Process. Impacts*, 17(6), 1070–1081.
- Gao, H., Tang, Q., Ferguson, C. R., Wood, E. F., and Lettenmaier, D. P. (2010). “Estimating the water budget of major US river basins via remote sensing.” *Int. J. Remote Sens.*, 31(14), 3955–3978.
- Genest, C., and Favre, A.-C. (2007). “Everything You Always Wanted to Know about Copula Modeling but Were Afraid to Ask.” *J. Hydrol. Eng.*, 12(4), 347–368.
- Graf, A., Bogena, H. R., Drüe, C., Hardelauf, H., Pütz, T., Heinemann, G., and Vereecken, H. (2014). “Spatiotemporal relations between water budget components and soil water content in a forested tributary catchment.” *Water Resour. Res.*, 50(6), 4837–4857.
- Gupta, V., Jain, M., Singh, P., and Singh, V. (2019). “An assessment of global satellite-based precipitation datasets in capturing precipitation extremes: A comparison with observed precipitation dataset in India.” *Int. J. Climatol.*
- Han, H., Jian, H., Peng, Y., and Yao, S. (2023). “A conditional copula model to identify the response of runoff probability to climatic factors.” *Ecol. Indic.*, 146, 109415.
- Han, X., Wei, Z., Zhang, B., Li, Y., Du, T., and Chen, H. (2021). “Crop evapotranspiration prediction by considering dynamic change of crop coefficient and the precipitation effect in back-propagation neural network model.” *J. Hydrol.*, 596, 126104.
- Hao, Z., Hao, F., Singh, V. P., Xia, Y., Shi, C., and Zhang, X. (2018). “A multivariate approach for statistical assessments of compound extremes.” *J. Hydrol.*, 565, 87–94.

- Hasan, E., and Tarhule, A. (2020). “GRACE: Gravity Recovery and Climate Experiment long-term trend investigation over the Nile River Basin: Spatial variability drivers.” *J. Hydrol.*, 586, 124870.
- Hasson, S., Lucarini, V., and Pascale, S. (2013). “Hydrological cycle over South and Southeast Asian river basins as simulated by PCMDI/CMIP3 experiments.” *Earth Syst. Dyn.*, 4(2), 199–217.
- Hentschel, R., Bittner, S., Janott, M., Biernath, C., Holst, J., Ferrio, J. P., Gessler, A., and Priesack, E. (2013). “Simulation of stand transpiration based on a xylem water flow model for individual trees.” *Agric. For. Meteorol.*, 182–183, 31–42.
- Hersbach, H., Bell, B., Berrisford, P., Hirahara, S., Horányi, A., Muñoz-Sabater, J., Nicolas, J., Peubey, C., Radu, R., Schepers, D., Simmons, A., Soci, C., Abdalla, S., Abellan, X., Balsamo, G., Bechtold, P., Biavati, G., Bidlot, J., Bonavita, M., Chiara, G., Dahlgren, P., Dee, D., Diamantakis, M., Dragani, R., Flemming, J., Forbes, R., Fuentes, M., Geer, A., Haimberger, L., Healy, S., Hogan, R. J., Hólm, E., Janisková, M., Keeley, S., Laloyaux, P., Lopez, P., Lupu, C., Radnoti, G., Rosnay, P., Rozum, I., Vamborg, F., Villaume, S., and Thépaut, J. (2020). “The ERA5 global reanalysis.” *Q. J. R. Meteorol. Soc.*, 146(730), 1999–2049.
- Hirschi, M., Seneviratne, S. I., and Schär, C. (2006). “Seasonal Variations in Terrestrial Water Storage for Major Midlatitude River Basins.” *J. Hydrometeorol.*, 7(1), 39–60.
- Hu, Z., Zhang, Z., Sang, Y.-F., Qian, J., Feng, W., Chen, X., and Zhou, Q. (2021). “Temporal and spatial variations in the terrestrial water storage across Central Asia based on multiple satellite datasets and global hydrological models.” *J. Hydrol.*, 596, 126013.
- Huffman, G. J., Adler, R. F., Bolvin, D. T., and Nelkin, E. J. (2010). The TRMM Multi-satellite Precipitation Analysis (TMPA). Chapter 1 in *Satellite Rainfall Applications for Surface Hydrology*. (M. Gebremichael and F. Hossain, eds.), Dordrecht: Springer Netherlands.
- Huffman, G. J., Bolvin, D. T., Nelkin, E. J., Wolff, D. B., Adler, R. F., Gu, G., Hong, Y., Bowman, K. P., and Stocker, E. F. (2007). “The TRMM Multisatellite Precipitation Analysis (TMPA): Quasi-Global, Multiyear, Combined-Sensor Precipitation Estimates at Fine Scales.” *J. Hydrometeorol.*, 8(1), 38–55.
- Huffman, G. J., Stocker, E. F., Bolvin, D. T., Nelkin, E. J., and Tan, J. (2019). “GPM IMERG Final Precipitation L3 1 day 0.1 degree x 0.1 degree V06, Edited by Andrey Savtchenko, Greenbelt, MD, Goddard Earth Sciences Data and Information Services Center (GES DISC).” <<https://doi.org/10.5067/GPM/IMERGDF/DAY/06>> (Mar. 9, 2020).
- Immerzeel, W. (2008). “Historical trends and future predictions of climate variability in the Brahmaputra basin.” *Int. J. Climatol.*, 28(2), 243–254.

- Islam, M. A., Yu, B., and Cartwright, N. (2020). "Assessment and comparison of five satellite precipitation products in Australia." *J. Hydrol.*, 590, 125474.
- Jato-Espino, D., Charlesworth, S. M., Perales-Momparler, S., and Andrés-Doménech, I. (2017). "Prediction of Evapotranspiration in a Mediterranean Region Using Basic Meteorological Variables." *J. Hydrol. Eng.*, 22(4), 04016064.
- Ji, X., Li, Y., Luo, X., He, D., Guo, R., Wang, J., Bai, Y., Yue, C., and Liu, C. (2020). "Evaluation of bias correction methods for APHRODITE data to improve hydrologic simulation in a large Himalayan basin." *Atmos. Res.*, 242, 104964.
- Jia, Y., Lei, H., Yang, H., and Hu, Q. (2020). "Terrestrial Water Storage Change Retrieved by GRACE and Its Implication in the Tibetan Plateau: Estimating Areal Precipitation in Ungauged Region." *Remote Sens.*, 12(19), 3129.
- Jian, J., Webster, P. J., and Hoyos, C. D. (2009). "Large-scale controls on Ganges and Brahmaputra river discharge on intraseasonal and seasonal time-scales." *Q. J. R. Meteorol. Soc.*, 135(639), 353–370.
- Jothityangkoon, C., Sivapalan, M., and Farmer, D. . (2001). "Process controls of water balance variability in a large semi-arid catchment: downward approach to hydrological model development." *J. Hydrol.*, 254(1–4), 174–198.
- Joyce, R. J., Janowiak, J. E., Arkin, P. A., and Xie, P. (2004). "CMORPH: A Method that Produces Global Precipitation Estimates from Passive Microwave and Infrared Data at High Spatial and Temporal Resolution." *J. Hydrometeorol.*, 5(3), 487–503.
- Kendall, M. G. (1938). "A New Measure of Rank Ccorrelation." *Biometrika*, 30(1–2), 81–93.
- Kidd, C., Becker, A., Huffman, G. J., Muller, C. L., Joe, P., Skofronick-Jackson, G., and Kirschbaum, D. (2017). "So, How Much of the Earth's Surface Is Covered by Rain Gauges?" *Bull. Am. Meteorol. Soc.*
- Kidd, C., and Huffman, G. (2011). "Global precipitation measurement." *Meteorol. Appl.*, 18(3), 334–353.
- Kidd, C., Huffman, G. J., Maggioni, V., Chambon, P., and Oki, R. (2021). "The Global Satellite Precipitation Constellation: Current Status and Future Requirements."
- Landerer, F. W., and Swenson, S. C. (2012). "Accuracy of scaled GRACE terrestrial water storage estimates." *Water Resour. Res.*, 48(4), 1–11.
- Legates, D. R., and McCabe, G. J. (1999). "Evaluating the use of 'goodness-of-fit' Measures in hydrologic and hydroclimatic model validation." *Water Resour. Res.*, 35(1), 233–241.
- Lehmann, F., Vishwakarma, B. D., and Bamber, J. (2022). "How well are we able to close the water budget at the global scale?" *Hydrol. Earth Syst. Sci.*, 26(1), 35–54.

- Li, B., Beaudoin, H., and Rodell, M. (2020). "GLDAS Catchment Land Surface Model L4 monthly 1.0 x 1.0 degree V2.1, Greenbelt, Maryland, USA, Goddard Earth Sciences Data and Information Services Center." NASA/GSFC/HSL.
- Li, C., Sun, G., Caldwell, P. V., Cohen, E., Fang, Y., Zhang, Y., Oudin, L., Sanchez, G. M., and Meentemeyer, R. K. (2020). "Impacts of Urbanization on Watershed Water Balances Across the Conterminous United States." *Water Resour. Res.*, 56(7).
- Li, J. Z., Wang, Y. X., Li, S. F., and Hu, R. (2015). "A Nonstationary Standardized Precipitation Index incorporating climate indices as covariates." *J. Geophys. Res. Atmos.*, 120(23), 12,082-12,095.
- Li, X. H., Zhang, Q., and Xu, C. Y. (2012). "Suitability of the TRMM satellite rainfalls in driving a distributed hydrological model for water balance computations in Xinjiang catchment, Poyang lake basin." *J. Hydrol.*, 426–427, 28–38.
- Li, X., Long, D., Han, Z., Scanlon, B. R., Sun, Z., Han, P., and Hou, A. (2019). "Evapotranspiration Estimation for Tibetan Plateau Headwaters Using Conjoint Terrestrial and Atmospheric Water Balances and Multisource Remote Sensing." *Water Resour. Res.*, 55(11), 8608–8630.
- Li, Z., and Quiring, S. M. (2021). "Investigating spatial heterogeneity of the controls of surface water balance in the contiguous United States by considering anthropogenic factors." *J. Hydrol.*, 601, 126621.
- Li, Z., Tang, G., Hong, Z., Chen, M., Gao, S., Kirstetter, P., Gourley, J. J., Wen, Y., Yami, T., Nabih, S., and Hong, Y. (2021). "Two-decades of GPM IMERG early and final run products intercomparison: Similarity and difference in climatology, rates, and extremes." *J. Hydrol.*, 594, 125975.
- Li, Z., Tang, G., Kirstetter, P., Gao, S., Li, J.-L. F., Wen, Y., and Hong, Y. (2022). "Evaluation of GPM IMERG and its constellations in extreme events over the conterminous united states." *J. Hydrol.*, 606, 127357.
- Li, Z., Yang, D., Gao, B., Jiao, Y., Hong, Y., and Xu, T. (2015). "Multiscale Hydrologic Applications of the Latest Satellite Precipitation Products in the Yangtze River Basin using a Distributed Hydrologic Model." *J. Hydrometeorol.*, 16(1), 407–426.
- Liu, C.-Y., Aryastana, P., Liu, G. R., and Huang, W. R. (2020). "Assessment of satellite precipitation product estimates over Bali Island." *Atmos. Res.*
- Liu, Y., Zheng, Y., Li, W., and Zhou, T. (2022). "Evaluating the Performance of Satellite-Based Precipitation Products Using Gauge Measurement and Hydrological Modeling: A Case Study in a Dry Basin of Northwest China." *J. Hydrometeorol.*, 23(4), 541–559.
- Liu, Z., Chen, X., Liu, F., Lin, K., He, Y., and Cai, H. (2018). "Joint Dependence Between River Water Temperature, Air Temperature, and Discharge in the Yangtze

- River: The Role of the Three Gorges Dam.” *J. Geophys. Res. Atmos.*, 123(21), 11,938–11,951.
- Liu, Z., Cheng, L., Wang, X., Lin, K., Chen, X., Zhao, T., Tu, X., and Zhou, P. (2022). “A probabilistic framework for sequential drought-fluvial identification, probability estimation and prediction.” *J. Hydrol.*, 612, 128115.
- Liu, Z., and Menzel, L. (2018). “Probabilistic dependence between streamflow and hydroclimatic variables and the possible linkages to large-scale atmospheric circulation: A case study in Baden-Württemberg, Southwest Germany.” *J. Hydrol.*, 565, 443–454.
- Liu, Z., Törnros, T., and Menzel, L. (2016). “A probabilistic prediction network for hydrological drought identification and environmental flow assessment.” *Water Resour. Res.*, 52(8), 6243–6262.
- Lorenz, C., and Kunstmann, H. (2012). “The Hydrological Cycle in Three State-of-the-Art Reanalyses: Intercomparison and Performance Analysis.” *J. Hydrometeorol.*, 13(5), 1397–1420.
- Lorenz, C., Kunstmann, H., Devaraju, B., Tourian, M. J., Sneeuw, N., and Riegger, J. (2014). “Large-Scale Runoff from Landmasses: A Global Assessment of the Closure of the Hydrological and Atmospheric Water Balances.” *J. Hydrometeorol.*, 15(6), 2111–2139.
- Luo, X., Fan, X., Li, Y., and Ji, X. (2020). “Bias correction of a gauge-based gridded product to improve extreme precipitation analysis in the Yarlung Tsangpo–Brahmaputra River basin.” *Nat. Hazards Earth Syst. Sci.*, 20(8), 2243–2254.
- Luo, Z., Li, H., Zhang, S., Wang, L., Wang, S., and Wang, L. (2023). “A Novel Two-Step Method for Enforcing Water Budget Closure and an Intercomparison of Budget Closure Correction Methods Based on Satellite Hydrological Products.” *Water Resour. Res.*
- Lv, M., Ma, Z., Yuan, X., Lv, M., Li, M., and Zheng, Z. (2017). “Water budget closure based on GRACE measurements and reconstructed evapotranspiration using GLDAS and water use data for two large densely-populated mid-latitude basins.” *J. Hydrol.*, 547, 585–599.
- Ma, Q., Li, Y., Liu, F., Feng, H., Biswas, A., and Zhang, Q. (2023). “SPEI and multi-threshold run theory based drought analysis using multi-source products in China.” *J. Hydrol.*, 616, 128737.
- Mann, H. B. (1945). “Nonparametric Tests Against Trend.” *Econometrica*, 13(3), 245.
- Marak, J. D. K., Sarma, A. K., and Bhattacharjya, R. K. (2020). “Innovative trend analysis of spatial and temporal rainfall variations in Umiam and Umtru watersheds in Meghalaya, India.” *Theor. Appl. Climatol.*, 142(3–4), 1397–1412.

- Marengo, J. A. (2005). "Characteristics and spatio-temporal variability of the Amazon River Basin Water Budget." *Clim. Dyn.*, 24(1), 11–22.
- Masood, M., Yeh, P. J.-F., Hanasaki, N., and Takeuchi, K. (2015). "Model study of the impacts of future climate change on the hydrology of Ganges–Brahmaputra–Meghna basin." *Hydrol. Earth Syst. Sci.*, 19(2), 747–770.
- Maxwell, R. M., and Condon, L. E. (2016). "Connections between groundwater flow and transpiration partitioning." *Science* (80-.), 353(6297), 377 LP – 380.
- Michelson, D. (2004). "Systematic correction of precipitation gauge observations using analyzed meteorological variables." *J. Hydrol.*
- Mitchell, V. G., McMahon, T. A., and Mein, R. G. (2003). "Components of the Total Water Balance of an Urban Catchment." *Environ. Manage.*, 32(6), 735–746.
- Mu, Q., Zhao, M., and Running, S. W. (2011). "Improvements to a MODIS global terrestrial evapotranspiration algorithm." *Remote Sens. Environ.*, 115(8), 1781–1800.
- Munier, S., Aires, F., Schlaffer, S., Prigent, C., Papa, F., Maisongrande, P., and Pan, M. (2014). "Combining data sets of satellite-retrieved products for basin-scale water balance study: 2. Evaluation on the Mississippi Basin and closure correction model." *J. Geophys. Res. Atmos.*, 119(21), 12,100–12,116.
- Munier, S., Palanisamy, H., Maisongrande, P., Cazenave, A., and Wood, E. F. (2012). "Global runoff anomalies over 1993–2009 estimated from coupled Land–Ocean–Atmosphere water budgets and its relation with climate variability." *Hydrol. Earth Syst. Sci.*, 16(10), 3647–3658.
- Music, B., and Caya, D. (2007). "Evaluation of the Hydrological Cycle over the Mississippi River Basin as Simulated by the Canadian Regional Climate Model (CRCM)." *J. Hydrometeorol.*, 8(5), 969–988.
- Music, B., and Caya, D. (2009). "Investigation of the Sensitivity of Water Cycle Components Simulated by the Canadian Regional Climate Model to the Land Surface Parameterization, the Lateral Boundary Data, and the Internal Variability." *J. Hydrometeorol.*, 10(1), 3–21.
- Muthuvel, D., and Mahesha, A. (2021). "Copula-Based Frequency and Coincidence Risk Analysis of Floods in Tropical-Seasonal Rivers." *J. Hydrol. Eng.*, 26(5), 05021007.
- Ndehedehe, C., Awange, J., Agutu, N., Kuhn, M., and Heck, B. (2016). "Understanding changes in terrestrial water storage over West Africa between 2002 and 2014." *Adv. Water Resour.*, 88, 211–230.
- Nelsen, R. B. (2006). *An Introduction to Copulas*. Springer Series in Statistics, New York, NY: Springer New York.

- Nguyen, P., Ombadi, M., Sorooshian, S., Hsu, K., Aghakouchak, A., Braithwaite, D., Ashouri, H., and Thorstensen, A. (2018). “The PERSIANN family of global satellite precipitation data: a review and evaluation of products.” *Hydrol. Earth Syst. Sci.*
- Nogueira, M. (2020). “Inter-comparison of ERA-5, ERA-interim and GPCP rainfall over the last 40 years: Process-based analysis of systematic and random differences.” *J. Hydrol.*, 583, 124632.
- Oliveira, P. T. S., Nearing, M. A., Moran, M. S., Goodrich, D. C., Wendland, E., and Gupta, H. V. (2014). “Trends in water balance components across the Brazilian Cerrado.” *Water Resour. Res.*, 50(9), 7100–7114.
- Oliveira, P. T. S., Wendland, E., Nearing, M. A., Scott, R. L., Rosolem, R., and Rocha, H. R. da. (2015). “The water balance components of undisturbed tropical woodlands in the Brazilian cerrado.” *Hydrol. Earth Syst. Sci.*, 19(6), 2899–2910.
- Öztopal, A., and Şen, Z. (2017). “Innovative Trend Methodology Applications to Precipitation Records in Turkey.” *Water Resour. Manag.*, 31(3), 727–737.
- Pan, M., Sahoo, A. K., Troy, T. J., Vinukollu, R. K., Sheffield, J., and Wood, E. F. (2012). “Multisource Estimation of Long-Term Terrestrial Water Budget for Major Global River Basins.” *J. Clim.*, 25(9), 3191–3206.
- Pan, M., and Wood, E. F. (2006). “Data Assimilation for Estimating the Terrestrial Water Budget Using a Constrained Ensemble Kalman Filter.” *J. Hydrometeorol.*, 7(3), 534–547.
- PAN, M., WOOD, E., WOJCIK, R., and MCCABE, M. (2008). “Estimation of regional terrestrial water cycle using multi-sensor remote sensing observations and data assimilation.” *Remote Sens. Environ.*, 112(4), 1282–1294.
- Pellet, V., Aires, F., Papa, F., Munier, S., and Decharme, B. (2020). “Long-term total water storage change from a Satellite Water Cycle reconstruction over large southern Asian basins.” *Hydrol. Earth Syst. Sci.*, 24(6), 3033–3055.
- Pervez, M. S., and Henebry, G. M. (2015). “Assessing the impacts of climate and land use and land cover change on the freshwater availability in the Brahmaputra River basin.” *J. Hydrol. Reg. Stud.*, 3, 285–311.
- Poncelet, C., Merz, R., Merz, B., Parajka, J., Oudin, L., Andréassian, V., and Perrin, C. (2017). “Process-based interpretation of conceptual hydrological model performance using a multinational catchment set.” *Water Resour. Res.*, 53(8), 7247–7268.
- Prakash, S. (2019). “Performance assessment of CHIRPS, MSWEP, SM2RAIN-CCI, and TMPA precipitation products across India.” *J. Hydrol.*, 571, 50–59.
- Prakash, S., Mitra, A. K., AghaKouchak, A., and Pai, D. S. (2015). “Error characterization of TRMM Multisatellite Precipitation Analysis (TMPA-3B42) products over India for different seasons.” *J. Hydrol.*, 529, 1302–1312.

- Praveen, B., Talukdar, S., Shahfahad, Mahato, S., Mondal, J., Sharma, P., Islam, A. R. M. T., and Rahman, A. (2020). “Analyzing trend and forecasting of rainfall changes in India using non-parametrical and machine learning approaches.” *Sci. Rep.*, 10(1), 10342.
- Qian, L., Dang, S., Bai, C., and Wang, H. (2021). “Variation in the dependence structure between runoff and sediment discharge using an improved copula.” *Theor. Appl. Climatol.*, 145(1–2), 285–293.
- Qian, L., Wang, X., and Wang, Z. (2020). “Modeling the dependence pattern between two precipitation variables using a coupled copula.” *Environ. Earth Sci.*, 79(21), 486.
- Revel, M., Zhou, X., Yamazaki, D., and Kanae, S. (2023). “Assimilation of transformed water surface elevation to improve river discharge estimation in a continental-scale river.” *Hydrol. Earth Syst. Sci.*, 27(3), 647–671.
- Roads, J., Kanamitsu, M., and Stewart, R. (2002). “CSE Water and Energy Budgets in the NCEP?DOE Reanalysis II.” *J. Hydrometeorol.*, 3(3), 227–248.
- Rodell, M., Houser, P. R., Jambor, U., Gottschalck, J., Mitchell, K., Meng, C.-J., Arsenault, K., Cosgrove, B., Radakovich, J., Bosilovich, M., Entin*, J. K., Walker, J. P., Lohmann, D., and Toll, D. (2004). “The Global Land Data Assimilation System.” *Bull. Am. Meteorol. Soc.*, 85(3), 381–394.
- Ropelewski, C. F., and Yarosh, E. S. (1998). “The Observed Mean Annual Cycle of Moisture Budgets over the Central United States (1973–92).” *J. Clim.*, 11(9), 2180–2190.
- Sahana, V., and Timbadiya, P. V. (2020). “Spatiotemporal Variation of Water Availability under Changing Climate: Case Study of the Upper Girna Basin, India.” *J. Hydrol. Eng.*, 25(5), 05020004.
- Sahoo, A. K., Pan, M., Troy, T. J., Vinukollu, R. K., Sheffield, J., and Wood, E. F. (2011). “Reconciling the global terrestrial water budget using satellite remote sensing.” *Remote Sens. Environ.*, 115(8), 1850–1865.
- Sajeev, A., Deb Barma, S., Mahesha, A., and Shiau, J.-T. (2021). “Bivariate Drought Characterization of Two Contrasting Climatic Regions in India Using Copula.” *J. Irrig. Drain. Eng.*, 147(3), 05020005.
- Salvadori, G., and Michele, C. De. (2004). “Frequency analysis via copulas: Theoretical aspects and applications to hydrological events.” *Water Resour. Res.*, 40(12).
- Şan, M., Akçay, F., Linh, N. T. T., Kankal, M., and Pham, Q. B. (2021). “Innovative and polygonal trend analyses applications for rainfall data in Vietnam.” *Theor. Appl. Climatol.*, 144(3–4), 809–822.
- Savéan, M., Delclaux, F., Chevallier, P., Wagnon, P., Gongga-Saholiariliva, N., Sharma, R., Neppel, L., and Arnaud, Y. (2015). “Water budget on the Dudh Koshi River (Nepal): Uncertainties on precipitation.” *J. Hydrol.*, 531, 850–862.

- Sen, P. K. (1968). "Estimates of the Regression Coefficient Based on Kendall's Tau." *J. Am. Stat. Assoc.*, 63(324), 1379–1389.
- Şen, Z. (2012). "Innovative Trend Analysis Methodology." *J. Hydrol. Eng.*, 17(9), 1042–1046.
- Şen, Z. (2017). "Innovative trend significance test and applications." *Theor. Appl. Climatol.*, 127(3–4), 939–947.
- Şen, Z., Şişman, E., and Dabanli, I. (2019). "Innovative Polygon Trend Analysis (IPTA) and applications." *J. Hydrol.*, 575, 202–210.
- Seo, J., Won, J., Choi, J., Lee, J., and Kim, S. (2022). "A copula model to identify the risk of river water temperature stress for meteorological drought." *J. Environ. Manage.*, 311, 114861.
- Sevruk, B. (2006). "Rainfall Measurement: Gauges."
- Seyoum, W. M., and Kwon, D. (2020). "Suitability of satellite-based hydro-climate variables and machine learning for streamflow modeling at various scale watersheds." *Hydrol. Sci. J.*, 65(13), 2233–2248.
- Sezen, C. (2022). "A new wavelet combined innovative polygon trend analysis (W-IPTA) approach for investigating the trends in the streamflow regime in the Konya Closed Basin, Turkey." *Theor. Appl. Climatol.*
- Shamsudduha, M., and Taylor, R. G. (2020). "Groundwater storage dynamics in the world's large aquifer systems from GRACE: uncertainty and role of extreme precipitation." *Earth Syst. Dyn.*, 11(3), 755–774.
- Sharannya, T. M., Al-Ansari, N., Barma, S. D., and Mahesha, A. (2020). "Evaluation of Satellite Precipitation Products in Simulating Streamflow in a Humid Tropical Catchment of India Using a Semi-Distributed Hydrological Model." *Water* 2020, Vol. 12, Page 2400, 12(9), 2400.
- Sheffield, J., Ferguson, C. R., Troy, T. J., Wood, E. F., and McCabe, M. F. (2009). "Closing the terrestrial water budget from satellite remote sensing." *Geophys. Res. Lett.*, 36(7), 1–5.
- Sheffield, J., Wood, E. F., Pan, M., Beck, H., Coccia, G., Serrat-Capdevila, A., and Verbist, K. (2018). "Satellite Remote Sensing for Water Resources Management: Potential for Supporting Sustainable Development in Data-Poor Regions." *Water Resour. Res.*, 54(12), 9724–9758.
- Sheikholeslami, R., Gharari, S., Papalexiou, S. M., and Clark, M. P. (2021). "VISCOUS: A Variance-Based Sensitivity Analysis Using Copulas for Efficient Identification of Dominant Hydrological Processes." *Water Resour. Res.*, 57(7).
- Simon, D., and Tien Li Chia. (2002). "Kalman filtering with state equality constraints." *IEEE Trans. Aerosp. Electron. Syst.*, 38(1), 128–136.

- Singh, R., Sah, S., Das, B., Potekar, S., Chaudhary, A., and Pathak, H. (2021). “Innovative trend analysis of spatio-temporal variations of rainfall in India during 1901–2019.” *Theor. Appl. Climatol.*, 145(1–2), 821–838.
- Singh, R., Sah, S., Das, B., Vishnoi, L., and Pathak, H. (2021). “Spatio-temporal trends and variability of rainfall in Maharashtra, India: Analysis of 118 years.” *Theor. Appl. Climatol.*, 143(3–4), 883–900.
- Sinha, J., Jha, S., and Goyal, M. K. (2019). “Influences of watershed characteristics on long-term annual and intra-annual water balances over India.” *J. Hydrol.*, 577, 123970.
- Sklar, A. (1959). “Fonctions de répartition à n dimensions et leurs marges.” *Publ. l’Institut Stat. l’Université Paris*, 8, 229–231.
- Sridhar, V., Ali, S. A., and Lakshmi, V. (2019). “Assessment and validation of total water storage in the Chesapeake Bay watershed using GRACE.” *J. Hydrol. Reg. Stud.*, 24, 100607.
- Strong, G. S., Proctor, B., Wang, M., Soulis, E. D., Smith, C. D., Seglenieks, F., and Snelgrove, K. (2002). “Closing the Mackenzie basin water budget, water years 1994/95 to 1996/97.” *Atmosphere-Ocean*, 40(2), 113–124.
- Su, F., and Lettenmaier, D. P. (2009). “Estimation of the Surface Water Budget of the La Plata Basin.” *J. Hydrometeorol.*, 10(4), 981–998.
- Sun, A. Y., Wang, D., and Xu, X. (2014). “Monthly streamflow forecasting using Gaussian Process Regression.” *J. Hydrol.*, 511, 72–81.
- Tao, Y., Wang, Y., Wang, D., Ni, L., and Wu, J. (2020). “A probabilistic modeling framework for assessing the impacts of large reservoirs on river thermal regimes – A case of the Yangtze River.” *Environ. Res.*, 183, 109221.
- Tapley, B. D., Bettadpur, S., Ries, J. C., Thompson, P. F., and Watkins, M. M. (2004). “GRACE Measurements of Mass Variability in the Earth System.” *Science* (80-.), 305(5683), 503–505.
- Tavakol, A., Rahmani, V., and Harrington Jr., J. (2020). “Probability of compound climate extremes in a changing climate: A copula-based study of hot, dry, and windy events in the central United States.” *Environ. Res. Lett.*, 15(10), 104058.
- Troy, T. J., Sheffield, J., and Wood, E. F. (2011). “Estimation of the Terrestrial Water Budget over Northern Eurasia through the Use of Multiple Data Sources.” *J. Clim.*, 24(13), 3272–3293.
- Uttarwar, S. B., Deb Barma, S., and Mahesha, A. (2020). “Bivariate Modeling of Hydroclimatic Variables in Humid Tropical Coastal Region Using Archimedean Copulas.” *J. Hydrol. Eng.*, 25(9), 05020026.

- Villarini, G., Serinaldi, F., and Krajewski, W. F. (2008). "Modeling radar-rainfall estimation uncertainties using parametric and non-parametric approaches." *Adv. Water Resour.*, 31(12), 1674–1686.
- Voisin, N., Wood, A. W., and Lettenmaier, D. P. (2008). "Evaluation of Precipitation Products for Global Hydrological Prediction." *J. Hydrometeorol.*, 9(3), 388–407.
- Wable, P. S., and Jha, M. K. (2018). "Application of Archimedean copulas to the impact assessment of hydro-climatic variables in semi-arid aquifers of western India." *Hydrogeol. J.*, 26(1), 89–108.
- Wang, H., Guan, H., Gutiérrez-Jurado, H. A., and Simmons, C. T. (2014). "Examination of water budget using satellite products over Australia." *J. Hydrol.*, 511, 546–554.
- Wang, S., Huang, J., Li, J., Rivera, A., McKenney, D. W., and Sheffield, J. (2014). "Assessment of water budget for sixteen large drainage basins in Canada." *J. Hydrol.*, 512, 1–15.
- Wang, S., Huang, J., Yang, D., Pavlic, G., and Li, J. (2015). "Long-term water budget imbalances and error sources for cold region drainage basins." *Hydrol. Process.*, 29(9), 2125–2136.
- Wang, S., McKenney, D. W., Shang, J., and Li, J. (2014). "A national-scale assessment of long-term water budget closures for Canada's watersheds." *J. Geophys. Res. Atmos.*, 119(14), 8712–8725.
- Wang, Y., Xu, Y., Tabari, H., Wang, J., Wang, Q., Song, S., and Hu, Z. (2020). "Innovative trend analysis of annual and seasonal rainfall in the Yangtze River Delta, eastern China." *Atmos. Res.*, 231, 104673.
- Watkins, M. M., Wiese, D. N., Yuan, D.-N., Boening, C., and Landerer, F. W. (2015). "Improved methods for observing Earth's time variable mass distribution with GRACE using spherical cap mascons." *J. Geophys. Res. Solid Earth*, 120(4), 2648–2671.
- Wehbe, Y., Temimi, M., Ghebreyesus, D. T., Milewski, A., Norouzi, H., and Ibrahim, E. (2018). "Consistency of precipitation products over the Arabian Peninsula and interactions with soil moisture and water storage." *Hydrol. Sci. J.*, 63(3), 408–425.
- Wei, L., Jiang, S., Ren, L., Wang, M., Zhang, L., Liu, Y., Yuan, F., and Yang, X. (2021). "Evaluation of seventeen satellite-, reanalysis-, and gauge-based precipitation products for drought monitoring across mainland China." *Atmos. Res.*, 263, 105813.
- Wei, L., Link, T. E., Hudak, A. T., Marshall, J. D., Kavanagh, K. L., Abatzoglou, J. T., Zhou, H., Pangle, R. E., and Flerchinger, G. N. (2016). "Simulated water budget of a small forested watershed in the continental/maritime hydroclimatic region of the United States." *Hydrol. Process.*, 30(13), 2000–2013.
- Wu, Y., and Chen, J. (2013). "Analyzing the Water Budget and Hydrological Characteristics and Responses to Land Use in a Monsoonal Climate River Basin in South China." *Environ. Manage.*, 51(6), 1174–1186.

- Xu, C.-Y., and Singh, V. P. (1998). "A Review on Monthly Water Balance Models for Water Resources Investigations." *Water Resour. Manag.*, 12(1), 20–50.
- Xue, X., Hong, Y., Limaye, A. S., Gourley, J. J., Huffman, G. J., Khan, S. I., Dorji, C., and Chen, S. (2013). "Statistical and hydrological evaluation of TRMM-based Multi-satellite Precipitation Analysis over the Wangchu Basin of Bhutan: Are the latest satellite precipitation products 3B42V7 ready for use in ungauged basins?" *J. Hydrol.*, 499, 91–99.
- Yang, X., Chen, Z., and Qin, M. (2023). "Joint probability analysis of streamflow and sediment load based on hybrid copula." *Environ. Sci. Pollut. Res.*, 30(16), 46489–46502.
- Yao, Y., Liang, S., Xie, X., Cheng, J., Jia, K., Li, Y., and Liu, R. (2014). "Estimation of the terrestrial water budget over northern China by merging multiple datasets." *J. Hydrol.*, 519(PA), 50–68.
- Yatagai, A., Kamiguchi, K., Arakawa, O., Hamada, A., Yasutomi, N., and Kitoh, A. (2012). "APHRODITE: Constructing a Long-Term Daily Gridded Precipitation Dataset for Asia Based on a Dense Network of Rain Gauges." *Bull. Am. Meteorol. Soc.*, 93(9), 1401–1415.
- Yuan, R.-Q., Chang, L.-L., Gupta, H., and Niu, G.-Y. (2019). "Climatic forcing for recent significant terrestrial drying and wetting." *Adv. Water Resour.*, 133, 103425.
- Zeng, N. (1999). "Seasonal cycle and interannual variability in the Amazon hydrologic cycle." *J. Geophys. Res. Atmos.*, 104(D8), 9097–9106.
- Zhang, D., Zhang, Q., Werner, A. D., and Gu, R. (2016). "Assessment of the reliability of popular satellite products in characterizing the water balance of the Yangtze River Basin, China." *Hydrol. Res.*, 47(S1), 8–23.
- Zhang, L., Li, X., Cao, Y., Nan, Z., Wang, W., Ge, Y., Wang, P., and Yu, W. (2020). "Evaluation and integration of the top-down and bottom-up satellite precipitation products over mainland China." *J. Hydrol.*, 581, 124456.
- Zhang, L., and Singh, V. P. (2006). "Bivariate Flood Frequency Analysis Using the Copula Method." *J. Hydrol. Eng.*, 11(2), 150–164.
- Zhang, Y., Pan, M., and Wood, E. F. (2016). "On Creating Global Gridded Terrestrial Water Budget Estimates from Satellite Remote Sensing." *Surv. Geophys.*, 37(2), 249–268.
- Zhou, W., Guan, K., Peng, B., Shi, J., Jiang, C., Wardlow, B., Pan, M., Kimball, J. S., Franz, T. E., Gentile, P., He, M., and Zhang, J. (2020). "Connections between the hydrological cycle and crop yield in the rainfed U.S. Corn Belt." *J. Hydrol.*, 590, 125398.

Zhu, M., Li, M., Liu, C., Wang, Y., Li, J., and Li, Y. (2020). “Spatial Distribution and Temporal Trends in the Daily Precipitation Concentration across the Yarlung Tsangpo River Basin: Eastern Himalaya of China.”

Zscheischler, J., and Seneviratne, S. I. (2017). “Dependence of drivers affects risks associated with compound events.” *Sci. Adv.*, 3(6), e1700263.

APPENDIX

Table AI.1 Daily metrics obtained for evaluation of satellite precipitation of winter season of the upper basin

| Metrics | CHIRPS | CMORPH | IMERG | SM2RAIN | TRMM |
|----------------|-------------|--------|-------------|-------------|-------------|
| POD | 0.92 | 0.99 | 1 | 0.76 | 1 |
| FAR | 0.06 | 0.07 | 0.07 | 0.06 | 0.07 |
| CSI | 0.87 | 0.92 | 0.93 | 0.72 | 0.93 |
| R ² | 0 | 0 | 0 | 0.02 | 0.01 |
| Mean (mm) | 4.74 | 3.81 | 4.68 | 5.41 | 3.53 |
| RBIAS | 0.02 | -0.18 | 0.01 | 0.17 | -0.24 |
| ME (mm) | 0.11 | -0.81 | 0.06 | 0.78 | -1.1 |
| MAE (mm) | 3.3 | 3.63 | 3.43 | 2.86 | 3.98 |
| RMSE (mm) | 4.79 | 5.02 | 4.89 | 4.44 | 5.25 |

Note: Daily mean of APHRODITE = 4.63 mm.

Table AI.2 Daily metrics obtained for evaluation of satellite precipitation of winter season of the middle basin

| Metrics | CHIRPS | CMORPH | IMERG | SM2RAIN | TRMM |
|----------------|-------------|--------|-------|-------------|------|
| POD | 0.79 | 1 | 1 | 0.74 | 1 |
| FAR | 0.17 | 0.2 | 0.2 | 0.17 | 0.2 |
| CSI | 0.68 | 0.8 | 0.8 | 0.64 | 0.8 |
| R ² | 0.01 | 0 | 0 | 0 | 0.07 |
| Mean (mm) | 5.43 | 6.09 | 6.17 | 6.89 | 5.96 |
| RBIAS | 0.34 | 0.51 | 0.52 | 0.7 | 0.47 |
| ME (mm) | 1.39 | 2.04 | 2.12 | 2.85 | 1.91 |

| | | | | | |
|-----------|-------------|------|------|------|------|
| MAE (mm) | 4.51 | 5.24 | 4.98 | 5.04 | 6.07 |
| RMSE (mm) | 6.44 | 6.74 | 6.74 | 6.83 | 7.46 |

Note: Daily mean of APHRODITE = 4.04 mm.

Table AI.3 Daily metrics obtained for evaluation of satellite precipitation of winter season of the lower basin

| Metrics | CHIRPS | CMORPH | IMERG | SM2RAIN | TRMM |
|----------------|-------------|-------------|-------------|---------|-------------|
| POD | 0.81 | 1 | 1 | 1 | 1 |
| FAR | 0.21 | 0.23 | 0.22 | 0.23 | 0.22 |
| CSI | 0.67 | 0.77 | 0.78 | 0.77 | 0.78 |
| R ² | 0.01 | 0 | 0.02 | 0 | 0.03 |
| Mean (mm) | 5.14 | 4.79 | 5.04 | 6.27 | 4.93 |
| RBIAS | 0.42 | 0.32 | 0.39 | 0.73 | 0.36 |
| ME (mm) | 1.51 | 1.16 | 1.41 | 2.64 | 1.3 |
| MAE (mm) | 3.85 | 4.13 | 3.78 | 4.04 | 4.72 |
| RMSE (mm) | 5.28 | 5.47 | 5.22 | 5.41 | 5.84 |

Note: Daily mean of APHRODITE = 3.63 mm.

Table AI.4 Daily metrics obtained for evaluation of satellite precipitation of summer season of the upper basin

| Metrics | CHIRPS | CMORPH | IMERG | SM2RAIN | TRMM |
|----------------|------------|--------|-------|---------|------|
| POD | 0.97 | 1 | 1 | 0.81 | 1 |
| FAR | 0 | 0 | 0 | 0 | 0 |
| CSI | 0.97 | 1 | 1 | 0.81 | 1 |
| R ² | 0.06 | 0.03 | 0.08 | 0.13 | 0 |
| Mean (mm) | 3.1 | 1.77 | 2.76 | 2.38 | 2.04 |

| | | | | | |
|-----------|--------------|-------|-------------|-------|-------|
| RBIAS | -0.19 | -0.54 | -0.28 | -0.37 | -0.46 |
| ME (mm) | -0.71 | -2.04 | -1.05 | -1.43 | -1.77 |
| MAE (mm) | 2.67 | 2.96 | 2.36 | 2.66 | 3.11 |
| RMSE (mm) | 3.89 | 4.25 | 3.72 | 3.97 | 4.3 |

Note: Daily mean of APHRODITE = 3.81 mm.

Table AI.5 Daily metrics obtained for evaluation of satellite precipitation of summer season of the middle basin

| Metrics | CHIRPS | CMORPH | IMERG | SM2RAIN | TRMM |
|----------------|--------|-------------|--------------|---------|-------|
| POD | 0.91 | 1 | 1 | 0.59 | 1 |
| FAR | 0 | 0 | 0 | 0 | 0 |
| CSI | 0.91 | 1 | 1 | 0.59 | 1 |
| R ² | 0.01 | 0.02 | 0.04 | 0.01 | 0.01 |
| Mean (mm) | 5.17 | 4.19 | 6.08 | 2.69 | 5.24 |
| RBIAS | -0.19 | -0.34 | -0.05 | -0.58 | -0.18 |
| ME (mm) | -1.19 | -2.18 | -0.29 | -3.68 | -1.12 |
| MAE (mm) | 4.61 | 4.19 | 3.82 | 5.25 | 4.69 |
| RMSE (mm) | 6.05 | 5.34 | 5.37 | 6.57 | 6.37 |

Note: Daily mean of APHRODITE = 6.37 mm.

Table AI.6 Daily metrics obtained for evaluation of satellite precipitation of summer season of the lower basin

| Metrics | CHIRPS | CMORPH | IMERG | SM2RAIN | TRMM |
|---------|--------|--------|-------|---------|------|
| POD | 0.94 | 1 | 1 | 1 | 1 |
| FAR | 0 | 0.01 | 0.01 | 0.01 | 0.01 |
| CSI | 0.94 | 0.99 | 0.99 | 0.99 | 0.99 |

| | | | | | |
|----------------|------|-------------|-------------|-------|--------------|
| R ² | 0.24 | 0.4 | 0.43 | 0.15 | 0.37 |
| Mean (mm) | 8.18 | 5.93 | 8.08 | 5.6 | 7.36 |
| RBIAS | 0.08 | -0.22 | 0.07 | -0.26 | -0.03 |
| ME (mm) | 0.62 | -1.64 | 0.51 | -1.96 | -0.2 |
| MAE (mm) | 5.8 | 3.74 | 3.81 | 3.92 | 4.34 |
| RMSE (mm) | 8.77 | 5.02 | 5.4 | 5.23 | 5.98 |

Note: Daily mean of APHRODITE = 7.57 mm.

Table AI.7 Daily metrics obtained for evaluation of satellite precipitation of monsoon season of the upper basin

| Metrics | CHIRPS | CMORPH | IMERG | SM2RAIN | TRMM |
|----------------|--------|--------------|-------------|---------|------|
| POD | 0.99 | 1 | 1 | 1 | 1 |
| FAR | 0 | 0 | 0 | 0 | 0 |
| CSI | 0.99 | 1 | 1 | 1 | 1 |
| R ² | 0.27 | 0.28 | 0.41 | 0.08 | 0.31 |
| Mean (mm) | 3.58 | 2.68 | 3.69 | 0.32 | 3.89 |
| RBIAS | 0.27 | -0.05 | 0.31 | -0.89 | 0.38 |
| ME (mm) | 0.76 | -0.14 | 0.88 | -2.5 | 1.07 |
| MAE (mm) | 1.95 | 1.27 | 1.54 | 2.5 | 1.93 |
| RMSE (mm) | 2.79 | 1.94 | 2.25 | 3.11 | 2.87 |

Note: Daily mean of APHRODITE = 2.82 mm.

Table AI.8 Daily metrics obtained for evaluation of satellite precipitation of monsoon season of the middle basin

| Metrics | CHIRPS | CMORPH | IMERG | SM2RAIN | TRMM |
|---------|--------|--------|-------|---------|------|
|---------|--------|--------|-------|---------|------|

| | | | | | |
|----------------|--------------|-------------|------------|-------|------|
| POD | 0.98 | 1 | 1 | 0.79 | 1 |
| FAR | 0 | 0 | 0 | 0 | 0 |
| CSI | 0.98 | 1 | 1 | 0.79 | 1 |
| R ² | 0.16 | 0.18 | 0.3 | 0.01 | 0.25 |
| Mean (mm) | 5.46 | 3.56 | 7.24 | 0.13 | 7.81 |
| RBIAS | -0.06 | -0.39 | 0.24 | -0.98 | 0.34 |
| ME (mm) | -0.37 | -2.28 | 1.41 | -5.71 | 1.97 |
| MAE (mm) | 4.25 | 3.4 | 3.96 | 5.71 | 4.57 |
| RMSE (mm) | 6.13 | 4.39 | 5.95 | 6.65 | 7.01 |

Note: Daily mean of APHRODITE = 5.83 mm.

Table AI.9 Daily metrics obtained for evaluation of satellite precipitation of monsoon season of the lower basin

| Metrics | CHIRPS | CMORPH | IMERG | SM2RAIN | TRMM |
|----------------|--------|-------------|-------------|--------------|-------|
| POD | 1 | 1 | 1 | 1 | 1 |
| FAR | 0 | 0 | 0 | 0 | 0 |
| CSI | 1 | 1 | 1 | 1 | 1 |
| R ² | 0.43 | 0.51 | 0.68 | 0.29 | 0.58 |
| Mean (mm) | 13.63 | 9.9 | 15.07 | 10.54 | 14.95 |
| RBIAS | 1.66 | -2.07 | 3.1 | -1.43 | 2.98 |
| ME (mm) | 5.97 | 4.73 | 5.05 | 4.89 | 5.49 |
| MAE (mm) | 8.04 | 6.23 | 7.09 | 6.82 | 7.72 |
| RMSE (mm) | 1.66 | -2.07 | 3.1 | -1.43 | 2.98 |

Note: Daily mean of APHRODITE = 11.97 mm.

Table AI.10 Daily metrics obtained for evaluation of satellite precipitation of post monsoon season of the upper basin

| Metrics | CHIRPS | CMORPH | IMERG | SM2RAIN | TRMM |
|----------------|--------|--------------|-------|-------------|------|
| POD | 0.88 | 1 | 1 | 0.7 | 1 |
| FAR | 0.1 | 0.11 | 0.11 | 0.06 | 0.11 |
| CSI | 0.8 | 0.89 | 0.89 | 0.67 | 0.89 |
| R ² | 0.01 | 0 | 0.02 | 0.04 | 0.03 |
| Mean (mm) | 4.56 | 3.94 | 4.6 | 3.76 | 4.64 |
| RBIAS | 0.14 | -0.01 | 0.15 | -0.06 | 0.16 |
| ME (mm) | 0.57 | -0.04 | 0.61 | -0.22 | 0.66 |
| MAE (mm) | 3.16 | 3.68 | 3.02 | 3 | 4.06 |
| RMSE (mm) | 4.68 | 5.02 | 4.58 | 4.57 | 5.29 |

Note: Daily mean of APHRODITE = 3.99 mm.

Table AI.11 Daily metrics obtained for evaluation of satellite precipitation of post monsoon season of the middle basin

| Metrics | CHIRPS | CMORPH | IMERG | SM2RAIN | TRMM |
|----------------|-------------|--------|-------|-------------|------|
| POD | 0.75 | 1 | 1 | 0.66 | 1 |
| FAR | 0.17 | 0.22 | 0.22 | 0.17 | 0.22 |
| CSI | 0.65 | 0.78 | 0.78 | 0.58 | 0.78 |
| R ² | 0.06 | 0 | 0.06 | 0 | 0.01 |
| Mean (mm) | 5.05 | 6.2 | 6.01 | 5.05 | 5.05 |
| RBIAS | 0.25 | 0.54 | 0.49 | 0.26 | 0.76 |
| ME (mm) | 1.03 | 2.17 | 1.98 | 1.03 | 3.06 |
| MAE (mm) | 4.11 | 5.13 | 4.41 | 4.63 | 6.2 |

RMSE (mm) **6.21** 6.75 6.47 6.58 7.63

Note: Daily mean of APHRODITE = 4.03 mm.

Table AI.12 Daily metrics obtained for evaluation of satellite precipitation of post monsoon season of the lower basin

| Metrics | CHIRPS | CMORPH | IMERG | SM2RAIN | TRMM |
|----------------|--------|-------------|-------------|-------------|----------|
| POD | 0.79 | 0.99 | 1 | 0.99 | 1 |
| FAR | 0.19 | 0.25 | 0.25 | 0.25 | 0.25 |
| CSI | 0.67 | 0.75 | 0.75 | 0.74 | 0.75 |
| R ² | 0.35 | 0.24 | 0.43 | 0.02 | 0.29 |
| Mean (mm) | 5.2 | 5.67 | 5.92 | 5.07 | 6.23 |
| RBIAS | 0.26 | 0.37 | 0.43 | 0.22 | 0.5 |
| ME (mm) | 1.06 | 1.53 | 1.78 | 0.93 | 2.09 |
| MAE (mm) | 3.83 | 4.1 | 3.8 | 4.08 | 4.81 |
| RMSE (mm) | 5.86 | 5.48 | 5.59 | 5.98 | 6.18 |

Note: Daily mean of APHRODITE = 4.14 mm.

LIST OF PUBLICATIONS

Journal

1. Deb Barma, S., and Mahesha, A. (2023). “Discussion of ‘Innovative approaches to the trend assessment of streamflows in the Eastern Black Sea basin, Turkey’ *.” *Hydrol. Sci. J.*, 68(5), 731–732.
2. Deb Barma et al. (2022). Evaluation of ERA5 and IMERG Precipitation Data for Risk Assessment of Water Cycle Variables of a Large River Basin in South Asia using Satellite data and Archimedean Copulas. *Water Conserv. Manag.* 6, 61-69.

Journal publication through mentorship and collaboration

3. Chowdari, K., Deb Barma, S., Bhat, N., Girisha, R., Gouda, K. C., and Mahesha, A. (2023). “Trends of seasonal and annual rainfall of semi-arid districts of Karnataka, India: application of innovative trend analysis approach.” *Theor. Appl. Climatol.*, 152(1–2), 241–264.
4. Thieu, N. Van, Deb Barma, S., Lam, T. Van, Kisi, O., and Mahesha, A. (2023). “Groundwater level modeling using Augmented Artificial Ecosystem Optimization.” *J. Hydrol.*, 617, 129034.
5. Sajeev, A., Deb Barma, S., Mahesha, A., Shiau, J.-T., 2021. Bivariate Drought Characterization of Two Contrasting Climatic Regions in India Using Copula. *J. Irrig. Drain. Eng.* 147, 05020005.
6. Uttarwar, S.B., Deb Barma, S., Mahesha, A., 2020. Bivariate Modeling of Hydroclimatic Variables in Humid Tropical Coastal Region Using Archimedean Copulas. *J. Hydrol. Eng.* 25, 05020026.
7. Sharannya, T.M., Al-Ansari, N., Deb Barma, S., Mahesha, A., 2020. Evaluation of Satellite Precipitation Products in Simulating Streamflow in a Humid Tropical Catchment of India Using a Semi-Distributed Hydrological Model. *Water* 2020, Vol. 12, Page 2400 12, 2400.
8. Kumar, S.S., Deb Barma, S., Amai, M., 2020. Simulation of coastal aquifer using mSim toolbox and COMSOL multiphysics. *J. Earth Syst. Sci.* 129, 66.
9. Sailesh, K., Deb Barma, S., Amai, M., 2020. Sensitivity Analysis of a Conceptual, Lumped Model Using VARS-TOOL Applied to Western Ghats Catchments of India. Preprint EarthArxiv.

Conferences

Deb Barma, Surajit and Mahesha, Amai (2017). “Most appropriate streamflow model structure for humid river basins.” 3rd International Conference on the Status and Future of the World’s Large Rivers 18-21 April 2017, New Delhi, India.

Deb Barma, Surajit, Mahesha, Amai, Kikon, Ayilobeni, Deka, Paresh Chandra and Mudbhatkal, Amogh (2017). “A comparative analysis of hydrological signatures of two Western Ghat catchments.” Hydro-2017 International, 21- 23 December, 2017, L.D. College of Engineering Ahmedabad, India.

Deb Barma, Surajit and Mahesha, Amai (2018). “Evaluation of High Resolution Satellite Based Rainfall Estimates over a Humid River Basin in Western Ghats, India. International conference on “Sustainable Technology for Intelligent Water Management STIWM” 16-19 February 2018, IIT Roorkee, India.

BIOSKTECH



Name: SURAJIT DEB BARMA

Permanent Address: Vill- Rammmanik Para, P.O. Golaghati ,
Bishalgarh Dist: Sepahijala, Tripura- 799 102.

EDUCATION: MASTER OF TECHNOLOGY
Discipline: Water Resources Engineering
National Institute of Technology, Silchar, India

BACHELOR OF TECHNOLOGY
Discipline: Agricultural Engineering
NERIST, Nirjuli, Arunachal Pradesh
Formerly affiliated to: North Eastern Hill University, Shillong.

Contact No.: +91-8217796934

Email ID: surajitdb@gmail.com

ORCID: 0000-0003-0849-3033